UNIVERSITÀ
DEGLI STUDI
DI PADOVA

Head Office: Università degli Studi di Padova

Department of Biology

Ph.D COURSE IN: BIOSCIENCES

CURRICULUM: BIOCHEMISTRY AND BIOTECHNOLOGY

SERIES XXXI

Adaptation of mechanisms for regulation of photosynthetic electron transport upon land colonization

Coordinator: Ch.mo Prof. Ildikò Szabò

Supervisor: Ch.mo Prof. Tomas Morosinotto

Ph.D student: Mattia Storti

TABLE OF CONTENTS

ABSTRACT (ENGLISH)

Photosynthetic reactions sustain life on our planet providing organic carbon sources exploited by all heterotrophic organisms. In eukaryotic organisms, oxygenic photosynthesis is catalyzed by 4 multiprotein complexes present on the thylakoid membranes inside the chloroplasts: Photosystem (PS) II, Cytochrome b_6f (Cyt b_6f), PSI and chloroplast ATP synthase (ATPase). The three former are responsible for a Linear Electron Flow (LEF) from water which is oxidized at level of PSII, to $NADP^+$. Electrons are transported by carrier molecules: Plastoquinone (PQ) allows the transfer between PSII and Cyt b_6f, Plastocyanin (Pc) transports electron from Cyt b_6f to PSI and Ferredoxin (Fd) is the primary acceptor of PSI and it transfers an electron to $NADP^+$. Thanks to the LEF a proton gradient across the thylakoid membrane is generated supporting ATP synthesis. NADPH and ATP are exploited by Calvin Benson cycle to fix inorganic CO_2 in sugars available for the metabolism.

Photosynthetic process described above is accompanied by the formation of unstable excited molecules that can drive to the generation of reactive oxygen species (ROS) which can be harmful for the photosynthetic process and the cell overall. Photosynthetic organisms evolved specific regulatory mechanisms to balance the efficiency of photochemical reaction with the need for protection. Among these photoprotective mechanisms the Alternative Electron Flow (AEF) pathways hold a seminal role in diverting electrons from photosynthetic processes to prevent over-reduction of electron transporters and consequent possible production of reactive species. AEF mechanisms can be divided in Cyclic Electron Flow (CEF) and Pseudo-CEF (PCEF) according to the acceptors of the pathways, respectively the plastoquinone pool and oxygen. Two major CEF are known and mediated by PGR5/PGRL1 proteins or by NDH-1 complex. PCEF is instead mediated by Flavodiiron proteins (FLV) or can arise by direct oxygen reduction to form reactive oxygen species that are then detoxified by the Mehler reaction. Different classes of photosynthetic organisms show variable distribution of the AEF pathways. In this thesis I focused on the early land plant *Physcomitrella patens*, that diverged from vascular plant ancestors early after land colonization. This moss is particularly interesting in this context because it presents all the main AEF identified in algae and vascular plants (PGR5/PGRL1, NDH-1, FLV), and is thus a suitable model to directly compared their activity in the same organisms. The study of this model will also contribute to understand the evolutionary driving forces that lead to the variability of these mechanisms.

In chapter 2 of this thesis the distribution of different AEF mechanisms in eukaryotic organisms is discussed, particularly focusing on the role of FLV proteins. The latter were already present in

cyanobacteria and found in green algae, non-vascular plants and gymnosperms but they were lost in Angiosperms. In this chapter we reviewed recent evidences on the function of these proteins and discussed the possible hypotheses of FLV loss in flowering plants. One of the plausible explanations is that another AEF mechanism replaces their function, making FLV dispensable. FLV were shown to be fundamental to respond to light fluctuation that occurs in the natural environments, a function that in angiosperms was replaced by PGR5/PGRL1.

In order to evaluate the hypothesis that PGRL1/PGR5 CEF mediated pathway can replace FLV role, in chapter 3 there is the description of the isolation of a *P. patens* double Knockout mutant defective for both FLV and PGRL1. Our experiments highlighted a strong synergy between the 2 pathways especially when plants were exposed to stressful light regimes mimicking natural environment. The comparison of single and double knock-out mutants showed that even if FLV have a major role in response to light fluctuation, their absence can be partially compensated by PGR5/PGRL1, suggesting that this functional overlap allowed the possible replacement of one pathway over the other during evolution. Further analysis allowed us to establish that FLV and PGRL1 are particularly important for protection of photosystem I (PSI) from over-reduction, thus preventing photodamage.

In chapter 4, we characterized NDH-1 complex in *P. patens*. NDH-1 is not generally found in green algae and was acquired in the green lineage by streptophyta algae. NDH-1 composition is conserved in most land plants, but several accessory subunits were acquired later and are missing from non-vascular plants. For instance, two antenna proteins involved in the formation of a PSI-NDH-1 supercomplex in *A. thaliana* are not present in the liverwort *Marchantia polymorpha*. Despite several reports trying to unravel the function of NDH-1 in plants, its physiological role in natural conditions is still unclear. In order to answer this question in chapter 4 we isolated a line defective for NDH-1 function by knocking out the gene coding a core subunit of the complex from *P. patens* genome. Biochemical characterization of *P. patens* WT plants allowed the detection of NDH-1 in a supercomplex, but the latter did not contain PSI, suggesting that a PSI-NDH-1 complex is not formed in *P. patens*. The comparison of photosynthetic activity of NDH-1 defective mutants with WT plants showed a small defect in PSI functionality in the first moment after light exposure or after light switch off. Reiterating cycle of dark and light, the defect observed increased significantly in NDH-1 defective plants suggesting that this complex may be important to avoid PSI over-reduction consuming electrons stored in stromal acceptors. However, this defect did not impact the plant growth not even in fluctuating light conditions, probably because of the compensation from other mechanisms present in the chloroplast.

In order to entangle this possible functional compensation in chapter 5 NDH-1 was knocked out in plants depleted of both PGRL1 and FLV, by isolating a double mutant lacking both CEF pathways (*pgrl1-ndhm*) and a triple mutant defective for both CEF and PCEF (*flva-pgrl1-ndhm*). All plants considered were grown in different light regimes analyzing growth and photosynthesis. *pgrl1-ndhm* and *flva-pgrl1-ndhm* exhibited a drastic decrease in growth and photosynthetic performances with increasing light intensities respect both single mutants and WT. This revealed that NDH-1 depletion has a much larger effect if other mechanisms for AEF are also absent, eliminating the compensating effects. Again, we found a synergic effect between AEF pathway since single mutant phenotype was much smaller than their combinations. The triple CEF-PCEF mutant showed growth defects even in non-stressing conditions suggesting these mechanisms are important also for steady state photosynthesis, not only for stress response. *In vivo* spectroscopic experiments and gas exchange measurements revealed that photosynthetic electron transport in *flva-ndhm-pgrl1* KO was less than in WT mosses. Spectroscopic and biochemical characterization detected extensive damage to PSI, correlated with the growth and electron transport defects. Thus, AEF are fundamental to sustain photosynthetic activity. Different AEF have a clear functional redundancy to ensure a correct photosynthetic activity and plant survival in many environmental conditions.

All the AEF pathways we considered compete for Fd or NADPH in the stroma of chloroplast with Ferredoxin-NADPH Reductase (FNR), which transfer an electron from reduced Fd to $NADP^+$. Thus, it is possible that the activities of FNR and AEF pathways can regulate each other during photosynthetic activity. In appendix 1 we analyzed FNR enzymes present in *P. patens* with the perspective to study them in the regulation of photosynthesis. In *P. patens* we identified 2 FNR isoforms similar to Root-type FNR of vascular plants. Nevertheless, the 2 isoforms are expressed differentially in photosynthetic and non-photosynthetic tissues. Moreover, we found that in *P. patens* FNR is poorly bounded to the thylakoid membrane at difference from angiosperms, possibly because of the absence of proteins involved in membrane docking.

Another interesting aspect linked to the evolution of first land plants is the acquisition of the de/rehydration tolerance. To investigate this aspect in the early plants *P. patens*, in appendix 2 we exploited the genetically encoded sensor Cameleon YC3.60 to study role of calcium signaling in the perception of dehydration stimuli. Interestingly, in response to an osmoticum we detected a systemic signal starting from the base of the plant (probably involved in the perception) and ending in the tips of phyllids. The signal measured was very slow compared to those measured in *A. thaliana* plants and compatible with a cell-cell communication mechanism.

RIASSUNTO (ITALIANO)

Le reazioni fotosintetiche permettono la vita sul nostro pianeta sia influenzando la composizione dei gas atmosferici che fornendo una fonte di carbonio organico utilizzabile dagli organismi eterotrofi. Negli organismi eucarioti, la fotosintesi ossigenica è mediata da 4 complessi situati nelle membrane tilacoidali dei cloroplasti: Il fotosistema (PS) II, il complesso dei citocromi b_6 ed f (Cyt b_6f), il PSI e l'ATP sintasi cloroplastica (ATPase). I primi 3 permettono il trasporto lineare degli elettroni (LEF) dall'acqua, ossidata a livello del PSII, fino al $NADP^+$. Inoltre, gli elettroni sono trasportati dal plastochinone (PQ) tra il PSII e il Cyt b_6f, mentre dal Cyt b_6f al PSI sono traportati dalla plastocianina (Pc). Infine, la ferredossina-$NADP^+$ reduttasi (FNR) ossida la ferredossina (Fd), accettore primario del PSI, portando alla sintesi di NADPH. Durante il LEF, un gradiente protoni è generato dalle reazioni di ossidoriduzione e utilizzato per sostenere l'attività dell'ATPase quindi sintetizzare ATP. NADPH e ATP sono utilizzati dal ciclo di Calvin Benson per fissare la CO_2 inorganica in zuccheri disponibili per il metabolismo.

Durante il processo fotosintetico si originano molecole cariche e specie reattive dell'ossigeno (ROS) che possono essere dannose per il processo stesso e per il metabolismo cellulare in genere. Per evitare la formazione dei ROS, gli organismi fotosintetici hanno evoluto diverse strategie che permettono di bilanciare la protezione dell'apparato fotosintetico e la sua produttività. Tra questi meccanismi vi sono i flussi alternativi degli elettroni (AEF) che hanno un ruolo fondamentale, spostando gli elettroni in eccesso dal LEF e cosi prevenendo l'accumulo di specie cariche reattive. I AEF possono essere divisi in trasporto ciclico (CEF) e pseudo-ciclico (PCEF) in base all'accettore finale degli elettroni, rispettivamente il plastochinone e l'ossigeno. Le 2 vie principali di CEF sono mediate rispettivamente dalle proteine PGR5/PGRL1 e dal complesso NDH-1. Il PCEF invece avviene grazie alle proteine FLV (Flavodiiron protein) o può derivare dalla riduzione dell'ossigeno a livello del PSI, generando così ROS che possono essere detossificati dalla reazione di Mehler. La distribuzione dei AEF non è omogenea nelle diverse classi di organismi fotosintetici. In questa tesi mi sono focalizzato sulla pianta non vascolare *Physcomitrella patens*, che si è diversificato dalle piante vascolari in prossimità della colonizzazione dell'ambiente terrestre. Questo organismo è un ottimo modello di studio in quanto potenzialmente utilizza tutti i AEF studiati nelle alghe e nelle piante vascolari (PGR5/PGRL1, NDH-1 e FLV) e permetterebbe il confronto diretto delle 3 vie. Lo studio di questo modello potrebbe anche contribuire a capire quali sono le ragioni evolutive che hanno portato ad una distribuzione così disomogenea delle vie di trasporto considerate nelle diverse classi di organismi.

Nel capitolo 2 di questa tesi ci siamo soffermati sulla relazione tra i diversi AEF negli organismi eucarioti, con un occhio di riguardo al ruolo delle FLV. Queste proteine infatti, pur essendo state acquisite precocemente nell'evoluzione (già nei cianobatteri) e poi conservate fino alle gimnosperme, non sono presenti nelle angiosperme. In questo capitolo abbiamo quindi discusso quali possano essere le ragioni della perdita delle FLV nel corso dell'evoluzione. Una delle possibili spiegazioni a questo fatto è che un altro AEF abbia rimpiazzato la loro funzione. Le FLV sono fondamentali per rispondere ai cambi improvvisi di intensità luminosa che si verificano in ambienti naturali e le angiosperme utilizzano la via mediata da PGR5/PGRL1 per rispondere almeno in parte a queste fluttuazioni di luce. Per verificare la possibilità che la via PGR5/PGRL1 abbia rimpiazzato le FLV, nel lavoro presentato nel capitolo 3 è descritto l'isolamento linee di *P. patens* in cui sono stati rimossi i geni che codificano per PGRL1 e una delle proteine FLV. Grazie a questi mutanti abbiamo individuato una forte correlazione tra l'attività delle 2 vie specialmente quando questi sono stati cresciuti in condizioni di luce stressanti che possono mimare quelle dell'ambiente naturale. Il confronto tra il doppio mutante per le 2 vie e i singoli mutanti per ognuna di esse ha evidenziato che il ruolo principale delle FLV è quello di sostenere l'attività fotosintetica in condizioni di luce fluttuante e la via PGR5/PGRL1 può in parte compensare la loro perdita in *P. patens*, suggerendo una possibile sovrapposizione funzionale delle vie. Ulteriori analisi ci hanno permesso di stabilire che le FLV e PGRL1 sono fondamentali per proteggere il PSI dalle condizioni di stress luminoso, non solo dissipando gli elettroni in eccesso ma anche regolando il flusso stesso di questi a livello della membrana agendo sull'attività del Cyt b_6f.

Nel capitolo 4, mi sono focalizzato sulla caratterizzazione del complesso NDH-1 di *P. patens*. Il complesso NDH-1 è stato acquisito dalle alghe streptofite durante il processo di colonizzazione delle terre emerse da parte degli organismi fotosintetici eucarioti. Nonostante una parte funzionale comune che catalizza la funzione sia presente nella maggior parte delle piante terrestri, diverse subunità accessorie sono state acquisite nel corso dell'evoluzione. Ad esempio, 2 proteine antenna coinvolte nella formazione di un supracomplesso tra NDH-1 e il PSI che si ritrovano nelle angiosperme, non sono invece presenti nelle marcanzie, ma una di queste, LHCA5 è stata ritrovata nel genoma di *P. patens*. Nonostante diversi lavori cerchino di capire il ruolo di NDH-1 nelle piante, la sua funzione fisiologica primaria non è ancora del tutto chiara. Per risolvere questo quesito, nel capitolo 4 sono stati studiati mutanti di *P. patens* difettivi per la funzione del complesso NDH-1, ottenuti dalla rimozione sito-specifica di un gene codificante una proteina fondamentale per l'attività dello stesso. La caratterizzazione biochimica dell'apparato fotosintetico di *P. patens*, ha permesso di individuare un supracomplesso contenente NDH-1, ma non il PSI, suggerendo che LHCA5 da sola non è in grado di mediare una stabile interazione tra i due complessi. Il confronto tra l'attività fotosintetica del

mutante del complesso NDH-1 e le piante selvatiche non ha messo in luce grandi differenze, eccetto per un lieve difetto nella funzione del PSI nel momento in cui le piante sono sottoposte ad un trattamento luminoso ed al termine di quest'ultimo. Reiterando cicli di luce e buio, il difetto osservato aumentava significativamente ad ogni ciclo, suggerendo che il complesso NDH-1 possa essere importante nell'innescare l'attività fotosintetica dopo un periodo di buio o durante lo stesso. Tuttavia, crescendo le piante mutanti nelle stesse condizioni di luminosità non sono stati riscontrati difetti nella crescita o foto-inibizione, lasciando aperta l'ipotesi che l'induzione di altri meccanismi di trasporto presenti nel cloroplasto possa aver compensato il difetto osservato nel breve tempo.

La possibile interazione tra il complesso NDH-1 e gli altri AEF è stata quindi ricercata nel capitolo 5, grazie ad un'analisi comparata di piante mutanti per una o più vie. Per questo motivo sono stati isolati un doppio mutante di *P. patens* difettivo delle 2 vie di CEF (*pgrl1-ndhm* KO) e un triplo mutante difettivo sia del ciclico che della via mediata dalle proteine FLV (*flva-pgrl1-ndhm* KO). Tutte le piante utilizzate per il confronto sono state coltivate in diversi regimi luminosi, analizzando il tasso di crescita e l'efficienza fotosintetica. Sia il doppio che il triplo mutante hanno mostrato un grosso fenotipo di crescita più evidente all'aumentare dell'intensità luminosa applicata. Mentre solo *flva-pgrl1-ndhm* ma non *pgl1-ndhm* KO ha mostrato una maggiore sensibilità alla luce fluttuante rispetto i ceppi parentali, evidenziando ancora una volta il ruolo delle proteine FLV in questa condizione. Come nel capitolo 3, i mutanti multipli hanno evidenziato un effetto sinergico tra i AEF, non solo durante uno stress luminoso ma anche in condizioni ottimali per la crescita. Analisi spettroscopiche e misure di evoluzione di ossigeno hanno rivelato che *flva-pgrl1-ndhm* KO è in grado di trasportare meno della metà degli elettroni rispetto i muschi selvatici, spiegando così la scarsa crescita. Altre analisi spettroscopiche e biochimiche hanno inoltre evidenziato che questo scarso flusso degli elettroni è correlato a notevoli danni a carico del PSI. I AEF non solo sono importanti per regolare la fotosintesi in condizioni di stress luminoso, ma sono anche fondamentali per sostenere il normale LEF proteggendo le proteine coinvolte nel processo. Inoltre, quando questi sono rimossi uno ad uno, non si sono evidenziate grandi differenze rispetto le piante selvatiche tranne che in particolari condizioni, specifiche per un determinato meccanismo. Tuttavia, quando questi vengono a mancare contemporaneamente, grossi difetti fotosintetici sono presenti, sottolineando una ridondanza funzionale nell'azione dei AEF.

Tutti i AEF considerati competono con la FNR per l'utilizzo di Fd e NADPH, questo enzima infatti trasferisce elettroni da Fd ridotta a $NADP^+$. Esiste quindi la possibilità che i AEF e la FNR possano interagire, influenzandosi a vicenda durante l'attività fotosintetica. In appendice 1 abbiamo analizzato le diverse isoforme della proteina FNR presenti in *P. patens* con la prospettiva di capire il loro ruolo

nella regolazione fotosintetica. In questo muschio sono presenti 2 isoforme per questa proteina, entrambe simili, a livello di sequenza, alle FNR della radice delle piante vascolari. Nonostante ciò, le 2 isoforme sono espresse differenziale in tessuti fotosintetici ed eterotrofi. Inoltre, in *P. patens* l'enzima FNR sembra essere scarsamente legato alle membrane se confrontato con le angiosperme, questo potrebbe essere dovuto all'assenza nel genoma di questo muschio dei geni codificanti le proteine coinvolte nell'ancoraggio della FNR alla membrana.

Un altro aspetto interessante riguardo l'evoluzione delle piante terrestri è l'acquisizione della tolleranza alla de/reidratazione. In appendice 2 abbiamo studiato la propagazione dei segnali calcio dopo la percezione di uno stress idrico, utilizzando il sensore Cameleon YC3.60 geneticamente codificato dal genoma di *P. patens*. Abbiamo rivelato la presenza di segnali sistemici che iniziano alla base della pianta e si propagano fino alla punta dei filloidi, quando essa viene sottoposta ad uno stress osmotico. Il segnale che abbiamo misurato è molto lento rispetto quello visto nelle piante vascolari e fa pensare ad un meccanismo di trasmissione da una cellula ad un'altra adiacente.

CHAPTER 1

INTRODUCTION

1.1 OXYGENIC PHOTOSYNTHESIS

Oxygenic photosynthesis is at the base of life on our planet and it allows plants, algae and cyanobacteria to convert sunlight into chemical energy available for the metabolism. In Eukaryotes the entire process takes place in specific organelles, the chloroplasts, separated by the envelope. Chloroplast contains the thylakoids, another membrane system, which divides the inner space (lumen) from the outer space (stroma) (Figure 1). Thylakoids constitute a three-dimensional network organized in stacked membrane regions (grana) connected by non-appressed regions (stroma lamellae). Photosynthetic process can be divided in two phases, named "light" and "dark" phase. The light phase takes place at the level of thylakoid membranes and exploits sunlight to produce ATP and NADPH.

$$NADP^+ + 2\ H_2O + 1.3\ ADP + 1.3\ P_i + light \rightarrow NADPH + O_2 + 2\ H^+ + 1.3\ ATP$$

Light reactions depend on the presence of four major complexes embedded in the thylakoid membrane: Photosystem II (PSII), Photosystem I (PSI), cytochrome *b6/f* (Cyt b_6f) and ATP synthase (ATPase) (Figure 1).

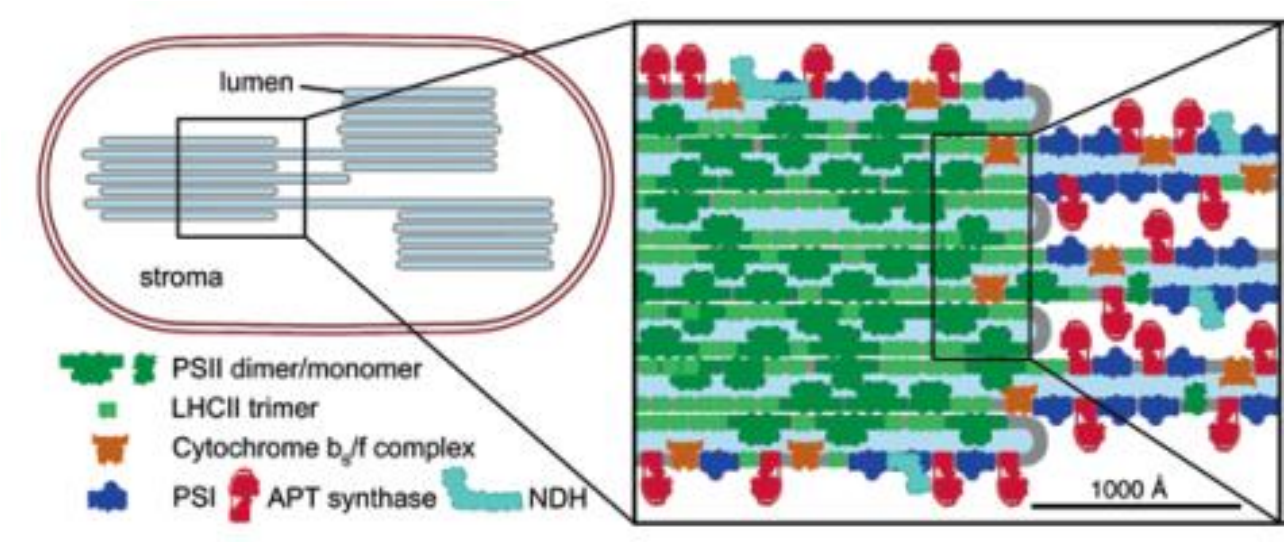

Figure 1 Chloroplasts contain thylakoid membranes which divide the stroma from the lumen. Thylakoid membranes are organized in stacked regions called grana and non-appressed regions, the stroma lamellae. The complexes involved in oxygenic photosynthesis are not homogeneously distributed in the thylakoids, PSII and LHCII antennae are located in grana regions, while PSI and ATP synthase are found exclusively in stroma lamellae or in grana margins (Kouřil et al. 2018).

Photosynthetic pigments, chlorophylls (Chl) and carotenoids (Car), allow the harvesting of solar radiation. After light absorption, excited electrons in these pigments can decay through rapid transfer of energy to another molecule. In thylakoid membranes, pigments are bounded to specific antenna proteins called LHC (light harvesting complexes). These proteins when associated to photosystems coordinate the rapid transfer of solar energy from a pigment to another until it reaches the photosystem reaction center (RC) to fuel a charge separation event. Alternatively pigments excited state can decay by dissipating the absorbed energy in form of fluorescence or heat.

Light reactions start at the level of grana localized PSII. Three of the subunits of the complex core, D1, D2 and Cyt b_{559} coordinate the molecules involved in the charge separation reaction: a special Chl a pair (P_{680}), another Chl a molecule termed Chl_{D1}, pheophytin (Phe) and the acceptors, plastoquinone A and B (PQ_A and PQ_B). Excited P_{680} donates an electron to Chl_{D1} which in turn passes it to Phe. Reduced Phe donates one electron to PQ_A tightly bound to the RC and in turns reduces the secondary plastoquinone PQ_B (Figure 2).

$$P_{680}^* \rightarrow P680^+Chl_{D1}^- \rightarrow Chl_{D1}Phe^- \rightarrow PheQ_A^-Q_B \rightarrow PheQ_AQ_B^-$$

When a second electron reduces PQ_B^- it becomes protonated into plastoquinol (PQH_2) by two H^+ from stroma (H^+_{out}). In its reduced form PQH_2 is hydrophobic and can diffuse in the membrane. Once P_{680} undergoes charge separation it became oxidized (P_{680}^+) and needs one electron to recover neutrality. This is possible thanks to the activity of the Oxygen Evolving Complex (OEC). OEC splits a water molecule releasing O_2 and H^+ (H^+_{in}) on the lumenal side of the thylakoid membrane (Figure 2). The net result of the light dependent water splitting at the level of PSII is:

$$H_2O + PQ + 2H^+_{out} \rightarrow ½\ O_2 + PQH_2 + 2H^+_{in}$$

PSII activity thus results in the reduction of PQH_2 but also generates an electrochemical gradient thanks to H^+ liberation in the lumen (H^+_{in}) and their consumption on the stromal side of thylakoid membrane (H^+_{out}).

Cyt b_6f serves as interconnection between PSII and PSI, transferring electrons from PQH_2 to water soluble Plastocyanin (Pc) the primary donor of PSI. Cyt b_6f is considered also the rate limiting step of electron transport chain under strong illumination, since the rate of oxidation of PQH_2 is much slower than Pc oxidation by PSI (Kirchhoff 2014). Cyt b_6f is organized in a functional dimer, each monomer consists of four subunits: the iron-sulfur protein Rieske, Cyt b_6, Cyt f and the subunit IV. Catalytic function is provided by four redox centers: an iron-sulfur cluster, two hemes of $Cytb_6$ and one heme f. Cyt b_6f contains 2 PQ binding sites: the Q_o (quinol oxidase) in the Rieske protein with higher affinity for PQH_2 and the Q_i (quinone reductase) located in the stroma side of the complex

(Yamashita, Zhang, and Cramer 2007). Oxidation of PQH_2 at Q_o site releases two H^+ in the lumen increasing the ΔpH. The two electrons dissociated by PQH_2 oxidation are bifurcated in two different chain according to the Q-cycle mechanisms (Figure 2, Mitchell 1976). One electron is transferred to Pc through the high potential chain (PQH_2 → Rieske → Cyt f → Pc), the other is directed to PQ in the Q_i-site mean the low potential chain (PQH_2 → b_6^L → b_6^H → PQ). Every two successive steps of PQ reduction, two protons are taken from the stroma to regenerate PQH_2. The net products of the Q-cycle are thus 2 reduced Pc, 4 H^+ pumped in the lumen (4 H^+_{in}), 2 H^+ consumed in the stroma and 1 PQH_2 regenerate each 2 PQH_2 molecules oxidized.

Pc reduced by $Cytb_6f$ fast diffuses through the lumen to PSI (P_{700}^+) which catalyzes its oxidation, transferring the electron to the Fd (ferredoxin) located in the stroma. PSI complex is constituted by a monomeric core of 14 polypeptides, PsaA and PsaB proteins coordinate two Chl a which constitute the primary electron donor (P_{700}). Steric extrusion of the complex precludes its insertion in grana stacks, so PSI is exclusively present in non-appressed region (lamellae and grana margins). Light induces charge separation of P_{700} which becomes oxidized donating an electron to its primary acceptor (another Chl molecules). The electron chain consists of other 2 molecules of Chl beside P_{700}, 1 phylloquinone (A1) and 3 $[FeS]_4$ clusters which donates electron to Fd (Figure 2, P700→ Chl_1→Chl_2→Chl_3 →A_1→F_X→F_A→F_B→Fd). Finally, electrons are transferred from reduced Fd to $NADP^+$ via FNR (Ferredoxin-NADPH reductase), 2 reduced Fd must be oxidized to synthesize one NADPH molecule then used by CBB cycle.

The described linear flow of the electrons (LEF) which involve PSII, $Cytb_6f$ and PSI, overall results in the oxidation of 2 H_2O molecules, the synthesis of 1 molecules of NADPH and the pumping of 6 H^+ in the lumen.

$$2H_2O + NADP^+ + 2H^+_{out} + h\nu \rightarrow NADPH + 6\ H^+_{in}$$

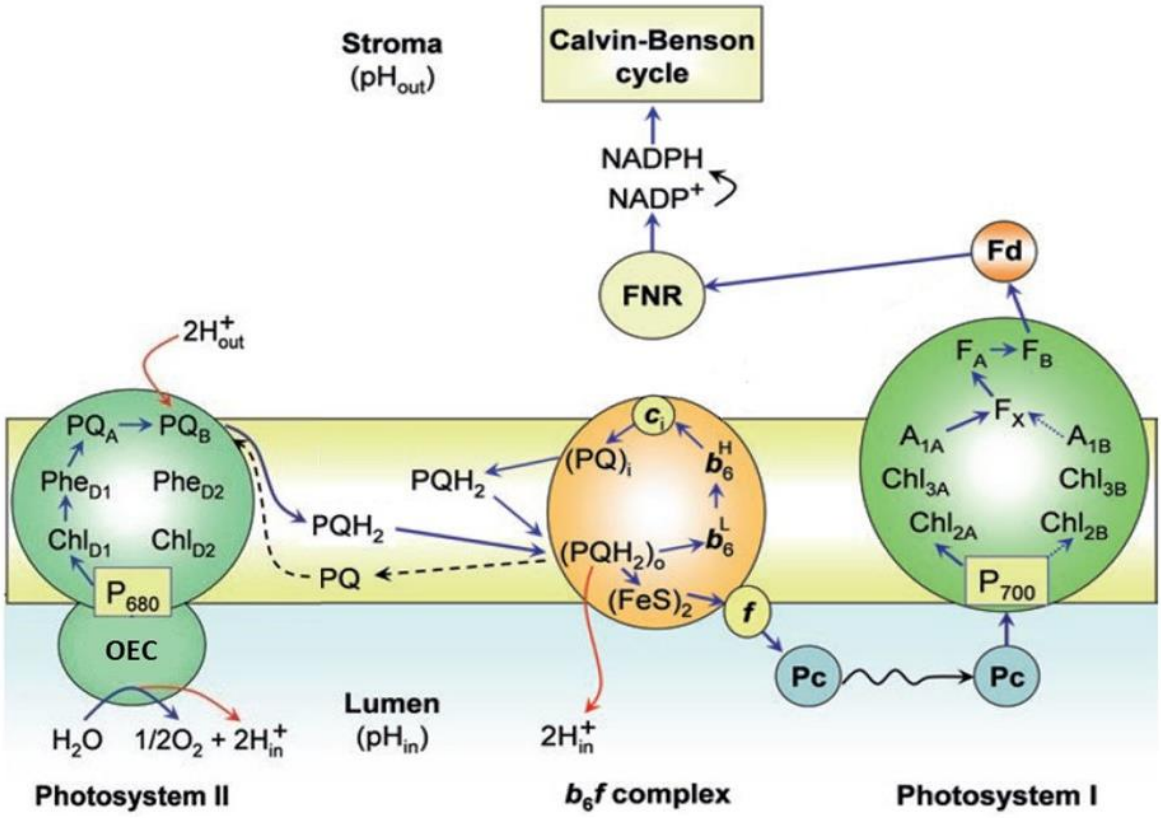

Figure 2 Scheme of photosynthetic Linear Electron Flow (LEF). Electrons donated from H_2O are energized by light reactions in PSII. The electrons are then transferred to the membrane-soluble carrier PQ, which is oxidized by Cyt b_6f and in turn transfers the electrons the water-soluble PC. PC is the electron donor of PSI; the latter energizes again the electrons using solar energy to transfer them to Fd. Finally, FNR transfers electrons from Fd to NADPH which feeds the cbb Cycle. Together with this electron transfer protons are released in the lumen at the level of OEC and Cyt b_6f complex. Adapted from (Tikhonov 2018).

During LEF the H^+ released in the lumen by OEC and Cytb_6f lead to a generation of a trans-thylakoid potential, also called proton motive force (pmf), including an electric ($\Delta\Psi$) and chemical (ΔpH) component, that represents the driving force for operation of chloroplast ATPase. The fourth major photosynthetic complex, ATPase, thus exploits pmf generated by LEF for ATP synthesis. ATPase as well as PSI is exclusively located in stroma lamellae. It is composed by 26 subunits which constitute the hydrophilic head (cF_1) involved in catalytic ATP synthesis and a membrane rotary motor (cF_0). cF_0 presents two hydrophilic channel spanning the membrane, which allow the dissipation of pmf to sustain catalytic activity (Hahn et al. 2018).

The products of LEF are finally consumed by the dark phase which takes place in the stroma, where the CBB cycle consumes ATP and NADPH to fix CO_2 in organic compounds:

$$6\ NADPH + 9\ ATP + 3\ CO_2 \rightarrow 6\ NADP^+ + 9\ ADP + G3P\ (Glyceraldehyde\ 3\text{-}phosphate)$$

1.2 PHOTOSYNTHETIC REGULATORY MECHANISMS

Environmental conditions are highly dynamic and variable illumination, temperature, water and gas availability can easily lead to overreduction of electron transport chain, limiting photosynthetic efficiency. In these conditions several reactive oxygen species (ROS) can be generated and contribute to damage photosynthetic machinery and further decrease its efficiency (Krieger-Liszkay 2005). ROS are produced both at the level of PSII, where the exited chlorophylls (Chl) can react with molecular oxygen, and PSI RC which directly reacts with O_2 when stromal acceptors are not available. Photosynthetic organisms thus need to continuously regulate light harvesting and electron transport to avoid the mentioned oxidative damage.

Mechanisms for Regulation of light harvesting

One important group of photosynthetic regulatory mechanisms modulates light harvesting efficiency, thus the plant ability to harvest light and use it for photochemistry. The fastest mechanisms, called Non-Photochemical Quenching (NPQ) consists in thermal dissipation of excess light energy through the de-excitation of excited chl molecules. NPQ involves different component distinguished from their activation kinetics. The fastest and largest component qE (Energy-dependent quenching) is activated and relaxed in a few seconds, while the slower qI (inhibitory quenching) recovers instead in hour time-scale. One intermediate component is instead correlated with zeaxanthin accumulation (qZ, see below) and it relaxes in minute time-scale (Müller, Li, and Niyogi 2001). In microalgae the main trigger for NPQ are LHCSR (LHC Stress-Related, Peers et al. 2009) proteins while in higher plants PSBS is responsible for qE activation.

LHCSR are antenna proteins but they show the specific ability to dissipate excitation energy as heat upon protonation of C-terminal residues (Liguori et al. 2013). In *Chlamydomonas reinhardtii*, LHCSR proteins bind both chlorophylls and carotenoids (lutein, violaxanthin) and when excited show short chl fluorescence lifetime, indicating that they can quench energy very efficiently (Bonente et al. 2011). PSBS protein is instead responsible for qE activation in vascular plants (X P Li et al. 2000). PSBS is a four-helix integral membrane protein which does not bind pigments (Fan et al. 2015). Two luminal-exposed glutamate residues in PSBS are protonated upon pH decrease (X P Li et al. 2004), leading to a conformational change which reorganizes the photosynthetic apparatus and activates NPQ.

Another protection mechanism conserved in most unicellular algae and higher plants depends from xanthophyll cycle (K. Niyogi, Bjorkman, and Grossman 1997). A key enzyme of this cycle is violaxanthin de-epoxidase (VDE, Arnoux et al. 2009), which is located in the lumen and upon pH decrease catalyzes the conversion of violaxanthin into zeaxanthin. The latter is a pigment with a central role in photoprotection in chloroplasts, since it is involved in ROS scavenging and excited chlorophyll quenching. Zeaxanthin is rapidly accumulated upon light illumination, but its reconversion in violaxanthin takes several minutes. All the mechanisms responsible of qE and qZ are triggered by lumenal acidification during electron transfer (see section 1, Figure 6). The activation of electron transport is thus fundamental to induce NPQ and activate energy dissipation in conditions in which light is in excess with respect to electron transport chain capacity.

Another mechanism for light harvesting regulation is the state transition, where LHCII are moved between PSII and PSI. This mechanism is triggered by electron transfer at the level of Cyt b_6f, where the binding of PQH_2 to Q_o subunits serves as a signal for the activation of a kinase (STN7 kinase, Bellaflore et al. 2005), which phosphorylates LHCII. Phosphorylated LHCII move from PSII to PSI in a conformation called "State II". LHCII can then be dephosphorylated (TAP38/PPH1, Pribil et al. 2010; Shapiguzov et al. 2010) and return to initial conformation "State I". During photosynthetic activity "State II" conformation alleviates the PQ pool reduction, limiting the light absorbed from PSII and allowing PSI to dissipate excess electrons thanks to its increased light harvesting capacity. Thus, state transition allows light absorption optimization between PSI and PSII (Wollman 2001).

Regulation of electron transport: Photosynthetic control

Another important mechanism to avoid photoinhibition is the "photosynthetic control" through Cyt b_6f regulation. Cyt b_6f exerts the photosynthetic control by controlling the rate of reduction of Pc (Kirchhoff 2014) so the amount of PSI electron donors (see section 1). When PSI is limited by the availability of stromal acceptors, electrons in excess can directly react with oxygen or react with the Iron Sulphur clusters of the complex, leading to photodamage. In order to avoid PSI over-reduction Cyt b_6f activity is regulated, again in response to lumenal acidification (Nishio and Whitmarsh 1993; Rumberg and Smgel 1968)(Figure 6) which decreases Q_o binding affinity for PQH_2. In case of intense illumination, thus, the decrease in luminal pH causes a reduction in electron transfer from PQH_2 to Pc. This regulation was shown to be important for PSI protection from excessive light (Joliot and Johnson 2011; Suorsa et al. 2015).

Regulation of Electron transport: Cyclic Electron Flow

Theoretical calculations on light phase of photosynthesis estimate that 3 H^+ are released in the lumen per each transported electron. Assuming that ATP synthesis requires 4.7 H^+ per molecules, it derives that every 4 electrons transported 2 molecules of NADPH and 2.6 molecules of ATP (corresponding to 12 H^+) are produced with a ratio ATP:NADPH of 1.3. Fixation of 1 molecule of CO_2 by CBB cycle requires 3 ATP and 2 NADPH (ratio 1.5) with thus a shortfall of ATP supply, which would lead to a slowdown of photosynthesis at the level of final acceptors. Based on LEF and CBB cycle stochiometric calculation, Arnon and Chain (Arnon and Chain 1975) first postulated a mechanism called cyclic electron flow (CEF) able to reinject electrons stored in PSI acceptors into membrane transporters at level of PQH_2 or Cyt b_6f. Doing this, CEF would prevent formation of NADPH recycling electrons to the membrane forming PQH_2, moreover the re-oxidation of PQH_2 at the level of Q-cycle leads to further proton gradient formation. So CEF would increase ATP:NADPH ratio to satisfy CBB cycle demand. Moreover, proton pumping CEF dependent activity possibly triggers those mechanisms dependent on lumenal pH for their activation, such as photosynthetic control and NPQ, influencing also membrane transport rate (Figure 6). Up to now two major routes of CEF have been described and mediated respectively by Proton Gradient Regulator 5/PGR5-Like 1 (PGR5/PGRL1) proteins and by a multi-subunit complex named NDH-1 (NADH De-Hydrogenase like 1). CEF is not the only way to increase ATP:NADPH ratio but other mechanisms such as pseudo-CEF can lead to electron dissipation preventing NADPH formation but still allowing ATP synthesis by the electron transfer in the membrane.

CEF mediated by PGR5/PGRL1

PGR5 was first identified by forward genetic approach in *A. thaliana* as a protein affecting proton gradient across the thylakoid membranes (Munekage et al. 2002). *pgr5* mutant showed defective NPQ induction, underlining the role of PGR5 in proton pumping through Cyt b_6f. Moreover, *in vitro* assays on ruptured chloroplast highlighted that *pgr5* had lower ability to reduce PQ pool and its behavior was affected by antimycin A (Figure 3)(Munekage et al. 2002), for this reason the CEF mediated by PGR5 was called “antimycin-sensitive”. Antimycin A binding site was also localized in PGR5 protein, although this is not conserved in all photosynthetic organisms (Sugimoto et al. 2013). Another protein, PGRL1 was then found to hold a role similar to PGR5 and *A. thaliana pgrl1* mutants

do not accumulate PGR5 (DalCorso et al. 2008), suggesting that the two proteins form a complex cooperating in the same pathway. *PGR5* and *PGRL1* genes are present in most of green algae and higher plants genome but only *PGR5* is also found in cyanobacteria indicating that this pathway is widespread in eukaryotic photosynthetic organisms (Peltier et al. 2010). PGR5/PGRL1 CEF mechanisms is still not fully elucidated and the exact components of the pathway have not been found. It has been proposed that the pathway acts as an FQR (ferredoxin-plastoquinone-reductase) able to transfer electrons from Fd to PQ, or alternatively directly to Cyt b_6f complex. The first hypothesis is sustained by the fact that recombinant PGRL1 is able to reduce PQ analogue *in vitro* (Hertle et al. 2013), while the latter hypothesis is supported by the finding that PGRL1 can form a PSI-type membrane supercomplex including also Cyt b_6f in *C. reinhardtii* (Iwai et al. 2010).

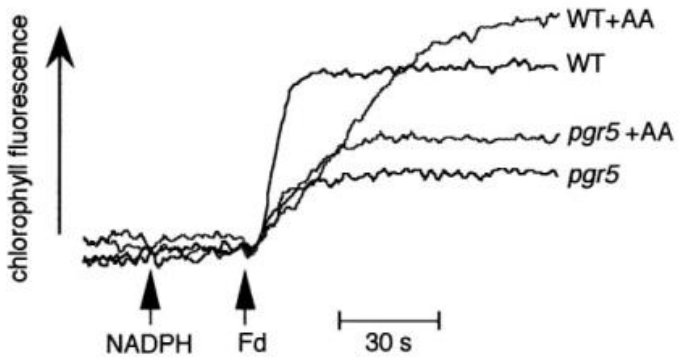

Figure 3: Induction od chlorophyll fluorescence rise by addition of Fd and NADPH. AA (Antimycin) decrease fluorescence rise velocity in WT chloroplast, while addiction of AA on *pgr5* chloroplast does not affect chlorophyll fluorescence (Munekage et al. 2002).

PGR5/PGRL1 pathway sustains pmf formation (C. Wang, Yamamoto, and Shikanai 2015), and thus contributes to NPQ activation *in vivo* (Munekage et al. 2002), thus it is fundamental to rapidly respond to increases in light intensity and protect photosynthetic apparatus. However its main role seems to prevent accumulation of electrons in the stroma acceptor pool, thus avoiding PSI overreduction in saturating light condition (Munekage et al. 2002). The control of redox state of PSI is also crucial in fluctuating light condition, since CBB cycle contribution in consuming NADPH produced by LEF is not continuous and PSI acceptors can easily become limiting. In this contest the activity of alternative pathways are fundamental and indeed in fluctuating light *pgr5* mutants of *A. thaliana* showed a lethal phenotype (Suorsa et al. 2012) and preferential damage to PSI (Kono, Noguchi, and Terashima 2014; Suorsa et al. 2012). It was also proposed that PGR5/PGRL1 can control linear electron transport rate through photosynthetic control, rather than only act at PSI acceptor side (Suorsa et al. 2016).

CEF mediated by NDH-1 complex

A second CEF pathway identified in plant is mediated by NDH-1 (NADH DeHydorgenase-like1) complex. NDH-1 complex was first identified thanks to *N. tabacum* chloroplast genome sequencing, which revealed 11 genes coding subunits sharing sequence homology with respiratory complex I of bacteria and mitochondria (Shinozaki et al. 1986). In cyanobacteria complex I is involved in control of PQ redox poise (Mi et al. 2001) and CEF (Ohkawa, Pakrasi, and Ogawa 2000). Battchikova, Eisenhut, and Aro reviewed that in *Synechocystis 6803* complex I can function in respiration, CO_2 concentration and CEF when different accessory subunits are bounded to the same core of the complex. The multifunctionality of complex I present in cyanobacteria was lost in eukaryotic organisms which kept the distinct functions separated (e.g. respiration and photosynthesis) in distinct cellular sub-compartment.

Structure of NDH-1 complex

Chloroplast NDH-1 is a large multi-protein complex that counts more than 30 subunits. Its shares a conserved L-shaped structure with respiratory complex I and its topology could be subdivided in 5 minor subcomplexes in angiosperms: membrane subcomplex (M), subcomplex A, lumenal subcomplex (L), electron donor-binding (EDB) subcomplex and subcomplex B (Figure 4). The membrane subcomplex is embedded in the thylakoid membrane, it is homolog of the proton pumping P module of respiratory complex I and is composed by proteins (Figure 4) encoded by plastid genome (Ifuku et al. 2011). The subcomplex A, located in the stroma side of the membrane, is composed of 7 subunits encoded by both nuclear and plastidial genomes. Plastidial encoded subunits of subcomplex A are homologue to the Q module of respiratory complex I that serves as an electron transporter. While the nuclear encoded genes of Subcomplex A have no homologous to complex I but their presence is fundamental for the NDH-1 activity (Rumeau et al. 2005). The subcomplex A is not essential for the stability of the whole NDH-1 complex, that is detectable even in its absence (Peng, Shimizu, and Shikanai 2008).

Respiratory complex I also includes a N module involved in NADH binding, that is not present in NDH-1 complex and apparently it has been replaced by the EDB domain constituted by nuclear encoded proteins (Yamamoto et al. 2011). The latter stabilizes subcomplex A and is involved in Fd binding (Yamamoto et al. 2011). The subcomplex B is important for the stability of the entire complex

but its role is still not clear (Peng et al. 2009). Nuclear encoded subunits of subcomplex B are present in *Marchantia* and *Physcomitrella* genomes but not in cyanobacteria, subcomplex B is thus considered to be incorporated in NDH-1 during early phase of land plant evolution. Finally, the lumenal subcomplex accounts 5 nuclear encoded subunits in *Arabidopsis* while only 1 was detected in *Marchantia*. Notably in *Arabidopsis* subcomplex A stability is affected by lumenal subcomplex impairment (Peng et al. 2009) while this is obviously not true for cyanobacteria where the subcomplex is not present.

In angiosperms NDH-1 interacts with PSI by two antenna proteins LHCA5 and LHCA6 to form a NDH-1-PSI supercomplex (Kouril et al. 2014; Peng et al. 2009) constituted of 2 PSI docked at 2 different sides of NDH-1 (Kouril et al. 2014). In *Marchantia* which lacks LHCA5 and LHCA6 the PSI-NDH1 protein was not detected, suggesting that the acquisition of this antennae was seminal to the formation of this structure (Ueda et al. 2012). It was also proposed that the subunits of lumenal subcomplex, also absent in non-vascular plants, were acquired to stabilize the interaction of NDH-1 to PSI through the 2 antennae.

In addition to subunits composing NDH-1 complex many other genes has been identified to lead to defects in NDH-1 functionality, these were named *chlororespiratory reduction* (*crr,* Hashimoto et al. 2003). A group of these genes are involved in editing of plastid-encoded *ndh-1* genes (Kotera, Tasaka, and Shikanai 2005), while others seem to be important for the accumulation and correct assembly of chloroplast NDH-1 complex (reviewed in Kato, Sugimoto, and Shikanai 2017).

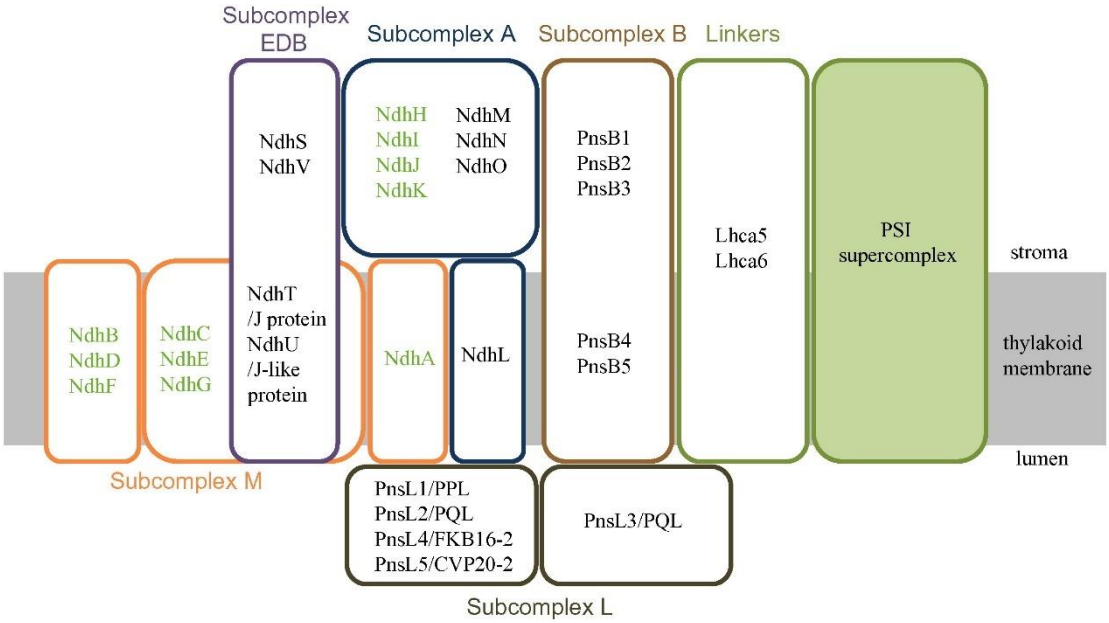

Figure 4. Schematic representation of NDH-1 complex in angiosperms. The complex is composed by 5 subcomplexs (EDB, M, A, B, L) and is associate to PSI thanks to 2 antenna proteins acting as linkers. The protein which constitute NDH-1 complex can be coded both by nuclear (black letters) or chloroplast (green letters) genomes (Shikanai 2016a).

Physiological role of NDH-1 complex in vascular plant

Several mutants partially or completely defective for NDH-1 activity were isolated and analyzed in the past years in tobacco, rice, *Arabidopsis* and *Marchantia* (T Shikanai et al. 1998; Rumeau et al. 2005; Ueda et al. 2012; Yamori et al. 2011; Grossman et al. 2003; Martin et al. 2015; P. Wang et al. 2006; Nashilevitz et al. 2010; Nellaepalli et al. 2012; Munekage et al. 2004), all sharing common features. These works showed that in WT plants exposed to low light irradiation, chlorophyll florescence transiently increase after light is switch off. The same is not true for NDH-1 defective mutants which showed no increase or lower increase in chlorophyll fluorescence after actinic light switch off (Figure 5A). This effect is thought to be due to a transient reduction of PQ by NDH-1 complex, that leads to an increase of chlorophyll fluorescence because of a partial saturation of PSII acceptors (Maxwell and Johnson 2000).

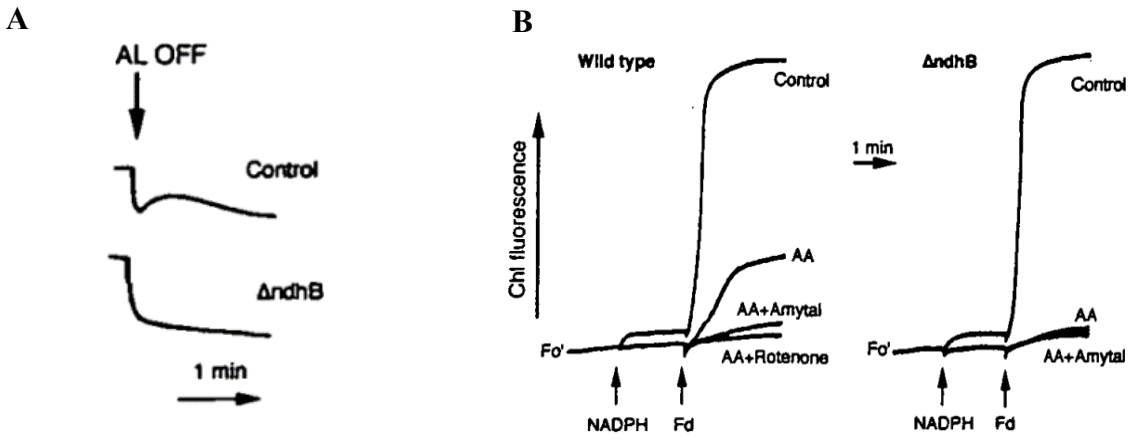

Figure 5 NDH-1 complex activity (adapted from endo et al. 1998). A) transient increase of chlorophyll fluorescence after AL switch off, WT (Control) shows an increase in chlorophyll fluorescence while *ndhb* mutant have little or none chlorophyll rise upon AL switch off. B) addiction of Fd to isolated *Arabidopsis* chloroplast induces a chlorophyll florescence rise, AA only decreases PQ reduction activity in WT thylakoids while completely deletes it in *ndhb* mutant thylakoids which have no NDH-1 residual activity.

It was demonstrated (Endo et al. 1998) that NDH-1 dependent PQ reduction *in vitro* is strictly dependent by the addition of reduced Fd, suggesting that the latter is the electron donor rather than NADPH (Figure 5B). Fd binding was also proposed to occur through Ndh-S subunit located in the lumenal EDB (Electron Binding Domain) subcomplex (Yamamoto et al. 2011). Strictly speaking, NDH-1 complex is not an NADH dehydrogenase as suggested by its name, but rather a Fd-dependent PQ reductase.

Since the complex includes a P-module-like domain (subcomplex A), it has been proposed that NDH-1 can pump 4 H^+ in the lumen in addition to the 4 H^+ translocated from the Q cycle in Cyt b_6f so contributing with the translocation of 8 H^+ for every 2 electrons transported, in contrast antimycin-sensitive pathway that depends solely on Q cycle to generate ΔpH (Toshiharu Shikanai 2016b). Despite the role of NDH-1 in photosynthetic membrane has been shown, is still not clear how relevant NDH-1 activity is *in vivo* for plant viability. Indeed, mutants lacking NDH-1 activity in several plant species rarely show any detectable photosynthetic or growth defect, even if this complex seems to be more important in C4 respect to C3 photosynthetic metabolism (Ishikawa et al. 2016). NDH-1 defective plants were shown to have a small reduction of photosynthetic efficiency at low light intensity (Ueda et al. 2012; Yamori et al. 2011; Ishikawa, Endo, and Sato 2008), in fluctuating light conditions (Yamori, Makino, and Shikanai 2016; Martin et al. 2015) and under chilling and warming condition (Q. Li, Yao, and Mi 2016; X. Li et al. 2004). An increase in NDH-1 activity was also observed in salt stress (He et al. 2015) and in mutants of sugar catabolism (Strand et al. 2015). All these phenotypes were nevertheless mild.

The importance of NDH-1 complexes was revealed only in absence of antimycin-sensitive CEF pathway where NDH-1 inactivation causes a major phenotype (Munekage et al. 2004). Indeed the double mutant showed a much larger defect in electron transport rate capacity compared to the two single mutants depleted respectively in PGR5 and NHD-1 activity (Munekage et al. 2004). This suggests that the 2 pathways can compensate each other activity by their overlapping function.

NDH-1 role in the evolution of photosynthetic organisms

While chlororespiratory function of NDH-1 first evolved in cyanobacteria (Battchikova, Eisenhut, and Aro 2011), in several microalgal plastidial genomes analyzed NDH-1 genes are absent (De Cambiaire et al. 2006; Pombert, Lemieux, and Turmel 2006; Wakasugi et al. 1997) with the only exception of Prasinophyceae in which some species conserve genes coding NDH-1 subunits (Turmel et al. 2009). In *C. reinhardtii* CEF function was shown to be mediated by another type of dehydrogenase called Nda2 which belong to type II NADH-dehydrogenase (Jans et al. 2008). NDH-1 is present in lower and higher branching streptophyte algae, the algae that latest diverged from plants ancestors (Turmel, Otis, and Lemieux 2006,reviewed by Vries et al. 2016). These evidences suggest that NDH-1 complexes could have played a role during land colonization process (Vries et al. 2016; Martín and Sabater 2010). During the evolution of seed plants other NDH-1 related genes

were acquired, these include transcription factors, RNA editing proteins, assembly factors, and antennae involved in NDH-1 coordination. The evolutionary history of NDH-1 complex is still not fully understood, the comprehension of its physiological role in eukaryotic organisms could clarify its role during the adaptation of photosynthesis to land environment.

Mehler reaction

The LEF from PSI to Fd and $NADP^+$ is the preferential route when CO_2 is available for carbon fixation and thus electrons are not in excess respect to the acceptor capacity. However, in some conditions such as carbon limitation or stressful light regimes LEF is not able to use all available excited electrons and other reactions become relevant. One of these is the formation of a superoxide anion (O_2^-) through an electron donated to molecular oxygen (O_2) from PSI. Superoxide anion is then converted to H_2O_2 and finally to water by superoxide dismutase and ascorbate peroxidase, the so called Mehler reaction (Mehler 1951; Mehler and Brown 1952). Mehler reaction has been termed also water-water cycle, or pseudo-CEF (PCEF)(Kozi Asada 1999; K. Asada 2000) because it uses electron derived from water splitting by PSII subsequently flow through PSI to regenerate water. The net result of the reaction is the formation of proton gradient, which leads to ATP synthesis without the production of NADPH, so contributing to increase the ATP/NADPH ratio available for the metabolism. Proton gradient derives from the water splitting in the OEC, at level o Q cycle and the oxygen reduction, the first 2 reactions increase the number of H^+ in the lumen while the last consumes H^+ present in the stroma.

However the main function of Mehler reaction is scavenge and detoxify ROS, which are harmful molecules but can also function as signal molecules inducing transcription of genes and activation of other pathways involved in photosynthetic regulatory mechanisms (Foyer and Noctor 2009).

Flavodiiron proteins

Flavodiiron proteins (FLVs or FDPs) are a large class of enzymes conserved in bacteria, protozoa and archaea (Wasserfallen et al. 1998). All FLVs have two conserved domains: a N-terminal metallo-β-lactamase-like domain and a C-terminal flavodoxin-like domain (Goncalves et al. 2011; Vicente et al. 2008). The first can reduce O_2 or NO coordinated by a diiron center, while the second contains a

flavin mononucleotide (FMN) moiety. FLVs are grouped in 5 classes based on an additional C-terminal extension they can harbor (Vicente et al. 2008). Class C FLVs are specific for photosynthetic organisms (Allahverdiyeva et al. 2015) and carry an additional flavin reductase-like domain. This domain was shown *in vitro* to allow direct oxidation of NADPH, which serves as electron donor for O_2 reduction to H_2O without ROS production (Vicente et al. 2002). In this thesis FLVs will be referred to class C FLVs involved in photosynthetic process. In cyanobacteria *FLV* genes are grouped in two clusters, one with *FLV1* and *FLV2* while the other with *FLV3* and *FLV4*. Moreover, the pairs composed by FLV1-3 or FLV2-4 are functionally related (Zhang et al. 2009). Indeed FLV2-4 heterodimer was found (Zhang et al. 2012) and despite there are no biochemical evidences for FLV1-3 heterodimerization, analysis of single KO mutants suggests that the proteins interact to exert their role (Yagut Allahverdiyeva et al. 2011).

FLV1-3 are involved in Mehler like reaction thus allowing PCEF (Allahverdiyeva et al. 2013; Allahverdiyeva et al. 2011; Helman et al. 2003; Helman et al. 2005). This process allows dissipation of excess electrons coming from PSI and reducing O_2 to water instead of O_2^-, the lack of ROS production in cyanobacteria is crucial since they are very sensitive to these molecules (Drábková et al. 2007; Matthijs et al. 2012). At difference from Mehler reaction, FLV mediated electron flow to O_2 in some conditions is a substantial fraction and can vary 15% to 40% of gross oxygen evolution (Helman et al. 2003; Helman et al. 2005; Yagut Allahverdiyeva et al. 2011). Despite the considerable amount of electrons transported by FLV1-3, mutants for these proteins did not show any sensitivity even in high light condition (Zhang et al. 2009; Helman et al. 2003; Allahverdiyeva et al. 2011; Allahverdiyeva et al. 2013). FLV1-3 seem to be more active after long time dark exposure, supporting the idea that their role is more important when CO_2 fixation machinery is inactive (Helman et al. 2003). Confirmation of their role is the fact that, *flv1/flv3* mutants are more sensitive to fluctuating light conditions, in which CO_2 fixation is continuously turned on and off and the maintenance of redox balance is mandatory to protect PSI from oxidative stress (Allahverdiyeva et al. 2013). On the other hand, FLV2-4 heterodimer are able to redirect excess excitation to an unknow electrons acceptor, rather than O_2 (Bersanini et al. 2014; Zhang et al. 2009; Zhang et al. 2012). This mechanism is still not clear, but it is involved in PSII photoprotection in high light condition (Chukhutsina et al. 2015). *FLV2-4* genes are not present in eukaryotes, which conserved only the pseudo-cyclic electron flow pathway. Moreover, the loss of *FLV* during angiosperms evolution occurred quite early, limiting the presence FLV to early land plant (Allahverdiyeva et al. 2015) and gymnosperms (Ilík et al. 2017; Hanawa et al. 2017).

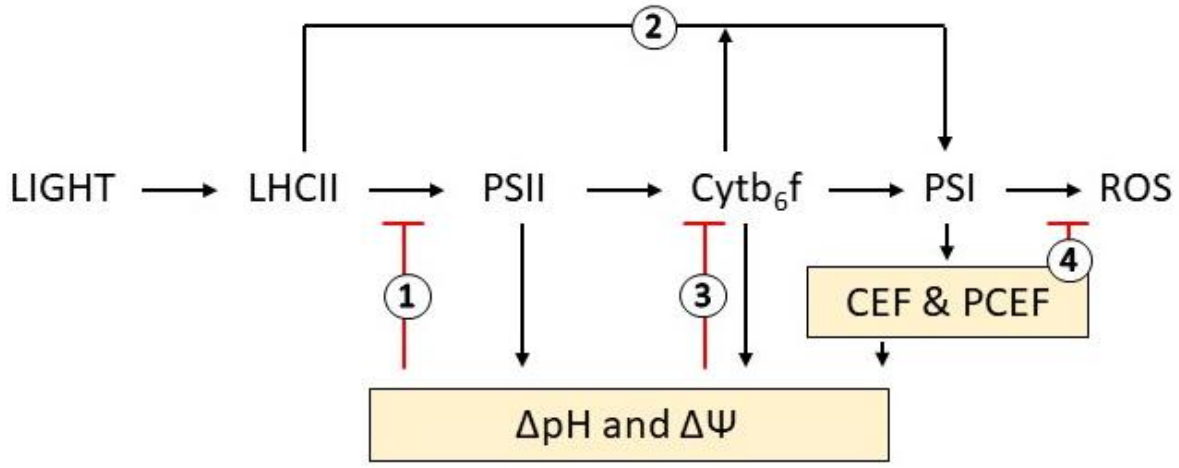

Figure 6: Interactions between photosynthetic regulatory mechanisms. 1 Non-photochemical quenching; 2 State transition; 3 Photosynthetic control; 4 CEF and PCEF. Red lines represent negative feedback, while black arrows are positive regulation.

1.3 *PHYSCOMITRELLA PATENS* AS MODEL ORGANISM FOR PHOTOSYNTHETIC STUDIES

Mosses diverged from vascular plants early after land colonization

Mosses (*phylum* Bryophyta) belong to bryophytes together with liverworts and hornworts (Figure 7A, Puttick et al. 2018). Bryophytes are non-vascular embryophytes which diverged from tracheophytes ancestors about 450 million years ago, early after the colonization of land environment, so forming one of the oldest plant groups (Kenrick and Crane 1997). Mosses are also characterized by the alternation of two generations: the gametophyte and the sporophyte but in contrast to vascular plants, in mosses the gametophyte represents the predominant generation and start with germination of a haploid spore. Gametophyte sexual reproduction generates a diploid sporophyte where meiotic process takes place to regenerate haploid spores (Strotbek, Krinninger, and Frank 2013). Mosses lack lignin in their cell wall, thus their dimension is quite small (few millimeter) limited by the lack of mechanical support and a proper vascular system. Moreover, they lack true leaves and roots, relying on pseudo leaves called phyllids (made by a single cell layer) and on unicellular rhizoids for anchoring and water uptake. Mosses were able to colonize a diverse spectrum of habitats ranging from Antarctic

tundra to desert areas but, lacking an efficient vascular system, stomata on the plant body and an efficient water uptake system, mosses hydration is strongly dependent from the surrounding environment, so they colonize preferentially shady and damp habitats such as forests and peatlands. The colonization of different habitats by these organisms was supported by the development of new abilities which allows them to survive to land environment, such as the acquisition of de/rehydration tolerance and adaptation to different light regimes accompanied by the improvement of signaling capacities to interact and cope with the same environment (Rensing et al. 2008). Mosses hold a key evolutionary position between algae end seed plants and in some cases they share features with both, so they are suitable candidates to study processes allowing land colonization.

The moss Physcomitrella patens

Physcomitrella patens is a moss of the family *Funariaceae* (order *Funariales*), which has become a model organism for the study of specific features connecting aquatic and terrestrial life. The positive features allowing the study of these moss account the relative short life cycle (Figure 7B, Ortiz-Ramírez et al. 2016), the easy manipulation and the high homologous recombination efficiency that made it a model for molecular biology studies. As other bryophytes the life cycle comprises two alternating generations. The gametophytic one starts with the germination of a spore that forms a branched filamentous tissue called protonema. This consists in 2 distinct cell types, the chloronema with chloroplast enriched cells, which apical cells divide about once a day to form new chloronema cells. Chloronemal cells can also divide by subapical cell to shape branched filaments. The second cell type called caulonema differentiates from chloronema apical cells and contains fewer and less developed chloroplasts. Some subapical cell-branches can form meristematic buds which developed in gametophores with a shoot surrounded by phyllids. Female (archegonia) and male (antheridia) sexual organs develop at the tip of gametophore (monoecious species), where fertilization of egg cells in the archegonia by sperms is water dependent. Upon fertilization a diploid sporophyte develops from the zygote where meiotic process leads to haploid spore formation (Figure 7B, Cove 2005). Cultivation of *P. patens* for experimental use is very simple, indeed almost any tissue or single cell is capable to regenerate an entire plant. Thus *P. patens* cultures can be maintained both photo-autotrophically and heterotrophically in early protonema stage vegetatively, soaking it on synthetic agarified medium after mechanical rupture of the tissue. Another interesting feature of *P. patens* is its high rate of homologous recombination (Kammerer and Cove 1996) allowing the specific gene targeting in the nuclear genome simply with the uptake of exogenous DNA harboring homologous

regions by protoplast cells. This feature combined with the availability of different selection markers and genome sequencing (Rensing et al. 2008) allowed the development of different reverse genetic strategies to address biological question. Among these we can find targeted knockout and knockin of in frame sequences, constitutive or inducible overexpression of endogenous gene or transgene, RNA interference (RNAi, or artificial miRNAs) and recently CRISPR-Cas9 technology (Strotbek, Krinninger, and Frank 2013; Lopez-Obando et al. 2016). Moreover, being the haploid gametophyte the dominant phase, is possible to obtain complete gene deletion without the selection of F2 homozygous generation like occurs in higher plants, considerably facilitating the isolation of mutants.

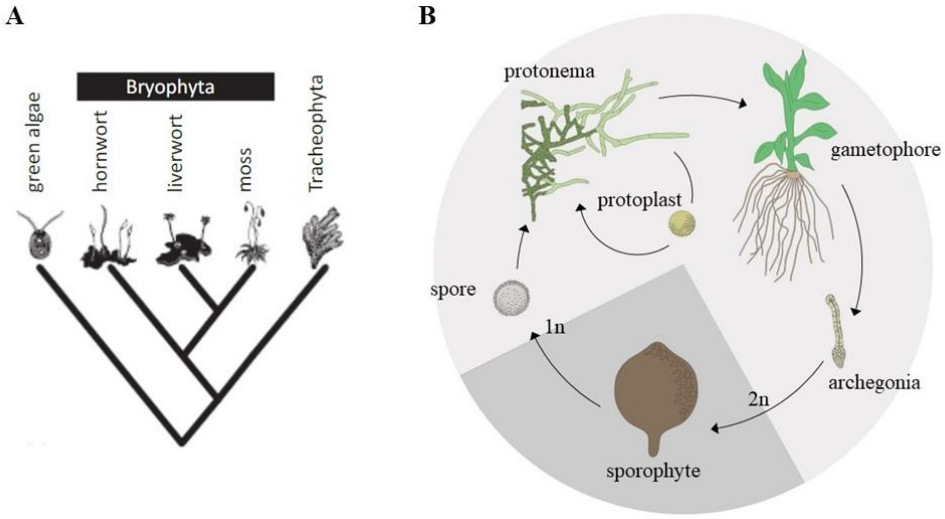

Figure 7: The early land plant *Physcomitrella patens*. A) Phylogenetic relationship between early land plant, the moss *P. patens* belong to Bryophyta together with hornworts and liverworts (Puttick et al. 2018). B) *P. patens* lifecycle (adapted from Ortiz-Ramírez et al. 2016).

P. patens to study photosynthesis evolution

As mentioned before, land plant evolution required the adaptation to new environmental conditions through the development of morphological and physiological features (Vries et al. 2016). One of these adaptations, is the emerging of new photosynthetic regulatory mechanisms mandatory to allows plants to cope with different irradiation conditions present in various lands habitats. For instance, NPQ regulation is based on the activity of different proteins in algae and higher plant (LHCSR and PSBS, Peers et al. 2009; Li et al. 2000), while the presence of AEF mechanisms is not homogenously conserved along photosynthetic organisms evolution (discussed in chapter 2). *P. patens* evolutionary position is reflected also in the composition/regulation of its photosynthetic apparatus which presents common and overlapping functions to both algae and vascular plants. NPQ for example is dependent on both LHCSR and PSBS, highlighting the evolution of new function before the loss of algae type mechanisms (Alboresi et al. 2010). *P. patens* also relies on an abundant and diverse set of LHC proteins (Iwai and Yokono 2017; Alboresi et al. 2008). Interestingly, also *P. patens* AEF mechanisms set appears to be one of the most complete among photosynthetic organisms. Indeed, it relies on FLV proteins as PCEF mechanisms (Gerotto et al. 2016), and on both PGR5/PGRL1 (Kukuczka et al. 2014) and NDH1 mediated CEF pathways. PGR5/PGRL1 pathway is not sensitive to antimycin in *P. patens*, indeed a single amino acid mutation confers resistance to the drug (Sugimoto et al. 2013). The function of this pathway has been studied thanks to a specific KO mutant for *PGRL1* gene. *P. patens pgrl1* showed a higher sensitivity to high light and reduced survival of the plants after anoxia treatment underling a regulatory role of PGRL1 during stressing conditions (Kukuczka et al. 2014). NDH1 instead has never been studied in *P. patens* but NDH1 coding genes are present in its genome except for those coding subunits of luminal subcomplex and LCHA6 linker antenna (Armbruster et al. 2013). The absence of both antennae linker was shown to prevent stably PSI-NDH1 super-complex formation in the liverwort *Marchantia polymorph*a (Ueda et al. 2012). It is not known if the presence of the only LHCA5 linker is sufficient to allow PSI-NDH1 super-complex formation in *P. patens*, even if molecular evidences suggests that *A. thaliana* mutants for LHC6 are not able to accumulate the super-complex (Otani, Yamamoto, and Shikanai 2017). Finally, the role of FLV has been studied in KO mutants showing particular sensitivity to fluctuating light (Gerotto et al. 2016), FLV role in eukaryotes is reviewed in chapter 2. Notably *P. patens flv* mutants showed an increased level of CEF compared to WT (Gerotto et al. 2016), this suggest us a relationship and a possible complementary role between CEF and PCEF in *P. patens*.

REFERENCES

Alboresi, Alessandro, Stefano Caffarri, Fabien Nogue, Roberto Bassi, and Tomas Morosinotto. 2008. "In Silico and Biochemical Analysis of Physcomitrella Patens Photosynthetic Antenna: Identification of Subunits Which Evolved upon Land Adaptation." *PLoS ONE* 3 (4). doi:10.1371/journal.pone.0002033.

Alboresi, Alessandro, Caterina Gerotto, Giorgio M Giacometti, Roberto Bassi, and Tomas Morosinotto. 2010. "Physcomitrella Patens Mutants Affected on Heat Dissipation Clarify the Evolution of Photoprotection Mechanisms upon Land Colonization." *Proceedings of the National Academy of Sciences of the United States of America* 107 (24): 11128–33. doi:10.1073/pnas.1002873107.

Allahverdiyeva, Y., H. Mustila, M. Ermakova, L. Bersanini, P. Richaud, G. Ajlani, N. Battchikova, L. Cournac, and E.-M. Aro. 2013. "Flavodiiron Proteins Flv1 and Flv3 Enable Cyanobacterial Growth and Photosynthesis under Fluctuating Light." *Proceedings of the National Academy of Sciences* 110 (10): 4111–16. doi:10.1073/pnas.1221194110.

Allahverdiyeva, Yagut, Maria Ermakova, Marion Eisenhut, Pengpeng Zhang, Pierre Richaud, Martin Hagemann, Laurent Cournac, and Eva Mari Aro. 2011. "Interplay between Flavodiiron Proteins and Photorespiration in Synechocystis Sp. PCC 6803." *Journal of Biological Chemistry* 286 (27): 24007–14. doi:10.1074/jbc.M111.223289.

Allahverdiyeva, Yagut, Janne Isojärvi, Pengpeng Zhang, and Eva-Mari Aro. 2015. "Cyanobacterial Oxygenic Photosynthesis Is Protected by Flavodiiron Proteins." *Life* 5 (1): 716–43. doi:10.3390/life5010716.

Armbruster, U., T. Ruhle, Renate Kreller, Christoph Strotbek, J. Zuhlke, Luca Tadini, Thomas Blunder, et al. 2013. "The PHOTOSYNTHESIS AFFECTED MUTANT68-LIKE Protein Evolved from a PSII Assembly Factor to Mediate Assembly of the Chloroplast NAD(P)H Dehydrogenase Complex in Arabidopsis." *The Plant Cell* 25 (10): 3926–43. doi:10.1105/tpc.113.114785.

Arnon, D I, and R K Chain. 1975. "Regulation of Ferredoxin-Catalyzed Photosynthetic Phosphorylations." *Proceedings of the National Academy of Sciences of the United States of America* 72 (12): 4961–65.

Arnoux, Pascal, Tomas Morosinotto, Giorgia Saga, Roberto Bassi, and David Pignol. 2009. "A Structural Basis for the PH-Dependent Xanthophyll Cycle in Arabidopsis Thaliana." *The Plant Cell* 21 (7): 2036–44. doi:10.1105/tpc.109.068007.

Asada, K. 2000. "The Water-Water Cycle as Alternative Photon and Electron Sinks." *Philosophical Transactions of the Royal Society B: Biological Sciences* 355 (1402): 1419–31. doi:10.1098/rstb.2000.0703.

Asada, Kozi. 1999. "THE WATER-WATER CYCLE IN CHLOROPLASTS: Scavenging of Active Oxygens and Dissipation of Excess Photons." *Annual Review of Plant Physiology and Plant Molecular Biology* 50 (1): 601–39. doi:10.1146/annurev.arplant.50.1.601.

Battchikova, Natalia, Marion Eisenhut, and Eva Mari Aro. 2011. "Cyanobacterial NDH-1 Complexes: Novel Insights and Remaining Puzzles." *Biochimica et Biophysica Acta - Bioenergetics* 1807 (8): 935–44. doi:10.1016/j.bbabio.2010.10.017.

Bellaflore, Stéphane, Frédy Barneche, Gilles Peltler, and Jean David Rochalx. 2005. "State

Transitions and Light Adaptation Require Chloroplast Thylakoid Protein Kinase STN7." *Nature* 433 (7028): 892–95. doi:10.1038/nature03286.

Bersanini, L., N. Battchikova, M. Jokel, A. Rehman, I. Vass, Y. Allahverdiyeva, and E.-M. Aro. 2014. "Flavodiiron Protein Flv2/Flv4-Related Photoprotective Mechanism Dissipates Excitation Pressure of PSII in Cooperation with Phycobilisomes in Cyanobacteria." *PLANT PHYSIOLOGY* 164 (2): 805–18. doi:10.1104/pp.113.231969.

Bonente, Giulia, Matteo Ballottari, Thuy B. Truong, Tomas Morosinotto, Tae K. Ahn, Graham R. Fleming, Krishna K. Niyogi, and Roberto Bassi. 2011. "Analysis of LHcSR3, a Protein Essential for Feedback de-Excitation in the Green Alga Chlamydomonas Reinhardtii." *PLoS Biology* 9 (1). doi:10.1371/journal.pbio.1000577.

Carol, P. 1999. "Mutations in the Arabidopsis Gene IMMUTANS Cause a Variegated Phenotype by Inactivating a Chloroplast Terminal Oxidase Associated with Phytoene Desaturation." *THE PLANT CELL ONLINE* 11 (1): 57–68. doi:10.1105/tpc.11.1.57.

Chukhutsina, Volha, Luca Bersanini, Eva Mari Aro, and Herbert Van Amerongen. 2015. "Cyanobacterial Flv4-2 Operon-Encoded Proteins Optimize Light Harvesting and Charge Separation in Photosystem II." *Molecular Plant* 8 (5): 747–61. doi:10.1016/j.molp.2014.12.016.

Cournac, Laurent, Kevin Redding, Jacques Ravenel, Dominique Rumeau, Eve Marie Josse, Marcel Kuntz, and Gilles Peltier. 2000. "Electron Flow between Photosystem II and Oxygen in Chloroplasts of Photosystem I-Deficient Algae Is Mediated by a Quinol Oxidase Involved in Chlororespiration." *Journal of Biological Chemistry* 275 (23): 17256–62. doi:10.1074/jbc.M908732199.

Cove, David. 2005. "The Moss *Physcomitrella Patens*." *Annual Review of Genetics* 39 (1): 339–58. doi:10.1146/annurev.genet.39.073003.110214.

DalCorso, Giovanni, Paolo Pesaresi, Simona Masiero, Elena Aseeva, Danja Schünemann, Giovanni Finazzi, Pierre Joliot, Roberto Barbato, and Dario Leister. 2008. "A Complex Containing PGRL1 and PGR5 Is Involved in the Switch between Linear and Cyclic Electron Flow in Arabidopsis." *Cell* 132 (2): 273–85. doi:10.1016/j.cell.2007.12.028.

De Cambiaire, Jean Charles, Christian Otis, Claude Lemieux, and Monique Turmel. 2006. "The Complete Chloroplast Genome Sequence of the Chlorophycean Green Alga Scenedesmus Obliquus Reveals a Compact Gene Organization and a Biased Distribution of Genes on the Two DNA Strands." *BMC Evolutionary Biology* 6. doi:10.1186/1471-2148-6-37.

Drábková, M., H. C P Matthijs, W. Admiraal, and B. Maršálek. 2007. "Selective Effects of H2O2 on Cyanobacterial Photosynthesis." *Photosynthetica* 45 (3): 363–69. doi:10.1007/s11099-007-0062-9.

Endo, Tsuyoshi, Toshiharu Shikanai, Fumihiko Sato, and Kozi Asada. 1998. "NAD(P)H Dehydrogenase-Dependent, Antimycin A-Sensitive Electron Donation to Plastoquinone in Tobacco Chloroplasts." *Plant and Cell Physiology* 39 (11): 1226–31. doi:10.1093/oxfordjournals.pcp.a029324.

Fan, Minrui, Mei Li, Zhenfeng Liu, Peng Cao, Xiaowei Pan, Hongmei Zhang, Xuelin Zhao, Jiping Zhang, and Wenrui Chang. 2015. "Crystal Structures of the PsbS Protein Essential for Photoprotection in Plants." *Nature Structural and Molecular Biology* 22 (9): 729–35. doi:10.1038/nsmb.3068.

Feilke, Kathleen, Peter Streb, Gabriel Cornic, François Perreau, Jerzy Kruk, and Anja Krieger-Liszkay. 2016. "Effect of Chlamydomonas Plastid Terminal Oxidase 1 Expressed in Tobacco

on Photosynthetic Electron Transfer." *Plant Journal* 85 (2): 219–28. doi:10.1111/tpj.13101.

Foyer, C. H., and G. Noctor. 2009. "Redox Regulation in Photosynthetic Organisms: Signaling, Acclimation, and Practical Implications." *Antioxidants & Redox Signaling* 11 (4): 861–905. doi:10.1089/ars.2008.2177.

Gerotto, Caterina, Alessandro Alboresi, Andrea Meneghesso, Martina Jokel, Marjaana Suorsa, Eva-mari Aro, and Tomas Morosinotto. 2016. "Flavodiiron Proteins Act as Safety Valve for Electrons in Physcomitrella Patens." *Proceedings of the National Academy of Sciences of the United States of America* 113 (43): 12322–27. doi:10.1073/pnas.1606685113.

Goncalves, Vera L, Joao B Vincente, Ligia M Saraiva, and Miguel Teixeira. 2011. "Flavodiiron Proteins and Their Role in Cyanobacteria." In *Bioenergetic Processes of Cyanobacteria*, 632–53. doi:10.1007/978-94-007-0388-9.

Grossman, Arthur R., Elizabeth E. Harris, Charles Hauser, Paul A. Lefebvre, Diego Martinez, Dan Rokhsar, Jeff Shrager, et al. 2003. "Chlamydomonas Reinhardtii at the Crossroads of Genomics." *Eukaryotic Cell*. doi:10.1128/EC.2.6.1137-1150.2003.

Hahn, Alexander, Janet Vonck, Deryck J. Mills, Thomas Meier, and Werner Kühlbrandt. 2018. "Structure, Mechanism, and Regulation of the Chloroplast ATP Synthase." *Science* 360 (6389). doi:10.1126/science.aat4318.

Hanawa, Hitomi, Kimitsune Ishizaki, Kana Nohira, Daisuke Takagi, Ginga Shimakawa, Takehiro Sejima, Keiichiro Shaku, Amane Makino, and Chikahiro Miyake. 2017. "Land Plants Drive Photorespiration as Higher Electron-Sink: Comparative Study of Post-Illumination Transient O2-Uptake Rates from Liverworts to Angiosperms through Ferns and Gymnosperms." *Physiologia Plantarum* 161 (1): 138–49. doi:10.1111/ppl.12580.

Hashimoto, Mihoko, Tsuyoshi Endo, Gilles Peltier, Masao Tasaka, and Toshiharu Shikanai. 2003. "A Nucleus-Encoded Factor, CRR2, Is Essential for the Expression of Chloroplast NdhB in Arabidopsis." *Plant Journal* 36 (4): 541–49. doi:10.1046/j.1365-313X.2003.01900.x.

He, Yi, Junliang Fu, Chenliang Yu, Xiaoman Wang, Qinsu Jiang, Jian Hong, Kaixing Lu, et al. 2015. "Increasing Cyclic Electron Flow Is Related to Na+ Sequestration into Vacuoles for Salt Tolerance in Soybean." *Journal of Experimental Botany* 66 (21): 6877–89. doi:10.1093/jxb/erv392.

Helman, Yael, Eugeni Barkan, Doron Eisenstadt, Boaz Luz, and Aaron Kaplan. 2005. "Fractionation of the Three Stable Oxygen Isotopes by Oxygen-Producing and Oxygen-Consuming Reactions in Photosynthetic Organisms." *Plant Physiology* 138 (4): 2292–98. doi:10.1104/pp.105.063768.

Helman, Yael, Dan Tchernov, Leonora Reinhold, Mari Shibata, Teruo Ogawa, Rakefet Schwarz, Itzhak Ohad, and Aaron Kaplan. 2003. "Genes Encoding A-Type Flavoproteins Are Essential for Photoreduction of O2 in Cyanobacteria." *Current Biology* 13 (3): 230–35. doi:10.1016/S0960-9822(03)00046-0.

Hertle, Alexander P., Thomas Blunder, Tobias Wunder, Paolo Pesaresi, Mathias Pribil, Ute Armbruster, and Dario Leister. 2013. "PGRL1 Is the Elusive Ferredoxin-Plastoquinone Reductase in Photosynthetic Cyclic Electron Flow." *Molecular Cell* 49 (3). Elsevier: 511–23. doi:10.1016/j.molcel.2012.11.030.

Ifuku, Kentaro, Tsuyoshi Endo, Toshiharu Shikanai, and Eva Mari Aro. 2011. "Structure of the Chloroplast NADH Dehydrogenase-like Complex: Nomenclature for Nuclear-Encoded Subunits." *Plant and Cell Physiology* 52 (9): 1560–68. doi:10.1093/pcp/pcr098.

Ilík, Petr, Andrej Pavlovič, Roman Kouřil, Alessandro Alboresi, Tomas Morosinotto, Yagut Allahverdiyeva, Eva Mari Aro, Hiroshi Yamamoto, and Toshiharu Shikanai. 2017. "Alternative Electron Transport Mediated by Flavodiiron Proteins Is Operational in Organisms from Cyanobacteria up to Gymnosperms." *New Phytologist* 214 (3): 967–72. doi:10.1111/nph.14536.

Ishikawa, Noriko, Tsuyoshi Endo, and Fumihiko Sato. 2008. "Electron Transport Activities of Arabidopsis Thaliana Mutants with Impaired Chloroplastic NAD(P)H Dehydrogenase." *Journal of Plant Research* 121 (5): 521–26. doi:10.1007/s10265-008-0180-x.

Ishikawa, Noriko, Atsushi Takabayashi, Ko Noguchi, Youshi Tazoe, Hiroshi Yamamoto, Susanne Von Caemmerer, Fumihiko Sato, and Tsuyoshi Endo. 2016. "NDH-Mediated Cyclic Electron Flow around Photosystem I Is Crucial for C4photosynthesis." *Plant and Cell Physiology* 57 (10): 2020–28. doi:10.1093/pcp/pcw127.

Iwai, Masakazu, Kenji Takizawa, Ryutaro Tokutsu, Akira Okamuro, Yuichiro Takahashi, and Jun Minagawa. 2010. "Isolation of the Elusive Supercomplex That Drives Cyclic Electron Flow in Photosynthesis." *Nature* 464 (7292): 1210–13. doi:10.1038/nature08885.

Iwai, Masakazu, and Makio Yokono. 2017. "Light-Harvesting Antenna Complexes in the Moss Physcomitrella Patens: Implications for the Evolutionary Transition from Green Algae to Land Plants." *Current Opinion in Plant Biology*. doi:10.1016/j.pbi.2017.04.002.

Jans, F., E. Mignolet, P.-A. Houyoux, P. Cardol, B. Ghysels, S. Cuine, L. Cournac, G. Peltier, C. Remacle, and F. Franck. 2008. "A Type II NAD(P)H Dehydrogenase Mediates Light-Independent Plastoquinone Reduction in the Chloroplast of Chlamydomonas." *Proceedings of the National Academy of Sciences* 105 (51): 20546–51. doi:10.1073/pnas.0806896105.

Joliot, Pierre, and Giles N Johnson. 2011. "Regulation of Cyclic and Linear Electron Fl Ow in Higher Plants." doi:10.1073/pnas.1110189108.

Kammerer, Wolfgang, and David J. Cove. 1996. "Genetic Analysis of the Effects of Re-Transformation of Transgenic Lines of the Moss Physcomitrella Patens." *Molecular and General Genetics* 250 (3): 380–82. doi:10.1007/s004380050089.

Kato, Yoshinobu, Kazuhiko Sugimoto, and Toshiharu Shikanai. 2017. "NDH-PSI Supercomplex Assembly Precedes Full Assembly of the NDH Complex in Chloroplast." *Plant Physiology*, pp.01120.2017. doi:10.1104/pp.17.01120.

Kenrick, Paul, and Peter R. Crane. 1997. "The Origin and Early Evolution of Plants on Land." *Nature*. doi:10.1038/37918.

Kirchhoff, Helmut. 2014. "Diffusion of Molecules and Macromolecules in Thylakoid Membranes." *Biochimica et Biophysica Acta - Bioenergetics* 1837 (4): 495–502. doi:10.1016/j.bbabio.2013.11.003.

Kono, Masaru, Ko Noguchi, and Ichiro Terashima. 2014. "Roles of the Cyclic Electron Flow around PSI (CEF-PSI) and O2-Dependent Alternative Pathways in Regulation of the Photosynthetic Electron Flow in Short-Term Fluctuating Light in Arabidopsis Thaliana." *Plant and Cell Physiology* 55 (5): 990–1004. doi:10.1093/pcp/pcu033.

Kotera, Emi, Masao Tasaka, and Toshiharu Shikanai. 2005. "A Pentatricopeptide Repeat Protein Is Essential for RNA Editing in Chloroplasts." *Nature* 433 (7023): 326–30. doi:10.1038/nature03229.

Kouril, Roman, Ond??ej Strouhal, Luk???? Nosek, Ren?? Lenobel, Ivo Chamr??d, Egbert J. Boekema, Marek ??ebela, and Petr Il??k. 2014. "Structural Characterization of a Plant

Photosystem i and NAD(P)H Dehydrogenase Supercomplex." *Plant Journal* 77 (4): 568–76. doi:10.1111/tpj.12402.

Kouřil, Roman, Lukáš Nosek, Dmitry Semchonok, Egbert J. Boekema, and Petr Ilík. 2018. "Organization of Plant Photosystem II and Photosystem I Supercomplexes." In *Subcellular Biochemistry*, 87:259–86. doi:10.1007/978-981-10-7757-9_9.

Krieger-Liszkay, Anja. 2005. "Singlet Oxygen Production in Photosynthesis." In *Journal of Experimental Botany*, 56:337–46. doi:10.1093/jxb/erh237.

Kukuczka, B., L. Magneschi, D. Petroutsos, J. Steinbeck, T. Bald, M. Powikrowska, C. Fufezan, G. Finazzi, and M. Hippler. 2014. "PGRL1-Mediated Cyclic Electron Flow Is Crucial for Acclimation to Anoxia and Complementary to Non-Photochemical Quenching in Stress Adaptation." *Plant Physiology* 165 (August): pp.114.240648-. doi:10.1104/pp.114.240648.

Lemieux, Claude, Christian Otis, and Monique Turmel. 2000. "Ancestral Chloroplast Genome in Mesostigma Viride Reveals an Early Branch of Green Plant Evolution." *Nature* 403 (6770): 649–52. doi:10.1038/35001059.

Lennon, Adrian M., Peerada Prommeenate, and Peter J. Nixon. 2003. "Location, Expression and Orientation of the Putative Chlororespiratory Enzymes, Ndh and IMMUTANS, in Higher-Plant Plastids." *Planta* 218 (2): 254–60. doi:10.1007/s00425-003-1111-7.

Li, Qinghua, Zheng-Ju Yao, and Hualing Mi. 2016. "Alleviation of Photoinhibition by Co-Ordination of Chlororespiration and Cyclic Electron Flow Mediated by NDH under Heat Stressed Condition in Tobacco." *Frontiers in Plant Science* 7 (March): 1–9. doi:10.3389/fpls.2016.00285.

Li, X P, O Björkman, C Shih, A R Grossman, M Rosenquist, S Jansson, and K K Niyogi. 2000. "A Pigment-Binding Protein Essential for Regulation of Photosynthetic Light Harvesting." *Nature* 403 (6768): 391–95. doi:10.1038/35000131.

Li, Xiao Ping, Adam M. Gilmore, Stefano Caffarri, Roberto Bassi, Talila Golan, David Kramer, and Krishna K. Niyogi. 2004. "Regulation of Photosynthetic Light Harvesting Involves Intrathylakoid Lumen PH Sensing by the PsbS Protein." *Journal of Biological Chemistry* 279 (22): 22866–74. doi:10.1074/jbc.M402461200.

Li, Xin-guo, Wei Duan, Qing-wei Meng, Qi Zou, and Shi-jie Zhao. 2004. "The Function of Chloroplastic NAD (P) H Dehydrogenase in Tobacco during Chillin ..." *Agriculture* 45 (1): 103–8.

Liguori, Nicoletta, Laura M. Roy, Milena Opacic, Grégory Durand, and Roberta Croce. 2013. "Regulation of Light Harvesting in the Green Alga Chlamydomonas Reinhardtii: The c-Terminus of Lhcsr Is the Knob of a Dimmer Switch." *Journal of the American Chemical Society* 135 (49): 18339–42. doi:10.1021/ja4107463.

Lopez-Obando, M., B. Hoffmann, C. Gery, A. Guyon-Debast, E. Teoule, C. Rameau, S. Bonhomme, and F. Nogue. 2016. "Simple and Efficient Targeting of Multiple Genes Through CRISPR-Cas9 in Physcomitrella Patens." *G3: Genes|Genomes|Genetics*, 1–27. doi:10.1534/g3.116.033266.

Martin, Mercedes, Dolores M. Noarbe, Patricia H. Serrot, and BartolomÃ© Sabater. 2015. "The Rise of the Photosynthetic Rate When Light Intensity Increases Is Delayed in Ndh Gene-Defective Tobacco at High but Not at Low CO2 Concentrations." *Frontiers in Plant Science* 6 (February): 1–11. doi:10.3389/fpls.2015.00034.

Martín, Mercedes, and Bartolomé Sabater. 2010. "Plastid Ndh Genes in Plant Evolution." *Plant*

Physiology and Biochemistry. doi:10.1016/j.plaphy.2010.04.009.

Matthijs, Hans C.P., Petra M. Visser, Bart Reeze, Jeroen Meeuse, Pieter C. Slot, Geert Wijn, Renée Talens, and Jef Huisman. 2012. "Selective Suppression of Harmful Cyanobacteria in an Entire Lake with Hydrogen Peroxide." *Water Research* 46 (5): 1460–72. doi:10.1016/j.watres.2011.11.016.

Maxwell, K, and G N Johnson. 2000. "Chlorophyll Fluorescence - a Practical Guide." *J.Exp.Bot.* 51 (345): 659–68.

Mehler, Alan H. 1951. "Studies on Reactions of Illuminated Chloroplasts. II. Stimulation and Inhibition of the Reaction with Molecular Oxygen." *Archives of Biochemistry and Biophysics* 34 (2): 339–51. doi:10.1016/0003-9861(51)90012-4.

Mehler, Alan H., and Allan H. Brown. 1952. "Studies on Reactions of Illuminated Chloroplasts. III. Simultaneous Photoproduction and Consumption of Oxygen Studied with Oxygen Isotopes." *Archives of Biochemistry and Biophysics* 38 (1): 365–70. doi:10.1016/0003-9861(52)90042-8.

Mi, Hualing, Yong Deng, Yoshito Tanaka, Takashi Hibino, and Teruhiro Takabe. 2001. "Photo-Induction of an NADPH Dehydrogenase Which Functions as a Mediator of Electron Transport to the Intersystem Chain in the Cyanobacterium Synechocystis PCC6803." *Photosynthesis Research* 70 (2): 167–73. doi:10.1023/A:1017946524199.

Mitchell, Peter. 1976. "Possible Molecular Mechanisms of the Protonmotive Function of Cytochrome Systems." *Journal of Theoretical Biology* 62 (2): 327–67. doi:10.1016/0022-5193(76)90124-7.

Müller, P, X P Li, and K K Niyogi. 2001. "Non-Photochemical Quenching. A Response to Excess Light Energy." *Plant Physiology* 125 (4): 1558–66. doi:10.1104/pp.125.4.1558.

Munekage, Yuri, Mihoko Hashimoto, Chikahiro Miyake, Ken-ichi Tomizawa, Tsuyoshi Endo, Masao Tasaka, and Toshiharu Shikanai. 2004. "Cyclic Electron Flow around Photosystem I Is Essential for Photosynthesis." *Nature* 429 (6991): 579–82. doi:10.1038/nature02598.

Munekage, Yuri, Masaya Hojo, Jörg Meurer, Tsuyoshi Endo, Masao Tasaka, and Toshiharu Shikanai. 2002. "PGR5 Is Involved in Cyclic Electron Flow around Photosystem I and Is Essential for Photoprotection in Arabidopsis." *Cell* 110 (3): 361–71. doi:10.1016/S0092-8674(02)00867-X.

Nashilevitz, S., C. Melamed-Bessudo, Y. Izkovich, I. Rogachev, S. Osorio, M. Itkin, A. Adato, et al. 2010. "An Orange Ripening Mutant Links Plastid NAD(P)H Dehydrogenase Complex Activity to Central and Specialized Metabolism during Tomato Fruit Maturation." *The Plant Cell* 22 (6): 1977–97. doi:10.1105/tpc.110.074716.

Nellaepalli, Sreedhar, Sireesha Kodru, Malavath Tirupathi, and Rajagopal Subramanyam. 2012. "Anaerobiosis Induced State Transition: A Non Photochemical Reduction of PQ Pool Mediated by NDH in Arabidopsis Thaliana." *PLoS ONE* 7 (11). doi:10.1371/journal.pone.0049839.

Nishio, John N, and John Whitmarsh. 1993. "Dissipation of the Proton Electrochemical Potential in Lntact Chloroplasts ' II . The PH Gradient Monitored by Cytochrome f Reduction Kinetics," 89–96.

Niyogi, Kk, O Bjorkman, and Ar Grossman. 1997. "Chlamydomonas Xanthophyll Cycle Mutants Identified by Video Imaging of Chlorophyll Fluorescence Quenching." *The Plant Cell* 9 (8): 1369–80. doi:10.1105/tpc.9.8.1369.

Niyogi, Krishna K. 2000. "Safety Valves for Photosynthesis." *Current Opinion in Plant Biology* 3 (6): 455–60. doi:10.1016/S1369-5266(00)00113-8.

Ohkawa, Hiroshi, Himadri B. Pakrasi, and Teruo Ogawa. 2000. “Two Types of Functionally Distinct NAD(P)H Dehydrogenases in Synechoeystis Sp. Strain PCC6803.” *Journal of Biological Chemistry* 275 (41): 31630–34. doi:10.1074/jbc.M003706200.

Okegawa, Yuki, Yoshichika Kobayashi, and Toshiharu Shikanai. 2010. “Physiological Links among Alternative Electron Transport Pathways That Reduce and Oxidize Plastoquinone in Arabidopsis.” *Plant Journal* 63 (3): 458–68. doi:10.1111/j.1365-313X.2010.04252.x.

Ortiz-Ramírez, Carlos, Marcela Hernandez-Coronado, Anna Thamm, Bruno Catarino, Mingyi Wang, Liam Dolan, José A A. Feijó, and Jörg D D. Becker. 2016. “A Transcriptome Atlas of Physcomitrella Patens Provides Insights into the Evolution and Development of Land Plants.” *Molecular Plant* 9 (2): 205–20. doi:10.1016/j.molp.2015.12.002.

Otani, Takuto, Hiroshi Yamamoto, and Toshiharu Shikanai. 2017. “Stromal Loop of Lhca6 Is Responsible for the Linker Function Required for the NDH-PSI Supercomplex Formation.” *Plant and Cell Physiology* 58 (4): 851–61. doi:10.1093/pcp/pcx009.

Peers, Graham, Thuy B Truong, Elisabeth Ostendorf, Andreas Busch, Dafna Elrad, Arthur R Grossman, Michael Hippler, and Krishna K Niyogi. 2009. “An Ancient Light-Harvesting Protein Is Critical for the Regulation of Algal Photosynthesis.” *Nature* 462 (7272): 518–21. doi:10.1038/nature08587.

Peltier, Gilles, Dimitri Tolleter, Emmanuelle Billon, and Laurent Cournac. 2010. “Auxiliary Electron Transport Pathways in Chloroplasts of Microalgae.” *Photosynthesis Research* 106: 19–31. doi:10.1007/s11120-010-9575-3.

Peng, Lianwei, Yoichiro Fukao, Masayuki Fujiwara, Tsuneaki Takami, and Toshiharu Shikanai. 2009. “Efficient Operation of NAD(P)H Dehydrogenase Requires Supercomplex Formation with Photosystem I via Minor LHCI in Arabidopsis.” *The Plant Cell* 21 (11): 3623–40. doi:10.1105/tpc.109.068791.

Peng, Lianwei, Hideyuki Shimizu, and Toshiharu Shikanai. 2008. “The Chloroplast NAD(P)H Dehydrogenase Complex Interacts with Photosystem I in Arabidopsis.” *Journal of Biological Chemistry* 283 (50): 34873–79. doi:10.1074/jbc.M803207200.

Pombert, Jean Francois, Claude Lemieux, and Monique Turmel. 2006. “The Complete Chloroplast DNA Sequence of the Green Alga Oltmannsiellopsis Viridis Reveals a Distinctive Quadripartite Architecture in the Chloroplast Genome of Early Diverging Ulvophytes.” *BMC Biology* 4. doi:10.1186/1741-7007-4-3.

Pribil, Mathias, Paolo Pesaresi, Alexander Hertle, Roberto Barbato, and Dario Leister. 2010. “Role of Plastid Protein Phosphatase TAP38 in LHCII Dephosphorylation and Thylakoid Electron Flow.” *PLoS Biology* 8 (1). doi:10.1371/journal.pbio.1000288.

Puttick, Mark N., Jennifer L. Morris, Tom A. Williams, Cymon J. Cox, Dianne Edwards, Paul Kenrick, Silvia Pressel, et al. 2018. “The Interrelationships of Land Plants and the Nature of the Ancestral Embryophyte.” *Current Biology* 28 (5): 733–745.e2. doi:10.1016/j.cub.2018.01.063.

Rensing, Stefan A, Daniel Lang, Andreas D Zimmer, Astrid Terry, Asaf Salamov, Harris Shapiro, Tomoaki Nishiyama, et al. 2008. “The Physcomitrella Genome Reveals Evolutionary Insights into the Conquest of Land by Plants.” *Science (New York, N.Y.)* 319 (5859): 64–69. doi:10.1126/science.1150646.

Rosso, D., A. G. Ivanov, A. Fu, J. Geisler-Lee, L. Hendrickson, M. Geisler, G. Stewart, et al. 2006. “IMMUTANS Does Not Act as a Stress-Induced Safety Valve in the Protection of the Photosynthetic Apparatus of Arabidopsis during Steady-State Photosynthesis.” *PLANT*

PHYSIOLOGY 142 (2): 574–85. doi:10.1104/pp.106.085886.

Rumberg, B, and U Smgel. 1968. "PH Changes in the Inner Phase of the Thylakoids during Photosynthesis" 622 (1963): 1968–70.

Rumeau, Dominique, Noëlle Bécuwe-Linka, Audrey Beyly, Mathilde Louwagie, Jérôme Garin, and Gilles Peltier. 2005. "New Subunits NDH-M, -N, and -O, Encoded by Nuclear Genes, Are Essential for Plastid Ndh Complex Functioning in Higher Plants." *The Plant Cell* 17 (1): 219–32. doi:10.1105/tpc.104.028282.

Segura, María V., and María J. Quiles. 2015. "Involvement of Chlororespiration in Chilling Stress in the Tropical Species Spathiphyllum Wallisii." *Plant Cell and Environment* 38 (3): 525–33. doi:10.1111/pce.12406.

Shapiguzov, A., B. Ingelsson, I. Samol, C. Andres, F. Kessler, J.-D. Rochaix, A. V. Vener, and M. Goldschmidt-Clermont. 2010. "The PPH1 Phosphatase Is Specifically Involved in LHCII Dephosphorylation and State Transitions in Arabidopsis." *Proceedings of the National Academy of Sciences* 107 (10): 4782–87. doi:10.1073/pnas.0913810107.

Shikanai, T, T Endo, T Hashimoto, Y Yamada, K Asada, and A Yokota. 1998. "Directed Disruption of the Tobacco NdhB Gene Impairs Cyclic Electron Flow around Photosystem I." *Proceedings of the National Academy of Sciences of the United States of America* 95 (16): 9705–9. doi:10.1073/pnas.95.16.9705.

Shikanai, Toshiharu. 2016a. "Chloroplast NDH: A Different Enzyme with a Structure Similar to That of Respiratory NADH Dehydrogenase." *Biochimica et Biophysica Acta - Bioenergetics*. doi:10.1016/j.bbabio.2015.10.013.

———. 2016b. "Regulatory Network of Proton Motive Force: Contribution of Cyclic Electron Transport around Photosystem I in Arabidopsis." *Photosynthesis Research*. Springer Netherlands. doi:10.1007/s11120-016-0227-0.

Shinozaki, K, M Ohme, M Tanaka, T Wakasugi, N Hayashida, T Matsubayashi, N Zaita, et al. 1986. "The Complete Nucleotide Sequence of the Tobacco Chloroplast Genome: Its Gene Organization and Expression." *EMBO J.* 5: 2043–50.

Strand, Deserah D., Aaron K. Livingston, Mio Satoh-Cruz, John E. Froehlich, Veronica G. Maurino, and David M. Kramer. 2015. "Activation of Cyclic Electron Flow by Hydrogen Peroxide in Vivo." *Proceedings of the National Academy of Sciences* 112 (17): 5539–44. doi:10.1073/pnas.1418223112.

Strotbek, Christoph, Stefan Krinninger, and Wolfgang Frank. 2013. "The Moss Physcomitrella Patens: Methods and Tools from Cultivation to Targeted Analysis of Gene Function." *The International Journal of Developmental Biology* 57 (6–8): 553–64. doi:10.1387/ijdb.130189wf.

Sugimoto, Kazuhiko, Yuki Okegawa, Akihiko Tohri, Terri A. Long, Sarah F. Covert, Toru Hisabori, and Toshiharu Shikanai. 2013. "A Single Amino Acid Alteration in PGR5 Confers Resistance to Antimycin a in Cyclic Electron Transport around PSI." *Plant and Cell Physiology* 54 (9): 1525–34. doi:10.1093/pcp/pct098.

Suorsa, Marjaana, Michele Grieco, Markus Nurmi, Malgorzata Pietrzykowska, Marjaana Rantala, Virpi Paakkarinen, Mikko Tikkanen, Stefan Jansson, and Eva-mari Aro. 2012. "PROTON GRADIENT REGULATION5 Is Essential for Proper Acclimation of Arabidopsis Photosystem I to Naturally and Arti Fi Cially Fluctuating Light Conditions" 24 (July): 2934–48. doi:10.1105/tpc.112.097162.

Suorsa, Marjaana, Fabio Rossi, Luca Tadini, Mathias Labs, Monica Colombo, Peter Jahns, Martin M M. Kater, et al. 2016. "PGR5-PGRL1-Dependent Cyclic Electron Transport Modulates Linear Electron Transport Rate in Arabidopsis Thaliana." *Molecular Plant* 9 (2): 271–88. doi:10.1016/j.molp.2015.12.001.

Tikhonov, Alexander N. 2018. "The Cytochrome B6f Complex: Biophysical Aspects of Its Functioning in Chloroplasts." In *Subcellular Biochemistry*, 87:287–328. doi:10.1007/978-981-10-7757-9_10.

Turmel, Monique, Marie Christine Gagnon, Charley J. O'Kelly, Christian Otis, and Claude Lemieux. 2009. "The Chloroplast Genomes of the Green Algae Pyramimonas, Monomastix, and Pycnococcus Shed New Light on the Evolutionary History of Prasinophytes and the Origin of the Secondary Chloroplasts of Euglenids." *Molecular Biology and Evolution* 26 (3): 631–48. doi:10.1093/molbev/msn285.

Turmel, Monique, Christian Otis, and Claude Lemieux. 2006. "The Chloroplast Genome Sequence of Chara Vulgaris Sheds New Light into the Closest Green Algal Relatives of Land Plants." *Molecular Biology and Evolution* 23 (6): 1324–38. doi:10.1093/molbev/msk018.

Ueda, Minoru, Tetsuki Kuniyoshi, Hiroshi Yamamoto, Kazuhiko Sugimoto, Kimitsune Ishizaki, Takayuki Kohchi, Yoshiki Nishimura, and Toshiharu Shikanai. 2012. "Composition and Physiological Function of the Chloroplast NADH Dehydrogenase-like Complex in Marchantia Polymorpha." *Plant Journal* 72 (4): 683–93. doi:10.1111/j.1365-313X.2012.05115.x.

Vicente, João B., Cláudio M. Gomes, Alain Wasserfallen, and Miguel Teixeira. 2002. "Module Fusion in an A-Type Flavoprotein from the Cyanobacterium Synechocystis Condenses a Multiple-Component Pathway in a Single Polypeptide Chain." *Biochemical and Biophysical Research Communications* 294 (1): 82–87. doi:10.1016/S0006-291X(02)00434-5.

Vicente, João B, Maria Arménia Carrondo, Miguel Teixeira, and Carlos Frazão. 2008. "Structural Studies on Flavodiiron Proteins." *Methods in Enzymology* 437 (January): 3–19. doi:10.1016/S0076-6879(07)37001-8.

Vries, Jan De, Amanda Stanton, John M Archibald, and Sven B Gould. 2016. "Streptophyte Terrestrialization in Light of Plastid Evolution." *Trends in Plant Science* xx. Elsevier Ltd: 1–10. doi:10.1016/j.tplants.2016.01.021.

Wakasugi, T., T. Nagai, M. Kapoor, M. Sugita, M. Ito, S. Ito, J. Tsudzuki, et al. 1997. "Complete Nucleotide Sequence of the Chloroplast Genome from the Green Alga Chlorella Vulgaris: The Existence of Genes Possibly Involved in Chloroplast Division." *Proceedings of the National Academy of Sciences* 94 (11): 5967–72. doi:10.1073/pnas.94.11.5967.

Wang, Caijuan, Hiroshi Yamamoto, and Toshiharu Shikanai. 2015. "Role of Cyclic Electron Transport around Photosystem I in Regulating Proton Motive Force." *Biochimica et Biophysica Acta* 1847 (9). Elsevier B.V.: 931–38. doi:10.1016/j.bbabio.2014.11.013.

Wang, Peng, Wei Duan, Atsushi Takabayashi, Tsuyoshi Endo, and Toshiharu Shikanai. 2006. "Chloroplastic NAD (P) H Dehydrogenase in Tobacco Leaves Functions in Alleviation of Oxidative Damage Caused by Temperature Stress 1 [OA]" 141 (June): 465–74. doi:10.1104/pp.105.070490.1.

Wasserfallen, Alain, Sandra Ragettli, Yves Jouanneau, and Thomas Leisinger. 1998. "A Family of Flavoproteins in the Domains Archaea and Bacteria." *European Journal of Biochemistry* 254 (2): 325–32. doi:10.1046/j.1432-1327.1998.2540325.x.

Wollman, F. A. 2001. "State Transitions Reveal the Dynamics and Flexibility of the Photosynthetic

Apparatus." *EMBO Journal*. doi:10.1093/emboj/20.14.3623.

Yamamoto, Hiroshi, Lianwei Peng, Yoichiro Fukao, and Toshiharu Shikanai. 2011. "An Src Homology 3 Domain-like Fold Protein Forms a Ferredoxin Binding Site for the Chloroplast NADH Dehydrogenase-like Complex in Arabidopsis." *The Plant Cell* 23 (4): 1480–93. doi:10.1105/tpc.110.080291.

Yamashita, E., H. Zhang, and W. A. Cramer. 2007. "Structure of the Cytochrome B6f Complex: Quinone Analogue Inhibitors as Ligands of Heme Cn." *Journal of Molecular Biology* 370 (1): 39–52. doi:10.1016/j.jmb.2007.04.011.

Yamori, Wataru, Amane Makino, and Toshiharu Shikanai. 2016. "A Physiological Role of Cyclic Electron Transport around Photosystem I in Sustaining Photosynthesis under Fluctuating Light in Rice." *Scientific Reports* 6 (July 2015). Nature Publishing Group: 1–12. doi:10.1038/srep20147.

Yamori, Wataru, Naoki Sakata, Yuji Suzuki, Toshiharu Shikanai, and Amane Makino. 2011. "Cyclic Electron Flow around Photosystem i via Chloroplast NAD(P)H Dehydrogenase (NDH) Complex Performs a Significant Physiological Role during Photosynthesis and Plant Growth at Low Temperature in Rice." *Plant Journal* 68 (6): 966–76. doi:10.1111/j.1365-313X.2011.04747.x.

Zhang, P., M. Eisenhut, A.-M. Brandt, D. Carmel, H. M. Silen, I. Vass, Y. Allahverdiyeva, T. A. Salminen, and E.-M. Aro. 2012. "Operon Flv4-Flv2 Provides Cyanobacterial Photosystem II with Flexibility of Electron Transfer." *The Plant Cell* 24 (5): 1952–71. doi:10.1105/tpc.111.094417.

Zhang, Pengpeng, Yagut Allahverdiyeva, Marion Eisenhut, and Eva-Mari Aro. 2009. "Flavodiiron Proteins in Oxygenic Photosynthetic Organisms: Photoprotection of Photosystem II by Flv2 and Flv4 in Synechocystis Sp. PCC 6803." *PloS One* 4 (4): e5331. doi:10.1371/journal.pone.0005331.

CHAPTER 2

Balancing protection and efficiency in the regulation of photosynthetic electron transport across plant evolution

Authors name and affiliation

Alessandro Alboresi, Mattia Storti, Tomas Morosinotto

Department of Biology, University of Padova, Via Ugo Bassi 58B, 35121 Padua, Italy

THIS CHAPTER WAS PUBLISHED IN "*NEW PHYTOLOGIST*" (2018).

The format of this chapter conforms editorial request of the journal.

CONTRIBUTION

In this chapter MS wrote the manuscript and revised the text

SUMMARY

Photosynthetic electron transport requires continuous modulation to maintain the balance between light availability and metabolic demands. Multiple mechanisms for the regulation of electron transport have been identified and are unevenly distributed among photosynthetic organisms. Flavodiiron proteins (FLVs) influence photosynthetic electron transport by accepting electrons downstream of photosystem I to reduce oxygen to water. FLV activity has been demonstrated in cyanobacteria, green algae and mosses to be important in avoiding photosystem I overreduction upon changes in light intensity. FLV-encoding sequences were nevertheless lost during evolution by angiosperms, suggesting that these plants increased the efficiency of other mechanisms capable of accepting electrons from photosystem I, making the FLV activity for protection from overreduction superfluous or even detrimental for photosynthetic efficiency.

I. INTRODUCTION

Photosynthesis supports life using light energy to fix CO_2 and producing oxygen (O_2) as a by-product. In oxygenic photosynthetic organisms, sunlight fuels the linear electron flow (LEF) from water to $NADP^+$, relying on two photosystems (PSI and PSII) embedded in the thylakoid membranes (Fig. 1). Electron transport is coupled with proton accumulation in the thylakoid lumen and the generation of an electrochemical gradient that drives ATP synthesis. All cell metabolism, starting with the Calvin–Benson (CB) cycle, responsible for CO_2 fixation, is supported by the NADPH and ATP produced by these reactions.

Plant metabolism demand in a dynamic environment is continuously changing. As an example, stomata closure can cause CO_2 limitation with a major impact on ATP/NADPH consumption rates by the CB cycle. The imbalance between the rate of metabolism of ATP/NADPH utilization and excitation energy available is dangerous because excited electrons cannot be stored and their accumulation leads to the formation of reactive oxygen species that, if in excess, can damage the photosynthetic apparatus (Eberhard *et al*., 2008; Li *et al*., 2009). Photosynthetic organisms evolved a sophisticated machinery to efficiently repair PSII from light damage (Tikkanen *et al*., 2014), whereas there is no analogous mechanism for PSI. The recovery of any PSI damage requires the complete

resynthesis of the supercomplex, a slow and costly process that in plants can require weeks (Teicher *et al*., 2000).

Photosynthetic organisms also evolved multiple regulatory mechanisms to balance light-dependent processes and metabolic exploitation of photosynthesis products. Notable examples are the dissipation of excess excitation energy as heat (called nonphotochemical quenching, NPQ), the state transition to equilibrate excitation between PSI and PSII, and the photosynthetic control to reduce electron transport capacity under excess illumination – see Eberhard *et al*. (2008) and Li *et al*. (2009) for overall reviews.

Electron transport capacity is also regulated by the presence of pathways feeding or diverting electrons from the LEF, such as cyclic electron flow (CEF) and pseudo-CEF (PCEF) (Fig. 1). CEF recycles electrons from PSI to the thylakoid plastoquinone (PQ) pool, decreasing NADPH formation and promoting proton pumping by cytochrome (Cyt) b_6f. Two CEF pathways have been identified, one dependent on PGR5/PGRL1 (Munekage *et al*., 2002; DalCorso *et al*., 2008) and the other resulting from the activity of a chloroplast NADH dehydrogenase-like (NDH-1) complex (Shikanai *et al*., 1998). Two pathways have also been identified for PCEF: the Mehler reaction occurs when PSI directly oxidizes O_2 to form O_2^-, which is then converted first into hydrogen peroxide (H_2O_2) and finally to O_2 and H_2O by superoxide dismutase and ascorbate peroxidase (Asada, 2000). More recently, PCEF was shown to be mediated also by a class of enzymes called flavodiiron proteins (FLVs or FDPs) that accept electrons downstream of PSI to reduce oxygen to water (Fig. 1). PCEF is also called the water-to-water cycle, because H_2O is split by PSII and then resynthesized when O_2 acts as the final electron acceptor from PSI instead of $NADP^+$.

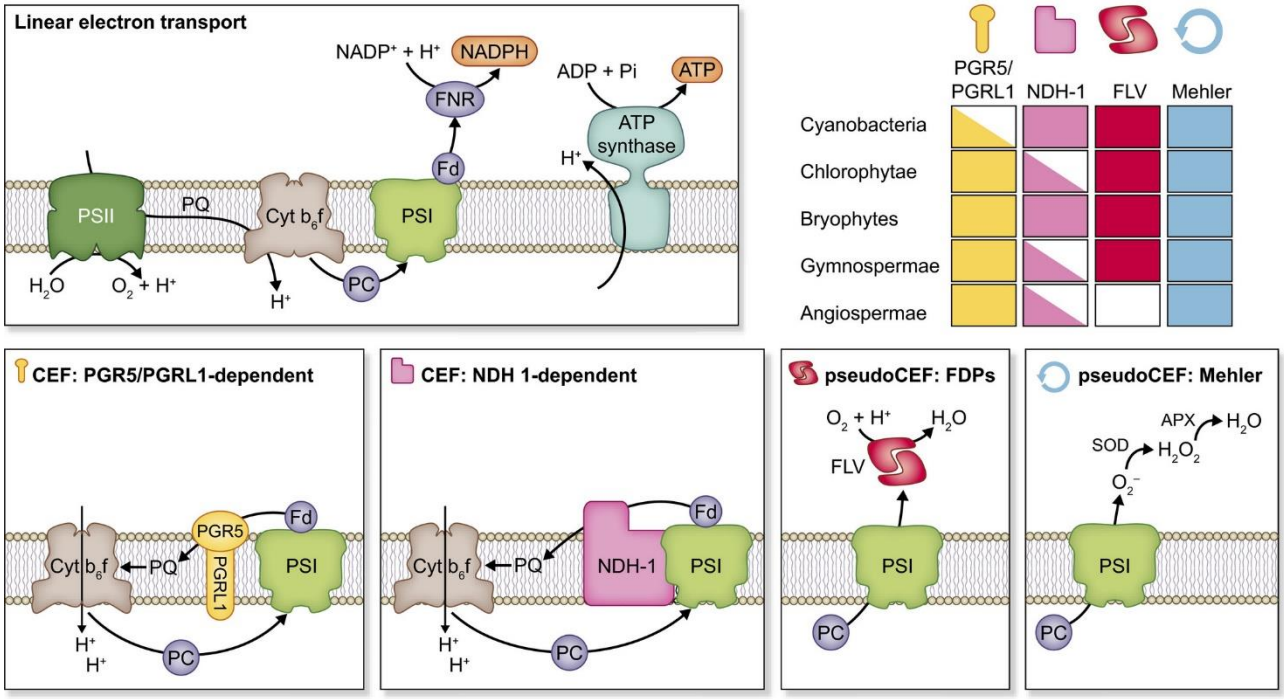

Figure 1. Diversity and distribution of electron transport pathways in oxygenic photosynthetic organisms. Linear electron flow (LEF) involves the transport of electrons from water to $NADP^+$, catalyzed by four protein complexes present in the thylakoid membranes (photosystem I, PSI; photosystem II, PSII; cytochrome (Cyt)b_6f, ATP synthase) conserved from cyanobacteria to vascular plants. PSII reduces plastoquinone (PQ) to plastoquinol (PQH_2), while $Cytb_6f$ transports electrons from PQH_2 to the water-soluble plastocyanin (PC), which serves as electron donor to PSI. Electrons from PSI are then transferred to the stromal acceptor ferredoxin (Fd) and through ferredoxin-$NADP^+$ reductase (FNR), finally used to synthesize NADPH. Alternative electron pathways are also present to modulate electron transport efficiency. This modulation involves cyclic electron flow (CEF) around PSI (PGR5/PGRL1-dependent and NDH-1-dependent) and pseudo-CEF (or water–water cycle) (i.e. Mehler reaction and flavodiiron protein (FLV or FDP)-dependent). These pathways are instead not equally distributed in different phylogenetic groups, and their distribution is represented with color coding to indicate their presence (split in case of presence only in some family members). In some cases, the activity was not functionally demonstrated and is thus inferred from genome sequence analyses. APX, ascorbate peroxidase; Pi, inorganic phosphate; SOD, superoxide dismutase.

II. Diversity of molecular mechanisms for regulation of photosynthetic electron transport

CEF and PCEF activities are found in all photosynthetic organisms, but they are not equally distributed, as schematized in Fig. 1. This observation suggests that the mechanisms for the fine control of photosynthetic electron transport changed during colonization of novel ecological niches and adaptation to habitats with different light availability, ultraviolet radiation and water limitations (Hohmann-Marriott & Blankenship, 2011; de Vries & Archibald, 2018). Exploration of mechanistic diversity in different photosynthetic organisms is critical to better understand their evolution and the physiological role of these reactions.

The PGR5/PGRL1-mediated CEF has been identified in plants (Munekage *et al*., 2002; DalCorso *et al*., 2008), and corresponding genes were also found in green eukaryotic algae (Peltier *et al*., 2010; Jokel *et al*., 2018). The chloroplast multimeric NDH complex (NDH-1) (Shikanai *et al*., 1998) acts as a ferredoxin-dependent PQ reductase with proton-pumping activity and it has been characterized in angiosperms, but its presence was described also in the Streptophyta alga *Klebsormidium flaccidum* (Hori *et al*., 2014). However, some lineages of seed plants, mainly gymnosperms, showed the loss of plastid NDH genes (Ruhlman *et al*., 2015). Chlorophyte algae such as *Chlamydomonas reinhardtii* are instead missing NDH-1 and rely on the chloroplast monomeric NDH-2, an NAD(P)H dehydrogenase without proton-pumping activity (Peltier *et al*., 2010).

PSI in the presence of oxygen can produce superoxide, which is then reduced to H_2O_2, in a process called the Mehler reaction, before being reduced to water in a process generally called the water–water cycle (Asada, 2000). FLVs are instead more unevenly distributed, with up to six genes found in cyanobacteria (Zhang *et al*., 2009) involved in the photoprotection of both PSI and PSII (Allahverdiyeva *et al*., 2013). Eukaryotic photosynthetic organisms have maintained only two genes (named *FLVA* and *FLVB*), and molecular evidence of FLV activity has recently emerged in chlorophyte algae (Jokel *et al*., 2015; Chaux *et al*., 2017), nonvascular plants (Gerotto *et al*., 2016; Shimakawa *et al*., 2017) and gymnosperms (Ilík *et al*., 2017), whereas the corresponding genes are not found in any known angiosperm (Fig. 1). In eukaryotes, the FLVA–FLVB complex forms a heterodimer, and the oligomeric state is fundamental for protein function, since in *Physcomitrella patens* and *C. reinhardtii* the removal of one protein leads to the loss of the other (Gerotto *et al*., 2016; Chaux *et al*., 2017).

CEF and PCEF have been shown to play a fundamental role in PSI photoprotection; indeed, corresponding mutants showed PSI damage and sharp growth defects (Munekage *et al*., 2004; Takahashi *et al*., 2009; Suorsa *et al*., 2012; Gerotto *et al*., 2016). In *C. reinhardtii*, growth was shown to be drastically more impacted when PSI, rather than PSII, was damaged (Larosa *et al*., 2018). These observations suggest that photosynthetic organisms evolved a protection strategy with eventual photodamage targeting one PS, PSII, which is efficiently repaired while maintaining the activity of the other intact. This strategy could also provide another advantage, in that a protected PSI can still sustain some ATP synthesis even in the case of major PSII damage (Huang *et al*., 2018).

III. Role of FLVs in the regulation of photosynthesis in eukaryotes

Mutants depleted in FLVs showed strong photosensitivity when exposed to fluctuating light, demonstrating a physiological role particularly relevant to these conditions (Gerotto *et al*., 2016; Chaux *et al*., 2017; Shimakawa *et al*., 2017). As schematized in Fig. 2, based on data from *P. patens* (Gerotto *et al*., 2016), when dark-adapted plants are exposed to strong irradiance, linear electron transport takes a few minutes to become fully activated, in correspondence with the activation of the CB cycle. During the first seconds of illumination, FLVs are the main sink of electrons downstream of PSI and are responsible for 40–60% of the total electron flow (Gerotto *et al*., 2016; Chaux *et al*., 2017; Shimakawa *et al*., 2017).

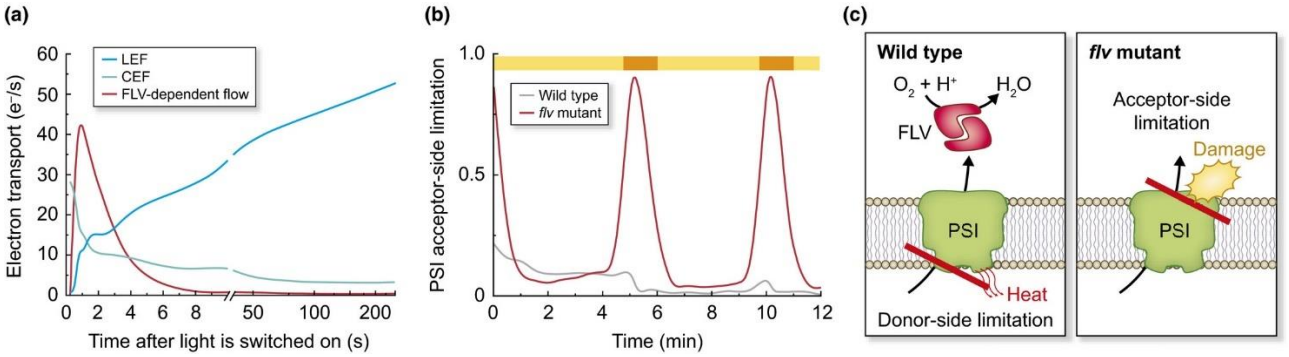

Figure 2. Flavodiiron protein (FLV) function in dissipating excess electrons, protecting photosystem I (PSI) from overexcitation. (a) Relative contribution to total electron transport after light is switched on in *Physcomitrella patens* plants, based on data from Gerotto *et al*. (2016). Cyclic electron flow (CEF) is estimated using the photosystem II (PSII) inhibitor 3-(3,4-dichlorophenyl)-1,1-dimethylurea and the FLV-dependent pseudo-(CEF) from the differences between the wild-type (WT) and *flv* plants, and linear electron flow (LEF) represents all residual electron flow, thus including the Mehler reaction. The data used to build the graph have up to 20% standard deviation, not reported. (b) Effect of FLV activity in *P. patens* response to fluctuation, based on data from Gerotto *et al*. (2016). The *flv* mutants exposed to alternating limiting/strong illumination (indicated by yellow/orange bars) show acceptor-side limitation every time the light in increased, whereas the WT plants are limited from the donor side. (c) Scheme of FLV role. In WT electron transport, the rate-limiting step is the transport from cytochrome b_6f to PSI, making the latter limited from the donor side, where it can withstand even intense illumination. In *flv* mutants, instead, every time the light suddenly increases, electron transport is limited by the ability of PSI to donate electrons. Electrons accumulated at the stromal side of PSI are dangerous, leading to damage to iron–sulfur clusters.

Sustained FLV electron transport activity is transient, but it avoids the accumulation of electrons at the PSI acceptor side when LEF is limited and NADPH consumption is thus slow. This effect is clear in *flv* mutants that show a PSI acceptor-side limitation upon saturating illumination, meaning that the activity is limited by $NADP^+$ availability (Gerotto *et al*., 2016), whereas wild-type plants are limited from the donor side (Fig. 2). This difference has major implications for photosensitivity because PSI can sustain intense illumination when oxidized as $P700^+$, owing to its efficient ability to dissipate energy as heat (Bukhov & Carpentier,2003), although it is damaged by overreduction when electron donors are available but acceptors are limiting. In these conditions, in fact, electrons accumulated at the PSI acceptor side can react with the iron–sulfur centers present in the stromal side of the complex, causing oxidative damage (Tiwari *et al*., 2016).

FLV activity, while relaxing PSI overreduction, also contributes to the generation of a ΔpH across the thylakoid membrane because of $Cytb_6f$ activity and the different localization of water splitting and regeneration. FLV activity thus still supports some ATP synthesis and allows the activation of other mechanisms for regulation of photosynthesis, which requires a low lumenal pH such as NPQ. Photosynthetic control, a decrease in $Cytb_6f$ activity, is also induced by a pH decrease, slowing down the electron supply to PSI and thus reducing the risks of overreduction (Eberhard *et al*., 2008).

It is fundamental to mention that the roles of FLVs are biologically relevant not only in dark to light transitions but also every time there is an abrupt change in illumination intensity that causes an imbalance between the photosynthetic electron transport and metabolism capacity of consuming NADPH. This role is eco-physiologically important because, whereas dark-to-light transitions are less frequent, plants and algae are continuously exposed to fluctuations in irradiation in their natural environment. In those dynamic light conditions, FLVs can act as a safety valve for excess electrons, reducing their accumulation at the acceptor side of PSI whenever required. As schematized in Fig. 2, mutants depleted of FLVs show a limitation at the acceptor side of PSI every time the light increases, eventually leading to damage and growth reduction (Gerotto *et al*., 2016).

Another remarkable feature of FLVs in photosynthetic organisms is their ability to support intense electron transport for a limited time while their activity become later undetectable. FLVs are competing for reducing power with carbon fixation, and thus a constitutive activity is potentially detrimental for overall photosynthetic efficiency. There is presently no experimental evidence supporting that the decrease in FLV activity is simply due to a lower affinity for electron donors or if post-translational mechanisms are responsible for its inactivation. An inspiring hypothesis is that

FLVs could be inhibited by light via redox regulation in the stroma, since this signal also activates its major competing pathway for electrons, namely carbon fixation.

IV. Why were FLVs lost in angiosperms?

Considering the recent evidence showing the prominent FLV role in response to light dynamics in cyanobacteria, algae and nonvascular plants, it is puzzling to observe that this protein was lost in angiosperms. Moss FLVA and -B are indeed functional upon expression in *Arabidopsis* and rice (*Oryza sativa*) (Yamamoto *et al*., 2016; Wada *et al*., 2017), showing that they do not require any other accessory components to function and demonstrating that there are no structural or mechanistic reasons for their loss. By contrast, this observation suggests that, at some point, FLVs must have provided some selective disadvantage to angiosperm ancestors.

One possible explanation is that FLV activity represents an energy loss, since electrons are going back to O_2 with a futile water–water cycle. FLV activity sustains ΔpH and increases the ATP/NADPH ratio, but it is less efficient than CEF, which does not lose electrons but recycles them to the PQ pool. As mentioned earlier, FLVs are inhibited when CB is active, but it is not possible to exclude the presence of a low constitutive activity that could be detrimental when electron transport is limiting for carbon fixation (Foyer *et al*., 2012).

For this energetic cost to be adequately relevant, however, other adaptations are required to cover the role of FLVs in photoprotection by increasing the ability of other pathways to accept electrons from PSI and avoid the risks of acceptor-side limitation. Angiosperms indeed rely more than mosses do on CEF for supporting electron transport after an abrupt change in illumination and avoid PSI overreduction (Joliot & Johnson, 2011; Kono *et al*., 2014). Indeed, ablation of the PGR5/PGRL1 CEF in *Arabidopsis* results in a lethal phenotype when exposed to fluctuating light (Suorsa *et al*., 2012), whereas analogous mutants in the same conditions do not show a growth phenotype in *P. patens* (Kukuczka *et al*., 2014). *P. patens* plants consistently show small cyclic electron transport activity (Fig. 2), but this is enhanced in *flv* mutants (Gerotto *et al*., 2016).

It should also be considered that other adaptations can play a major influence in altering the NADPH demand. One interesting possibility comes from the observation that angiosperms and gymnosperms differ in leaf morphology and stomata regulation, with implications on gas exchange efficiency. Investigations of paleoclimate suggested that angiosperm origination corresponds with a decrease in atmospheric CO_2 levels, as these plants were allegedly favored owing to their higher density of

vascular veins and stomata and their improved ability to control CO_2 levels in leaves while also minimizing water losses (McElwain *et al.*, 2016). If angiosperms are indeed more efficient in gas exchange management, then CO_2 will be on average more available, making FLV activity less strategic. In other words, if conditions where CO_2 is strongly limiting are less frequent, this reduces the advantage of FLV activity, potentially making CEF and other electron acceptor pathways sufficient to ensure PSI protection.

V. CONCLUSIONS

FLVs have been recently shown in cyanobacteria, green algae, mosses and liverworts to be seminal in protecting photosynthetic apparatus upon abrupt increases of light intensity. Mutants impaired in FLV expression showed severe phenotypes if exposed to fluctuating illumination. FLV-encoding sequences were nevertheless lost during evolution by angiosperms thanks to an increased efficiency of other mechanisms capable of accepting electrons from PSI, making the FLV activity in protection from overreduction superfluous or even detrimental.

ACKNOWLEDGEMENTS

A.A. acknowledges the support from Università degli Studi di Padova, Dipartimento di Biologia (BIRD173749/17). T.M. acknowledges the financial support by the European Research Council (BIOLEAP grant no. 309485).

REFERENCES

Allahverdiyeva Y, Mustila H, Ermakova M, Bersanini L, Richaud P, Ajlani G, Battchikova N, Cournac L, Aro E-M. 2013. Flavodiiron proteins Flv1 and Flv3 enable cyanobacterial growth and photosynthesis under fluctuating light. *Proceedings of the National Academy of Sciences, USA* 110: 4111–4116.

Asada K. 2000. The water–water cycle as alternative photon and electron sinks. *Philosophical Transactions of the Royal Society B: Biological Sciences* 355: 1419–1431.

Bukhov NG, Carpentier R. 2003. Measurement of photochemical quenching of absorbed quanta in photosystem I of intact leaves using simultaneous measurements of absorbance changes at 830 nm and thermal dissipation. *Planta* 216: 630–638.

Chaux F, Burlacot A, Mekhalfi M, Auroy P, Blangy S, Richaud P, Peltier G. 2017. Flavodiiron proteins promote fast and transient O_2 photoreduction in *Chlamydomonas*. *Plant Physiology* 174: 1825–1836.

DalCorso G, Pesaresi P, Masiero S, Aseeva E, Schünemann D, Finazzi G, Joliot P, Barbato R, Leister D. 2008. A complex containing PGRL1 and PGR5 is involved in the switch between linear and cyclic electron flow in Arabidopsis. *Cell* 132: 273–285.

Eberhard S, Finazzi G, Wollman F-A. 2008. The dynamics of photosynthesis. *Annual Review of Genetics*42: 463–515.

Foyer CH, Neukermans J, Queval G, Noctor G, Harbinson J. 2012. Photosynthetic control of electron transport and the regulation of gene expression. *Journal of Experimental Botany* 63: 1637–1661.

Gerotto C, Alboresi A, Meneghesso A, Jokel M, Suorsa M, Aro E-M, Morosinotto T. 2016. Flavodiiron proteins act as safety valve for electrons in *Physcomitrella patens*. *Proceedings of the National Academy of Sciences, USA* 113: 12322–12327.

Hohmann-Marriott MF, Blankenship RE. 2011. Evolution of photosynthesis. *Annual Review of Plant Biology* 62: 515–548.

Hori K, Maruyama F, Fujisawa T, Togashi T, Yamamoto N, Seo M, Sato S, Yamada T, Mori H, Tajima N *et al*. 2014. *Klebsormidium flaccidum* genome reveals primary factors for plant terrestrial adaptation. *Nature Communications* 5: e3978.

Huang W, Yang Y-J, Zhang S-B, Liu T. 2018. Cyclic electron flow around photosystem I promotes ATP synthesis possibly helping the rapid repair of photodamaged photosystem II at low light. *Frontiers in Plant Science* 9: e239.

Ilík P, Pavlovič A, Kouřil R, Alboresi A, Morosinotto T, Allahverdiyeva Y, Aro E-M, Yamamoto H, Shikanai T. 2017. Alternative electron transport mediated by flavodiiron proteins is operational in organisms from cyanobacteria up to gymnosperms. *New Phytologist* 214: 967–972.

Jokel M, Johnson X, Peltier G, Aro E-M, Allahverdiyeva Y. 2018. Hunting the main player enabling *Chlamydomonas reinhardtii* growth under fluctuating light. *Plant Journal: For Cell and Molecular Biology*94: 822–835.

Jokel M, Kosourov S, Battchikova N, Tsygankov AA, Aro EM, Allahverdiyeva Y. 2015. *Chlamydomonas*flavodiiron proteins facilitate acclimation to anoxia during sulfur deprivation. *Plant & Cell Physiology* 56: 1598–1607.

Joliot P, Johnson GN. 2011. Regulation of cyclic and linear electron flow in higher plants. *Proceedings of the National Academy of Sciences, USA* 108: 13317–13322.

Kono M, Noguchi K, Terashima I. 2014. Roles of the cyclic electron flow around PSI (CEF-PSI) and O_2-dependent alternative pathways in regulation of the photosynthetic electron flow in short-term fluctuating light in *Arabidopsis thaliana*. *Plant & Cell Physiology* 55: 990–1004.

Kukuczka B, Magneschi L, Petroutsos D, Steinbeck J, Bald T, Powikrowska M, Fufezan C, Finazzi G, Hippler M. 2014. Proton gradient regulation5-Like1-mediated cyclic electron flow is crucial for acclimation to anoxia and complementary to nonphotochemical quenching in stress adaptation. *Plant Physiology* 165: 1604–1617.

Larosa V, Meneghesso A, La Rocca N, Steinbeck J, Hippler M, Szabò I, Morosinotto T. 2018. Mitochondria affect photosynthetic electron transport and photosensitivity in a green alga. *Plant Physiology* 176: 2305–2314.

Li Z, Wakao S, Fischer BB, Niyogi KK. 2009. Sensing and responding to excess light. *Annual Review of Plant Biology* 60: 239–260.

McElwain JC, Yiotis C, Lawson T. 2016. Using modern plant trait relationships between observed and theoretical maximum stomatal conductance and vein density to examine patterns of plant macroevolution. *New Phytologist* 209: 94–103.

Munekage Y, Hashimoto M, Miyake C, Tomizawa K, Endo T, Tasaka M, Shikanai T. 2004. Cyclic electron flow around photosystem I is essential for photosynthesis. *Nature* 429: 579–582.

Munekage Y, Hojo M, Meurer J, Endo T, Tasaka M, Shikanai T. 2002. *PGR5* is involved in cyclic electron flow around photosystem I and is essential for photoprotection in *Arabidopsis*. *Cell* 110: 361–371.

Peltier G, Tolleter D, Billon E, Cournac L. 2010. Auxiliary electron transport pathways in chloroplasts of microalgae. *Photosynthesis Research* 106: 19–31.

Ruhlman TA, Chang W-J, Chen JJ, Huang Y-T, Chan M-T, Zhang J, Liao D-C, Blazier JC, Jin X, Shih M-C *et al*. 2015. NDH expression marks major transitions in plant evolution and reveals coordinate intracellular gene loss. *BMC Plant Biology* 15: e100.

Shikanai T, Endo T, Hashimoto T, Yamada Y, Asada K, Yokota A. 1998. Directed disruption of the tobacco *ndhB* gene impairs cyclic electron flow around photosystem I. *Proceedings of the National Academy of Sciences, USA* 95: 9705–9709.

Shimakawa G, Ishizaki K, Tsukamoto S, Tanaka M, Sejima T, Miyake C. 2017. The liverwort, *Marchantia*, drives alternative electron flow using a flavodiiron protein to protect PSI. *Plant Physiology* 173: 1636–1647.

Suorsa M, Järvi S, Grieco M, Nurmi M, Pietrzykowska M, Rantala M, Kangasjärvi S, Paakkarinen V, Tikkanen M, Jansson S *et al*. 2012. PROTON GRADIENT REGULATION5 is essential for proper acclimation of *Arabidopsis* photosystem I to naturally and artificially fluctuating light conditions. *Plant Cell* 24: 2934–2948.

Takahashi S, Milward SE, Fan D-Y, Chow WS, Badger MR. 2009. How does cyclic electron flow alleviate photoinhibition in Arabidopsis? *Plant Physiology* 149: 1560–1567.

Teicher HB, Lindberg Møller B, Vibe Scheller H. 2000. Photoinhibition of Photosystem I in field-grown barley (*Hordeum vulgare* L.): induction, recovery and acclimation. *Photosynthesis Research* 64: 53–61.

Tikkanen M, Mekala NR, Aro E-M. 2014. Photosystem II photoinhibition-repair cycle protects Photosystem I from irreversible damage. *Biochimica et Biophysica Acta* 1837: 210–215.

Tiwari A, Mamedov F, Grieco M, Suorsa M, Jajoo A, Styring S, Tikkanen M, Aro E-M. 2016. Photodamage of iron–sulphur clusters in photosystem I induces non-photochemical energy dissipation. *Nature Plants*2: e16035.

de Vries J, Archibald JM. 2018. Plant evolution: landmarks on the path to terrestrial life. *New Phytologist*217: 1428–1434.

Wada S, Yamamoto H, Suzuki Y, Yamori W, Shikanai T, Makino A. 2017. Flavodiiron protein substitutes for cyclic electron flow without competing CO_2 assimilation. *Plant Physiology* 176: 1509–1518.

Yamamoto H, Takahashi S, Badger MR, Shikanai T. 2016. Artificial remodelling of alternative electron flow by flavodiiron proteins in *Arabidopsis*. *Nature Plants* 2: e16012.

Zhang P, Allahverdiyeva Y, Eisenhut M, Aro E-M. 2009. Flavodiiron proteins in oxygenic photosynthetic organisms: photoprotection of photosystem II by Flv2 and Flv4 in *Synechocystis* sp. PCC 6803. *PLoS ONE*4: e5331.

CHAPTER 3

Role of cyclic and pseudo-cyclic electron transport in response to dynamic light changes in *Physcomitrella patens*

Authors name and affiliation

Mattia Storti[1], Alessandro Alboresi[1], Caterina Gerotto[2], Eva-Mari Aro[2], Giovanni Finazzi[3] and Tomas Morosinotto[1]

[1] Dept. of Biology, University of Padova, 35121 Padova, Italy;

[2] Dept. of Biochemistry, Molecular Plant Biology, University of Turku, FI-20014 Turku, Finland

[3] Laboratoire de Physiologie Cellulaire et Végétale, UMR 5168, Centre National de la Recherche Scientifique (CNRS), Commissariat à l'Energie Atomique et aux Energies Alternatives (CEA), Université Grenoble Alpes, Institut National Recherche Agronomique (INRA), Institut de Recherche en Sciences et Technologies pour le Vivant (iRTSV), CEA Grenoble, F-38054 Grenoble cedex 9, France

THIS CHAPTER WAS ACCEPTED FOR PUBLICATION IN "*PLANT, CELL & ENVIRONMENT*".

CONTRIBUTION

MS performed most of the experiments presented in this work

ABSTRACT

Photosynthetic organisms support cell metabolism by harvesting sunlight and driving the electron transport chain at the level of thylakoid membranes. Excitation energy and electron flow in the photosynthetic apparatus is continuously modulated in response to dynamic environmental conditions. Alternative electron flow around photosystem I plays a seminal role in this regulation contributing to photo-protection by mitigating over-reduction of the electron carriers.

Different pathways of alternative electron flow coexist in the moss *Physcomitrella patens*, including cyclic electron flow mediated by the PGRL1/PGR5 complex and pseudo-cyclic electron flow mediated by the flavodiiron proteins FLV. In this work we generated *P. patens* plants carrying both *pgrl1* and *flva* knock-out (KO) mutations. A comparative analysis of the WT, *pgrl1*, *flva* and *pgrl1 flva* lines suggests that cyclic and pseudo-cyclic processes have a synergic role in the regulation of photosynthetic electron transport. However, while both contribute to photosystem I protection from over-reduction by modulating electron flow following changes in environmental conditions, FLV activity is particularly relevant in the first seconds after a light change while PGRL1 has a major role upon sustained strong illumination.

Keywords: Photosynthesis; Bryophyta; Evolution, Molecular; photoprotection; Energy metabolism; Photosynthetic Reaction Center Complex Proteins;

INTRODUCTION

Life on earth largely depends on oxygenic photosynthesis which enables plants, algae and cyanobacteria to convert light into chemical energy. Sunlight powers the transfer of electrons from water to $NADP^+$ by the activity of two photosystems (PS), PSII and PSI, generating NADPH and ATP to sustain cell metabolism. Natural environmental conditions are highly variable, and changes in sunlight irradiation drastically affect electron flow. ATP and NADPH consumption rates are also dynamic following the different demands from various metabolic pathways (Kulheim *et al.* 2002; Peltier, Tolleter, Billon & Cournac 2010; Allahverdiyeva, Suorsa, Tikkanen & Aro 2015b; Bailleul *et al.* 2015). Photosynthetic organisms are able to thrive in such a dynamic environment thanks to the evolution of mechanisms that divert/feed electrons from/to linear transport chain to adjust ATP and NADPH production based on metabolic and environmental constraints (Allen 2002; Shikanai 2016; Shikanai & Yamamoto 2017).

Photosynthetic electron transport is modulated by proton accumulation in the lumen that inhibits the activity of cytochrome b_6f (Cyt b_6f) (Stiehl & Witt 1969; Rumberg & Siggel 1969; Nishio & Whitmarsh 1993; Finazzi & Rappaport 1998), avoiding PSI over-reduction (Joliot & Johnson 2011). A second mechanism for regulation is cyclic electron flow (CEF) around PSI, in which electrons are redirected from PSI to PQ or Cyt b_6f (Arnon & Chain 1975), contributing to proton translocation and ATP synthesis without NADPH formation (Peltier, Aro & Shikanai; Munekage *et al.* 2002; Peng, Fukao, Fujiwara, Takami & Shikanai 2009; Joliot & Johnson 2011; Shikanai 2014). Cyclic electron activity is important to modulate electron transport under different illumination conditions in different plant species (Yamori, Sakata, Suzuki, Shikanai & Makino 2011; Suorsa *et al.* 2012; Kono, Noguchi & Terashima 2014; Kukuczka *et al.* 2014). Two CEF pathways have been identified in plants, one related to the PGR5/ PGRL1 complex (Munekage *et al.* 2002; DalCorso *et al.* 2008; Hertle *et al.* 2013) and the other to a NADH dehydrogenase like complex (Peltier *et al.*; Shikanai *et al.* 1998).
Alternative, electron flow can occur via the water-water cycles (i.e. Mehler reaction and Flavodiiron proteins), also known as pseudo-cyclic (PCEF) pathways, because they also contribute to the generation of ΔpH without net NADPH production (Shikanai & Yamamoto 2017). These cycles include Mehler reaction, i.e. electron flow from the PSI Fe-S clusters or from ferredoxin to molecular oxygen (Mehler 1951) and electron transport catalysed by Flavodiiron proteins (known as FLV or FDP, (Helman *et al.* 2003; Allahverdiyeva *et al.* 2013; Allahverdiyeva, Isojärvi, Zhang & Aro 2015a)) likely using ferredoxin (Jokel, Johnson, Peltier, Aro & Allahverdiyeva 2018) as electron donor. Two Flavodiiron proteins, called FLVA/B in eukaryotes, are especially active in mediating responses to dynamic light conditions, protecting PSI from light stress under fluctuating light conditions (Allahverdiyeva *et al.* 2013; Gerotto *et al.* 2016; Shimakawa *et al.* 2017; Chaux *et al.* 2017). FLVs are present in cyanobacteria, green algae, non-vascular plants and gymnosperms, but they were lost by Angiosperms (Ilík *et al.* 2017). In flowering plants, CEF would replace FLV activity, based on the observation that FLV can complement light sensitivity of angiosperm *pgr5* mutants (Yamamoto, Takahashi, Badger & Shikanai 2016; Wada *et al.* 2017).
In the moss *P. patens* both CEF and FLV are active and mutants depleted in the latter showed increased cyclic activity, suggesting a compensatory role of the two mechanisms (Gerotto *et al.* 2016). To test this hypothesis and further investigate the influence of these mechanisms of photosynthetic electron transport in an organism where they are naturally present, we generated *P. patens* mutants depleted in both FLVA and PRGL1. A comparison of the single and the double mutant showed that the latter had a more severe phenotype, showing that these mechanisms play a synergic role in protecting photosynthetic apparatus from over-reduction. The two mechanisms, however, differ for

their activation kinetics. FLV role is more prominent for the first minute after an increase in light intensity while PGRL1 takes longer to be activated but remains effective upon sustained illumination.

RESULTS

Double *flva pgrl1* KO mutants of *P. patens* were generated using homologous recombination to disrupt the *FLVA* gene (Gerotto *et al.* 2016) in a *pgrl1* KO background (Kukuczka *et al.* 2014) (Figure 1 and Supplementary Figure S1). Results from two independent lines are reported but more than 10 clones with an insertion in the expected target locus were isolated. *FLVA* expression was lost in *flva pgrl1* KO mutants as shown by RT-PCR (Figure 1A) and western blotting analysis confirmed the absence of FLVA protein accumulation (Figure 1B). We also observed that in the absence of FLVA, *FLVB* gene was transcribed but there was an impairment of FLVB protein accumulation, consistent with previous suggestions that FLVA and B form an hetero-tetramer in plants (Yamamoto *et al.* 2016; Wada *et al.* 2017). *PGRL1* expression was also verified to be absent and, even if antibodies against PGRL1 are not able to detect *P. patens* isoform, the absence of the corresponding protein was verified in parental *pgrl1* KO line by mass spectrometry (Kukuczka *et al.* 2014). Instead, immunoblot analysis showed that also PGR5 was depleted in *pgrl1* KO plants (Figure 1B), as observed in both green algae and angiosperms (DalCorso *et al.* 2008; Jokel *et al.* 2018). The *flva pgrl1* KO plants grown under control conditions showed no major alteration of the photosynthetic apparatus composition with respect to WT as assessed by the similar accumulation of Cyt f, γ-ATPase, PSII (D2 antibody) and of PSI (PSAD antibody, Figure 1B) and by the indistinguishable pigment content (Table S1). This finding is in agreement with previous observations in both *pgrl1* and *flva* single KO lines (Kukuczka *et al.* 2014; Gerotto *et al.* 2016). The content of PSBS and LHCSR, the proteins responsible of another major regulatory mechanism of photosynthesis, Non Photochemical Quenching, (Alboresi *et al.* 2010), were also found to have unaltered accumulation in all mutant lines (Figure 1B).

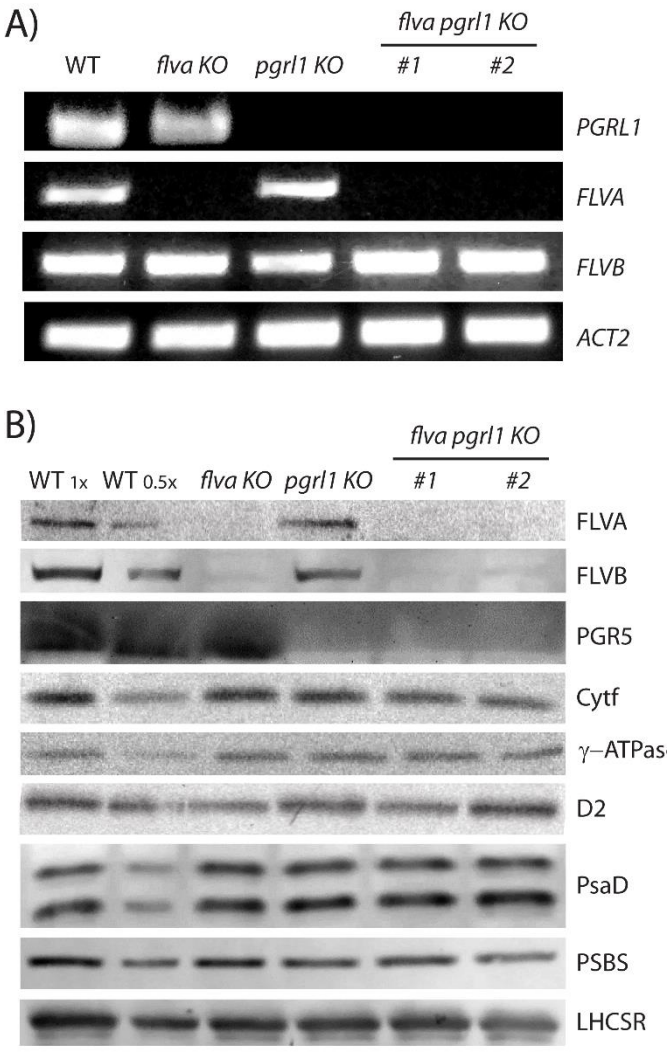

Figure 1. Isolation of *flva pgrl1* double KO plants. *FLVA* was knocked out in *pgrl1* KO plants using homologous recombination. After verifying that the resistance cassette was inserted in the expected genomic region (Figure S1), expression of *PGRL1, FLVA* and *FLVB* was verified by RT-PCR (**A**) and FLVA, FLVB, Cyt f, γ-ATPase, D2, PsaD, PSBS and LHCSR protein accumulation was verified by immunoblot analysis using specific antibodies (**B**). For *flva pgrl1* KO, two representative independent lines are shown. A total extract equivalent to 2.5 µg of Chl (for Cyt f, β-ATPase FLVB, D2 and PsaD) and 5 µg of Chl (for FLVA and PGR5) was loaded for each sample. For WT, 0.5X corresponds to loading half of the extract. For PsaD the double band is likely due to two protein isoforms (Busch *et al.* 2013) and for LHCSR is known to be due to LHCSR1 and LHCSR2 isoforms (Pinnola *et al.* 2013).

FLVA and PGRL1 have a synergic effect on P. patens growth under different light regimes.

The role of FLV and PGRL1 in response to light dynamics was assessed by exposing WT, *flva* KO, *pgrl1* KO and double *flva pgrl1* KO plants to different illumination regimes. Plants were first grown for 10 days in control conditions (CL, 50 µmol photons m^{-2} s^{-1}) and then moved to different light conditions. Some plants were exposed constant light of different intensity (CL; ML, 150 µmol photons m^{-2} s^{-1}; HL, 500 µmol photons m^{-2} s^{-1}) while others were grown in fluctuating light regimes, where cycles of saturating illumination (875, 525 or 250 µmol photons m^{-2} s^{-1}) and limiting light (25 or 50 µmol photons m^{-2} s^{-1}) were repeated during the day, as shown in Figure S2. In these experiments, the duration and intensity of the saturating light were chosen to maintain the total number of photons equivalent to a constant illumination of 150 µmol photons m^{-2} s^{-1} (Figure S2), i.e. the same as in the ML conditions, while exposing plants to dynamic light changes. There were no differences at the

beginning of the experiment, because protonema colonies of the same size were inoculated but they emerged in some cases during the following 3 weeks (Figure S3).

No significant differences in growth were observed between WT and mutant lines in CL conditions. However, clear differences emerged in other illumination regimes (Figure 2; Figure S4). *pgrl1* KO showed the strongest growth inhibition under constant HL but not under fluctuating light, conditions where *flva* KO turned out to be particularly sensitive (Figure 2; Figure S4). *flva pgrl1* KO growth was affected in both cases consistent with the phenotype of the parental lines. Under fluctuating illumination, the FLV effect was preponderant and no significant difference between *flva* KO and *flva pgrl1* KO was detectable provided that saturating light exposure was short (1-minute, Figure S4). However, when the duration of strong illumination was extended to 3 minutes, *flva pgrl1* KO plants showed a significantly stronger phenotype than both single KO genotypes, demonstrating a functional redundancy of FLV and PGRL1 in plants photo-protection. Their synergic phenotype was also evident under HL, where growth reduction became larger in *flva pgrl1* KO than in *pgrl1* KO mutant evidencing an influence of FLV. Overall the growth phenotypes support the hypothesis that FLV and PGRL1 have a partially overlapping role in modulating plant growth.

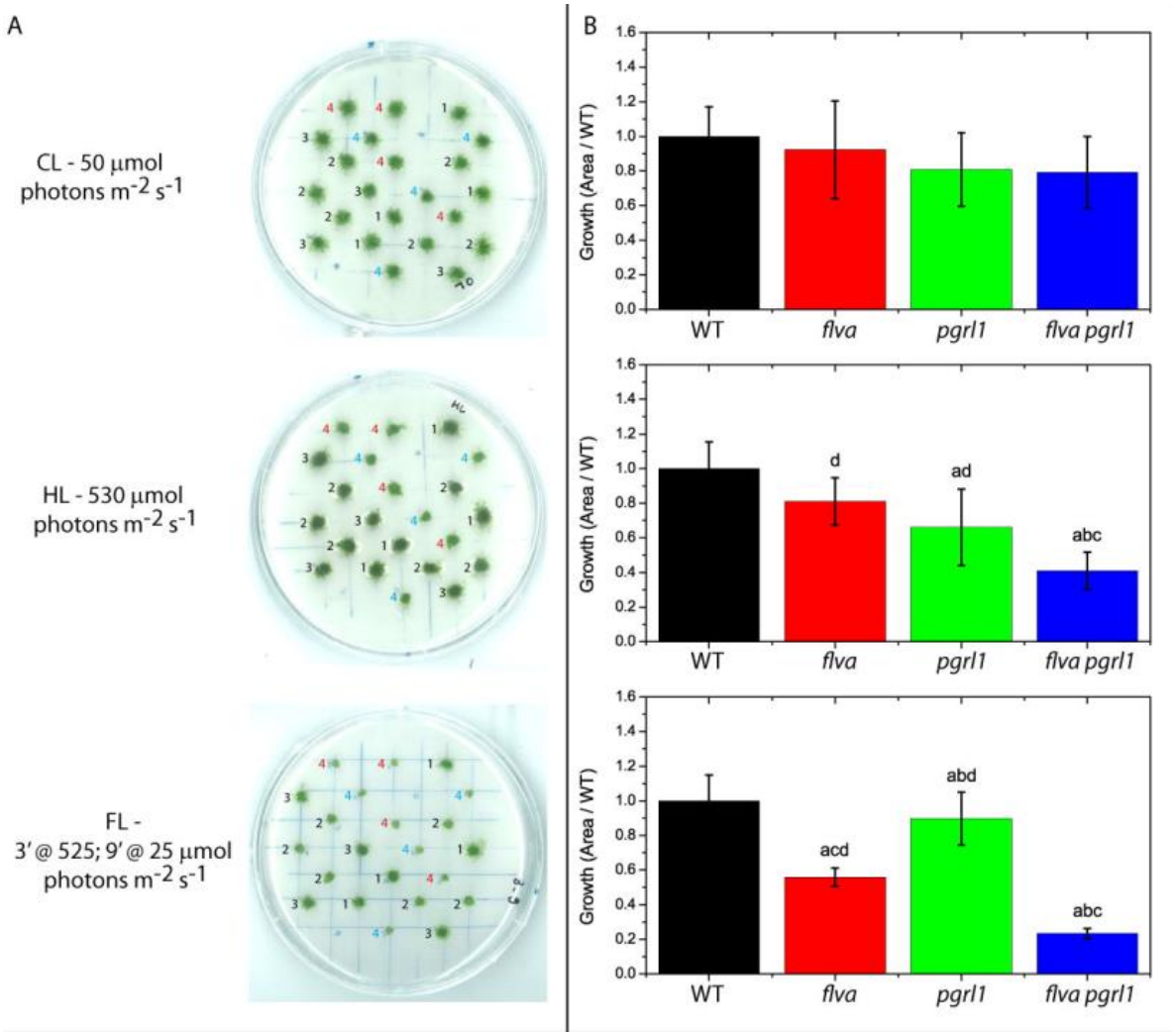

Figure 2. Growth phenotypes of *Physcomitrella patens* plants. A) Representative pictures of plants during growth experiments. **B**) Growth quantification. Plants were grown for 21 days under CL, HL and FL (the case of 3 minutes of intense illumination followed by 9 of low light is shown here). Results from additional conditions are reported in figure S3. Plant position was randomized for each biological replicate (n = 4) but was the same for different light regimes inside the same biological replicate. In panel A, the numbers on the left of each plant indicate the genotypes 1: WT; 2: *flva* KO; 3: *pgrl1* KO; 4: *flva pgrl1* KO. In the latter red and blue numbers indicate two independent lines. B) Plant growth quantified from the size of each plant and normalized to the WT. WT, *flva*, *pgrl1* and *flva pgrl1* KO are shown respectively in black, red, green and blue. a, b, c and d indicate statistically significant difference from WT, *flva*, *pgrl1* and *flva pgrl1* KO respectively. (n = 8-21, $p < 0.001$).

Consequences of different light regimes on photosynthetic activity was assessed by measuring the PSII maximum quantum yield (Figure 3A, Figure S5) and the active PSI/PSII ratio (Figure 3B), by measuring chlorophyll fluorescence and the amplitude of the electrochromic shift (ECS) signal induced by a single turnover saturating flash (Bailleul *et al.* 2010), respectively. The PSI/PSII ratios was largely reduced in the double mutant especially in HL and FL, indicating that the absence of both PGRL1 and FLV strongly affects the content of active PSI. Fluorescence data also revealed a reduction of PSII quantum yield. This suggest that PSII activity was also affected to some extent, although an indirect role due to the alteration in PSI content (e.g. due to the overreduction of PSII acceptors, see below) cannot be ruled out (Tikkanen, Rantala, Grieco & Aro 2017).

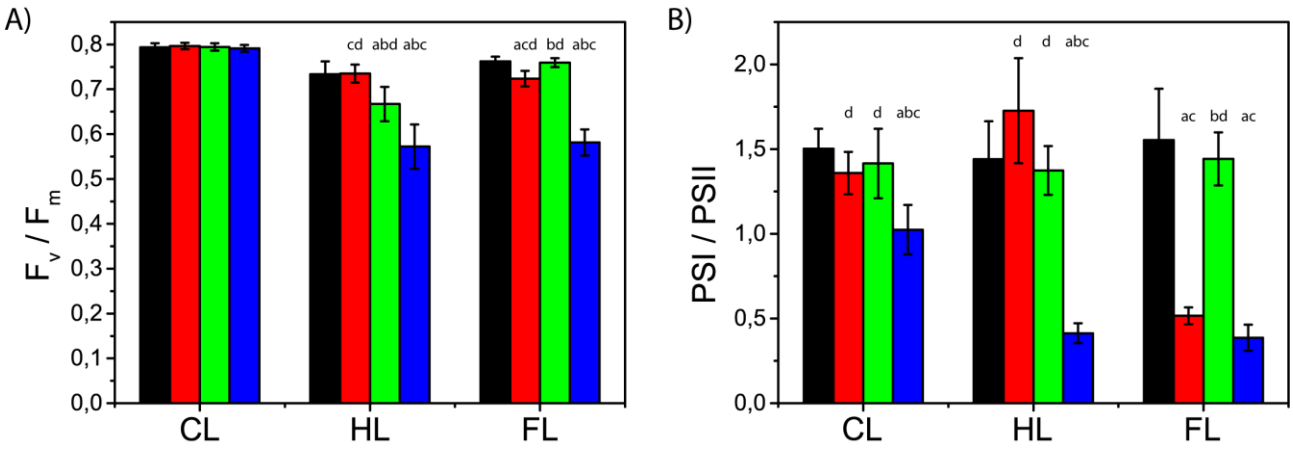

Figure 3 Effect of growing conditions on maximum PSII efficiency and PSI / PSII ratio. Measurements were performed on 12-day old plants exposed to the same growth conditions described in figure 2. **A**) F_v/F_m and **B**) PSI / PSII. WT, *flva*, *pgrl1* and *flva pgrl1* KO are shown respectively in black, red, green and blue. a, b, c and d indicate statistically significant difference from WT, *flva*, *pgrl1* and *flva pgrl1* KO respectively (n = 5-10, $p < 0.001$).

Functional investigation of the PGRL1 and FLV synergy

The influence of FLV and PGRL1 on photosynthetic activity was further investigated *in vivo*. Fluorescence parameters showed that PSII was oversaturated in the light in the absence of FLV and induction of photo-protective responses (NPQ) was slower (Figure S6). This phenomenon was essentially PGRL1 insensitive, *flva pgrl1* KO plants behaving as the single *flva* KO in terms of NPQ induction and PSII efficiency.

The effects on PSI were instead much larger in both *flva* and *flva pgrl1 KO,* which showed a lower Y_I than WT and *pgrl1* upon exposition to saturating light (Figure 4A). Such a reduction in Y_I can be due to a limitation from either the donor or acceptor side and the two cases can be distinguished *in vivo* by applying saturating light flashes to induce P700 oxidation followed by its reduction (Tikkanen, Rantala & Aro 2015). As shown in Figure 4B-C, the PSI efficiency under saturating illumination in WT plants is mainly limited by the donor side, i.e. by electrons transported from PSII via Cyt b_6f. *pgrl1* KO plants behaved in a similar way while *flva* and *flva pgrl1* KO showed a strong acceptor side limitation. *flva* KO plants however quickly recovered and after 2 minutes of illumination they were indistinguishable from the WT while in *flva pgrl1* KO PSI remained strongly limited at the acceptor side. This finding suggests that FLVA is seminal to avoid acceptor side limitation in WT plants after an increase in illumination and that PGRL1 is necessary to recover from this limitation in the absence of FLVA (Figure 4B). Overall, these measurements demonstrated a functional synergy between FLV and PGR5/PGRL1 pathways in maintaining PSI acceptor side oxidised upon illumination changes.

The acceptor side limitation observed in *flva* and *flva pgrl1* KO was dependent on the light intensity, being less pronounced when illumination was less intense. All genotypes, including *flva pgrl1* KO, were able to recover acceptor side limitation to WT levels at 50 µmol photons m^{-1} s^{-1} of actinic light suggesting that other mechanisms are active in accepting electrons from PSI but have lower capacity and are not able to sustain the required electron transport to respond to a strong increase in illumination (Figure 4).

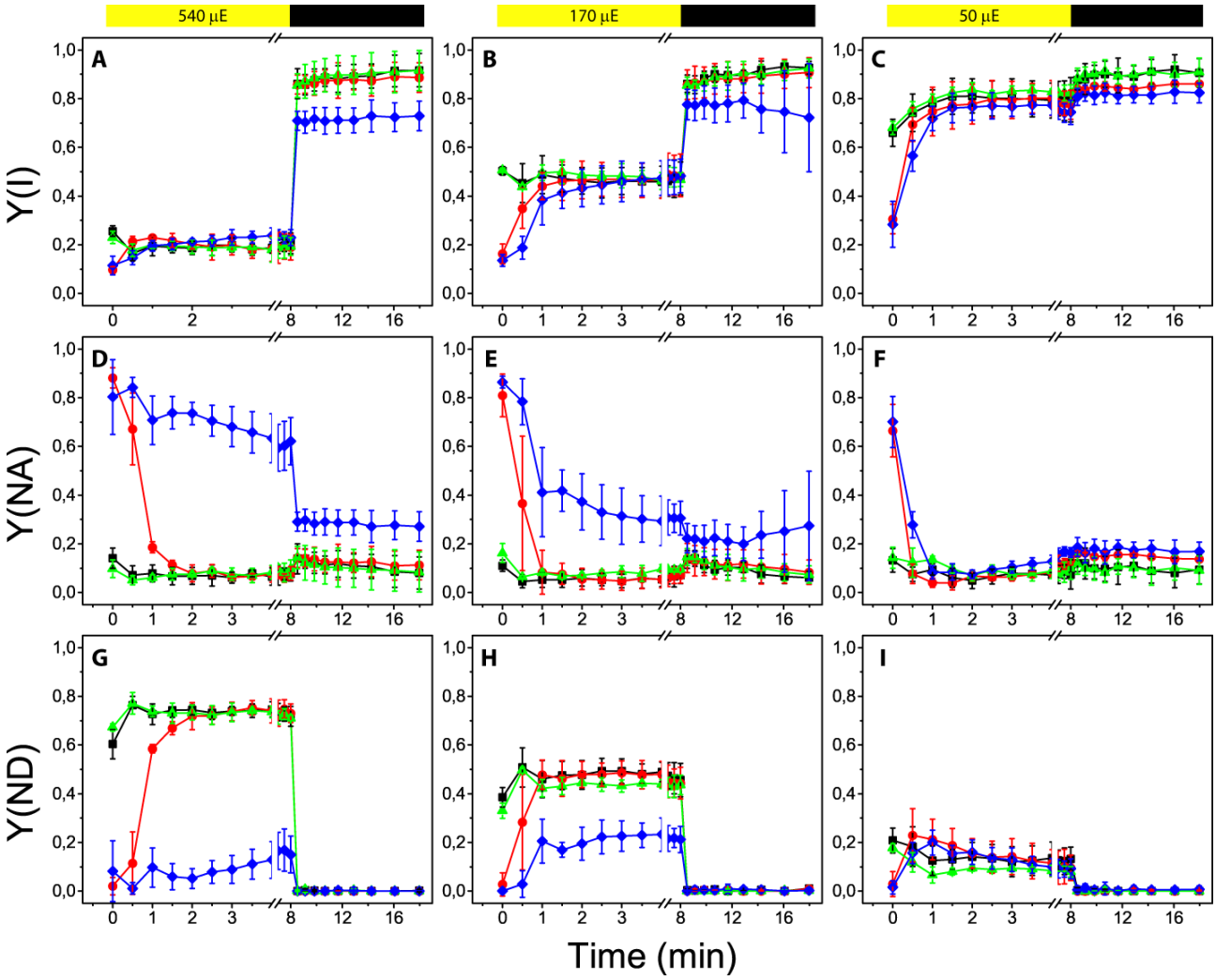

Figure 4. PSI efficiency in *flva pgrl1* KO plants. PSI efficiency was evaluated in different plants using $P700^+$ signal, treating dark adapted plants for 8 minutes by an actinic illumination ((A, D, G) 540, (B, E, H) 175 or (C, F, I) 50 µmol photons m^{-2} s^{-1}) followed by 10 minutes of dark. A-C) PSI yield (Y_I). D-F) PSI acceptor side limitation, Y(NA); G-I) PSI donor side limitation Y(ND). WT, *flva, pgrl1* and *flva pgrl1* are shown respectively as black squares, red circles, green triangles and blue diamonds. Values are expressed as average ± SD of 3-5 independent biological replicates.

To further investigate the effect of *flva* and *pgrl1* KO mutations on PSI activity, we monitored changes in the P700 oxidation state in the light by a different spectrophotometric approach (ΔOD_{705}, Figure S7). WT plants exposed to saturating light showed a largely oxidised P700 and at steady state after 180 seconds of saturating illumination, PSI becoming ≈ 80% oxidised (Figure 5A and S7). The *pgrl1* KO plants behaved as WT, while *flva* plants showed lower levels of PSI oxidation immediately after light was switched on, consistent with their high acceptor side limitation. PSI then was progressively oxidised and after 90 seconds of illumination reaching WT oxidation levels at steady state. Interestingly, no such recovery could be observed in *flva pgrl1* KO where P700 remained highly reduced even in the presence of saturating light, showing a strong and stable acceptor side limitation. These results clearly demonstrated that in the absence of both FLV and PGRL1, residual mechanisms

for PSI re-oxidation are unable to keep P700 oxidized under saturating illumination, consistently with results from Y_I.

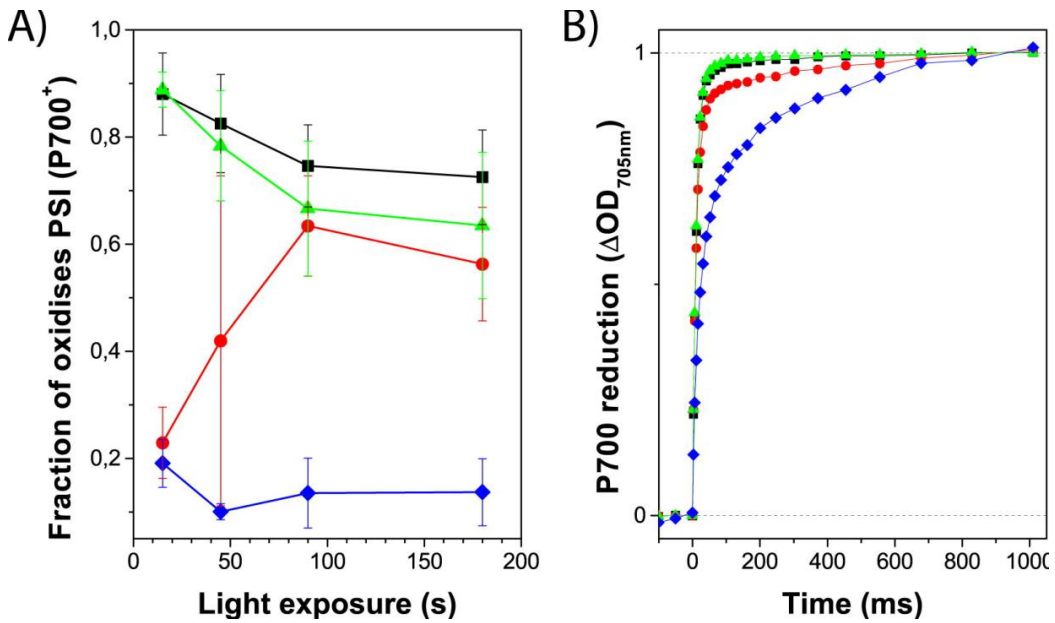

Figure 5. Dependence of PSI oxidation state from illumination duration. A) Dark adapted plants were subjected to saturating constant illumination (940 µmol photons m^{-2} s^{-1}) for different time intervals (15, 45, 90 or 180 s) before light was switched off. Oxidized fraction is expressed as the ratio between $P700^+$ signals at the end of illumination and the maximal oxidation levels obtained by addition of DCMU and DBIMB (examples in Figure S6). Reported values are average ± SD of at least 4 independent replicates for each time point. **B**) $P700^+$ reduction kinetics after 180s actinic light exposure in the different genotypes. WT is shown in black, *flva* KO in red, *pgrl1* KO in green and *flva pgrl1* in blue. Curves shown are average of 4-6 independent measurements.

Similar kinetic measurements were performed to assess the activity of Cyt b_6f, monitoring Cyt f oxidation state from its differential absorption signal at 554 nm (minus a baseline, see methods) in dark-acclimated plants and plants exposed to light for 3 minutes (Figure S8). Cyt b_6f kinetics in *flva pgrl1* KO plants were faster than in WT and both single mutants (Figure S8; Figure 6A). As shown in figure 6A, *flva pgrl1* KO kinetics are significantly different from the other genotypes since P700 and Cyt b_6f have comparable kinetics while in all other genotypes the reduction rate of the former is much faster. Immunoblot analysis showed that these differences in electron transport capacity cannot be explained by an altered accumulation of Cyt b_6f in *flva pgrl1* KO (Figure 1) and it should be attributed to differences in regulation at the level of electron transport.

We thus compared Cyt f^+ and $P700^+$ reduction kinetics to pinpoint the limiting step of photosynthetic electron transport. Electron flow between Cyt b_6f and PSI involves diffusion of Plastocyanin (PC), the electron carrier localized in the lumen of thylakoid membranes. PC diffusion can be restricted in microdomains of the lumen with a cross-section similar to PC size (approximately 3-4 nm in dark-acclimated leaves of *A. thaliana*), thus limiting the rate of electron flow (Kirchhoff, Schöttler, Maurer & Weis 2004). In illuminated thylakoids lumen expands and thus microdomains disappear facilitating

PC mobility, allowing a more efficient electron transport (Kirchhoff 2014; Koochak, Puthiyaveetil, Mullendore, Li & Kirchhoff 2018).

To assess possible differences in PC mobility, we compared the re-reduction kinetics of Cyt f^+ versus that of $P700^+$ in dark and light acclimated samples to evaluate the apparent equilibrium constant deduced, as described earlier (Kirchhoff *et al.* 2004) (Figure 6 C and D, respectively). The theoretical equilibrium constant between Cyt *f* and P700 calculated from the redox potentials of the two cofactors should be 64-312 (Kirchhoff *et al.* 2004). In WT, *pgrl1* KO and light acclimated *flva* KO we found similar values for the calculated equilibrium constant, witnessing an almost perfect redox equilibration between the two complexes. This finding is in agreement with previous results in plants (Kirchhoff *et al.* 2011). In *flva pgrl1* KO but also in dark acclimated *flva* KO, instead, the reduction of $P700^+$ reduction rate resulted in impaired redox equilibration between PSI and its electron donor PC with an apparent equilibrium constant between 1-3 (Figure C and D). Overall, these results suggest that limitation of electron flow at the PSI acceptor side prevents corrects equilibration of electrons between the two complexes.

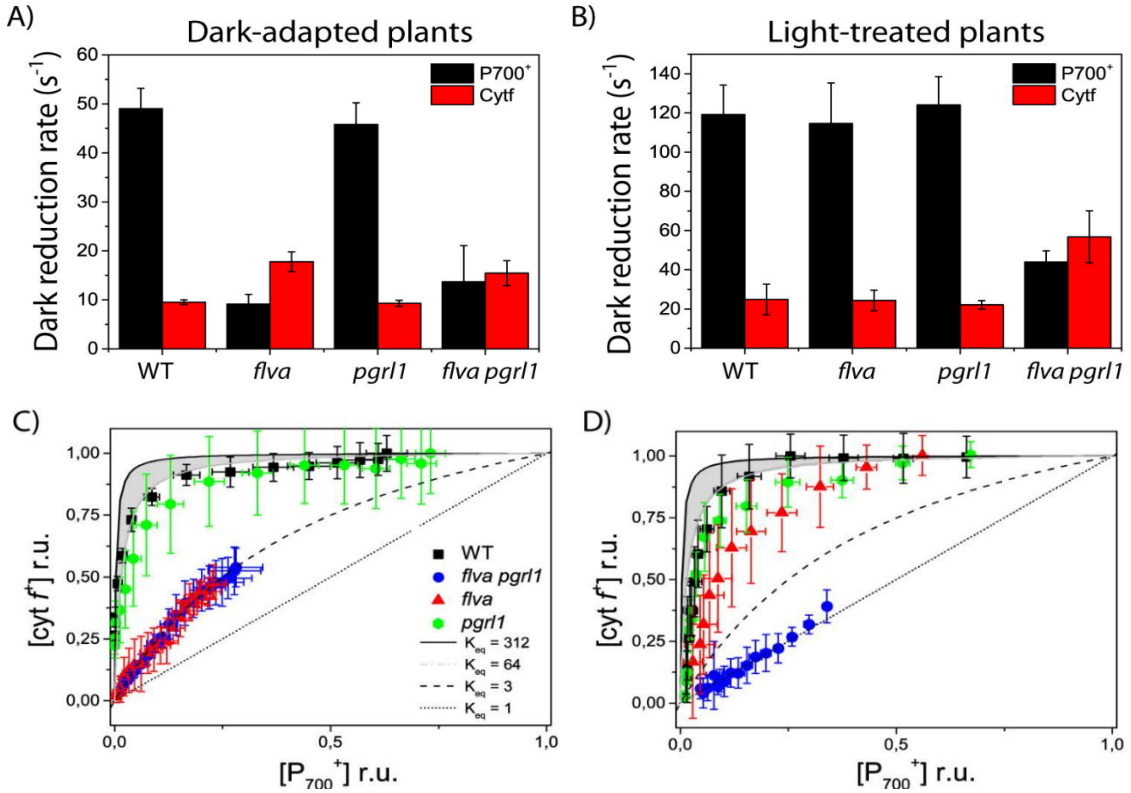

Figure 6. Dark reduction kinetics and equilibrium of P700 and cytochrome f. A-B) half-time of dark reduction kinetics reported in figure S7. Values for P700 (black bars) and Cyt f (red bars) were obtained from dark-adapted (A) and light-treated (B) protonema cells. **C-D**) Equilibration plot of cytochrome f and P700 in dark-adapted (C) and light-treated (D) protonema cells. WT is shown in black, *flva* KO in red, *pgrl1* KO in green and *flva pgrl1* in blue. The grey area indicates the range for theoretical equilibrium between cytochrome *f* and P700 based on their redox potential. Reported values are average ± SD of 4-6 independent replicates for each time point.

Plants maintain steady state proton motive force despite alteration in flva- and pgrl1-dependent electron transport activities

Electron flow generates a proton motive force (pmf), which is required for the synthesis of ATP and, via its ΔpH component, affects photosynthesis by inducing NPQ and lowering the electron transport activity of Cyt b_6f that can be monitored exploiting the ECS signal. Upon exposition to steady saturating illumination all genotypes showed the same ability to generate a transmembrane potential with ECS curves also showing similar kinetics (Figure 7A). Proton conductivity after steady state saturating illumination (180 seconds) was also indistinguishable between the different genotypes, confirming that plants have similar maximal capacity of generating pmf and using this to synthetize ATP (Figure 7B).

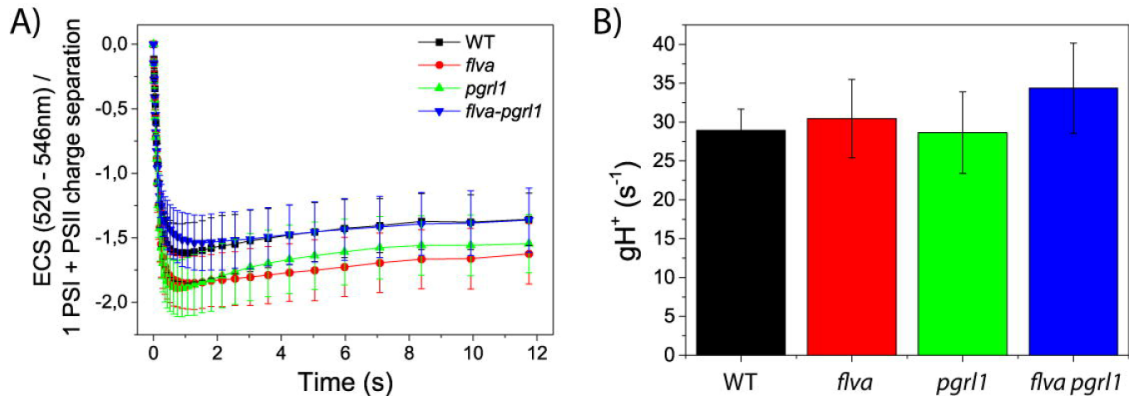

Figure 7. Proton motive force generation. Relaxation of ECS signal in the dark after a saturating light was switched off was exploited to evaluate plants capacity to generate a proton motive force. **A)** ECS signal kinetic after light is switched off. **B**) Proton conductivity (g_{H^+}) calculated form the rate of ECS decay after the actinic light was switched off. WT, *flva*, *pgrl1* and *flva pgrl1* KO are shown respectively in black, red, green and blue. Data reported are average ± SD of 6-10 independent replicates.

Cumulative effects of fluctuating light

Since mutants showed a strong growth phenotype under fluctuating light conditions, we also measured PSI and PSII yield under conditions where plants were exposed to short-term fluctuating light, alternating 3 minutes of saturating light to 9 minutes of limiting illumination. As shown in figure 8, the first high-light treatment has very similar effect on *flva* and *flva pgrl1* KO with an initial lower Y_I that recovered after 2 minutes, as previously observed. The repetitions of strong illumination treatments, however, showed an additive effect with PSI efficiency that did not recover under limiting light phases as in WT and *pgrl1* KO. Decreases in PSI efficiency were long-lasting, and Y_I did not recover even by applying a longer dark treatment at the end of the measurement.

The observed reduction in Y_I was due to acceptor side limitation, which appeared during high light exposure and in *flva pgrl1* KO did not recover during the 9 minutes of dim illumination. Consequently, the following high light treatments had an even larger effect with a consequent increase of severity in acceptor side limitation at each cycle of limiting/saturating illumination. As observed above PSII parameters Y(II), 1-qL and NPQ were similar for all genotypes upon exposition to a first strong light treatment (Figure 8D, E and F). With the repetition of strong illumination in a fluctuating light regime, however, PSII parameters were also affected with a reduction of Y(II) in *flva pgrl1* KO accompanied by an over-reduction of PQ redox state, as evidenced by the 1-qL parameter.

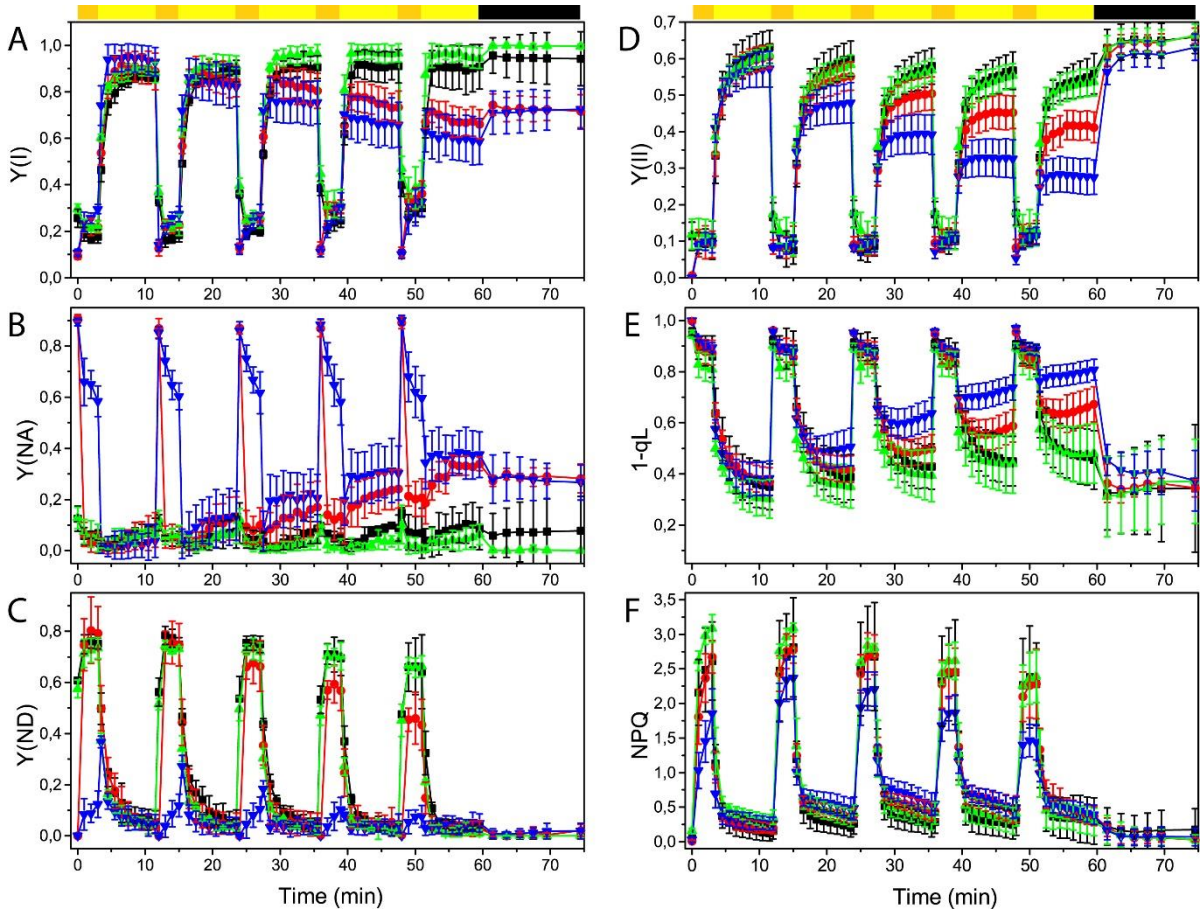

Figure 8. Effect of short-term fluctuating light treatments on PSI and PSII efficiency. PSI Efficiency (Y_I, **A**), its acceptor (YNA, **B**) and donor side limitations (YND, **C**) were monitored together with PSII efficiency parameters (Y_{II} (**D**), PQ redox state (1- qL, **E**) and NPQ (**F**)). Plants were exposed to a fluctuating light cycles by alternating 3 minutes of exposition to 525 µmol photons m^{-2} s^{-1} and 9 minutes to 25 µmol photons m^{-2} s^{-1}. After five cycles plants were left in the dark for 15 minutes. WT is shown in black, *flva* KO line in green, *pgrl1* KO line in blue and *flva pgrl1* KO in red. Values are expressed as average ± SD of at least 3 replicates.

DISCUSSION

Cyclic and pseudo-cyclic electron transport are active in synergy to protect PSI from over-reduction

Regulation of electron transport in photosynthetic organisms is seminal to maintain the balance between light availability and metabolic demands in a highly dynamic environment. Multiple mechanisms such as cyclic electron flow around PSI and pseudo-cyclic pathways capable to divert/feed electrons from/to linear transport chain have been identified unevenly distributed in photosynthetic organisms (Shikanai 2016; Shikanai & Yamamoto 2017; Alboresi, Storti & Morosinotto 2018).

In this work, we investigated the relative contribution of cyclic and pseudo-cyclic electron flow pathways in maintaining a high photosynthetic efficiency by generating a double knock-out mutant of *P. patens* depleted in both FLVA and PGRL1 (Figure 1) (Kukuczka *et al.* 2014; Gerotto *et al.* 2016). In *P. patens*, as in *C. reinhardtii* (Jokel *et al.* 2018) and *A. thaliana* (DalCorso *et al.* 2008), the loss of PGRL1 causes the loss of PGR5 attached to thylakoid membranes and therefore the inactivation of the whole PGR5/PGRL1-dependent CEF pathway. Analysis of the double KO evidenced a clear synergy between the activity of cyclic and pseudo-cyclic electron flow, as shown by the finding that the double mutant presents the most severe growth phenotype under different light conditions. Mutant analysis revealed that growth is reduced, mainly because of a damage to PSI, whose levels are strongly reduced in different conditions (Figure 3). The damage to PSI in turn also affects PSII via the PQ pool that is more easily over-reduced (Figure 8E).

Functional measurements help proposing a mechanistic explanation for the moss phenotypes observed in the different genotypes. The *flva* KO plants suffer strong PSI acceptor side limitation after light is switched on but they recover after a few seconds (Figure 4) (Gerotto *et al.* 2016). In *flva pgrl1* KO, where PGR5/PGRL1-dependent CEF pathway is also inactivated, this acceptor side limitation is instead not recovered, and PSI remains over-reduced. This difference in redox state is highly relevant because an oxidized PSI can withstand exposure to high light intensities, where $P700^+$ is stable thanks to its ability to dissipate energy as heat (Bukhov & Carpentier 2003). On the contrary, over-reduced PSI is instead prone to light damage to Fe-S clusters present on the stromal side of the protein complex (Sonoike, Terashima, Iwaki & Itoh 1995; Tiwari *et al.* 2016). To avoid this phenomenon, other mechanisms capable of accepting electron from PSI are still present and likely active in *flva pgrl1* KO plants (e.g. NDH-dependent cyclic electron transport or the Mehler reaction, whose corresponding genes are present in *P. patens* genome (Alboresi *et al.* 2018; Kato, Odahara, Fukao & Shikanai 2018)). The photorespiration pathway uses ATP and reducing power to regenerate

ribulose-1,5-bisphosphate (RuBP) from 2-phosphoglycolate and it has also been demonstrated to represent a significant electron sink in bryophytes like mosses (Aro, Gerbaud & André 1984) or liverworts (Hanawa *et al.* 2017). While all these remaining transport pathways can alleviate acceptor side limitation at lower light intensities (Figure 4), they are not able to sustain the elevated electron fluxes that are generated under strong illumination. Similar roles of CEF and FLV have been recently reported in the case of the green freshwater alga *Chlamydomonas reinhardtii* (Jokel *et al.* 2018). In this organism, however, CEF activity is mainly active in low oxygen/anaerobic conditions (Finazzi, Furia, Barbagallo & Forti 1999; Takahashi, Clowez, Wollman, Vallon & Rappaport 2013), where FLV are still active, but cannot evacuate alone all the electrons in excess generated by photosynthesis (Burlacot *et al.* 2018).

While acting in synergy, the CEF mediated by PGRL1/PGR5 and the PCEF catalysed by FLVs show different activation kinetics. Even if *flva pgrl1* KO generally showed a stronger phenotype than the single mutants, FLV role is in fact more relevant during the first seconds after abrupt changes in light intensity, while the PRGL1 influence is more evident under prolonged intense illumination (Figure 2, Figure S4).

Despite the observed alterations in the PSI redox state, the *flva pgrl1* KO plants still showed the ability to generate a steady state proton motive force similarly to WT plants, suggesting that there are compensating mechanisms to maintain pmf (Figure 7). Photosynthetic efficiency in dim stable illumination is not affected by the mutations and this can be explained considering that, at stationary state, electron transport activity is largely due to linear electron flow from water to NADPH (Kukuczka *et al.* 2014; Gerotto *et al.* 2016).

While all WT and mutant plants can generate the same pmf in stationary conditions, they show relevant differences when exposed to stronger illumination. In fact, the reduction in Y_I has limited consequences under steady dim illumination but has a strong impact when illumination increases and there is the need of alternative mechanisms capable of accepting extra electrons to avoid PSI over-reduction. Even if they play a minor contribution to electron transport in steady state conditions, thus, FLV and PGRL1/PGR5 ensure that there are extra acceptors for PSI available in case of sudden increases in illumination. The lower ceiling of electron transport capacity in *flva pgrl1* KO plants, as well as their lack of ability to properly equilibrate electrons between PSI and its electron donors (Figure 6C and D), certainly causes a limited ability of increasing their electron transport upon abrupt changes in illumination exposing plants to strong risks of over-reduction with a consequent damage to PSI and impact on growth.

Can alternative electron flows be a disadvantage in some conditions?

P. patens pgrl1 KO mutants can respond well to light fluctuations where they show neither alteration in growth nor significant photodamage (Figure 2-3), at variance with PGR5/PGRL1 mutants in *A. thaliana*, which are instead highly affected in fluctuating light (Suorsa *et al.* 2012). To explain this intriguing observation, we propose that the activity of FLVs can partially compensate for the altered cyclic electron transport, thus mitigating accumulation of electrons at the acceptor side and the consequent damage. This hypothesis is corroborated by results showing that over-expression of heterologous *P. patens* FLV is able to restore PSI acceptor side limitation phenotypes in *Arabidopsis* and rice plants depleted for PGR5 (Yamamoto *et al.* 2016; Wada *et al.* 2017).

This FLV ability to protect PSI from damage also in flowering plants is puzzling, since FLVs have been lost during angiosperm evolution (Ilík *et al.* 2017). Considering the functional overlap observed in this work, CEF is the most likely candidate to protect PSI in the absence of FLV. It is thus possible that upon acquirement of an efficient CEF the selective pressure to keep FLV decreased in Angiosperms ancestors, leading to the gene loss. However, another possibility can be conceived in which FLV were lost because they cause possible disadvantages, e.g. because of energy losses due to the transfer of electrons back to O_2 in a futile water-water cycle that is detrimental in limiting light conditions. The results presented here support this possibility. We in fact observe that *flva pgrl1* KO showed slower growth (Figure 2B), larger reduction of Fv/Fm and more PSI damage (Figure 3) when compared to *pgrl1* KO not only under fluctuating light, but also under constant saturating illumination. This suggests that FLVs are also active in these conditions of steady illumination and consequently it is possible that they have a basal activity even in steady conditions which would be detrimental in limiting light conditions.

MATERIALS AND METHODS

Plant material and treatments

Protonemal tissue of *P. patens*, Gransden wild-type (WT) strain, and knock-out (KO) lines were grown on minimum $PpNO_3$ media in controlled conditions: 24°C, 16 h light/ 8 h dark on photoperiod and light intensity of 50 µmol photons $m^{-2}s^{-1}$ (Control Light, CL), and analyzed after 10 days of growth. The growth phenotype of KO lines was evaluated by growing them at different constant light intensities: 5 (low light, LL), 50 (CL), 150 (medium light, ML) and 500 (high light, HL) µmol photons

$m^{-2}s^{-1}$; and with cycles of 5 min at 25 µmol photons $m^{-2}s^{-1}$ and 1 min 875 µmol photons $m^{-2}s^{-1}$, 9 min 25 µmol photons $m^{-2}s^{-1}$ and 3 min 525 µmol photons $m^{-2}s^{-1}$ or 10 min at 50 µmol photons $m^{-2}s^{-1}$ and 10 min 250 µmol photons $m^{-2}s^{-1}$. Growth test started by spotting clones of 2 mm diameter on solid medium using a custom steel tubular stencil and then was monitored by scanning the whole plates at different time points using Konica Minolta bizhub C280 with a resolution of 600 ppi. Colony growth was quantified by calculating integrated density (area * mean intensity) after the background exclusion with the imageJ (*https://imagej.nih.gov/ij/*) "threshold colour" plugin. Integrated density was used to quantify instead of "area" because this parameter better takes into account the three dimensional of *P. patens* colonies (Saavedra *et al.* 2011), whose morphology is influenced by the different light regimes used for the growth.

Moss Transformation and mutant selection

The *FLVA* KO construct (Gerotto *et al.* 2016) was used to remove *FLVA* from *pgrl1* single KO mutant genetic background (Kukuczka *et al.* 2014). Transformation was performed as in (Alboresi *et al.* 2010). After two rounds of selection, *in vivo* chlorophyll fluorescence was evaluated with Fluorcam 800 (PSI) to screen resistant lines. Colonies which differs in fluorescence tracks respect to background were homogenized using 3 mm zirconium glass beads (Sigma-Aldrich) and genomic DNA (gDNA) was isolated with rapid extraction protocol as in (Edwards, Johnstone & Thompson 1991) with minor modification. gDNA was then used to confirm insertion by PCR as in (Gerotto *et al.* 2016). RNA was afterwards purified with Tri Reagent (Sigma Aldrich) and used as template for cDNA synthesis with RevertAid Reverse Transcriptase (Thermo Scientific) to verify *FLVA* and *PGRL1* expression.

Thylakoid and Total Protein Extracts

Thylakoids from protonemal tissue were prepared as in (Gerotto, Alboresi, Giacometti, Bassi & Morosinotto 2012). Total extracts were obtained grinding tissues in solubilization buffer (50 mM TRIS pH 6.8, 100 mM DTT, 2% SDS and 10% glycerol). For immunoblotting analysis, following SDS-PAGE, samples were loaded at the same equivalent amount of chlorophylls and proteins were transferred to nitro-cellulose membranes (Pall Corporation) and detected with alkaline phosphatase conjugated antibody after hybridization with specific primary antibodies (anti-PsaD, Agrisera, catalog number AS09 461; anti-Cyt f, Agrisera, catalog number AS06 119; anti-γ-ATPase, Agrisera, catalog number AS08 312 ; custom-made anti-PGR5, anti-FLVA and anti-FLVB (Gerotto *et al.*

2016); anti-D2, in house polyclonal antibodies). Anti-PsaD recognizes a double band, likely corresponding to two protein isoforms as identified by mass spectrometry (Busch *et al.* 2013).

Spectroscopic measurements

In vivo chlorophyll fluorescence and P700 absorption signal were monitored simultaneously at room temperature with a Dual-PAM-100 fluorometer (Walz, Germany) in protonemal tissues grown for 10 days in $PpNO_3$ medium and CL condition or in a 10 days plant treated for the last 5 days in a different light condition. Before measurements, plants were dark-acclimated for 40 minutes. For induction/recovery kinetics actinic constant light was set to 540, 170 or 50 µmol photons $m^{-2}s^{-1}$. Fluctuating light responses were evaluated repeating 5 cycles of 3 min 540 µmol photons $m^{-2}s^{-1}$, 9 min 26 µmol photons $m^{-2}s^{-1}$.

PSII and PSI parameters were calculated as following: Fv/Fm as (Fm-Fo)/Fm, Y(II) as (Fm'-F)/Fm', relative qL as qL = (Fm'-F)/(Fm'-Fo') x Fo'/F, NPQ as (Fm-Fm')/ Fm', Y_I as 1 - Y(ND) - Y(NA), Y(NA) as (Pm-Pm')/Pm , Y(ND) as (1 - P700 red), where Fm and Fo represent the maximum and minimum fluoresce yields ((Maxwell & Johnson 2000)), while Pm and Pm' represent the P700 signals recorded just before (P) then briefly after onset of a saturating pulse (Pm')(Klughammer & Schreiber 1994).

Spectroscopic analysis on WT, *flva* KO and *pgrl1* KO and *flva pgrl1* KO lines was performed *in vivo* on 10-day old intact tissues using a JTS-10 spectrophotometer (Biologic). Relative amount of functional photosynthetic complexes and electron transport rates were evaluated measuring the Electrochromic Shift (ECS) spectral change on buffer infiltrated plants (HEPES 20mM pH 7.5, KCl 10mM) in presence and absence of 3-(3,4-dichlorophenyl)-1,1-dimethylurea (DCMU 20µM) and hydroxylamine (HA, 4 mM) as in (Bailleul, Cardol, Breyton & Finazzi 2010; Gerotto *et al.* 2016). Proton motive force (pmf) was evaluated following ECS relaxation kinetics for 20s after actinic light switch-off, gH^+ was evaluated by the same kinetics calculating the half relaxation time $t_{1/2}$ of ECS. $P700^+$ absorption kinetics were measured from the absorption at 705 nm (ΔOD_{705}), following the re-reduction after actinic light switch off. For light treated measures, plants were illuminated for 3 minutes at 940 µmol photons $m^{-2}s^{-1}$ before actinic light switch off and recording of re-reduction kinetics. Dark acclimated re-reduction kinetics were measured on plant acclimated for 10 minutes in the dark, following a 5 seconds light pulse at 940 µmol photons $m^{-2}s^{-1}$ not sufficient to reach the photosynthetic steady state. Fraction of oxidized P700 was calculated by comparing the maximum signal from $P700^+$ obtained with intense illumination before and after infiltrating plants with DBIMB 150 µM. P700 kinetic rate was estimated by relaxation time $t_{1/2}$ of $P700^+$ reduction in the dark. Cyt f

absorption was measured with the same mode describe for $P700^+$, with an interference filter at 554 nm. In this case 546 and 573 nm were used as background and removed to 554 signal (Finazzi *et al.* 1997). Oxidized Cyt f and Cyt f kinetic rate were calculated as for P700 measurements.

To assess the existence of restricted diffusion domains, we compared the theoretical equilibrium constants between PSI and its electron donor (K_{th}) with the experimental one (K_{exp}), following previous approaches in plants. K_{th} was estimated based on the redox potentials of Cyt f and of P700 in a range between 60 and 300 ms. To evaluate K_{exp} the following equation was used to relate redox changes of P700 and of Cyt f in an "equilibration plot" (Figure 6C, D) (Flori *et al.* 2017).

$$K_{exp} = \frac{[cyt\ f^+][P700]}{[cyt\ f][P700^+]} \quad [1]$$

where [*cytf*], [$cytf^+$], [P700] and [$P700^+$] represent the concentration, of the oxidized and reduced form of the cyt f and P_{700} pools.

From equation [1] the relationship between the relative amount of oxidized P_{700} and of cyt f can be derived as:

$$y = \frac{K_{\exp}.x}{1 + x.(K_{\exp} - 1)}, \quad [2]$$

$$\text{with } y = \frac{cyt\ f^+}{cyt\ f + cytf^+} \quad [3]$$

$$\text{and } x = \frac{P700^+}{P700^+ + P700} \quad [4]$$

AUTHOR CONTRIBUTIONS

AA and TM designed the research; MS, AA, CG, GF performed the experiments; MS, AA, EMA, GF and TM analysed the data; MS, AA, GF and TM wrote the paper.

ACKNOWLEDGEMENTS

AA acknowledges the financial support by the University of Padova. TM received financial support by the European Research Council (BIOLEAP grant no. 309485). We thank Michael Hippler (Munster, Germany) for providing P. patens *pgrl1* ko plants that served for the isolation of *flva pgrl1* KO and for useful discussion. The authors have no conflict of interest to declare.

REFERENCES

Alboresi A., Gerotto C., Giacometti G.M., Bassi R., Morosinotto T., Alboresia A., … Morosinotto T. (2010) Physcomitrella patens mutants affected on heat dissipation clarify the evolution of photoprotection mechanisms upon land colonization. *Proceedings of the National Academy of Sciences of the United States of America* **107**, 11128–33.

Alboresi A., Storti M. & Morosinotto T. (2018) Balancing protection and efficiency in the regulation of photosynthetic electron transport across plant evolution. *The New phytologist*.

Allahverdiyeva Y., Isojärvi J., Zhang P. & Aro E.-M. (2015a) Cyanobacterial Oxygenic Photosynthesis is Protected by Flavodiiron Proteins. *Life* **5**, 716–743.

Allahverdiyeva Y., Mustila H., Ermakova M., Bersanini L., Richaud P., Ajlani G., … Aro E.-M. (2013) Flavodiiron proteins Flv1 and Flv3 enable cyanobacterial growth and photosynthesis under fluctuating light. *Proceedings of the National Academy of Sciences of the United States of America* **110**, 4111–6.

Allahverdiyeva Y., Suorsa M., Tikkanen M. & Aro E.-M.E.-M. (2015b) Photoprotection of photosystems in fluctuating light intensities. *Journal of experimental botany* **66**, 2427–36.

Allen J. (2002) Photosynthesis of ATP-electrons, proton pumps, rotors, and poise. *Cell* **110**, 273–6.

Arnon D.I. & Chain R.K. (1975) Regulation of ferredoxin-catalyzed photosynthetic phosphorylations. *Proceedings of the National Academy of Sciences of the United States of America* **72**, 4961–5.

Aro E.M., Gerbaud A. & André M. (1984) CO(2) and O(2) Exchange in Two Mosses, Hypnum cupressiforme and Dicranum scoparium. *Plant physiology* **76**, 431–5.

Bailleul B., Berne N., Murik O., Petroutsos D., Prihoda J., Tanaka A., … Finazzi G. (2015) Energetic coupling between plastids and mitochondria drives CO2 assimilation in diatoms. *Nature* **524**, 366–9.

Bailleul B., Cardol P., Breyton C. & Finazzi G. (2010) Electrochromism: A useful probe to study algal photosynthesis. *Photosynthesis Research* **106**, 179–189.

Bukhov N.G. & Carpentier R. (2003) Measurement of photochemical quenching of absorbed quanta in photosystem I of intact leaves using simultaneous measurements of absorbance changes at 830 nm and thermal dissipation. *Planta* **216**, 630–8.

Burlacot A., Sawyer A., Cuiné S., Auroy-Tarrago P., Blangy S., Happe T. & Peltier G. (2018) Flavodiiron-Mediated O2 Photoreduction Links H2 Production with CO2 Fixation during the Anaerobic Induction of Photosynthesis. *Plant physiology* **177**, 1639–1649.

Busch A., Petersen J., Webber-Birungi M.T., Powikrowska M., Lassen L.M.M., Naumann-Busch

B., … Jensen P.E. (2013) Composition and structure of photosystem I in the moss Physcomitrella patens. *Journal of experimental botany* **64**, 2689–99.

Chaux F., Burlacot A., Mekhalfi M., Auroy P., Blangy S., Richaud P. & Peltier G. (2017) Flavodiiron Proteins Promote Fast and Transient O2Photoreduction inChlamydomonas. *Plant physiology* **174**, 1825–1836.

DalCorso G., Pesaresi P., Masiero S., Aseeva E., Schünemann D., Finazzi G., … Leister D. (2008) A complex containing PGRL1 and PGR5 is involved in the switch between linear and cyclic electron flow in Arabidopsis. *Cell* **132**, 273–85.

Edwards K., Johnstone C. & Thompson C. (1991) A simple and rapid method for the preparation of plant genomic DNA for PCR analysis. *Nucleic acids research* **19**, 1349.

Finazzi G., Büschlen S., de Vitry C., Rappaport F., Joliot P. & Wollman F.A. (1997) Function-directed mutagenesis of the cytochrome b6f complex in Chlamydomonas reinhardtii: involvement of the cd loop of cytochrome b6 in quinol binding to the Q(o) site. *Biochemistry* **36**, 2867–74.

Finazzi G., Furia A., Barbagallo R.P. & Forti G. (1999) State transitions, cyclic and linear electron transport and photophosphorylation in Chlamydomonas reinhardtii. *Biochimica et biophysica acta* **1413**, 117–29.

Finazzi G. & Rappaport F. (1998) In vivo characterization of the electrochemical proton gradient generated in darkness in green algae and its kinetic effects on cytochrome b6f turnover. *Biochemistry* **37**, 9999–10005.

Flori S., Jouneau P.-H., Bailleul B., Gallet B., Estrozi L.F., Moriscot C., … Finazzi G. (2017) Plastid thylakoid architecture optimizes photosynthesis in diatoms. *Nature communications* **8**, 15885.

Gerotto C., Alboresi A., Giacometti G.M.G.M., Bassi R. & Morosinotto T. (2012) Coexistence of plant and algal energy dissipation mechanisms in the moss Physcomitrella patens. *The New phytologist* **196**, 763–73.

Gerotto C., Alboresi A., Meneghesso A., Jokel M., Suorsa M., Aro E.-M.E.M. & Morosinotto T. (2016) *Flavodiiron proteins act as safety valve for electrons in Physcomitrella patens*. National Academy of Sciences.

Hanawa H., Ishizaki K., Nohira K., Takagi D., Shimakawa G., Sejima T., … Miyake C. (2017) Land plants drive photorespiration as higher electron-sink: comparative study of post-illumination transient O2 -uptake rates from liverworts to angiosperms through ferns and gymnosperms. *Physiologia plantarum* **161**, 138–149.

Helman Y., Tchernov D., Reinhold L., Shibata M., Ogawa T., Schwarz R., … Kaplan A. (2003)

Genes Encoding A-Type Flavoproteins Are Essential for Photoreduction of O2 in Cyanobacteria. *Current Biology* **13**, 230–235.

Hertle A.P., Blunder T., Wunder T., Pesaresi P., Pribil M., Armbruster U. & Leister D. (2013) PGRL1 is the elusive ferredoxin-plastoquinone reductase in photosynthetic cyclic electron flow. *Molecular cell* **49**, 511–23.

Ilík P., Pavlovič A., Kouřil R., Alboresi A., Morosinotto T., Allahverdiyeva Y., … Shikanai T. (2017) Alternative electron transport mediated by flavodiiron proteins is operational in organisms from cyanobacteria up to gymnosperms. *New Phytologist* **214**.

Jokel M., Johnson X., Peltier G., Aro E.-M. & Allahverdiyeva Y. (2018) Hunting the main player enabling Chlamydomonas reinhardtii growth under fluctuating light. *The Plant journal : for cell and molecular biology* **94**, 822–835.

Joliot P. & Johnson G.N. (2011) Regulation of cyclic and linear electron flow in higher plants. *Proceedings of the National Academy of Sciences of the United States of America* **108**, 13317–22.

Kato Y., Odahara M., Fukao Y. & Shikanai T. (2018) Stepwise evolution of supercomplex formation with photosystem I is required for stabilization of chloroplast NADH dehydrogenase-like complex: Lhca5-dependent supercomplex formation in Physcomitrella patens. *The Plant Journal*.

Kirchhoff H. (2014) Structural changes of the thylakoid membrane network induced by high light stress in plant chloroplasts. *Philosophical transactions of the Royal Society of London. Series B, Biological sciences* **369**, 20130225.

Kirchhoff H., Hall C., Wood M., Herbstová M., Tsabari O., Nevo R., … Reich Z. (2011) Dynamic control of protein diffusion within the granal thylakoid lumen. *Proceedings of the National Academy of Sciences of the United States of America* **108**, 20248–53.

Kirchhoff H., Schöttler M.A., Maurer J. & Weis E. (2004) Plastocyanin redox kinetics in spinach chloroplasts: evidence for disequilibrium in the high potential chain. *Biochimica et biophysica acta* **1659**, 63–72.

Klughammer C. & Schreiber U. (1994) An improved method, using saturating light pulses, for the determination of photosystem I quantum yield via P700+-absorbance changes at 830 nm. *Planta* **192**, 261–268.

Kono M., Noguchi K. & Terashima I. (2014) Roles of the cyclic electron flow around PSI (CEF-PSI) and O_2-dependent alternative pathways in regulation of the photosynthetic electron flow in short-term fluctuating light in Arabidopsis thaliana. *Plant & cell physiology* **55**, 990–1004.

Koochak H., Puthiyaveetil S., Mullendore D.L., Li M. & Kirchhoff H. (2018) The structural and

functional domains of plant thylakoid membranes. *The Plant journal : for cell and molecular biology*.

Kukuczka B., Magneschi L., Petroutsos D., Steinbeck J., Bald T., Powikrowska M., … Hippler M. (2014) Proton Gradient Regulation5-Like1-Mediated Cyclic Electron Flow Is Crucial for Acclimation to Anoxia and Complementary to Nonphotochemical Quenching in Stress Adaptation. *Plant physiology* **165**, 1604–1617.

Kulheim C., Agren J., Jansson S., Külheim C., Agren J. & Jansson S. (2002) Rapid regulation of light harvesting and plant fitness in the field. *Science (New York, N.Y.)* **297**, 91–3.

Maxwell K. & Johnson G.N. (2000) Chlorophyll fluorescence - A practical guide. *Journal of Experimental Botany* **51**, 659–668.

Mehler A.H. (1951) Studies on reactions of illuminated chloroplasts. *Archives of Biochemistry and Biophysics* **33**, 65–77.

Munekage Y., Hojo M., Meurer J., Endo T., Tasaka M. & Shikanai T. (2002) PGR5 is involved in cyclic electron flow around photosystem I and is essential for photoprotection in Arabidopsis. *Cell* **110**, 361–71.

Nishio J.N. & Whitmarsh J. (1993) Dissipation of the Proton Electrochemical Potential in Intact Chloroplasts (II. The pH Gradient Monitored by Cytochrome f Reduction Kinetics). *Plant physiology* **101**, 89–96.

Peltier G., Aro E.-M. & Shikanai T. NDH-1 and NDH-2 Plastoquinone Reductases in Oxygenic Photosynthesis. *Annual review of plant biology* **67**, 55–80.

Peltier G., Tolleter D., Billon E. & Cournac L. (2010) Auxiliary electron transport pathways in chloroplasts of microalgae. *Photosynthesis Research* **106**, 19–31.

Peng L., Fukao Y., Fujiwara M., Takami T. & Shikanai T. (2009) Efficient operation of NAD(P)H dehydrogenase requires supercomplex formation with photosystem I via minor LHCI in Arabidopsis. *The Plant cell* **21**, 3623–40.

Pinnola A., Dall'Osto L., Gerotto C., Morosinotto T., Bassi R. & Alboresi A. (2013) Zeaxanthin binds to light-harvesting complex stress-related protein to enhance nonphotochemical quenching in Physcomitrella patens. *The Plant cell* **25**, 3519–34.

Rumberg B. & Siggel U. (1969) pH changes in the inner phase of the thylakoids during photosynthesis. *Die Naturwissenschaften* **56**, 130–2.

Saavedra L., Balbi V., Lerche J., Mikami K., Heilmann I. & Sommarin M. (2011) PIPKs are essential for rhizoid elongation and caulonemal cell development in the moss Physcomitrella patens. *The Plant Journal* **67**, 635–647.

Shikanai T. (2014) Central role of cyclic electron transport around photosystem I in the regulation

of photosynthesis. *Current opinion in biotechnology* **26**, 25–30.

Shikanai T. (2016) Regulatory network of proton motive force: contribution of cyclic electron transport around photosystem I. *Photosynthesis research* **129**, 1–8.

Shikanai T., Endo T., Hashimoto T., Yamada Y., Asada K. & Yokota A. (1998) Directed disruption of the tobacco ndhB gene impairs cyclic electron flow around photosystem I. *Proceedings of the National Academy of Sciences of the United States of America* **95**, 9705–9.

Shikanai T. & Yamamoto H. (2017) Contribution of Cyclic and Pseudo-cyclic Electron Transport to the Formation of Proton Motive Force in Chloroplasts. *Molecular plant* **10**, 20–29.

Shimakawa G., Ishizaki K., Tsukamoto S., Tanaka M., Sejima T. & Miyake C. (2017) The Liverwort, Marchantia, Drives Alternative Electron Flow Using a Flavodiiron Protein to Protect PSI. *Plant physiology* **173**, 1636–1647.

Sonoike K., Terashima I., Iwaki M. & Itoh S. (1995) Destruction of photosystem I iron-sulfur centers in leaves of Cucumis sativus L. by weak illumination at chilling temperatures. *FEBS letters* **362**, 235–8.

Stiehl H.H. & Witt H.T. (1969) Quantitative Treatment of the Function of Plastoquinone in Photosynthesis. *Zeitschrift für Naturforschung B* **24**, 1588–1598.

Suorsa M., Järvi S., Grieco M., Nurmi M., Pietrzykowska M., Rantala M., … Aro E.-M. (2012) PROTON GRADIENT REGULATION5 is essential for proper acclimation of Arabidopsis photosystem I to naturally and artificially fluctuating light conditions. *The Plant cell* **24**, 2934–48.

Takahashi H., Clowez S., Wollman F.-A., Vallon O. & Rappaport F. (2013) Cyclic electron flow is redox-controlled but independent of state transition. *Nature communications* **4**, 1954.

Tikkanen M., Rantala S. & Aro E.-M. (2015) Electron flow from PSII to PSI under high light is controlled by PGR5 but not by PSBS. *Frontiers in plant science* **6**, 521.

Tikkanen M., Rantala S., Grieco M. & Aro E.-M. (2017) Comparative analysis of mutant plants impaired in the main regulatory mechanisms of photosynthetic light reactions - From biophysical measurements to molecular mechanisms. *Plant physiology and biochemistry : PPB* **112**, 290–301.

Tiwari A., Mamedov F., Grieco M., Suorsa M., Jajoo A., Styring S., … Aro E.-M. (2016) Photodamage of iron–sulphur clusters in photosystem I induces non-photochemical energy dissipation. *Nature Plants*, 16035.

Wada S., Yamamoto H., Suzuki Y., Yamori W., Shikanai T. & Makino A. (2017) Flavodiiron protein substitutes for cyclic electron flow without competing CO2 assimilation. *Plant physiology* **176**, 1509–1518.

Yamamoto H., Takahashi S., Badger M.R. & Shikanai T. (2016) Artificial remodelling of alternative electron flow by flavodiiron proteins in Arabidopsis. *Nature plants* **2**, 16012.

Yamori W., Sakata N., Suzuki Y., Shikanai T. & Makino A. (2011) Cyclic electron flow around photosystem I via chloroplast NAD(P)H dehydrogenase (NDH) complex performs a significant physiological role during photosynthesis and plant growth at low temperature in rice. *The Plant journal : for cell and molecular biology* **68**, 966–76.

SUPPLEMENTARY MATERIAL

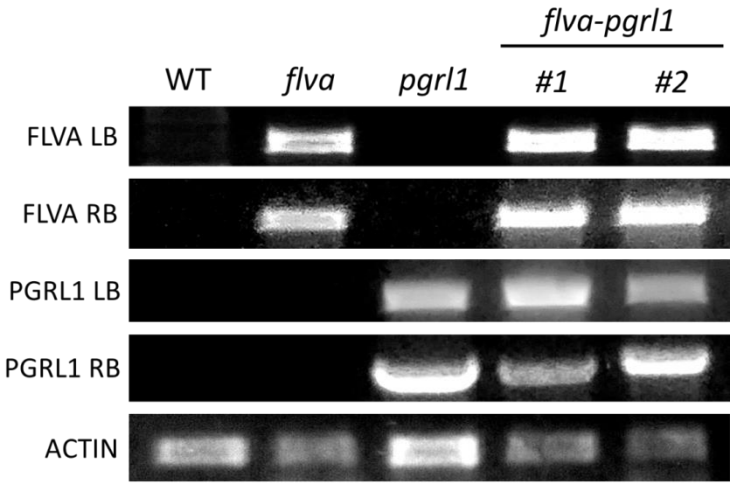

Figure S1. Verification of homologous recombination in *flva pgrl1* KO plants. Insertion of the resistance cassette in *FLVA* genetic locus was verified by PCR amplification of both left (LB) and right borders (RB). One primer annealed on the resistance cassette and the other on the genome. LB and RB were also verified for *pgrl1*. Actin was amplified by PCR as control of the quality of gDNA preparation.

Genotype	Chl a/b	Chl/Car
WT	2.68 ± 0.13	3.32 ± 0.37
flva	2.74 ± 0.09	3.41 ± 0.28
pgrl1	2.77 ± 0.17	3.15 ± 0.17
flva pgrl1	2.73 ± 0.17	3.42 ± 0.40

Table S1. Pigment content of *Physcomitrella patens* plants. Chl and carotenoid contents were evaluated in all lines grown for 10 days in control light conditions by measuring Chl a/b and Chl/car ratios (n > 3). In the case of *flva pgrl1* KO data from the two lines measured independently were averaged together (n= 6).

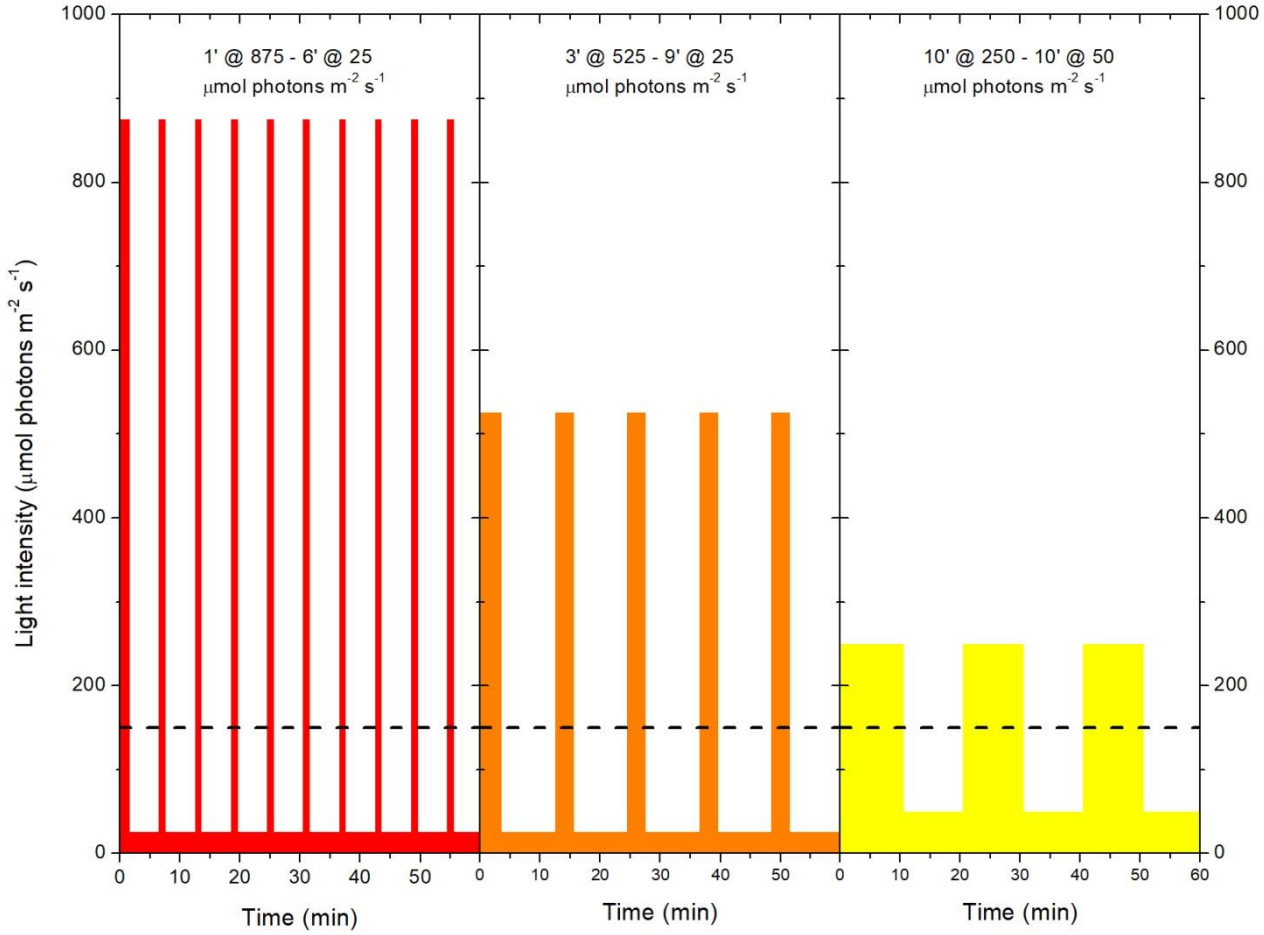

Figure S2. Scheme of fluctuating light protocols employed. Representation of 1 hour of dynamic light regimes used for *Physcomitrella patens* plants treatments reported in figure 2 and S3. Light regimes differ in frequency of light fluctuation (1-6 min, 3-9 min, 10-10 min) and in light intensity (875-25, 525-25, 250-50 µmol photons m^{-2} s^{-1}). The average light intensity is equivalent to a constant light of 150 µmol photons m^{-2} s^{-1} in all conditions (dashed line).

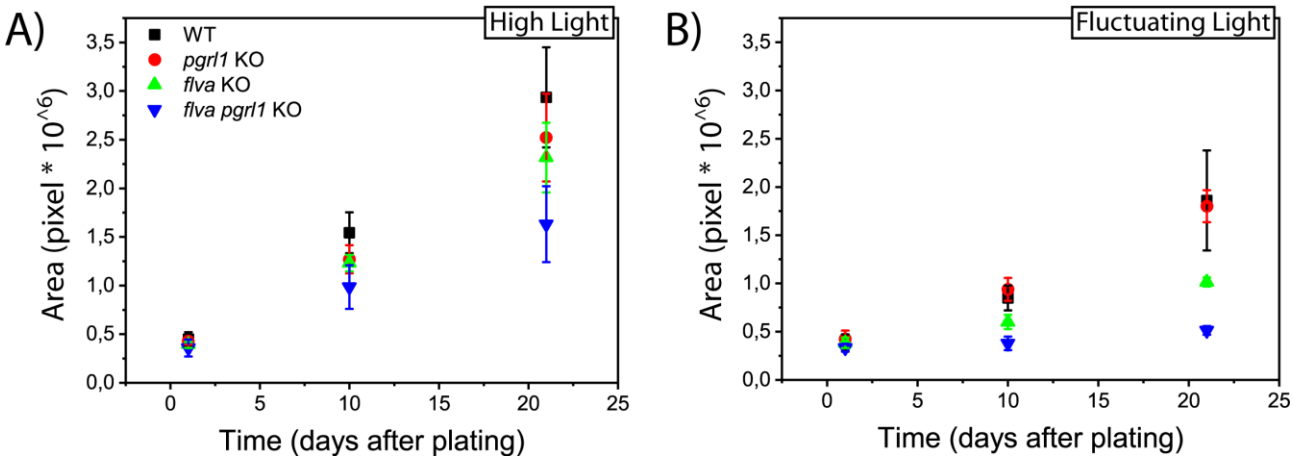

Figure S3. Effect of high light and fluctuating light on growth kinetics of *Physcomitrella patens* plants. Plants were grown under different light regimes as shown in Figure 2 and their size was evaluated after 1, 10 and 21 days of growth on minimum medium. Plants were exposed to (**A**) high light and (**B**) fluctuating light (3' at 500, 9' at 25 µmol photons m-2 s-1). WT, *flva*, *pgrl1* and *flva pgrl1* KO are shown respectively with black squares, red circles, green triangles and blue diamonds, respectively. (n = 8-21)

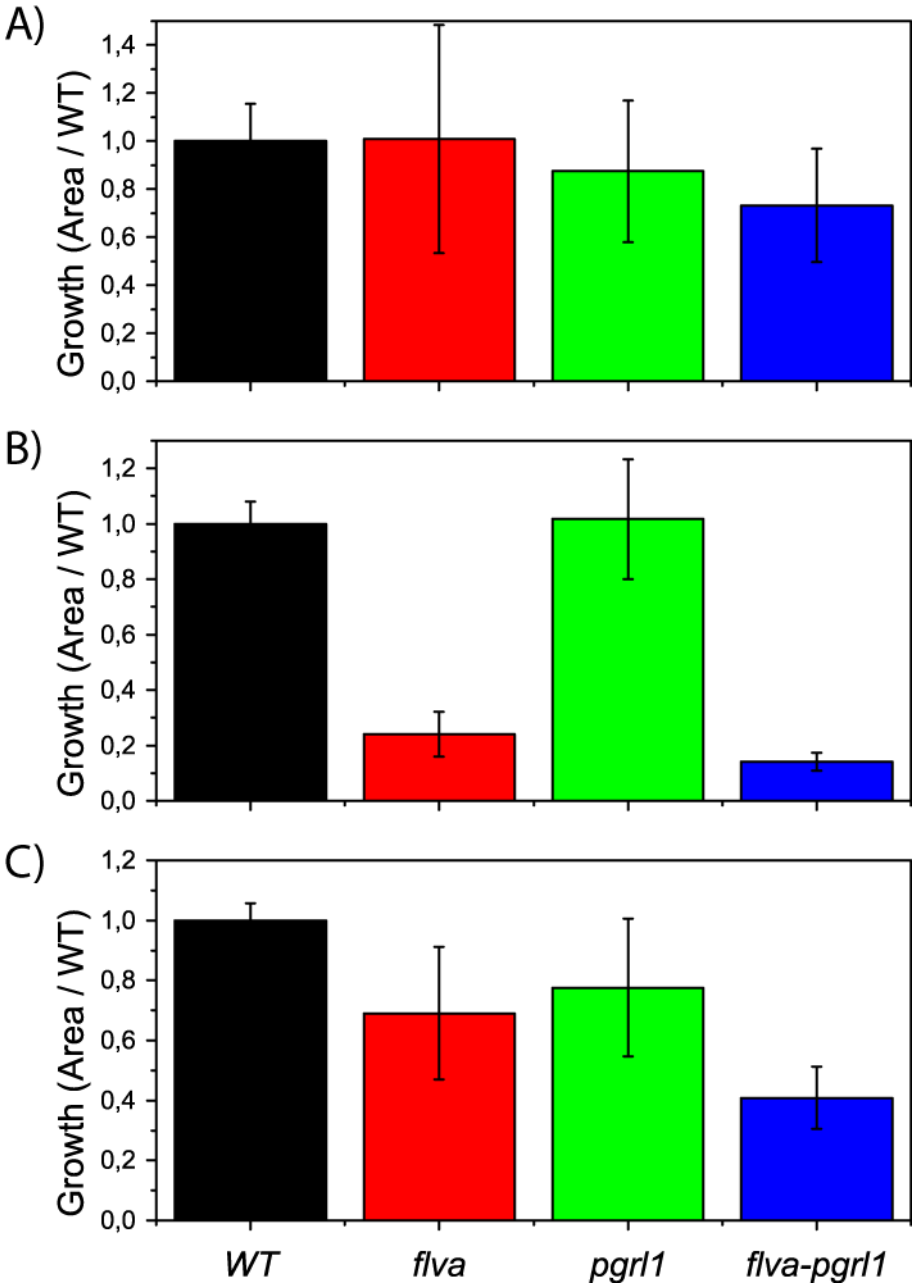

Figure S4. Effect of fluctuating light on growth of *Physcomitrella patens* plants. Plants were grown under different light regimes as shown in figure 2 and their size was evaluated after 21 days of growth on minimum medium. Plants exposed to constant 150 µ mol photons m^{-2} s^{-1} (A) are compared with others exposed to fluctuating light providing the same average light intensity (B and C). Light regimes differ in frequency of light fluctuation (1-6 min in B and 10-10 min in C) and in light intensity (875-25 in B and 250-25 150 µmol photons m^{-2} s^{-1} in C). WT, *flva*, *pgrl1* and *flva pgrl1* KO are shown respectively in black, red, green and blue (n = 4-12).

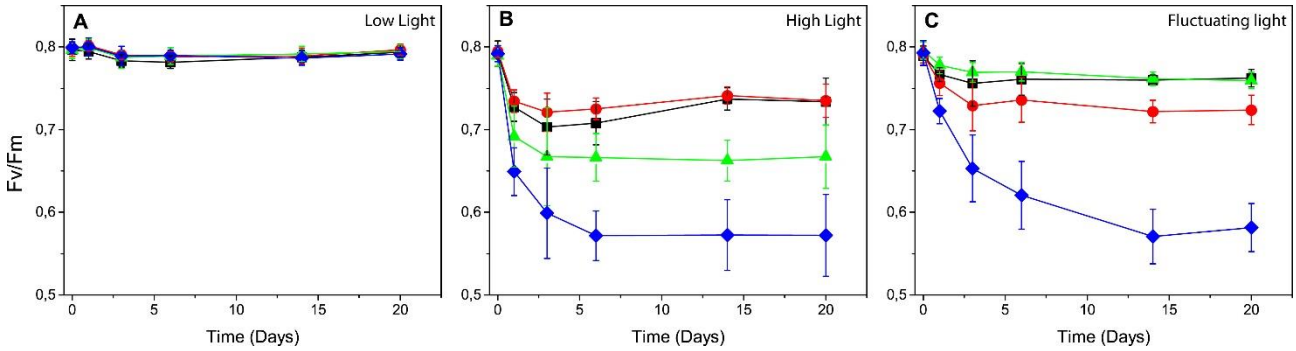

Figure S5. Maximum PSII efficiency of plants grown under different conditions. PSII efficiency in plants exposed in different conditions (shown in figure 2) was calculated after measurement of *in vivo* chlorophyll fluorescence with a PAM imaging system. A) Low Light; B) High Light; C) Fluctuating light (3' at 500, 9' at 25 µmol photons m^{-2} s^{-1}). WT, *flva*, *pgrl1* and *flva pgrl1* KO are shown respectively with black squares, red circles, green triangles and blue diamonds, respectively. (n = 8-21)

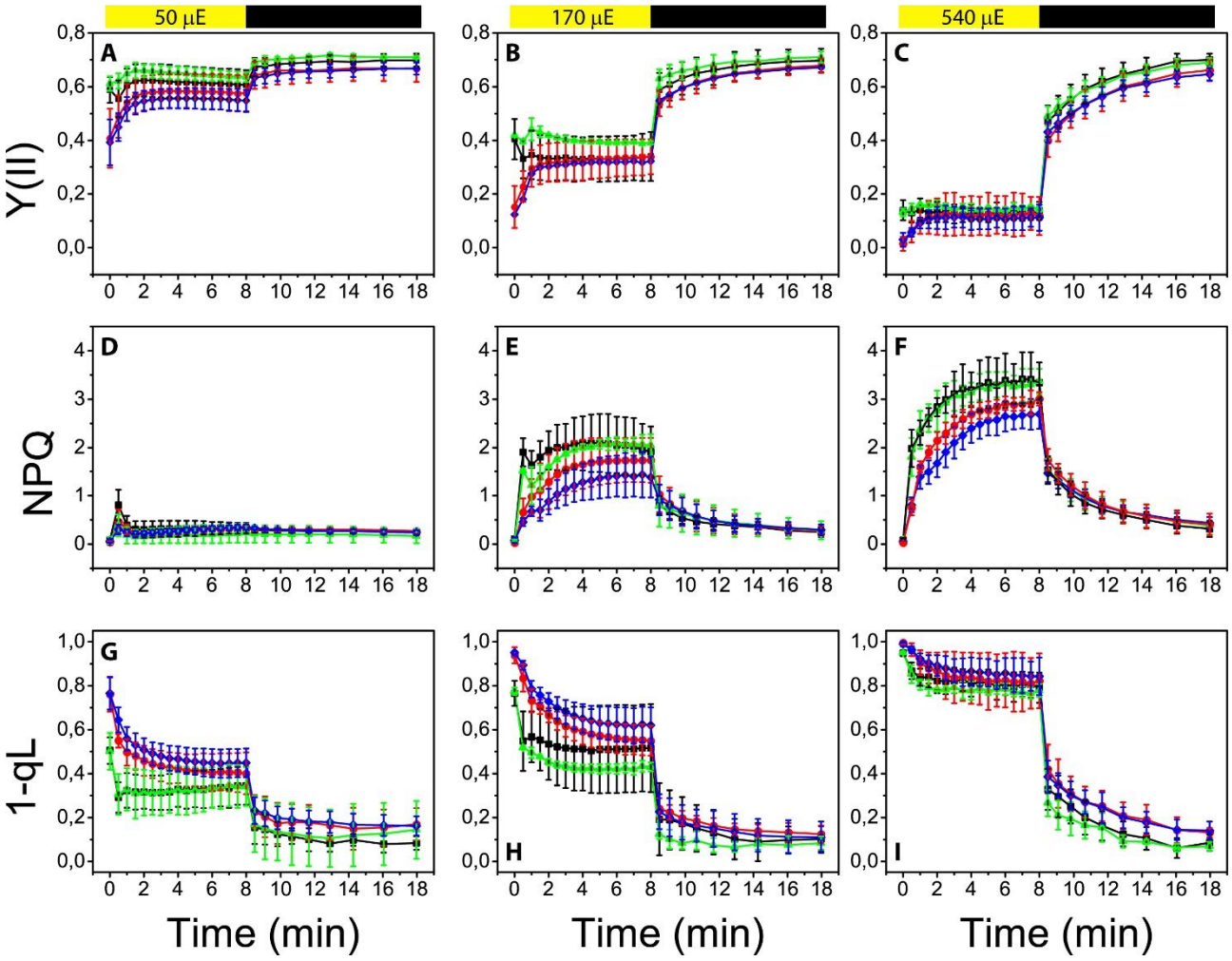

Figure S6. Effect of mutations on PSII efficiency and NPQ activation. YII (A-C), NPQ (D-F) and (G-I) were monitored in plants exposed to 50 (A, D, G), 170 (B, E, H) and 540 µmol photons m^{-2} s^{-1} (C, F, I) of actinic light. In all panels WT, *flva, pgrl1* and *flva pgrl1* are shown respectively as black squares, red circles green triangles and blue diamonds. Values are expressed as average ± SD of 3-5 independent replicates.

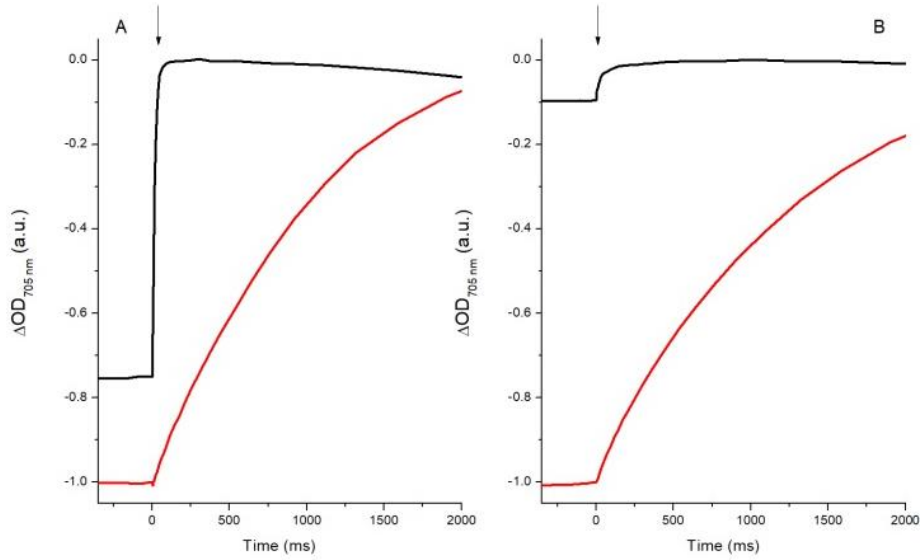

Figure S7. P700 oxidation state estimation. WT (A) and *flva pgrl1* KO (B) are here reported. P700 oxidation showed in Figure 5 was measured by comparing the maximal signal obtained after 180 seconds under a saturating illumination (black line) with the signal obtained after treating the same sample by DCMU and DBMIB (red line). All samples are normalized to the maximal signal. Arrows (t = 0): light off.

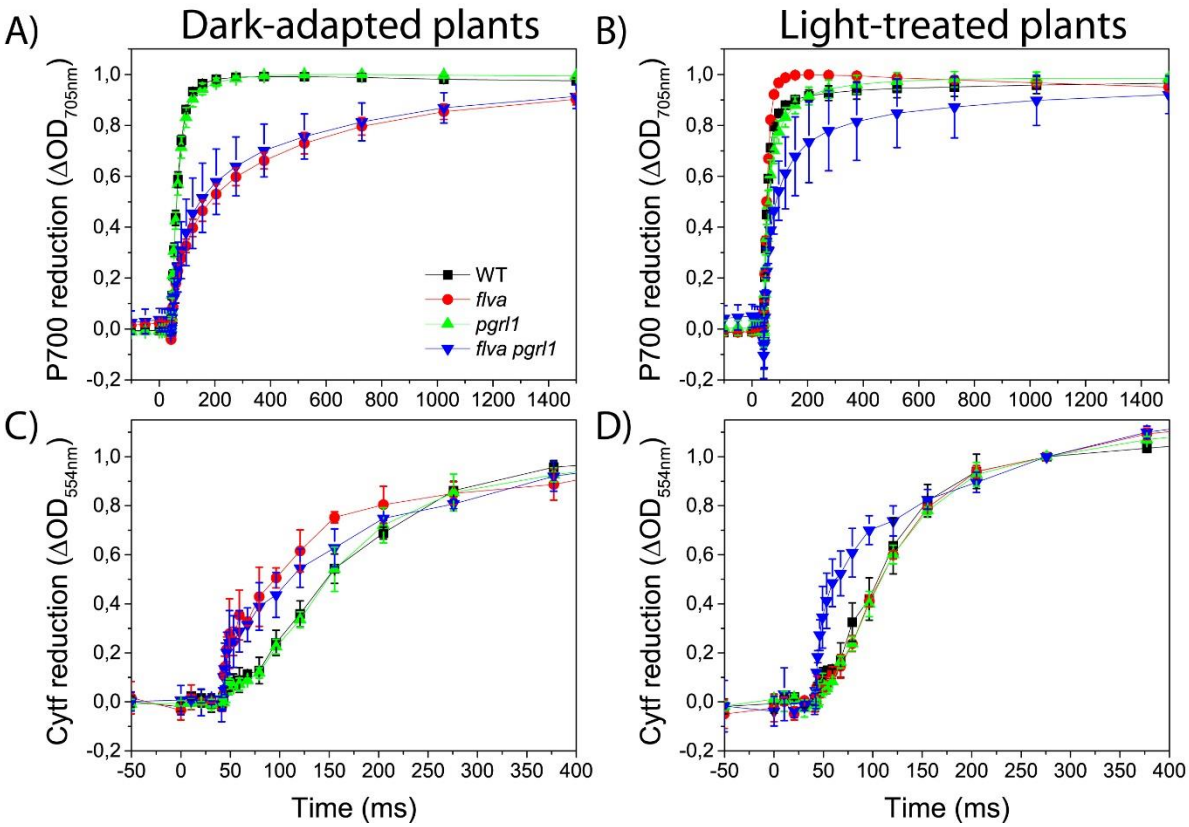

Figure S8. Redox kinetics of P700 and cytochrome f measured in dark-adapted (A, C) and light-adapted (B, D) protonema cells. Data were used to calculate dark-reduction half-time and equilibrium of P700 and Cyt f in Figure 6. WT is shown in black, *flva* KO in red, *pgrl1* KO in green and *flva pgrl1* in blue. Reported values are average ± SD of at least 4 independent replicates for each time point.

CHAPTER 4

Chloroplast NADH dehydrogenase-like complex role in dark to light transitions in the moss *Physcomitrella patens*

Authors name and affiliation

Mattia Storti[1], Maria Paola Puggioni[2], Anna Segalla[1], Tomas Morosinotto[1], Alessandro Alboresi[1]

[1] Dept. of Biology, University of Padova, 35121 Padova, Italy;

[2] Forschungszentrum Jülich, IBG-2, 52428 Jülich, Germany.

CONTRIBUTION

MS performed photosynthetic and biochemical characterization and growth experiments.

ABSTRACT

Alternative electron pathways contribute significantly to the regulation of photosynthetic light reactions to meet metabolic demands in a dynamic environment. Understanding the molecular mechanisms of their activity is seminal to decipher their role in response to environmental cues and in plant adaptation. The chloroplast NADH dehydrogenase-like (NDH) complex mediates cyclic electron transport pathway around photosystem I in different organisms like cyanobacteria, eukaryotic algae and various plant species but has a discontinuous distribution in green lineage. In order to assess how its activity and physiological role changed during plant evolution, we isolated *Physcomitrella patens* plants knocked out of the gene *NDHM* which encodes for a subunit fundamental for the stability and activity of the whole complex. *P. patens ndhm* KO mosses showed defects in PSI activity in the first seconds after plants were shifted from the dark to light, suggesting a role of NDH in these transitions. Reiterated dark/light cycles indeed enhanced the difference between WT and mutant leading also to a higher reduction of the plastoquinone pool in the latter, showing that NDH is active in alleviating redox pressure in thylakoid membrane upon changes in light intensity by maintaining PSI acceptor side oxidized in the dark.

INTRODUCTION

Photosynthetic reactions convert sunlight into chemical energy and sustain most lifeforms on earth. Light energy supports a linear electron flux (LEF) catalyzed by three major complexes imbedded in thylakoid membranes: (i) photosystem (PS) II, (ii) cytochrome b_6f (Cyt b_6f) and (iii) PSI. Overall electrons are transferred from water to $NADP^+$ *via* plastoquinone (PQ), plastocyanin, ferredoxin and ferredoxin-$NADP^+$ reductase. The electron transfer is coupled with proton (H^+) accumulation in the lumen, originating from the photolysis of H_2O and the reconversion of the reduced plastoquinone (PQH_2) to PQ at the level of Cyt b_6f. The LEF-generated H^+ gradient is exploited by chloroplast ATPase for the synthesis of ≈ 1.3 ATP molecules per molecule of NADPH. Yet, the Calvin-Benson-Bassham (CBB) cycle is demanding ≈ 1.5 molecules of ATP per NADPH (Shikanai, 2016*a*). The cyclic electron flow (CEF) around PSI is one of the strategies adopted by photosynthetic organisms to divert electrons from reduced ferredoxin to reduce PQ, diminishing NADPH formation and

increasing ATP biosynthesis (Arnon and Chain, 1975). Two major CEF pathways have been described so far although not conserved in all photosynthetic organisms (Peltier *et al.*; Yamori and Shikanai, 2016; Alboresi *et al.*, 2018). The first depends on PGR5/PGRL1 proteins (Munekage *et al.*, 2002; DalCorso *et al.*, 2008) and the second is mediated by chloroplast NADH dehydrogenase like complex (NDH also called NDH-1), a multimeric complex which share structural and evolutionary aspects with the mitochondrial respiratory complex I (Peltier *et al.*; Shikanai, 2016*b*). The NDH complex has a patchy distribution in the green lineage (Ruhlman *et al.*, 2015): it is present in cyanobacteria (Peltier *et al.*) and it has been identified in Gymnosperms, Angiosperms and also Streptophytae algae like *Klebsormidium flaccidum* (Hori *et al.*, 2014; Ruhlman *et al.*, 2015; de Vries *et al.*, 2016), but it is absent in some green algae like *Chlamydomonas reinhardtii* where a monomeric type II NADPH dehydrogenase (NDH-2; also called NDA2) was shown to play a role in CEF (Desplats *et al.*, 2009).

The NDH complex includes several subunits organized in various subcomplexes whose assembly is possible thanks to the activity of several ancillary proteins. In angiosperms NDH forms a supercomplex with PSI through the binding with two specific antenna proteins, LHCA5 and LHCA6, as demonstrated by genetic and structural evidences (Peng *et al.*, 2008, 2009; Kouřil *et al.*, 2014). Further studies in *Arabidopsis* demonstrated that LHCA5 and LHCA6 replace respectively LHCA4 and LHCA2 in PSI for the binding of two PSI per NDH (Otani *et al.*, 2018). In the liverwort *Marchantia polymorpha,* which lacks the genes encoding for LHCA5 and LHCA6, PSI-NDH complex was not detected (Ueda *et al.*, 2012) suggesting that these subunits were acquired during the evolution of land plants possibly to allow a more efficient operation of NDH-dependent CEF pathway (Ueda *et al.*, 2012). In the moss *Physcomitrella patens,* where NDH complex is also present (Armbruster *et al.*, 2010; Kukuczka *et al.*, 2014) and active (Ito *et al.*, 2018; Kato *et al.*, 2018), the genome encodes for a *LHCA5* gene but not for *LHCA6* (Alboresi *et al.*, 2008) and NDH was suggested to associate with only one PSI complex (Kato *et al.*, 2018). Because of these peculiar structural properties and because of moss position in the tree of life, the functional investigation of NDH in *P. patens* can provide important insights on the function of alternative electron transports and how they were shaped by adaptation to terrestrial life. In fact, mechanisms for regulation of electron transport evolved and changed during plant evolution; for example, flavodiiron proteins (FLVs) sustain an alternative pathway transferring electrons downstream PSI to O_2 as a final acceptor with the formation of H_2O. FLVs activity has been reported in photosynthetic eukaryotes (Gerotto *et al.*, 2016; Shimakawa *et al.*, 2017; Chaux *et al.*, 2017; Jokel *et al.*, 2018) and in cyanobacteria (Allahverdiyeva *et al.*, 2013; Bersanini *et al.*, 2014), but they are not present in angiosperm genomes. In *P. patens* mutants lacking FLVs their absence was suggested to be partially compensated by an increased CEF

(Gerotto *et al.*, 2016) and showed complementarity with PGRL1/PGR5 cyclic electron transport (Chapter 3), but their functional interaction with NDH complex has never been investigated so far.

We report the isolation of *P. patens* mutants in which *NDHM* gene was knocked out and the resulting functional characterization of chloroplast NDH in this moss. Since *P. patens*, unlike angiosperms, has an active FLV-dependent electron transport pathway (Gerotto *et al.*, 2016), we also investigated its functional overlap with NDH-dependent CEF pathway. Results evidenced the role of NDH in modulating PSI activity especially after dark-to-light transitions. Unlike FLVs that can sustain strong electron transport after an abrupt change in light intensity, NDH activity is relevant particularly in the dark where it keeps PSI acceptor side oxidized, an ideal condition to respond to the eventual return of the light.

RESULTS

Isolation and biochemical characterization of Physcomitrella patens ndhm knock-out mutant

The functional role of *P. patens* chloroplast NDH was investigated by generating plants where the gene encoding the NDHM subunit was knocked-out by homologous recombination (Fig. S1). In *Arabidopsis thaliana* nuclear-encoded subunits of subcomplex A (e.g. NDHM, NDHN and NDHO) (Fig. 1) are known to be essential for the activity of the whole NDH complex (Rumeau *et al.*, 2005). Among them, NDHM was chosen as target for mutagenesis because in *P. patens* genome it is encoded by a single gene *locus* and it has already been detected in *P. patens* thylakoids by proteomic analysis (Kukuczka *et al.*, 2014). Two independent KO lines were confirmed by PCR to have a single insertion in the target *locus* and to have lost *NDHM* expression (Fig. S1). The absence of NDHM protein was verified by western blotting using an antiserum raised against the full-length recombinant PpNDHM protein. Immunoblot analysis revealed that NDHH, a plastid-encoded subunit of subcomplex A, was also undetectable in *ndhm* KO lines (Fig. 1B), suggesting that the absence of NDHM caused the destabilization of NDH subcomplex A and inactivation of the whole NDH as observed in *A. thaliana* (Peng *et al.*, 2008).

The *ndhm* KO plants grown under optimum conditions did not show any morphological alteration as compared to the WT (Fig. 1). Pigment composition also was unchanged in both *ndhm* KO lines (Table S2). Moreover, the *ndhm* KO mutants showed no significant difference with abundance of PSI and II

core subunits (PsaD and D2) nor in Cyt f and γ-ATPase (Fig. 1B). Protein complexes from the thylakoid membrane were separated using a clear native (CN) gel after a mild solubilization (Fig. 2). There was no difference between WT and *ndhm* KO in the pattern of chlorophyll-containing green bands or in the protein bands after staining with Coomassie Brilliant Blue (Fig. 2A). CN-PAGE confirmed that under optimum growth conditions the photosynthetic apparatus of *ndhm* KO plants is very similar to the WT.

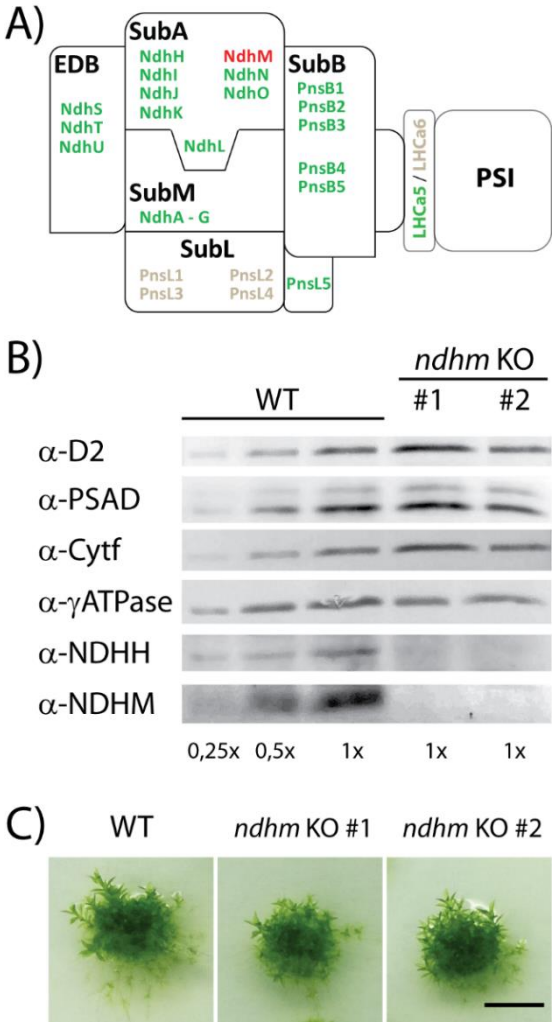

Figure 1. Phenotype of *NDHM* gene knockout (KO) mutants. A) Predicted structure of photosystem I (PSI)–NAD(P)H dehydrogenase (NDH) supercomplex of the model plant *Arabidopsis thaliana*. PSI-LHCI is connected to NDH through the antenna linkers LCHA5/LHCA6. Different sub-complexes form NDH complex, namely EDB, SubA, SubB, SubL and SubM and they are all indicated in black. All the sequences either putatively present or absent in *P. patens* genome are respectively labeled in green or grey. NDHM subunit is labeled in red. **B**) Western blotting analysis for detection of D2, PSAD, Cytf, γATPase, NDHH and NDHM in WT and *ndhm* KO #1 and #2. **C**) Moss colonies of WT and *ndhm* KO #1 and #2 grown for 21 days on $PPNO_3$ under 50 µmol photons m^{-2} s^{-1}. Scale bars = 0,5 cm.

In *A. thaliana* and *Hordeum vulgare*, a large supercomplex formed by one chloroplast NDH surrounded by two PSI has been characterized (Peng *et al.*, 2009; Kouřil *et al.*, 2014) and was detectable by native gel electrophoresis (Peng *et al.*, 2009; Järvi *et al.*, 2011). In *P. patens* CN-PAGE profile of *ndhm* KO was undistinguishable from WT and no band was identifiable as PSI-NDH supercomplex. Proteins in CN-PAGE were separated after denaturation in a second dimension by SDS-PAGE and analyzed by immunoblotting using specific antibodies (Fig. 2B). Anti-NDHM antibody revealed the presence of NDH complex in two major spots missing in the *ndhm* KO (Fig. 2B). The weaker spot corresponded to a native size of approx. 700 KDa, as expected for NDH monomers and described in *M. polymorpha* (Ueda *et al.*, 2012). A more intense NDHM signal was instead detected at higher MW (approx. 1000 KDa in the native gel), comigrating with PSI and PSII supercomplexes (Fig. 2B). This spot corresponds to the approximate size of a PSI-NDH supercomplex with a single NDH and PSI as recently suggested (Otani *et al.*, 2018). However, an immunoblot analysis using an anti-PSAD and LHCA1 antibodies failed to clearly reveal PSI subunits in the same region, suggesting that PSI-NDH, if present, represents a very small fraction of PSI particles in *P. patens*.

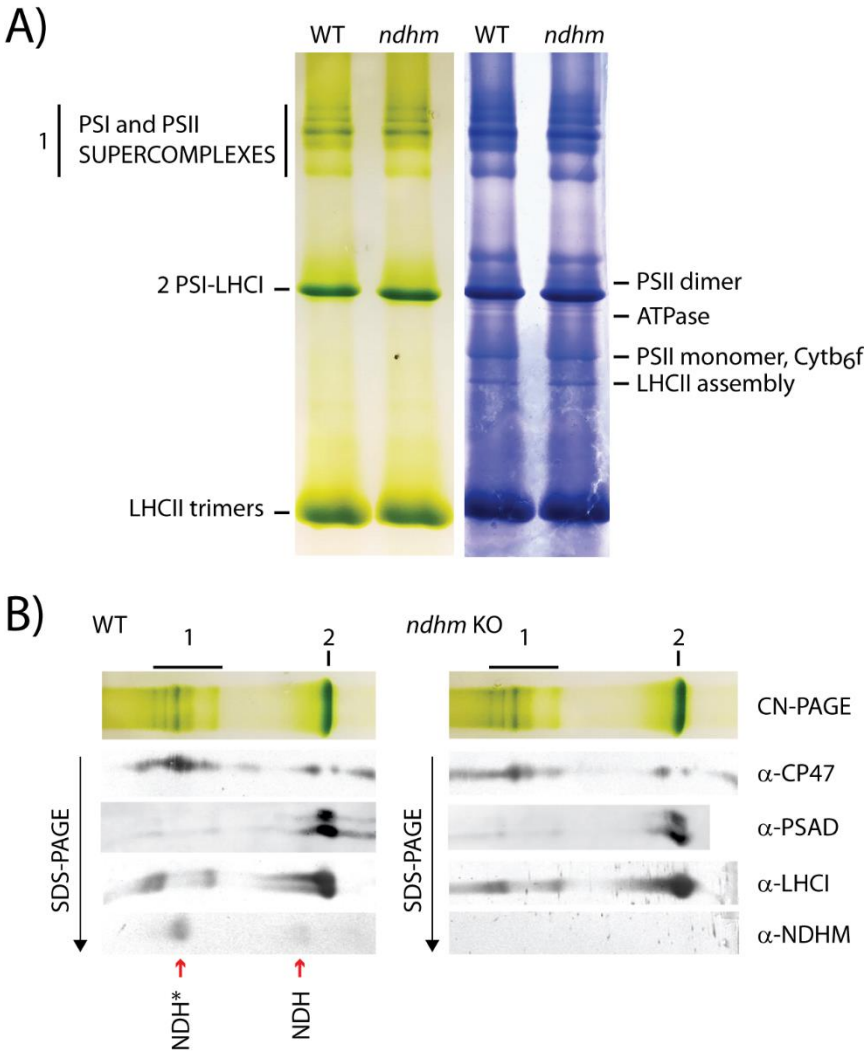

Figure 2. Native gel analysis of thylakoid membrane protein complexes. **A**) Protein complexes were solubilized from thylakoid membranes isolated from *Physcomitrella patens* protonema of WT and *ndhm* KO grown under control conditions. Protein complexes were separated by CN-PAGE and the known green bands were indicated on the left side while bands visible after Coomassie brilliant blue staining were indicated on the right side. **B**) The upper part of CN gel was further subjected to 2D SDS–PAGE and western blotting analysis using antibodies against CP47 for PSII, PSAD and LHCI for PSI and NDHM for NDH. Vertical red arrows indicate the positions of NDH as detected by the NDHM antibody. 1. PSI and PSII supercomplexes; 2. PSI-LHCI.

Response of the P. patens ndhm knock-out mutant to light

In order to assess the functional role of chloroplast NDH, a physiological characterization was performed analyzing the main photosynthetic parameters in plants exposed to increasing photosynthetic active radiation (Fig. 3 and Fig. S2). The maximum PSII efficiency was 0.83 ± 0.02 in WT and 0.84 ± 0.02 in *ndhm* KO and therefore it was not affected by NDHM depletion. PSII quantum efficiency [Y(II)] upon exposure to increasing light intensities was also indistinguishable in WT plants and in two independent clones on *ndhm* KO (Fig. 3). The efficiency of PSI [Y(I)] was instead slightly impaired in *ndhm* KO upon exposure to light (Fig. 3). While the limitation of PSI donor-side [Y(ND)] (Fig. S2) was unaffected, this difference was attributable to an increased acceptor-side limitation [Y(NA)] (Fig. S2) in *ndhm* KO mosses as compared to WT. It is interesting to notice that the impaired Y(I) translated into a lower electron transport rate of PSI over the one of PSII, as estimated by ETRI/ETRII (Fig. S2). These results thus suggest a small but significant impairment of PSI activity in *ndhm* KO well consistent with analogous mutants in other plant species (Peltier *et al.*; Yamori *et al.*, 2015).

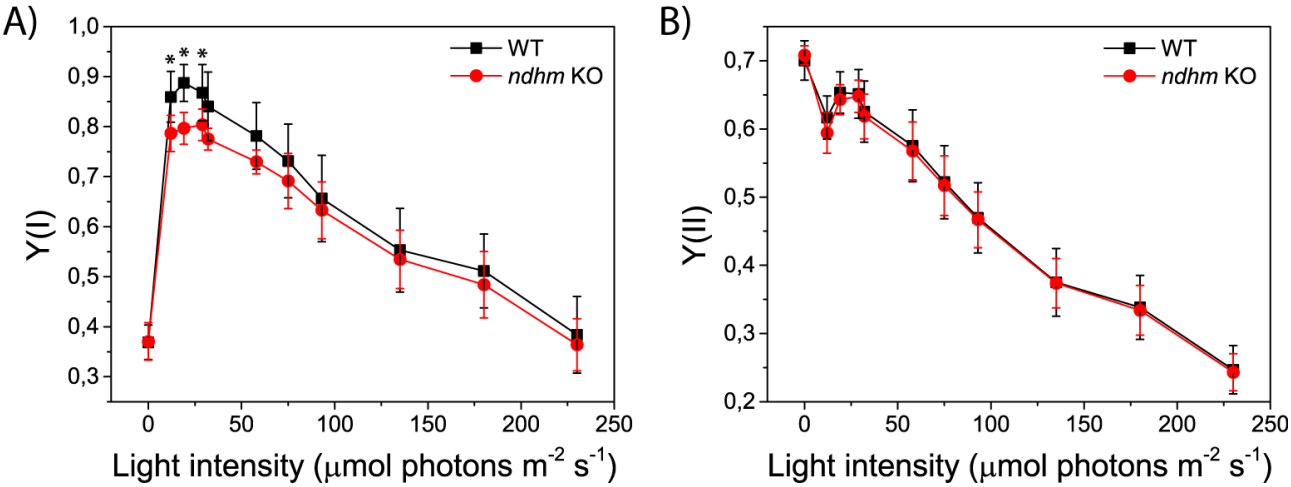

Fig. 3. Effect of the NDHM defect on photosystem activity. Light-intensity dependence of (**A**) Y(I) and (**B**) Y(II) in WT (black squares) and *ndhm* KO (red circles) plants. For *ndhm* KO mutants, experiments were always performed using two independent lines and for clarity reasons the average value obtained from the two lines was presented. * indicates significant differences (Student's t-test $p<0.01$), biological replicates n = 3-6 ± sd.

In order to deeper analyze the higher acceptor-side limitation of *ndhm* KO as compared to WT, we treated the plants for 8 minutes with constant actinic light at different intensities (Fig. 4 and Fig. S3). The Y(II), the NPQ level and the redox state of PQ (1-qL) did not show differences in the two genotypes independently from the light intensity (Fig. S3). When plants were treated with an actinic light comparable with the growth light intensity (50 µmol photons m^{-2} s^{-1}), Y(I) was found to be highly similar in both the genotypes with the exception of the first data point. Indeed, during the first second of actinic light exposure *ndhm* KO mutants showed a partially reduced donor-side limitation (Fig. 4B) and an increased acceptor-side limitation (Fig. 4C) compared to WT plants. Similar results were obtained by treating the plants with stronger illumination (540 µmol photons m^{-2} s^{-1}; Fig. 4D-F and Fig. S3) showing that *ndhm* KO mutation led to a higher Y(NA) limitation when the light was switched on. Interestingly acceptor side limitation (Y(NA)) was higher in *ndhm* KO than WT also when light was switched off and remained higher during the 10 minutes of dark recovery. This suggests that in absence of NDH activity stromal acceptors are not readily oxidized as in WT after the light is switched off (Fig. 4C and 4F).

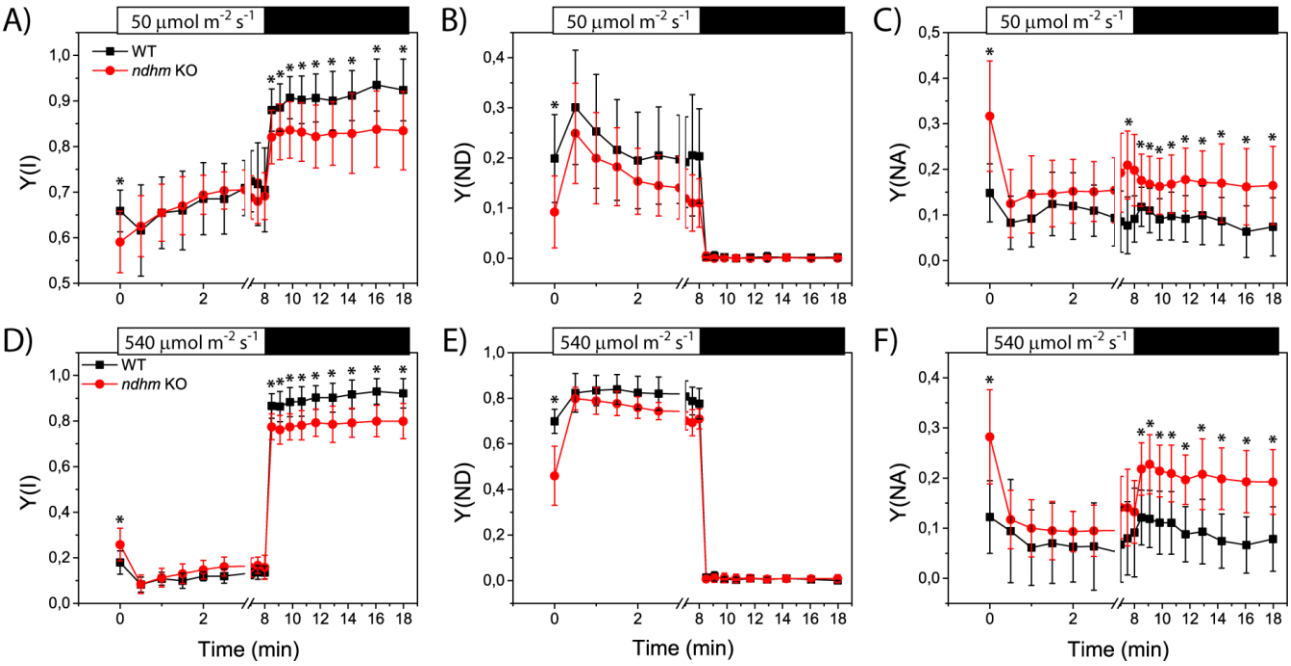

Fig. 4. Effect of the NDHM depletion on P700 redox state. Y(I) (**A**, **D**), Y(ND) (**B**, **E**) and Y(NA) (**C**, **F**). White bars on top of each graph represent the interval in which actinic light was switched on and black bars represent the period of dark recovery. The actinic light intensity was 50 µmol photons m^{-2} s^{-1} for A-C and 540 µmol photons m^{-2} s^{-1} for D-F. Data represent average values ± sd, n = 4 - 10. For *ndhm* KO mutants, experiments were always performed using two independent lines and for clarity reasons the average value obtained from the two lines was presented. WT (black) and *ndhm* KO (red). * indicates a significant difference between WT and mutant plants (examined by Student's t-test, $P < 0.01$).

Mutant lines are deficient in short-term response to changing light intensity

Previous data suggested an NDH complex activity in the dark and during the dark-to-light transitions. WT and the *ndhm* KO mutants were thus challenged by a reiterated exposure to dark/light cycles where 3 minutes of illumination with actinic light of 50 μmol photons m^{-2} s^{-1} were followed by 6 minutes of dark. This 9-minute cycle was then repeated 4 more times while monitoring P700 absorption and chlorophyll fluorescence signals to determine PSI and PSII activity (Fig. 5).The Y(I) decreased gradually over time in both genotypes and 6 minutes of dark treatment were not sufficient to fully recover to the initial value. The effect was however larger in *ndhm* KO, with the difference between WT and mutants becoming larger at each light/dark cycle (Fig. 5A). This difference in PSI efficiency is attributable to a progressive increase of acceptor side limitation (Y(NA), Fig. 5C) that did not recover during the dark phases. Remarkably Y(NA) seems to increase at each dark phase supporting the hypothesis that NDH is active in oxidizing PSI acceptor side in the dark. After a few cycles even PSII activity was affected in the absence of NDHM. In particular in the last cycle of the kinetic 1-qL was significantly higher in *ndhm* KO than in WT plants, suggesting that with the accumulation of the cycles PQ pool become more reduced in the absence of NDH complex (Fig. 5F).

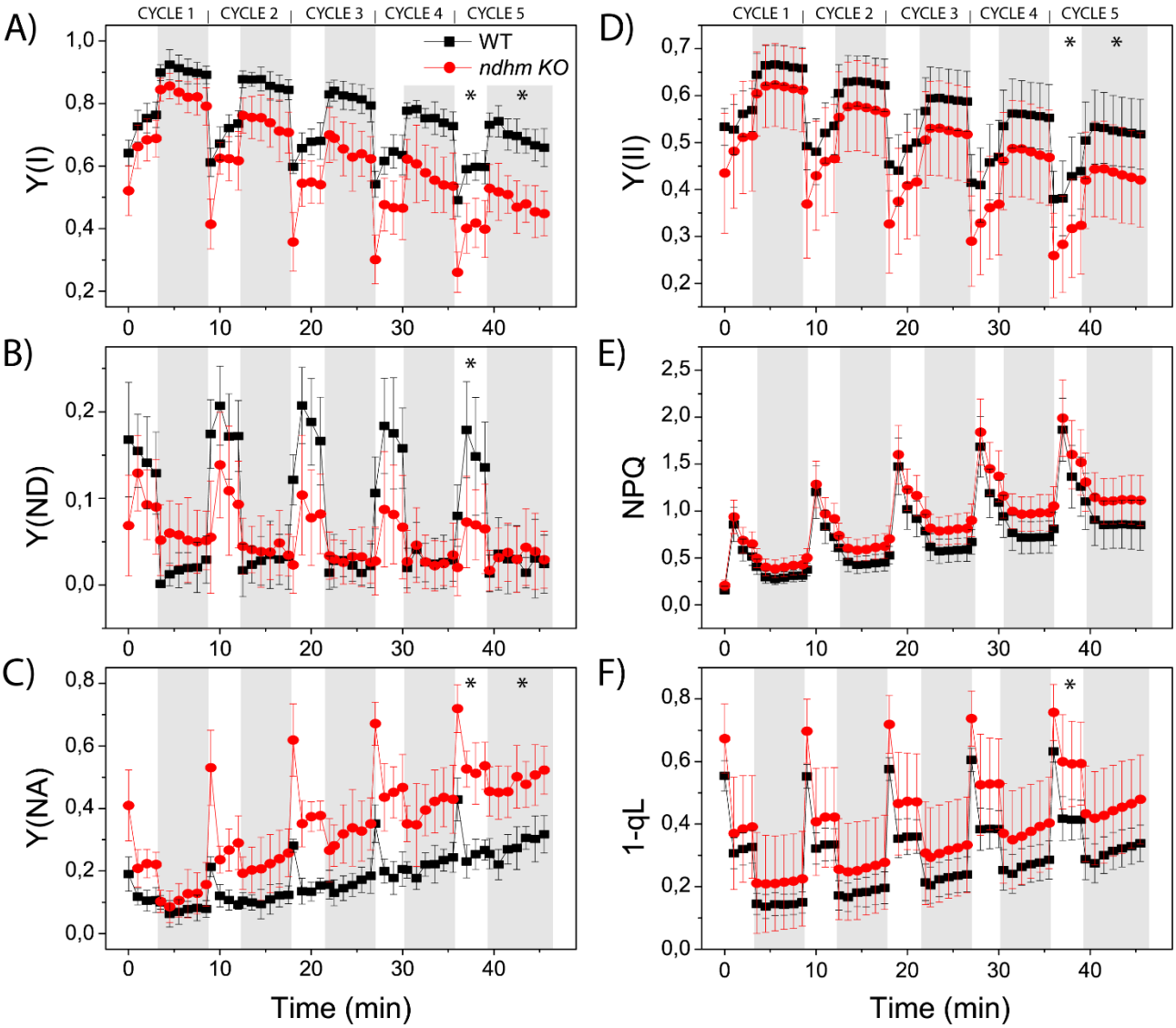

Fig. 5. NDH-dependent CET protects photosystem I under low intensity fluctuating light. Effect of fluctuating light on PSI and PSII: Y(I) (**A**), Y(ND) (**B**), Y(NA) (**C**), Y(II) (**D**), NPQ (**E**) and 1-qL (**F**) in WT (black) and *ndhm* KO (red) plants. Biological replicates, n = 4 ± sd for WT and 8 ± sd for *ndhm* KO. At time 0, after 40 minutes of dark adaptation, plants were treated with actinic light (50 µmol photons m^{-2} s^{-1}) for 3 minutes followed by 6 minutes in the dark. This 3+6 minutes cycle was repeated 4 more times. * indicates a significant difference between WT and mutant plants in the light and dark period of the cycle (examined by Student's t-test, $P < 0.01$).

Interaction of NDH and pseudo-cyclic electron transport

In *P. patens* the FLVs were shown to play a major role upon dark-to-light transitions and to be responsible for highly active electron transports in the first seconds after light was switched on (Gerotto *et al.*, 2016). Results present here also suggest that NDH contribute to the dark-to-light transition with a possible overlapping function between the two pathways. The putative functional interaction between NDH and FLV pathways was thus tested by introducing the *flva* KO mutation

(Gerotto *et al.*, 2016) in *ndhm* KO plants (Fig. S4). The homologous recombination event in the *FLVA* locus of *ndhm* KO mutant was verified at the level of gDNA and FLVA expression was verified both by RT-PCR and western blotting analysis and chlorophyll a fluorescence analysis (Fig. S4). All genotypes showed similar Fv/Fm, 0.82 ± 0.02 for WT, 0.83 ± 0.02 for *flva* KO and 0.83 ± 0.02 for *flva ndhm* KO. As expected, the Y(I) of *flva* KO mutants was low as compared to WT when actinic light was switched on (Fig. 6A and 6D). Interestingly the *flva* KO and *flva ndhm* KO plants shared very similar PSI and PSII activity, regardless of the actinic light used (50 and 540 µmol photons m^{-2} s^{-1}) (Fig 6 and Fig. S5). In particular, plants carrying *flva* mutation had high Y(NA) (Fig. 6C and 6F), but no significant difference between *flva* KO and *flva ndhm* KO was detected suggesting that lack of FLV had a larger effect than NDH.

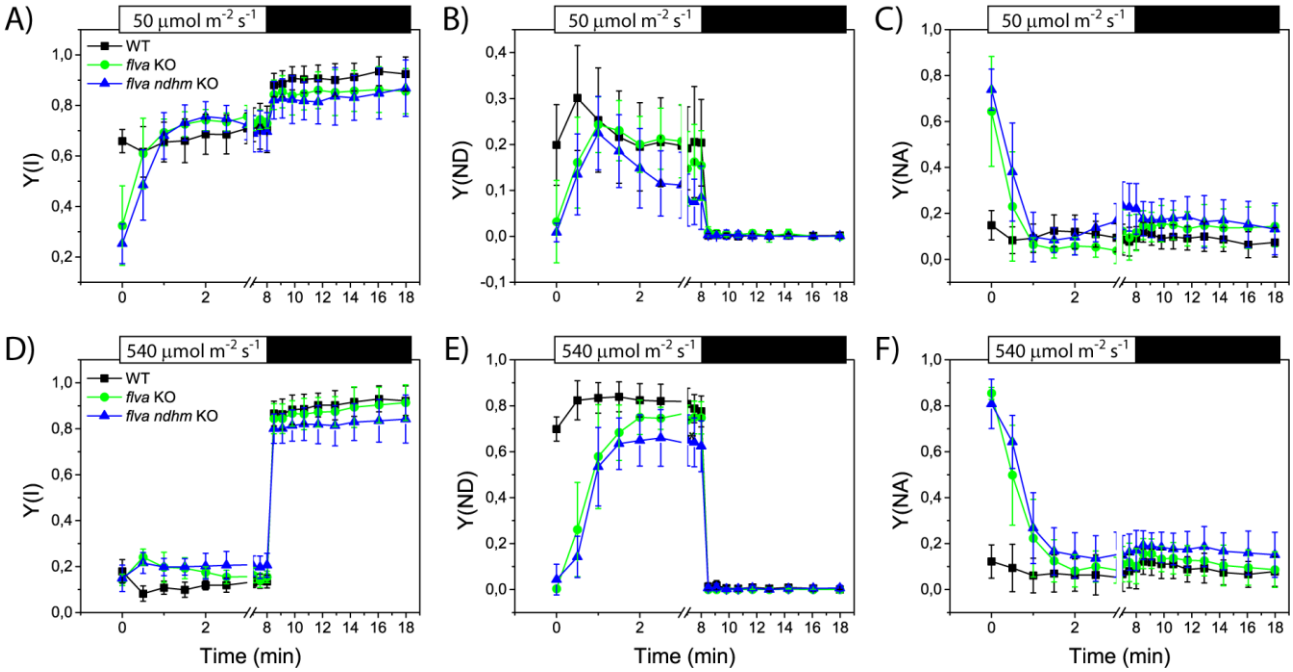

Fig. 6. Effect of the FLVA depletion in a *ndhm* KO background on P700 redox state. Y(I) (**A**, **D**), Y(ND) (**B**, **E**) and Y(NA) (**C**, **F**). White bars on top of each graph represent the interval in which actinic light was switched on and black bars represent the period of dark recovery. The actinic light intensity was 50 µmol photons m^{-2} s^{-1} for A-C and 540 µmol photons m^{-2} s^{-1} for D-F. Data represent average values ± sd, n = 4 - 6. For *flva ndhm* KO mutants, experiments were always performed using two independent lines and for clarity reasons the average value obtained from the two lines was presented. WT (black), *flva* KO (green) and flva *ndhm* KO (blue).

The estimation of total electron flow (TEF) using ECS signal in WT, *ndhm* KO, *flva* KO and *flva ndhm* KO showed that NDHM depletion had no detectable effect both in WT and *flva* KO background (Fig. 7A). When plants where treated by DCMU to block PSII activity and measure solely the electron flow through PSI, *flva* KO and *flva ndhm* KO showed a sustained transport as compared to WT and *ndhm* KO respectively (Fig. 7B). Mutants carrying *ndhm* KO mutation did not show a substantial reduction in CEF as compared to the corresponding backgrounds, either WT or *flva* KO (Fig. 7B).

Overall, these results clearly show that FLV activity has a substantial impact on electron transport and generation of pmf after light is switched on while the influence of NDH complex on light driven electron transport is instead quantitatively far less relevant.

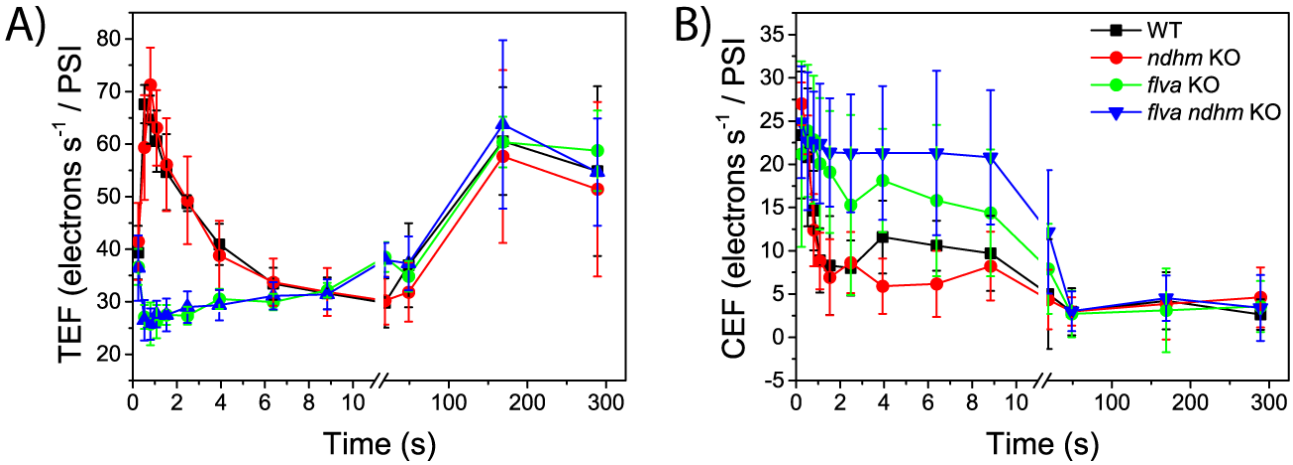

Fig. 7. Photosynthetic electron transport in *P. patens* plants. WT and mutant lines were grown in control light for 10 days. A) Total photosynthetic electron flow (TEF) and cyclic electron flow (CEF) measured *in vivo* in WT (black squares), *ndhm* KO (red circles), *flva* KO (green circles) and *flva ndhm* KO (blur triangles) at 940 µmol photons $m^{-2} \cdot s^{-1}$ actinic light, calculated from electrochromic shift signal. Electron transport rate values are normalized to xenon-induced PSI turnovers. Data presented are averages ± sd; n = 6-12.

DISCUSSION

It was recently proposed that NDH can form a supercomplex with one single PSI in *P. patens* (Kato *et al.*, 2018), instead of binding two PSI trough the antenna linkers LHCA5 and LHCA6 as in Angiosperms (Peng *et al.*, 2009; Kouřil *et al.*, 2014). Indeed, since *P. patens* genome contains LHCA5 but not a LHCA6 homologue (Alboresi *et al.*, 2008), only one PSI antenna should be available to bind NDH. Results presented here on *ndhm* KO of *P. patens* are consistent with this hypothesis. In fact, in wild-type plants NDHM was detected in a region of the gel compatible with the apparent molecular weight of PSI-NDH supercomplex. However, we could not demonstrate the comigration of NDH with PSI, leaving open alternative possibilities, such as for example the formation of an NDH dimer or another heterocomplex than PSI-NDH (Fig. 2B). If a PSI-NDH complex is indeed present, these 2D-immunoblot results suggest that it represents a very small fraction of the whole PSI population.

P. patens plants defective in NDH complex did not show any specific growth or developmental phenotype if compared to WT (Fig. 1), consistently to what was observed in several other organisms like *Marchantia, Nicotiana, Arabidopsis* and *Oryza* (Endo *et al.*, 1999; Ishikawa *et al.*, 2008; Yamori *et al.*, 2015). On the contrary NDH-mediated CEF might be essential in C4 plants, as demonstrated by NDHN suppression in *Flaveria bidentis* (Ishikawa *et al.*, 2016) and might have a key roles in the development of specific plant organs, as suggested by transposon-tagged tomato plants in which the loss of NDHM expression impair tomato fruit ripening (Nashilevitz *et al.*, 2010). This functional heterogeneity, together with the variable distribution of NDH complex among photosynthetic organisms (Ruhlman *et al.*, 2015), suggest that NDH complex had a meaningful physiological role during plastid evolution and that it specialized over time (de Vries *et al.*, 2016) but in some cases it has been juxtaposed or replaced by other mechanisms.

The analysis of photosynthetic parameters of *ndhm* KO plants at different light intensities revealed that NDH complex alleviates Y(NA) during the dark-to-light transitions (Fig. S2 and Fig. 4), both under control light (50 µmol photons m^{-2} s^{-1}) and under high light (540 µmol photons m^{-2} s^{-1}) conditions. The phenotype observed at the level of PSI acceptor side is congruent with previous work demonstrating that CEF is important during the first seconds of photosynthetic activity in C3 plants (Joliot and Joliot, 2006). When the NDH inactivation was combined with depletion of FLVs it emerged that the latter have a larger role in electron transport capacity than NDH complex. FLVs are responsible for the transport of a high number of electrons in the first seconds after light is switched on and their role cannot be compensated by the low electron transport capacity of NDH complex (Shikanai, 2016*a*; Strand *et al.*, 2017) (Fig. 6, Fig. 7 and Fig. S5). This observation is supported by the biochemical evidences presented here, with only a very small fraction of PSI involved in super-complexes with NDH. If this is the case, it can be understood why when PSI is fully active in transporting electrons NDH activity is not detectable.

However, NDH complex appears to be functionally different with respect to PGR5/PGRL1-dependent CEF where there are evidence of a partially overlapping function with FLV activity. In fact, the heterologous expression of *P. patens* FLVA/B in *A. thaliana* and rice was able to complement the phenotype of mutants impaired in PGR5 accumulation (Yamamoto *et al.*, 2016; Wada *et al.*, 2017). This was also confirmed in *P. patens* where the simultaneous absence of PGRL1 and FLV caused an enhanced Y(NA) with respect to each one of the two single mutants (Chapter 3).

The role of NDH and the differences between WT and *ndhm* KO are amplified when dark/light cycles are reiterated (Fig. 5). At each repetition the difference in acceptor side limitation between *ndhm* KO and WT plants increases, ultimately leading to a significant impairment in PSI yield (Fig. 5). The

repetition of the cycles also indirectly affects PSII activity, leading to a more pronounced reduction of PQ pool in *ndhm* KO plants than in WT (Fig. 5). The role of NDH complex is well compensated by other electron transport pathways when plants are grown in constant conditions of a growth chamber. This cyclic light experiment suggests that NDH complex physiological role could be much more relevant in natural environments, where the fluctuations in light intensities are frequent. In this case, NDH-dependent CEF pathway could provide higher flexibility to the chloroplast electron transport chain.

The physiological role in fluctuating light is apparently in contrast with the observations of a limited influence on photosynthetic electron transport. To reconcile this apparent conclusion, it should be underlined that while NDH is not abundant and active enough to have a major impact on electron transport when this is under full activity, the picture could instead be different in the dark, when light-driven electron transport is absent. Here even NDH activity could become physiologically relevant. Indeed, we observed that in *ndhm* KO PSI acceptor side remained high, suggesting that NDH could be active in maintaining PSI acceptor side oxidized after the light is switched off. The effect visible when light is switched back on, thus, would not be due to the NDH electron transport ability but rather to the fact that PSI in the absence of NDH is already partially reduced, limiting its acceptor capacity. A functional role of NDH complex in the dark period of fluctuating light treatments was already reported in the case of *O. sativa* (Yamori *et al.*, 2016) and *A. thaliana* (Strand *et al.*, 2017). In both cases, WT plants decreased the electron flow to PSI during the light phase, which seemed to be essential to prevent the over-reduction of PSI (Yamori *et al.*, 2016; Strand *et al.*, 2017). However, PSI is sensitive to excess electrons accumulating at the acceptor side where they damage the Fe-S cluster present here (Sonoike *et al.*, 1995; Tiwari *et al.*, 2016). NDH by keeping PSI oxidized after the light is switched off contributes to keeping PSI not limited at the acceptor side and reducing the probability of an acceptor side limitation when light is back on.

MATERIAL AND METHODS

Plant Material and growth conditions

WT and mutant lines of *P. patens* (Gransden) were grown on $PpNO_3$ medium at 24°C, 16 h light / 8 h dark photoperiod at control light intensity 50 µmol photons m^{-2} s^{-1}.

Construct Design, Moss Transformation and Screening of Resistant

Regions from *NDHM* gene (Phypa_170083) were amplified by PCR from WT gDNA and cloned up- and down-stream the coding sequence of bleomycin resistance cassette (Fig. S1). This construct was used for PEG-mediated heat-shock protoplast transformation as previously described (Alboresi *et al.*, 2010). The *flva ndhm* double KO plants were isolated by inserting *flva* mutation (Gerotto *et al.*, 2016) in *ndhm* #2. In all cases, after two rounds of selection on antibiotic supplemented media, gDNA from resistant lines and control plants was extracted by a quick extraction protocol (Edwards *et al.*, 1991) and used to confirm the presence of the insertion at the expected target locus (Fig. S1; Table S1). Total RNA was purified with TRI Reagent (Sigma Aldrich) and 1 µg was used as template for cDNA synthesis with RevertAid Transcriptase (Thermo Scientific) to verify *NDHM* and *ACT* gene expression using specific primers (Fig. S1, Table S1) (Gerotto *et al.*, 2016). All experiments were performed using two independent lines both *ndhm* and *flva ndhm* KO mutants. The average values obtained from the two lines are presented.

SDS-PAGE, CN-PAGE and western blotting

Total Protein extracts were obtained by grinding fresh tissues directly in Laemmli buffer before loading SDS-PAGE. For immunoblotting analysis, after SDS-PAGE, proteins were transferred onto nitro-cellulose membrane (Pall Corporation) and detected with specific commercial (anti-PsaD, anti-γATPase and anti-Cyt f, Agrisera, catalog numbers AS09 461,AS08 312 and AS06119) or in-house made polyclonal antibodies (CP47, LHCA1, D2 and NDHM) (Bassi *et al.*, 1992). Thylakoid membranes for CN-PAGE were purified as in (Gerotto *et al.*, 2012) and resuspended in 25mM BisTris pH7, 20% glycerol buffer at final concentration of 1 µg chl/µL. Pigment-protein complexes were solubilized with 0.75% n-Dodecyl-α-Maltoside as described in (Järvi *et al.*, 2011) adding 0.2% deoxycholic acid prior loading. CN-PAGE gel were casted as described in (Järvi *et al.*, 2011) using a 3.5-11 % acrylamide gradient for isolation. Chl a/b and Chl/Car ratios were obtained by fitting the spectrum of 80% acetone pigment extracts with spectra of the individual pigments (Croce *et al.*, 2002).

Fluorescence and P700 Measurement with Dual-PAM

Ten-day old plants grown on $PpNO_3$ medium were probed for chlorophyll fluorescence and $P700^+$ absorption with a Dual PAM-100 fluorometer (Walz). Plants were dark acclimated for 40 min before measurements. For light curves, light intensity increased every minute ranging from 0 to 230 µmol photons m^{-2} s^{-1}. For induction kinetics, 50 or 540 µmol photons m^{-2} s^{-1} actinic red light was used, for dark to light kinetics a cycle of 3 min 50 µmol photons m^{-2} s^{-1} and 6 min dark was repeated 5 times. PSII and PSI parameters were calculated as follow: Y(II), (Fm'-Fo)/Fm'; qL, (Fm'-F)/(Fm'-Fo') x Fo'/F; NPQ, (Fm-Fm')/Fm'; Y(I), 1-Y(ND)-Y(NA); Y(NA), (Pm-Pm')/Pm; Y(ND), (1 - P700 red).

Spectroscopic Analyses with Joliot-Type Spectrometer (JTS).

Spectroscopic analysis was performed *in vivo* on 10-day old intact tissues grown in control light using a JTS-10 spectrophotometer (Biologic). Electron transport rates (ETR) were evaluated measuring the Electrochromic Shift (ECS) spectral change on buffer infiltrated plants (Hepes 20mM pH 7.5, KCl 10mM) (Gerotto *et al.*, 2016). Relative amount of functional PSI was evaluated by xenon-induced single flash turnover in presence of 3-(3,4-dichlorophenyl)-1,1-dimethylurea (DCMU 20µM) and hydroxylamine (HA, 4 mM) and used to normalize electron transport rate values. Because of the presence of double PSI turnovers using a xenon lamp (Bailleul *et al.*, 2010), ETR absolute values are underestimated by ~40% (Gerotto *et al.*, 2016).

ABBREVIATIONS

gDNA, genomic DNA; PSII, photosystem II; Cyt b_6f, cytochrome b_6f; PSI, photosystem I; PQH_2, plastoquinone; LEF, linear electron flux; CBB, Calvin Benson Bassham; CEF, cyclic electron flux; LHC, light harvesting complex; ETR I, electron transport rate through photosystem I; ETR II, electron transport rate through photosystem II;

REFERENCES

Alboresi A, Caffarri S, Nogue F, Bassi R, Morosinotto T. 2008. In silico and biochemical analysis of Physcomitrella patens photosynthetic antenna: Identification of subunits which evolved upon land adaptation. PLoS ONE 3.

Alboresi A, Gerotto C, Giacometti GM, Bassi R, Morosinotto T, Alboresia A, Gerottob C, Giacomettib GM, Bassia R, Morosinotto T. 2010. Physcomitrella patens mutants affected on heat dissipation clarify the evolution of photoprotection mechanisms upon land colonization. Proceedings of the National Academy of Sciences of the United States of America 107, 11128–33.

Alboresi A, Storti M, Morosinotto T. 2018. Balancing protection and efficiency in the regulation of photosynthetic electron transport across plant evolution. The New phytologist.

Allahverdiyeva Y, Mustila H, Ermakova M, Bersanini L, Richaud P, Ajlani G, Battchikova N, Cournac L, Aro E-M. 2013. Flavodiiron proteins Flv1 and Flv3 enable cyanobacterial growth and photosynthesis under fluctuating light. Proceedings of the National Academy of Sciences of the United States of America 110, 4111–6.

Armbruster U, Zühlke J, Rengstl B, *et al.* 2010. The Arabidopsis thylakoid protein PAM68 is required for efficient D1 biogenesis and photosystem II assembly. The Plant cell 22, 3439–60.

Arnon DI, Chain RK. 1975. Regulation of ferredoxin-catalyzed photosynthetic phosphorylations. Proceedings of the National Academy of Sciences of the United States of America 72, 4961–5.

Bailleul B, Cardol P, Breyton C, Finazzi G. 2010. Electrochromism: A useful probe to study algal photosynthesis. Photosynthesis Research 106, 179–189.

Bassi R, Soen SY, Frank G, Zuber H, Rochaix JD. 1992. Characterization of chlorophyll a/b proteins of photosystem I from Chlamydomonas reinhardtii. The Journal of biological chemistry 267, 25714–21.

Bersanini L, Battchikova N, Jokel M, Rehman A, Vass I, Allahverdiyeva Y, Aro E-M. 2014. Flavodiiron protein Flv2/Flv4-related photoprotective mechanism dissipates excitation pressure of PSII in cooperation with phycobilisomes in Cyanobacteria. Plant physiology 164, 805–18.

Chaux F, Burlacot A, Mekhalfi M, Auroy P, Blangy S, Richaud P, Peltier G. 2017. Flavodiiron Proteins Promote Fast and Transient O2Photoreduction inChlamydomonas. Plant physiology 174, 1825–1836.

Croce R, Canino G, Ros F, Bassi R. 2002. Chromophore Organization in the Higher-Plant Photosystem II Antenna Protein CP26. Biochemistry 41, 7334–7343.

DalCorso G, Pesaresi P, Masiero S, Aseeva E, Schünemann D, Finazzi G, Joliot P, Barbato R, Leister D. 2008. A complex containing PGRL1 and PGR5 is involved in the switch between linear and cyclic electron flow in Arabidopsis. Cell 132, 273–85.

Desplats C, Mus F, Cuiné S, Billon E, Cournac L, Peltier G. 2009. Characterization of Nda2, a plastoquinone-reducing type II NAD(P)H dehydrogenase in chlamydomonas chloroplasts. The Journal of biological chemistry 284, 4148–57.

Edwards K, Johnstone C, Thompson C. 1991. A simple and rapid method for the preparation of plant genomic DNA for PCR analysis. Nucleic acids research 19, 1349.

Endo T, Shikanai T, Takabayashi A, Asada K, Sato F. 1999. The role of chloroplastic NAD(P)H dehydrogenase in photoprotection. FEBS letters 457, 5–8.

Gerotto C, Alboresi A, Giacometti GMGM, Bassi R, Morosinotto T. 2012. Coexistence of plant and algal energy dissipation mechanisms in the moss Physcomitrella patens. The New phytologist 196, 763–73.

Gerotto C, Alboresi A, Meneghesso A, Jokel M, Suorsa M, Aro E-MEM, Morosinotto T. 2016. *Flavodiiron proteins act as safety valve for electrons in Physcomitrella patens*. National Academy of Sciences.

Hori K, Maruyama F, Fujisawa T, *et al.* 2014. Klebsormidium flaccidum genome reveals primary factors for plant terrestrial adaptation. Nature communications 5, 3978.

Ishikawa N, Endo T, Sato F. 2008. Electron transport activities of Arabidopsis thaliana mutants with impaired chloroplastic NAD(P)H dehydrogenase. Journal of Plant Research 121, 521–526.

Ishikawa N, Takabayashi A, Noguchi K, Tazoe Y, Yamamoto H, von Caemmerer S, Sato F, Endo T. 2016. NDH-Mediated Cyclic Electron Flow Around Photosystem I is Crucial for C $_4$ Photosynthesis. Plant and Cell Physiology 57, 2020–2028.

Ito A, Sugita C, Ichinose M, Kato Y, Yamamoto H, Shikanai T, Sugita M. 2018. An evolutionarily conserved P-subfamily pentatricopeptide repeat protein is required to splice the plastid *ndhA* transcript in the moss *Physcomitrella patens* and *Arabidopsis thaliana*. The Plant Journal 94, 638–648.

Järvi S, Suorsa M, Paakkarinen V, Aro E-M. 2011. Optimized native gel systems for separation of

thylakoid protein complexes: novel super- and mega-complexes. The Biochemical journal 439, 207–14.

Jokel M, Johnson X, Peltier G, Aro E-M, Allahverdiyeva Y. 2018. Hunting the main player enabling Chlamydomonas reinhardtii growth under fluctuating light. The Plant journal : for cell and molecular biology 94, 822–835.

Joliot P, Joliot A. 2006. Cyclic electron flow in C3 plants. Biochimica et biophysica acta 1757, 362–8.

Kato Y, Odahara M, Fukao Y, Shikanai T. 2018. Stepwise evolution of supercomplex formation with photosystem I is required for stabilization of chloroplast NADH dehydrogenase-like complex: Lhca5-dependent supercomplex formation in Physcomitrella patens. The Plant Journal.

Kouřil R, Strouhal O, Nosek L, Lenobel R, Chamrád I, Boekema EJ, Šebela M, Ilík P. 2014. Structural characterization of a plant photosystem I and NAD(P)H dehydrogenase supercomplex. The Plant journal : for cell and molecular biology 77, 568–76.

Kukuczka B, Magneschi L, Petroutsos D, Steinbeck J, Bald T, Powikrowska M, Fufezan C, Finazzi G, Hippler M. 2014. Proton Gradient Regulation5-Like1-Mediated Cyclic Electron Flow Is Crucial for Acclimation to Anoxia and Complementary to Nonphotochemical Quenching in Stress Adaptation. Plant physiology 165, 1604–1617.

Munekage Y, Hojo M, Meurer J, Endo T, Tasaka M, Shikanai T. 2002. PGR5 is involved in cyclic electron flow around photosystem I and is essential for photoprotection in Arabidopsis. Cell 110, 361–71.

Nashilevitz S, Melamed-Bessudo C, Izkovich Y, *et al.* 2010. An orange ripening mutant links plastid NAD(P)H dehydrogenase complex activity to central and specialized metabolism during tomato fruit maturation. The Plant cell 22, 1977–97.

Otani T, Kato Y, Shikanai T. 2018. Specific substitutions of light-harvesting complex I proteins associated with photosystem I are required for supercomplex formation with chloroplast NADH dehydrogenase-like complex. Plant Journal 94, 122–130.

Peltier G, Aro E-M, Shikanai T. NDH-1 and NDH-2 Plastoquinone Reductases in Oxygenic Photosynthesis. Annual review of plant biology 67, 55–80.

Peng L, Fukao Y, Fujiwara M, Takami T, Shikanai T. 2009. Efficient operation of NAD(P)H dehydrogenase requires supercomplex formation with photosystem I via minor LHCI in

Arabidopsis. The Plant cell 21, 3623–40.

Peng L, Shimizu H, Shikanai T. 2008. The chloroplast NAD(P)H dehydrogenase complex interacts with photosystem I in Arabidopsis. Journal of Biological Chemistry 283, 34873–34879.

Ruhlman TA, Chang W-J, Chen JJ, *et al.* 2015. NDH expression marks major transitions in plant evolution and reveals coordinate intracellular gene loss. BMC Plant Biology 15, 100.

Rumeau D, Bécuwe-Linka N, Beyly A, Louwagie M, Garin J, Peltier G. 2005. New subunits NDH-M, -N, and -O, encoded by nuclear genes, are essential for plastid Ndh complex functioning in higher plants. The Plant cell 17, 219–32.

Shikanai T. 2016*a*. Regulatory network of proton motive force: contribution of cyclic electron transport around photosystem I. Photosynthesis research 129, 1–8.

Shikanai T. 2016*b*. Chloroplast NDH: A different enzyme with a structure similar to that of respiratory NADH dehydrogenase. Biochimica et biophysica acta 1857, 1015–22.

Shimakawa G, Ishizaki K, Tsukamoto S, Tanaka M, Sejima T, Miyake C. 2017. The Liverwort, Marchantia, Drives Alternative Electron Flow Using a Flavodiiron Protein to Protect PSI. Plant physiology 173, 1636–1647.

Sonoike K, Terashima I, Iwaki M, Itoh S. 1995. Destruction of photosystem I iron-sulfur centers in leaves of Cucumis sativus L. by weak illumination at chilling temperatures. FEBS letters 362, 235–8.

Strand DD, Fisher N, Kramer DM. 2017. The higher plant plastid NAD(P)H dehydrogenase-like complex (NDH) is a high efficiency proton pump that increases ATP production by cyclic electron flow. Journal of Biological Chemistry 292, 11850–11860.

Tiwari A, Mamedov F, Grieco M, Suorsa M, Jajoo A, Styring S, Tikkanen M, Aro E-M. 2016. Photodamage of iron–sulphur clusters in photosystem I induces non-photochemical energy dissipation. Nature Plants, 16035.

Ueda M, Kuniyoshi T, Yamamoto H, Sugimoto K, Ishizaki K, Kohchi T, Nishimura Y, Shikanai T. 2012. Composition and physiological function of the chloroplast NADH dehydrogenase-like complex in Marchantia polymorpha. The Plant journal : for cell and molecular biology 72, 683–93.

de Vries J, Stanton A, Archibald JM, Gould SB. 2016. Streptophyte Terrestrialization in Light of Plastid Evolution. Trends in Plant Science 21, 467–476.

Wada S, Yamamoto H, Suzuki Y, Yamori W, Shikanai T, Makino A. 2017. Flavodiiron protein substitutes for cyclic electron flow without competing CO2 assimilation. Plant physiology 176, 1509–1518.

Yamamoto H, Takahashi S, Badger MR, Shikanai T. 2016. Artificial remodelling of alternative electron flow by flavodiiron proteins in Arabidopsis. Nature plants 2, 16012.

Yamori W, Makino A, Shikanai T. 2016. A physiological role of cyclic electron transport around photosystem I in sustaining photosynthesis under fluctuating light in rice. Scientific reports 6, 20147.

Yamori W, Sakata N, Suzuki Y, Shikanai T, Makino A. 2011. Cyclic electron flow around photosystem I via chloroplast NAD(P)H dehydrogenase (NDH) complex performs a significant physiological role during photosynthesis and plant growth at low temperature in rice. The Plant journal : for cell and molecular biology 68, 966–76.

Yamori W, Shikanai T. 2016. Physiological Functions of Cyclic Electron Transport Around Photosystem I in Sustaining Photosynthesis and Plant Growth. Annual review of plant biology 67, 81–106.

Yamori W, Shikanai T, Makino A. 2015. Photosystem I cyclic electron flow via chloroplast NADH dehydrogenase-like complex performs a physiological role for photosynthesis at low light. Scientific reports 5, 13908.

SUPPLEMENTARY MATERIAL

Table S1. Primers employed for *ndhm* KO generation and screening. The table reports all the primers used to generate and characterize *Physcomitrella patens ndhm* KO lines. Primers were designed to disrupt *NDHM* coding sequence with the insertion of the bleomycin resistance cassette (ble). Genomic DNA from WT strain was used as a template to amplify selected homologous regions (P1 + P2 and P3 + P4). All the PCR products were cloned into BZRf vector for moss transformation using the restriction enzymes (REs) indicated. Moss protoplasts were transformed with *NDHM* KO construct linearized with PmlI and PacI. After transformation and two rounds of selection on zeocin, resistant lines were evaluated for correct homologous recombination using P5 + P6 (Left Border, LB) and P7 + P8 (Right Border, RB) primers. Primers NDHM_F and NDHM_R were used on cDNA libraries to verify *NDHM* expression by RT-PCR. ACTIN2_F and ACTIN2_R were used to controls the quality of genomic DNA and cDNA templates.

Primer name	Gene	Sequence	Use (RE)
P1	*NDHM*	atCACGTGCAGCTGCAACAAGTACCCAG	Vector design (PmlI)
P2	*NDHM*	atCTCGAGAATTCGCACATGACGAGTCG	Vector design (XhoI)
P3	*NDHM*	atGTTAACTTGGACTGTAGGGTGCTGAAC	Vector design (HpaI)
P4	*NDHM*	atTTAATTAATTACAAGCCAGCAAAGCAAA	Vector design (PacI)
P5	*NDHM*	TTGGAAGTCTGTTCACGCTTT	KO screening
P6	ble	GTGTCGTGCTCCACCATGT	KO screening
P7	ble	CCCCGCTTAAAAATTGGTAT	KO screening
P8	*NDHM*	TTCTGCCAATAGGATGTGAGG	KO screening
NDHM_F	*NDHM*	AGTGTCCTCCGCTTTTCTCA	RT-PCR
NDHM_R	*NDHM*	CTCCGTCAAATCTGCACCTG	RT-PCR
ACTIN2_F	*ACTIN2_F*	GCGAAGAGCGAGTATGACGAG	RT-PCR
ACTIN2_R	*ACTIN2_R*	AGCCACGAATCTAACTTGTGATG	RT-PCR

Table S2. Pigment composition of *Physcomitrella patens* WT and *ndhm* KO plants. Chlorophyll a/b and chlorophyll/carotenoid ratios (mol/mol) of protonema with SDs are shown (n = 5 to 8 for each genotype).

	Chl a/b	chl/car
WT	2.56 ± 0,11	3,85 ± 0,43
ndhm#1 KO	2,62 ± 0,15	4,08 ± 0,47
ndhm#2 KO	2,63 ± 0,13	3,67 ± 0,33

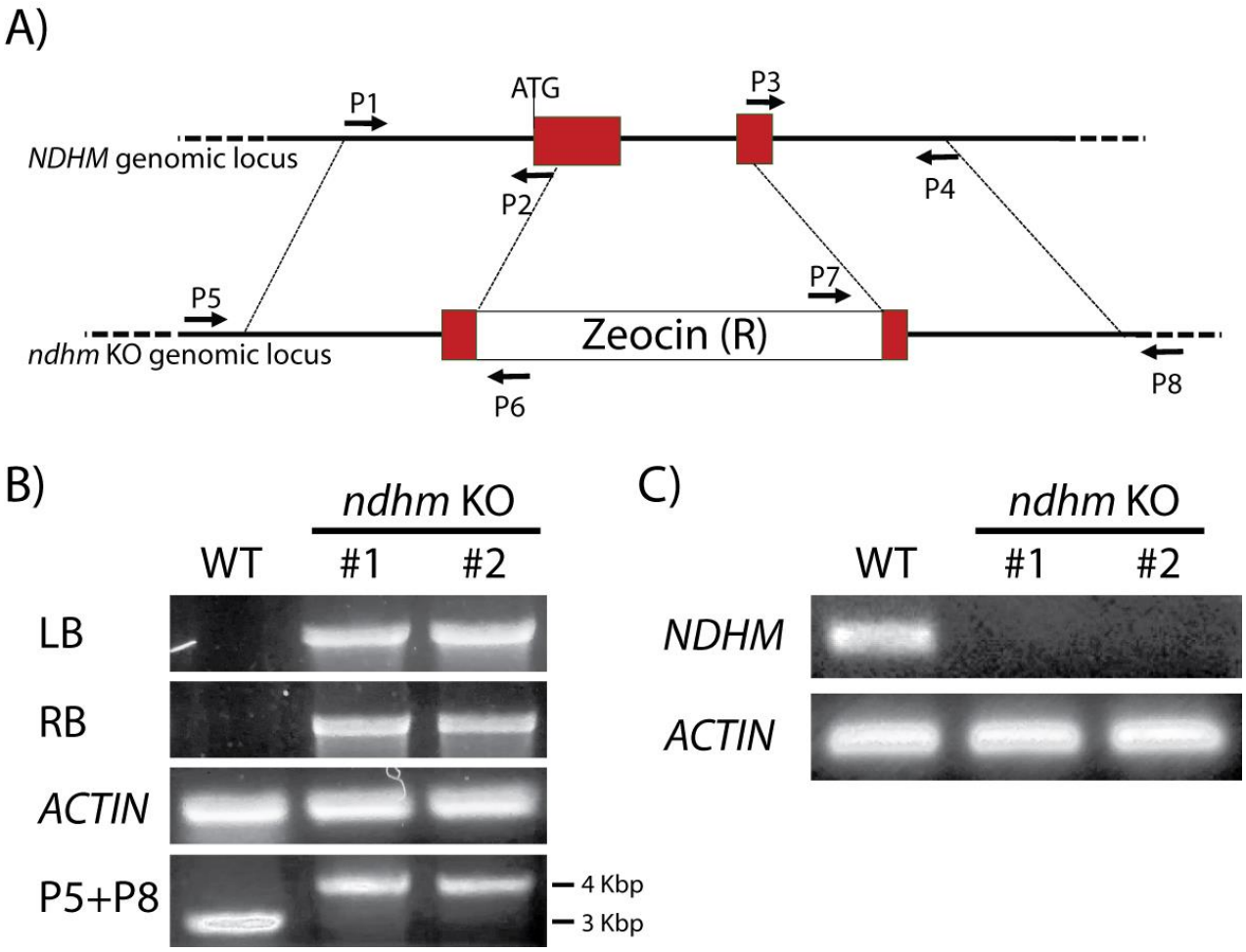

Fig. S1. Isolation of *ndhm* KO mutants. A) Schematic representation of the *NDHM* gene and corresponding *ndhm* KO. Red rectangles indicate exons and black arrows represent the primers used for cloning (from P1 to P4) and screening (from P5 to P8) procedures. After homologous recombination, the central part of the gene is substituted by the resistance cassette conferring zeocine resistance to *ndhm* KO. Dotted lines indicate the regions of the gene used to perform homologous recombination. B) Confirmation of homologous recombination event in the *NDHM* locus. LB stands for left border obtained by P5 and P6 primers, RB stands for right border obtained by P7 and P8. *ACTIN* primers were used as quality control for gDNA. The whole locus was amplified with primers P5 and P8 amplify WT target locus (~3 Kbp) and to confirm that *ndhm* KO #1 and #2 had one single insertion in the target locus (~4 Kbp). Multiple insertions in the target locus gave rise to a to larger fragment that was could not be amplified by PCR, those lines were discarded to focus on lines #1 and #2. C) RT-PCR analysis for the detection of *NDHM* and *ACTIN* transcripts in WT and two independent putative KO mosses. Primer sequences is reported in Table S1.

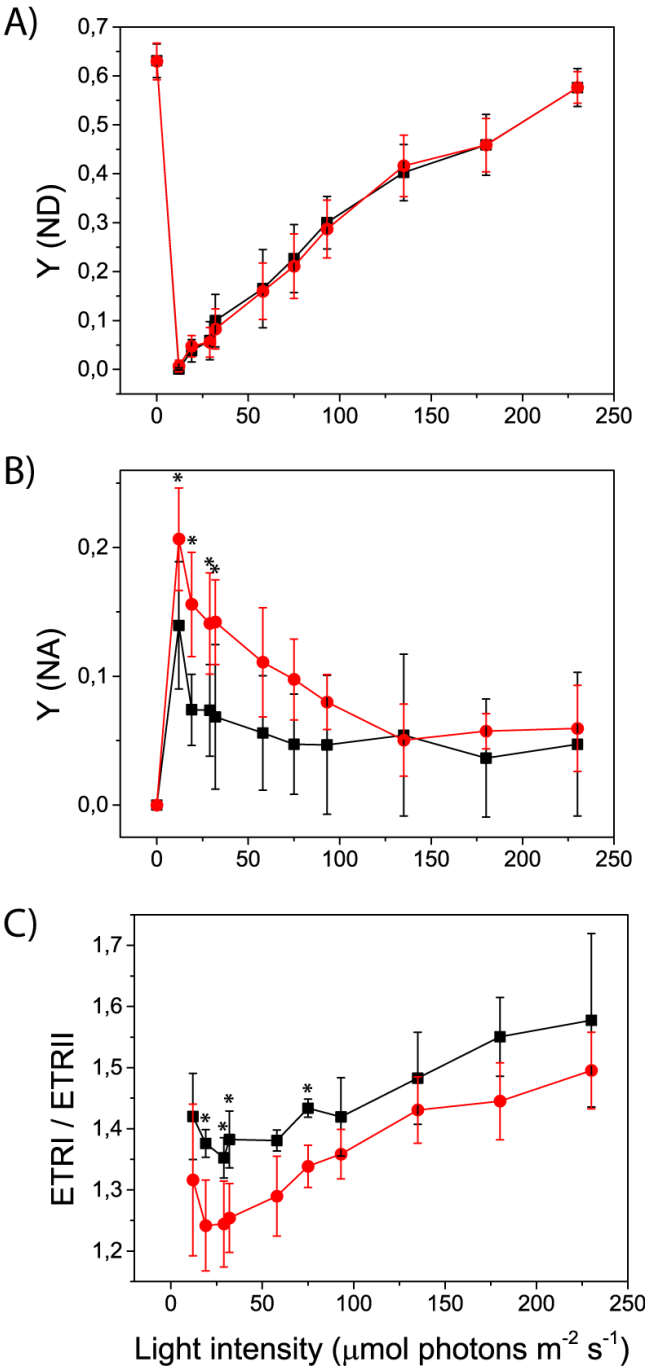

Fig. S2. Effect of the NDHM defect on photosystem II activity. Light-intensity dependence of (A) Y(ND), (B) Y(NA) and (C) ETRI/ETRII in WT (black squares) and two independent lines of *ndhm* KO (red circles), biological replicates n=3-6 ± sd. For *ndhm* KO mutants, experiments were always performed using two independent lines and for clarity reasons the average value obtained from the two lines was presented.

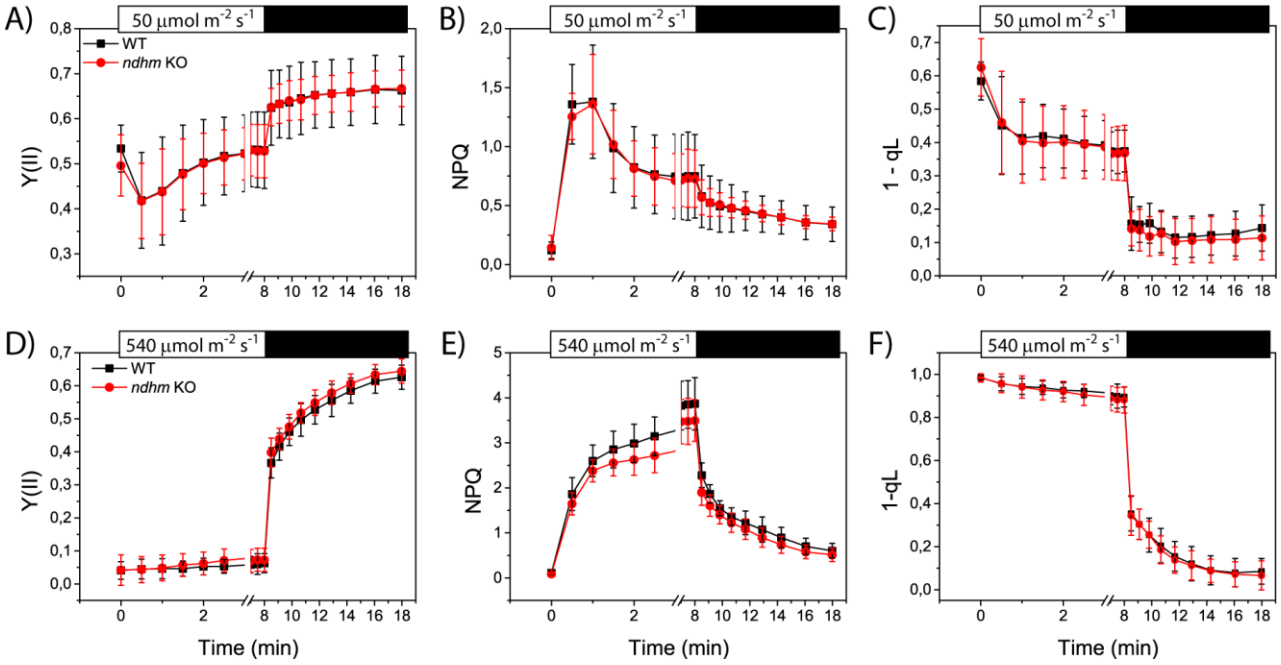

Fig. S3. Effect of the NDHM depletion on photosystem II activity. Chlorophyll fluorescence was measured to calculate time course of Y(II) (A, D), NPQ (B, E) and 1-qL (C, F). White and black bars on top of each graph represent the interval in which actinic light was switched respectively on and off. Actinic light intensity was 50 mmol photons m^{-2} s^{-1}; (A-C) and 540 mmol photons m^{-2} s^{-1} (D-F). For *ndhm* KO mutants, experiments were always performed using two independent lines and for clarity reasons the average value obtained from the two lines was presented. WT (black) and *ndhm* KO (red). Data represent mean values ± sd, n = 4 - 10.

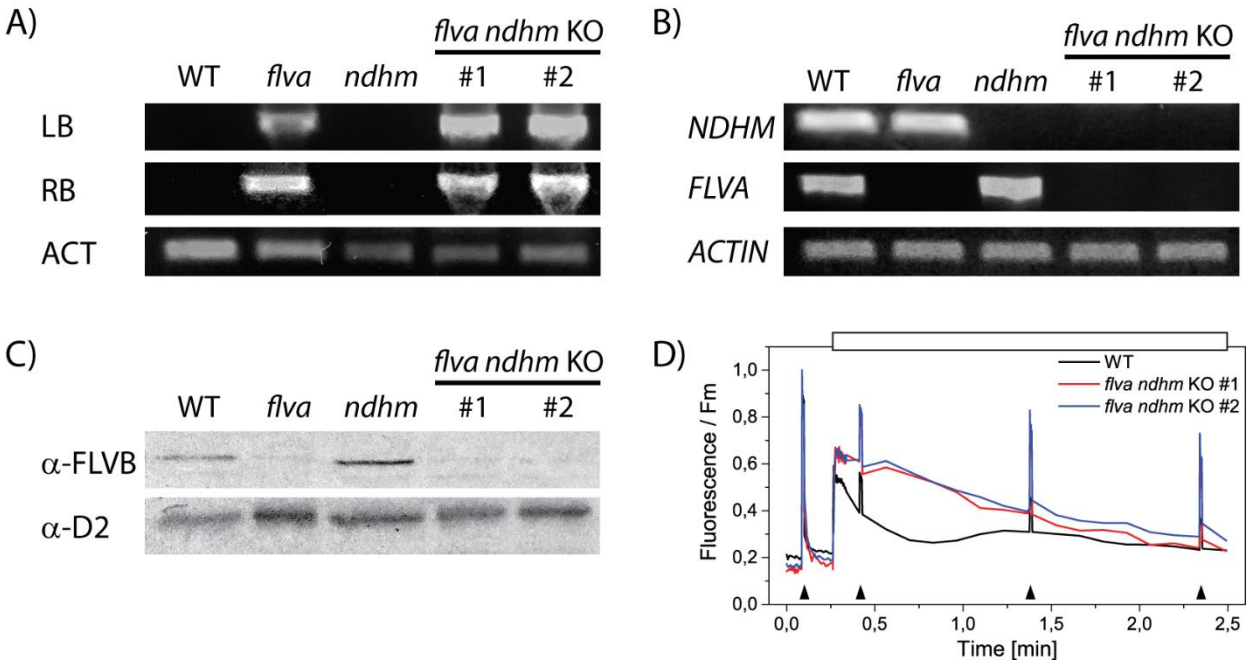

Fig. S4. Isolation of *flva ndhm* KO mutants. A) Confirmation of homologous recombination event in the *FLVA* locus of *ndhm* KO mutant. LB stands for left border, RB stands for right border obtained as previously described for the isolation of *flva* KO single mutants (Gerotto *et al.*, 2016). B) RT-PCR analysis for the detection of *NDHM*, *FLVA* and *ACTIN* transcripts in WT, *flva* KO, *ndhm* KO and two independent putative *flva ndhm* KO mosses. Primer sequences is reported in Table S1 and in the original publication describing the isolation of *flva* KO (Gerotto *et al.*, 2016). C) Western blotting analysis for detection of D2 and FLVB in WT and *flva ndhm* KO #1 and #2. D) Time courses of chlorophyll a fluorescence analysis for WT (black) and *flva ndhm* KO #1 and #2 (red and blue) exposed to 150 mmol photons m^{-2} s^{-1}. Exposure to actinic irradiance is indicated by a white bar at the top of the panel. Black triangles indicate the application of saturating flashes.

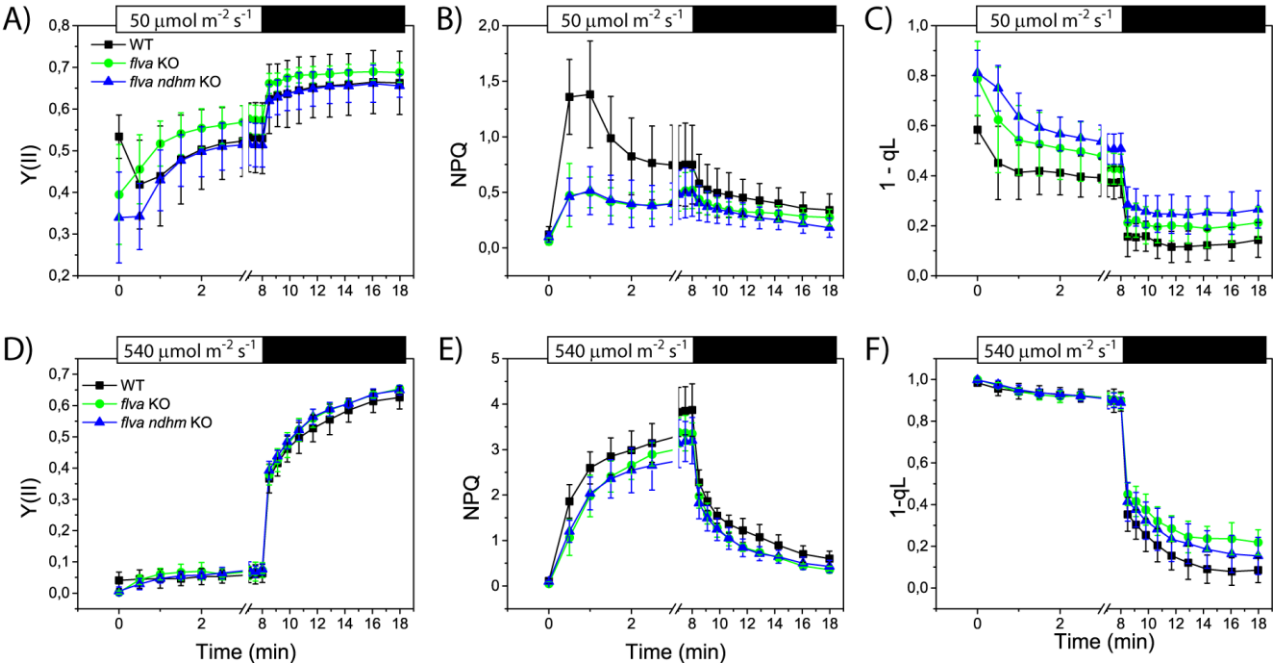

Fig. S5. Effect of the FLVA depletion in a *ndhm* KO background on photosystem II activity. Chlorophyll fluorescence was measured to calculate time course of Y(II) (A, D), NPQ (B, E) and 1-qL (C, F). White and black bars on top of each graph represent the interval in which actinic light was switched respectively on and off. Actinic light intensity was 50 mmol photons m^{-2} s^{-1}; (A-C) and 540 mmol photons m^{-2} s^{-1} (D-F). For *flva ndhm* KO mutants, experiments were always performed using two independent lines and for clarity reasons the average value obtained from the two lines was presented. WT (black), *flva* KO (green) and *flva ndhm* KO (blue). Data represent mean values ± sd, n = 4 - 10.

CHAPTER 5

Alternative Electron Flow Pathways Sustain Photosynthesis and Plant Growth

Authors name and affiliation

Mattia Storti, Federica Pennisi, Anna Segalla, Alessandro Alboresi, Tomas Morosinotto

Department of Biology, University of Padova, Via Ugo Bassi 58B, 35121 Padua, Italy

CONTRIBUTION

In this work MS performed growth test and photosynthetic characterization, analyzed the data and wrote most of the text.

ABSTRACT

Linear electron flow (LEF) allows the production of NADPH together with the generation of proton gradient (ΔpH) across the thylakoid membranes used for ATP synthesis. ΔpH is also important to modulate electron transport rate through non-photochemical quenching (NPQ) activation and Cyt b_6f down-regulation. Alternative electron flow (AEF) pathways transport electrons from LEF to other sinks to prevent overreduction and preserve photosynthetic apparatus. These pathways also control ATP/NADPH ratio in different light conditions. AEF include cyclic (CEF) and pseudo-cyclic electron flow (PCEF), the first recycles electrons form stroma pool downstream PSI to PQH_2 pool, while the second transports electrons back to oxygen. In this work we generated two new *P. patens* mutants, the first depleted for both CEF pathways and the second that in addition lacks also FLV mediated PCEF pathway. The two mutants showed strong sensitivity to light and defects in electrons transport rates, determining a reduced growth respect to WT plants in many different conditions. Severe PSI photoinhibition seems to be the primary cause of this reduced electrons transport. Plants partially recovered the phenotype when cultured in presence of glucose, suggesting that an external carbon source can support growth but also positively influence photosynthesis.

INTRODUCTION

As extensively discussed in the previous chapters, NADPH produced during linear electron flow (LEF) exceed that used for CO_2 fixation in Calvin-Benson-Bassam cycle (CBB cycle) (Yamori and Shikanai 2016) which is instead limited by ATP and CO_2 availability. The alternative electron flows (AEF) divert electrons from LEF final acceptors (Shikanai and Yamamoto 2017) preventing accumulation of reducing power in the stroma and membrane complexes, which can ultimately lead to photo-damage (Suorsa et al. 2012; Munekage et al. 2004; Gerotto et al. 2016). Cyclic electron flow (CEF) pathways can recycle electrons carried by reduced Fd and reintroduce them in the membrane at the level of PQ pool, decreasing NADPH formation while still sustaining ATP synthesis. Pseudo-CEF (PCEF) instead does not recycle electrons in the membrane but dissipate them through the so-called water-water cycle, using molecular oxygen as acceptor for electrons and thus producing water

(Allahverdiyeva et al. 2013; Helman et al. 2003). Again, this mechanism alleviates redox pressure in the stroma while still contributing to ATP synthesis.

Two major CEF pathways have been identified. The first one is mediated by the proteins PGR5 (proton gradient regulator 5) and PGRL1 (PGR5 like 1) and in flowering plants they were shown to be important in photoprotection and photosynthetic regulation during high light and fluctuating light (Munekage et al. 2002; DalCorso et al. 2008; Suorsa et al. 2016). The second CEF pathway is mediated by a supramolecular complex named NDH-1 (NADH dehydrogenase like 1, Shikanai 2015) which despite its ancient origin in cyanobacteria has not been conserved in many eukaryotic algae generation while being found in many land plants (Peltier et al. 2010; Vries et al. 2016). The function of NDH-1 on photosynthetic regulation is still controversial and it appears to be fundamental only when the other CEF route is absent (Munekage et al. 2004). PCEF is instead mediated by stromal soluble proteins able to oxidize NADPH and reduce O_2, called FLV (Flavodiiron proteins, (Allahverdiyeva et al. 2015) or by the reduction of reactive oxygen species by Mehler reaction (Mehler and Brown 1952; Mehler 1951).

In natural environment light irradiation is continuously changing, in timescales not always compatible with metabolic regulation. During these variations, electron transport chain can be rapidly over-reduced due to unbalance with metabolic demand. In these condition AEF are important in regulating membrane transport and avoid damage by multiple overlapping mechanisms (Suorsa et al. 2015; Gerotto et al. 2016; Shikanai and Yamamoto 2017; Munekage et al. 2004). As example, ΔpH promoted by AEF across thylakoid membranes contributes in trigger NPQ activation (Munekage et al. 2002; Gerotto et al. 2016) and regulate Cyt b_6f complex (Suorsa et al. 2015; Rumberg and Smgel 1968). Activation of both NPQ and Cyt b_6f control are important to decrease LEF activity and prevent stroma overreduction. FLV instead were shown to provide photoprotection during light fluctuation avoiding over-reduction and PSI acceptor side limitation (Allahverdiyeva et al. 2013; Gerotto et al. 2016).

CEF and PCEF physiological functions are thus partially overlapping and contribute to regulation of photosynthetic electron transport, as also evidenced in chapter 3. Here we investigated this functional overlap deeper by isolating a *Physcomitrella patens* double CEF mutant by knocking out *PGRL1* gene (Kukuczka et al. 2014) and *NDHM* (Chapter 4), and an triple mutant, where also *FLVA* gene (Gerotto et al. 2016) was depleted. We used the moss *P. patens* (Cove 2005; Rensing et al. 2008) as a model also because this non-vascular plant is one of the few model organisms known to rely on both the CEF pathways and PCEF to control the photosynthetic process, thus allowing to compare the activity of the pathways in a species where they are all present and active. Both the double and

triple mutants showed severe phenotypes in all light conditions analyzed with the latter suffering altered electron transport rate, highlighting that AEF are fundamental to maintain LEF.

RESULTS

CEF and PCEF mechanisms are fundamental for photosynthesis and growth

Double *pgrl1-ndhm* and triple *flva-pgrl1-ndhm* KO mutants of *P. patens* were generate using homologous recombination. Double mutants were obtain by using *PGRL1* KO construct (Kukuczka et al. 2014) on *ndhm* KO background (Chapter 4), isolating two independent lines that were used for the phenotypic characterization after confirmation of insertion in the expected *locus* (Supplementary figure 1) and RT PCR showing the absence of genes expression (Figure 1A). Triple mutants were obtained starting from different double mutant parental lines as described in material and methods, ensuring any effect of the background. After validation of resistance cassette insertion in each of the three *loci* disrupted (Supplementary figure 1) and absence of gene expression validated with RT PCR (Figure 1B), data of one mutant line from each two strategies were mediated in the phenotypic analysis.

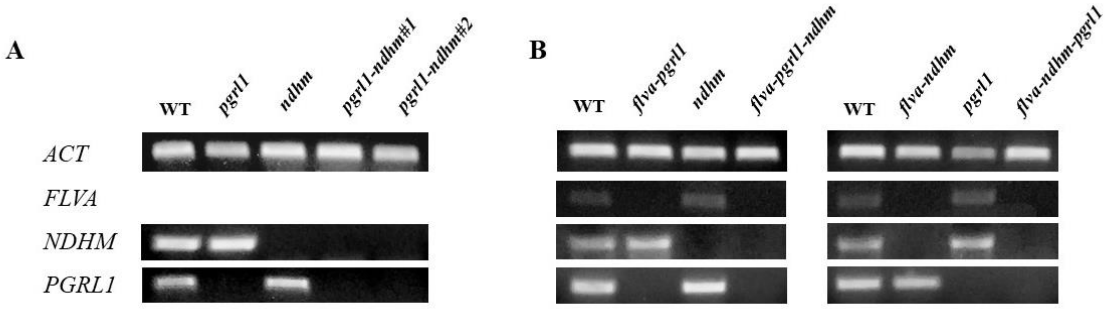

Figure 1 Isolation of *P. patens* KO lines: RT-PCR to assess the absence of both **A)** *NDHM* and *PGRL1* transcripts in *pgrl1-ndhm* lines and **B)** *FLVA*, *NDHM* and *PGRL1* transcripts in *flva-ndhm-pgrl1* (obtained by knocking out *PGRL1* from *flva-ndhm* KO) *and flva-pgrl*1*-ndhm* (obtained by knocking out NDHM from *flva-pgrl1* KO) lines.

Plants grown in control light condition (CL: 50 µmol photons m^{-2} s^{-1}) did not show any major alteration in pigments composition, with only chl a/b content in triple mutant slightly decreased respect to WT and single mutants (Table 1). Total Chl content instead did not differ in double and triple KO mutants (WT: 16.9 ± 4; *pgrl1-ndhm*: 18.7 ± 2; *flva-pgrl1-ndhm*: 17.2 ± 2.7 µg chl * mg^{-1} dry weight).

Table 1 Chlorophyll a / b ratio (Chl a/ Chl b) and total chlorophyll on carotenoids (chl/car) values obtained by the fitting of acetonic spectra, using extracts of WT, *ndhm*, *pgrl1*, *pgrl1-ndhm* and *flva-pgrl1-ndhm/flva-ndhm-pgrl1* lines. 5-7 independent pigment extracts were used per each genotype, errors are represented as standard deviation, letter "a" indicates statistically significative decrease respect WT plants (Anova $p<0.05$).

	Chl a/Chl b	**chl/car**
WT	2.59 ± 0.10	3.81 ± 0.48
ndhm	2.70 ± 0.08	3.82 ± 0.52
pgrl1	2.63 ± 0.08	3.79 ± 0.64
pgrl1-ndhm	2.56 ± 0.08	3.53 ± 0.43
flva-pgrl1-ndhm	2.41 ± 0.13 [a]	4.05 ± 0.77

PGRL1 and FLV were shown to be important in response to high light (HL) and fluctuating light (FL) regimes respectively (Chapter 3), while NDH-1 depletion alone has a small effect on photosynthetic efficiency in *P. patens* (Chapter 4). To unravel the role of CEF and PCEF pathways and their interaction WT, *ndhm*, *pgrl1*, *ndhm-pgrl1* and *flva-pgrl1-ndhm* KO mutants were grown in different light regimes for 21 days (Figure 2A) as previously described in chapter 3. Single *pgrl1* and *ndhm* KO did not show evident growth difference when compared to WT in all condition tested (Figure 2B). On the contrary strong effects were visible when the two genes were knocked out simultaneously with *pgrl1-ndhm* mutants showing a diminished growth in FL, but especially in medium light (ML) and HL conditions (Figure 2B), suggesting that CEF pathways are important at stronger irradiations and that in single mutants the other mechanism is compensating for its absence. PCEF pathway mediated by FLV was also depleted in *flva-pgrl1-ndhm* triple mutants that exhibited a severe phenotype, with a strongly reduced growth in all light condition tested even in CL (35 % of WT plants) or LL, highlighting that CEF and PCEF are seminal for growth in all light condition (Figure 2B).

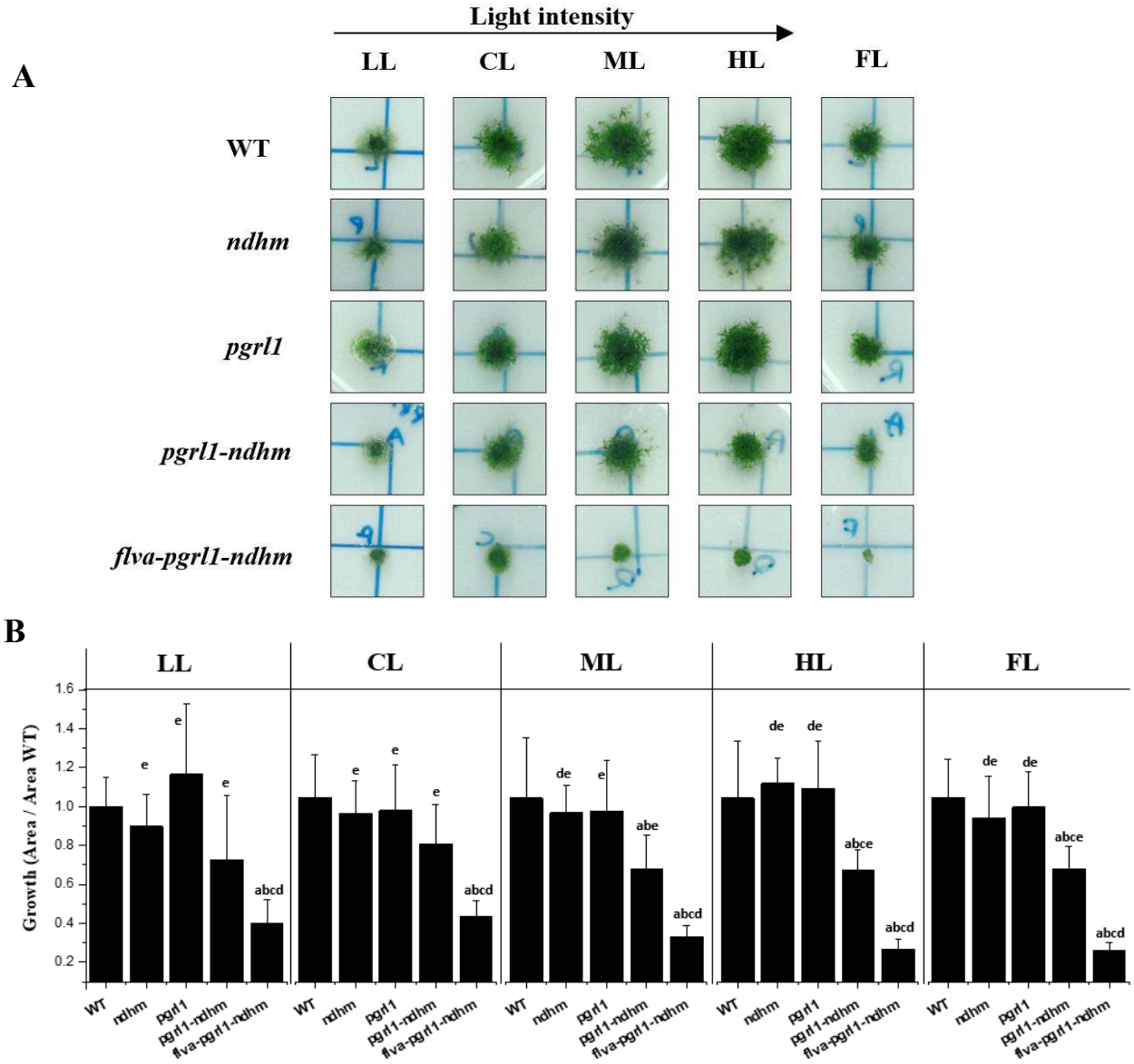

Figure 2 *P. patens* mutants grown in different light conditions. **A)** exemplificative colonies of WT, *ndhm*, *pgrl1*, *pgrl1-ndhm* and *flva-pgrl1-ndhm* grown in LL, CL, ML, HL or FL (respectively 10, 50, 150, 500 µmol photons m^{-2} s^{-1} or cycle of 3 min at 525 + 9 min at 25 µmol photons m^{-2} s^{-1}). **B)** Estimation of the colony sizes of plants grown for 21 days in different light conditions. a, b, c, d and e indicate statistically significant difference (Anova $p<0.001$, n=6-18) from WT, *ndhm*, *pgrl1*, *pgrl1-ndhm* and *flva-pgrl1-ndhm* respectively.

AEF protect PSI from photodamage also under low irradiances

In previous chapters we verified that growth phenotype of *P. patens* AEF mutants was associated to conditions leading PSI photodamage (Gerotto et al. 2016, Chapter 3). We thus evaluated PSI amount in *flva-pgrl1-ndhm* KO (Figure 3) quantifying PSI/PSII ratio spectroscopically using single flash turnover on plants grown in CL (Figure 3 A, B). In WT plants the PSI and PSII contribution to total charge separation was similar, while in triple mutants upon addition of DCMU, a PSII inhibitor,

charge separation recorded was very low (Figure 3A). Calculated PSI/PSII ratio was in fact decreased by 80% in *flva-pgrl1-nhdm* KO respect to WT, revealing that AEF are important to protect PSI even under the dim light. In *pgrl1-ndhm* KO plants, PSI/PSII ratio was also affected even if to a lesser extent. This suggests that FLV are important also under during constant light illumination at least in *pgrl1-ndhm* KO plants. PSI content was also assessed using CN-PAGE (Figure 3 C) that showed that in *flva-pgrl1-ndhm* KO PSI-LHCI band (Figure 3D) was 65% less than WT level (Figure 3E), confirming that PSI content was strongly reduced when these plants were cultured in dim light.

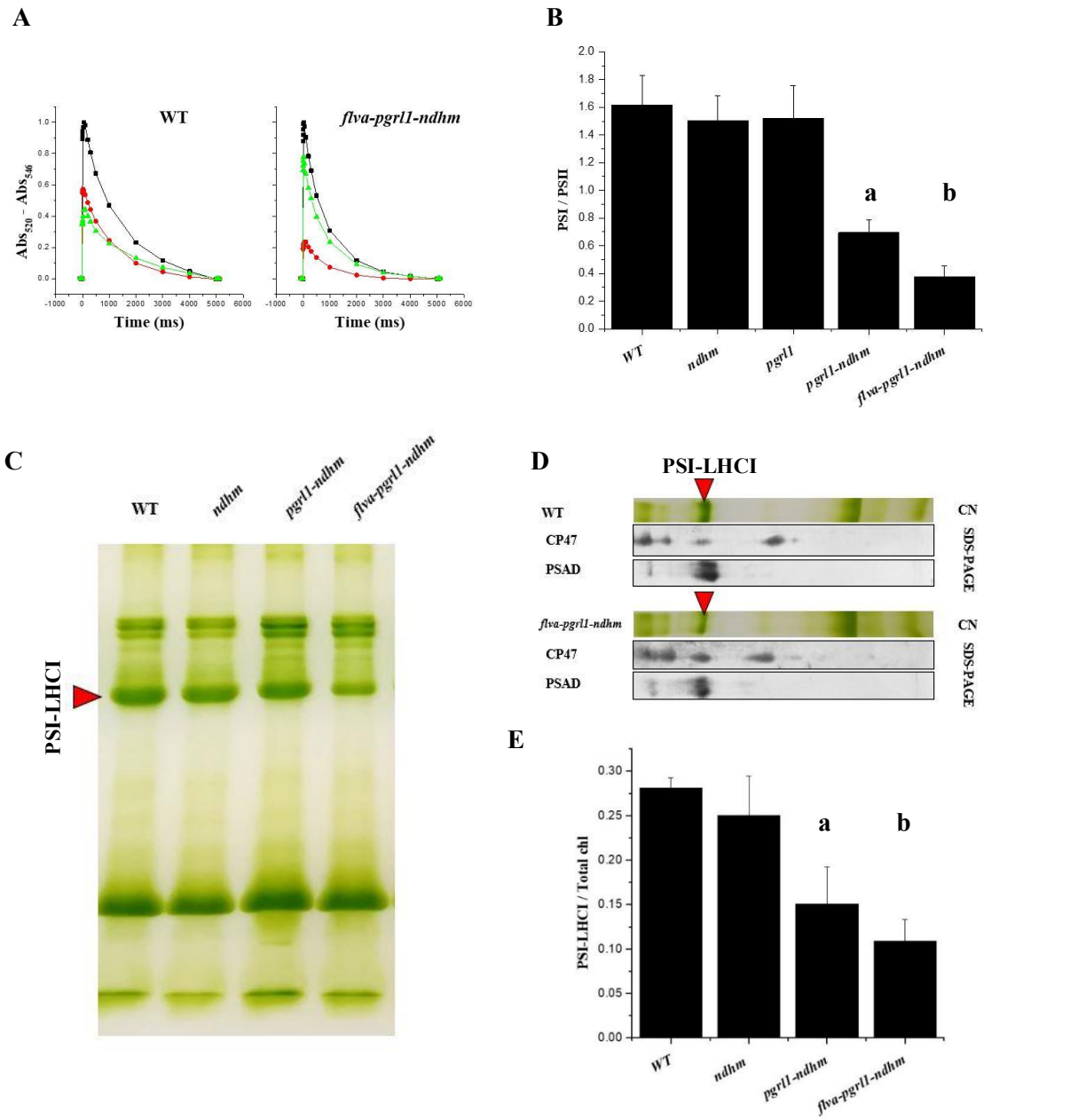

Figure 3 Spectroscopic (A-B) and biochemical (C-E) determination of PSI content in AEF mutants. Spectroscopic quantification of PSI/PSII ratio using single flash turnover: **A**) representative kinetics of single flash turnover of WT and triple mutant, PSII contribution (green) was calculated by the subtraction of total charge separation (black) and PSI charge separation (red) obtain by adding DCMU and HA; **B**) Calculation of PSI/PSII ratio of plants grown in CL (n=8 ± SD). **C**) Separation of protein complexes extracted from thylakoids with CN-PAGE, red arrow indicates PSI-LHCI band. **D**) identification of PSI and PSII band on second dimension SDS-PAGE using PSAD and CP47 specific antisera. **E**) Densitometry of PSI band in CN-PAGE, normalized on total chl content per lane (n=4 ± SD). Letters a and b indicate statistically difference respect the other genotypes (Anova $p<0.001$).

AEF are seminal to sustain PSI activity in all light conditions

We investigated the effect of PSI impairment in *flva-pgrl1-ndhm* and *pgrl1-ndhm* KO plants by pulse amplitude modulator (PAM) P700 absorption. Dark acclimated plants were exposed to a dim (50 µmol photons m^{-2} s^{-1}) or saturating (540 µmol photons m^{-2} s^{-1}) red light for 8 minutes, a time sufficient to reach photosynthetic steady state (Figure 4). In dim light, all photosynthetic parameters monitored for *pgrl1* and *ndhm* single mutants did not differ from WT (Figure 4A-C). On the contrary *pgrl1-ndhm* and *flva-pgrl1-ndhm* KO showed a drastic decrease in photosynthetic efficiency with the yield of PSI (Y(I), Figure 4A) reduced by 75% compared to WT plants upon exposition to dim light. PSI yield was shown to be limited in particular from the acceptor side (Y(NA), Figure 4B) in *pgrl1-ndhm* and *flva-pgrl1-ndhm* KO, while the donor side limitation (Y(ND), Figure 4C) was low in all genotype considered.

When plants were exposed to an intense 540 µmol photon m^{-2} s^{-1} actinic light instead Y(I) was very low for all genotypes, as expected since photosynthesis is saturated (Figure 4D). However, while in WT and single mutants PSI was limited from the donor side, as shown by the increase in Y(ND) (Figure 4F), *flva-pgrl1-ndhm* was limited by the acceptor side as evidenced by the high Y(NA) values (Figure 4E). *pgrl1-ndhm* KO PSI was also limited by the acceptor side (Figure 4E), but it also showed partial donor side limitation (Figure 4F).

This analysis suggests that CEF and PCEF pathways are seminal to maintain a high PSI yield by removing excess electron from PSI acceptor side.

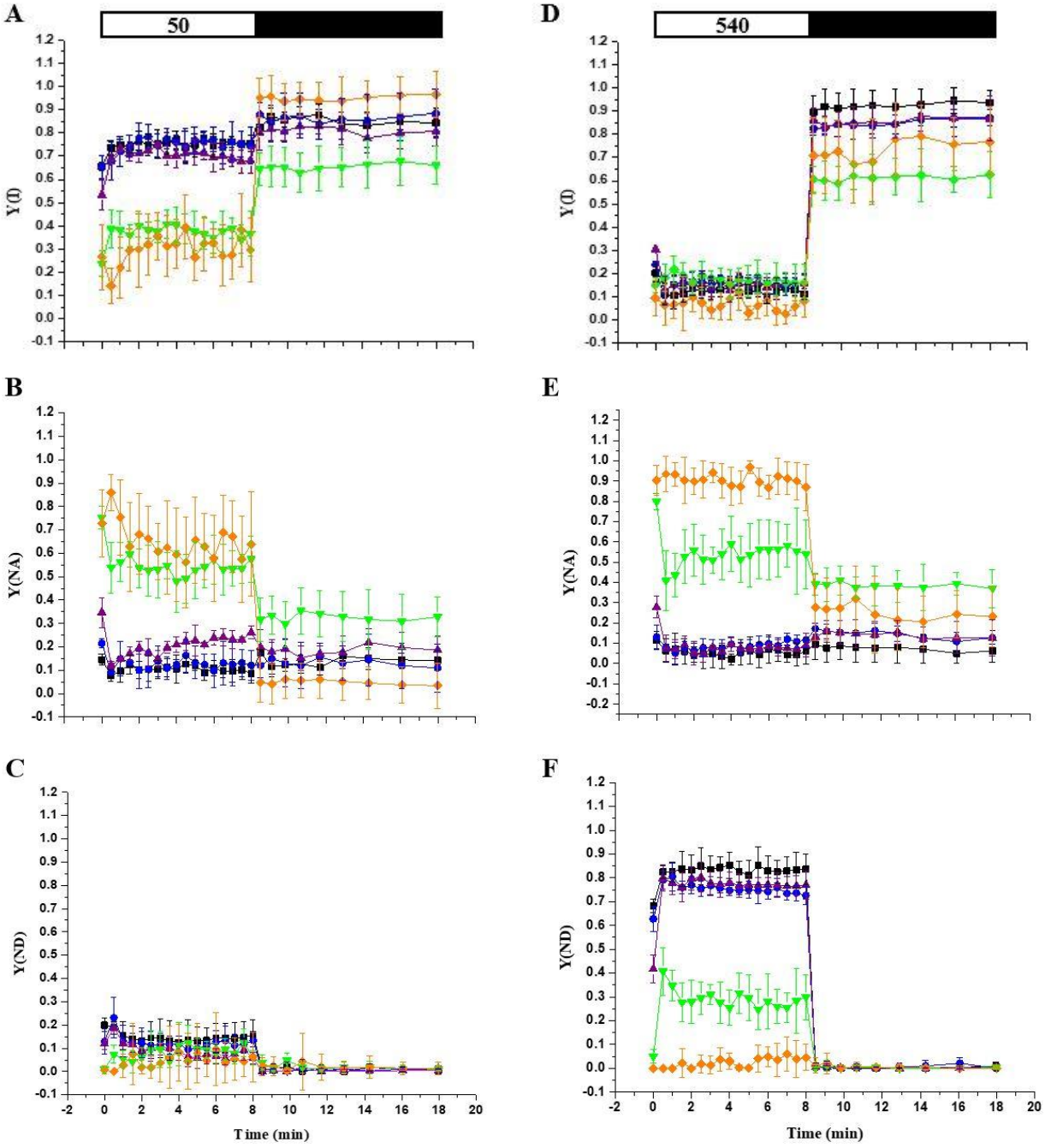

Figure 4 Dual-PAM analysis of PSI related parameters of plants grown in CL condition and treated at 50 (**A-C**) or 540 (**D-F**) µmol photons m^{-2} s^{-1}. **A, D)** Yield of PSI Y(I), **B, E)** yield of acceptor side Y(NA) and **C, F)** yield of donor side Y(ND). In each panel WT is represented in black, *ndhm* purple, *pgrl1* blue, *pgrl1-ndhm* green, *flva-pgrl1-ndhm* in orange. White bar on the top of **A)** and **D)** indicates 8 minutes of 50 or 540 µmol photons m^{-2} s^{-1} light exposure. Data are average of 5 biological replicates ± SD.

P700 re-reduction kinetics were also measured after exposure at different light intensities calculating both P700 oxidation level and the rate of $P700^+$ re-reduction in the dark (Figure 5A, B). In WT plants we observed an increase in $P700^+$ concentration concomitant with the increase in light intensity, reaching the maximum $P700^+$ at 940 µmol photons m^{-2} s^{-1} where PSI was completely oxidized (Figure 5C). In *flva-pgrl1-ndhm* KO, P700 showed a stronger oxidation at lower light intensities respect to WT plants. This could indicate that PSI electron transfer capacity is already close to saturation at 45 µmol photons m^{-2} s^{-1}. When FLV were present, in *pgrl1-ndhm* P700 was not fully oxidized, not even using the highest light intensities (Figure 5C), this phenotype can be attributable to charge recombination of P700. The rate of $P700^+$ reduction kinetics (1 * $T_{1/2}^{-1}$) after actinic light switch off for WT plants resulted slower at 45 µmol photons m^{-2} s^{-1}, reached the maximal value at 150 µmol photons m^{-2} s^{-1} and no further increases were observed at higher light intensities (Figure 5D). As in the previous experiments *ndhm* and *pgrl1* KO mutants showed a reduction rate similar to WT plants. The kinetic of P700 reduction was instead slower in *pgrl1-ndhm* KO and was even more impaired in the *flva-pgrl1-ndhm* KO (Figure 5D). Both more oxidized $P700^+$ and the relatively slow reduction kinetics suggests that despite the high acceptor side limitation observed in (Figure 4B, E), also the electron flux to PSI was strongly affected in triple mutants.

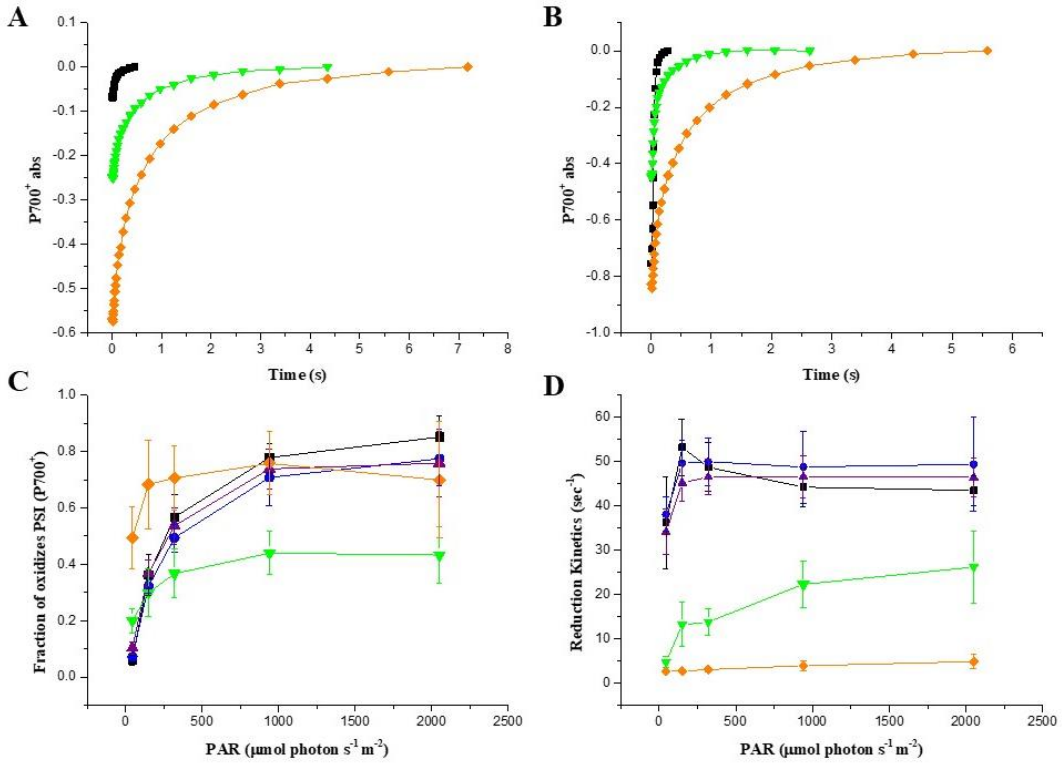

Figure 5 $P700^+$ kinetics at different light intensities (45, 150, 320, 940, 2050 µmol photons m^{-2} s^{-1}). Plant were exposed at 15 s actinic light and reduction kinetics of $P700^+$ recorded: **A**) exemplificative kinetics after actinic low (45 µmol photons m^{-2} s^{-1}) and **B**) high light (2050 µmol photons m^{-2} s^{-1}) switch off. For each kinetics **C**) the fraction of $P700^+$ on total P700 and **D**) the reduction half time in the dark were measured. In each panel WT is represented in black, *ndhm* purple, *pgrl1* blue, *pgrl1-ndhm* green, *flva-pgrl1-ndhm* orange. 8 independent biological samples were considered for each line, errors are represented as SD of single measurements.

PSII is also affected by PSI impaired electron transport capacity

The effect of PSI acceptor side limitation on PSII was analyzed assessing Fv/Fm parameters of plants grown in different light conditions (Figure 6). WT and *ndhm* KO maintained a high photosynthetic efficiency in LL, CL and FL, with a Fv/Fm decrease only in ML and HL proportionally to light intensity used for the growth. *pgrl1* KO showed a larger decrease in Fv/Fm in ML and HL when compared to WT. *flva-pgrl1-ndhm* triple mutant showed a significative reduction of Fv/Fm in all light conditions respect other genotypes (Figure 6), with a larger decrease with stronger light intensities. Similarly, also Fv/Fm of *pgrl1-ndhm* double KO was lower than WT when grown in constant light condition (CL, ML and HL), but it did not show sensitivity to FL.

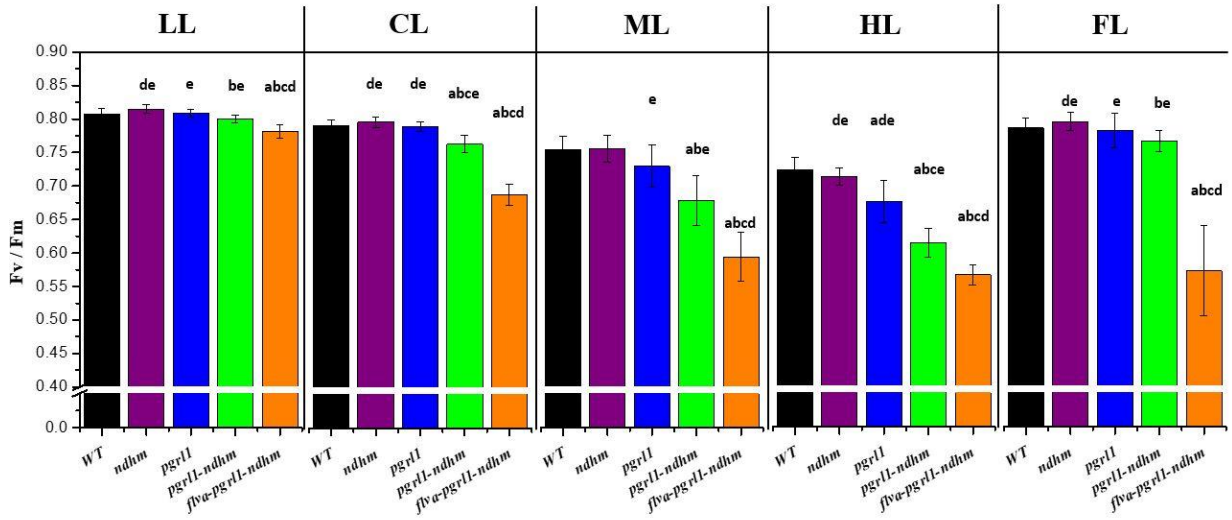

Figure 6 Fv/Fm parameters of WT, *ndhm*, *pgrl1*, *pgrl1-ndhm* and *flva-pgrl1-ndhm* grown for 21 days in LL, CL, ML, HL or FL. a, b, c, d and e indicate statistically significant difference (Anova $p<0.001$) from WT, *ndhm*, *pgrl1*, *pgrl1-ndhm* and *flva-pgrl1-ndhm* respectively (n=6-18, $p < 0.001$)

We performed *in vivo* PAM analysis to estimate PSII correlated parameters (Figure 7). As for PSI analysis, plants were dark adapted for 40 minutes before being exposed for eight minutes at 50 (Figure 7A-C) or 540 (Figure 7D-E) µmol photon m^{-2} s^{-1} actinic light. As well as PSI, PSII parameters of *ndhm* KO and *pgrl1* KO did not differ from those of WT plants independently from the actinic light intensity used.

Chlorophyll fluorescence derived parameters showed drastic decreases in photosynthetic efficiency of *flva-pgrl1-ndhm* KO already when the measure was performed with the lowest intensity, with yield of PSII (Y(II), Figure 7A) decreased of 80% compared to WT plants at steady state. NPQ seemed to

be little affected (Figure 7B), also because the dim light treatment was not sufficient to reasonably induce NPQ even in WT plants. In *flva-pgrl1-nhdm* KO NPQ only differed in the first 2 minutes where FLV activity was shown to be fundamental to induce ΔpH and NPQ activation (Gerotto et al. 2016). PQ pool reduction, estimated by 1-qL parameter (Figure 7C), was 2-fold higher in *flva-pgrl1-ndhm* KO respect to WT plants suggesting that PQ was highly reduced in this mutant even if exposed to dim light. Thus, the observed decrease in Y(II) in triple mutants at steady state was likely due to a saturation of PSII oxidized acceptors. Similarly, in *pgrl1-ndhm* KO both PSII yield and (Figure 7A) and PQ pool reduction (Figure 7C) were affected when compared to WT, but to a less extent respect *flva-pgrl1-ndhm* KO. Thus, pointing out again that FLV contribute to sustain steady state photosynthetic activity when the CEF pathways are absent.

When induction kinetics were performed with saturating light, Y(II) and 1-qL of *flva-pgrl1-ndhm* KO were closer to WT plants (Figure 7D, F). In this condition a significant difference in ability to induce NPQ emerged, indeed at steady state NPQ level of *flva-pgrl1-ndhm* KO was 60% less than in WT (Figure 7E). Even if NPQ was not impaired in CEF single KO mutants, when considered together with FLV depletion a strong phenotype was present, suggesting that the AEF are seminal to sustain ΔpH formation and thus NPQ induction. At photosynthetic steady state also *pgrl1-ndhm* KO showed a lower NPQ level than WT plants but this was higher than in *flva-pgrl1-ndhm* KO at steady state (Figure 7B). Thus, in absence of CEF pathways, FLV contributes to ΔpH formation and NPQ induction.

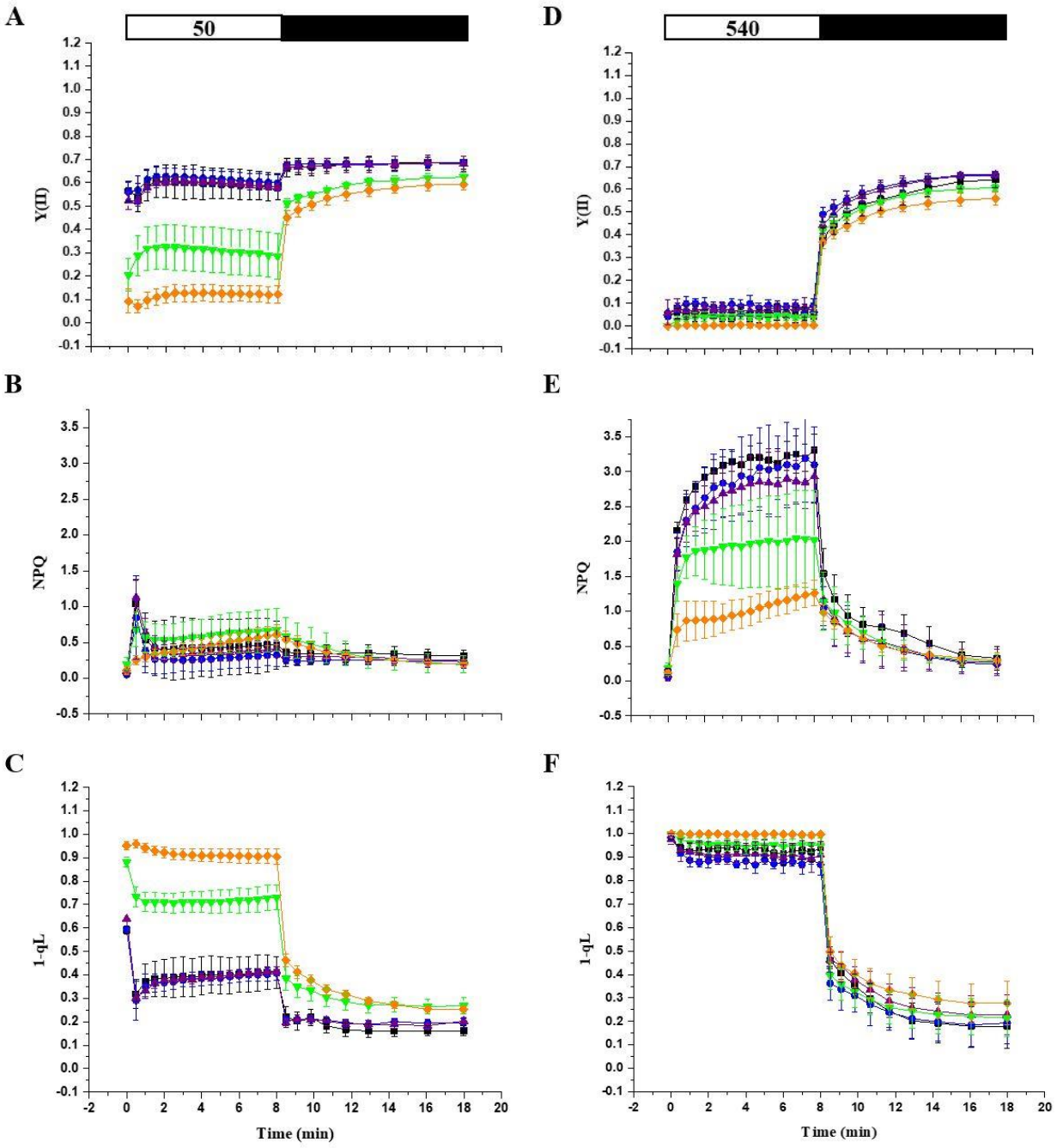

Figure 7 Dual-PAM analysis of PSII related parameters in plants exposed to 50 (**A-C**) or 540 (**D-F**) µmol photons m^{-2} s^{-1}. **A, D)** Yield of PSII Y(II), **B, E)** Non-photochemical quenching (NPQ) and **C, F)** PSII closed centers (1-qL). In each panel WT is represented in black, *ndhm* purple, *pgrl1* blue, *pgrl1-ndhm* green, *flva-pgrl1-ndhm* in orange. White bar on the top of **A)** and **D)** indicates 8 minutes of 50 or 540 µmol photons m^{-2} s^{-1} light exposure. Data are average of 5 biological replicates ± SD

AEF are fundamental to sustain photosynthetic electron transfer

Electron transport rate (ETR) was measured in all plants using dark induced relaxation kinetics (DIRK) analysis (Figure 8A). WT plants showed a peak in ETR between 1 and 2 s upon light switch on, dependent from FLV activity (Gerotto et al. 2016). After about 180 s ETR stabilized around a constant value of 42 ± 6 e^- * s^{-1} when photosynthetic steady state was reached.

ETR of *flva-pgrl1-ndhm* KO was severally impaired reaching level less than the half of those of WT plants, even at the stationary state (Figure 8A). Also pmf generated was impaired in *flva-pgrl1-ndhm* triple KO, which showed a decrease in both ΔpH and ΔΨ components (Figure 8B). In *pgrl1-ndhm* double mutants instead, steady state ETR was not impaired even if its activation upon light exposition was slowed, thus CEF appear to be more active in first seconds of light exposure (Chapter 2).

O_2 evolution (Figure 8C) was also evaluated to assess photosynthetic activity. O_2 consumed by respiration did not differ significantly in WT and *flva-pgrl1-ndhm* KO plants (Figure 8C) but upon light exposure, in triple mutants gross O_2 evolution was largely reduced in the latter (Figure 8C), consistent with the reduction in steady state ETR.

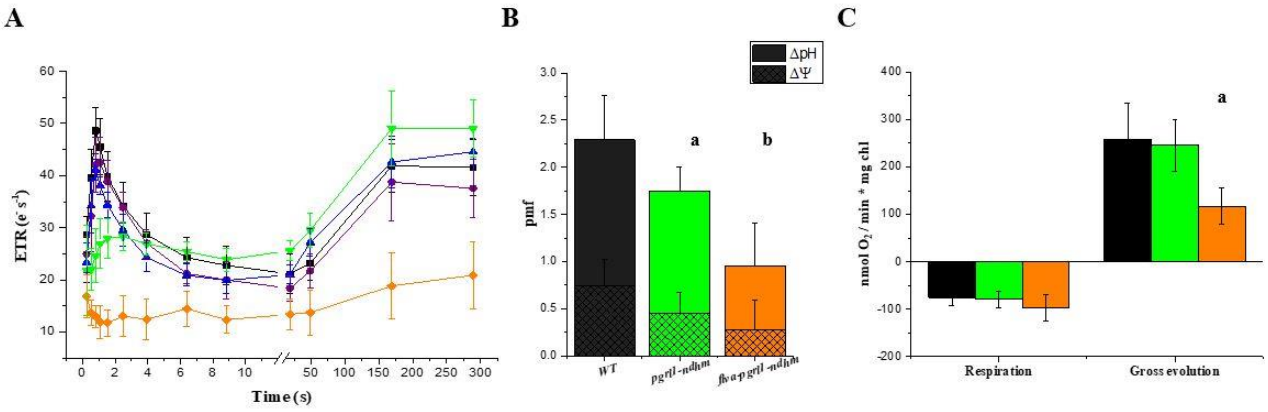

Figure 8 Photosynthetic electron transfer. **A**) Electron transport rate calculated from ECS spectra of dark acclimated plants after photosynthetic induction with 940 µmol photons m^{-2} s^{-1} actinic light. **B**) After light switch off the size of ECS decay was quantified to estimate ΔpH (gridded) and ΔΨ (empty). **C**) oxygen consumed by respiration during light period and gross oxygen evolution after actinic 850 µmol photons m^{-2} s^{-1} light exposition. In each panel WT is represented in black, *pgrl1-ndhm* green, *flva-pgrl1-ndhm* KO in orange. 10-15 independent samples were used for ECS measurements and 8 for oxygen evolution experiment. The errors is represented by SD and significative differences among genotypes are indicated by letters (Anova $p<0.001$)

External carbon source rescue mutant plants growth phenotype and alleviates photodamage

flva-pgrl1-ndhm KO showed a drastically affected photosynthetic activity (Figure 8) with a consequent severe growth phenotype (Figure 2). However, when grown at CL intensity in $PpNH_4$ medium, as during the mutant isolation process, containing glucose and ammonium tartrate (NH_4), triple KO were able to growth similarly to WT plants (Figure 9A). To investigate which nutrient sustained the growth of triple mutants, 2 mm spots of WT and *flva-pgrl1-ndhm* were laid on $PpNO_3$ solid medium containing glucose or NH_4. While NH_4 alone had no effect on the growth of triple mutant, glucose was able to partially rescue the growth (Figure 9A, B), indicating that an external carbon source was helpful in supporting plant growth when photosynthesis was impaired (Figure 9). The same behavior was observed when *flva-pgrl1-ndhm* KO was cultured on sucrose but not in non-metabolizable sugar mannitol, thus excluding both a signaling effect by glucose and an osmotic effect due to the presence of an osmolite in the medium and supporting the hypothesis of a metabolic effect.

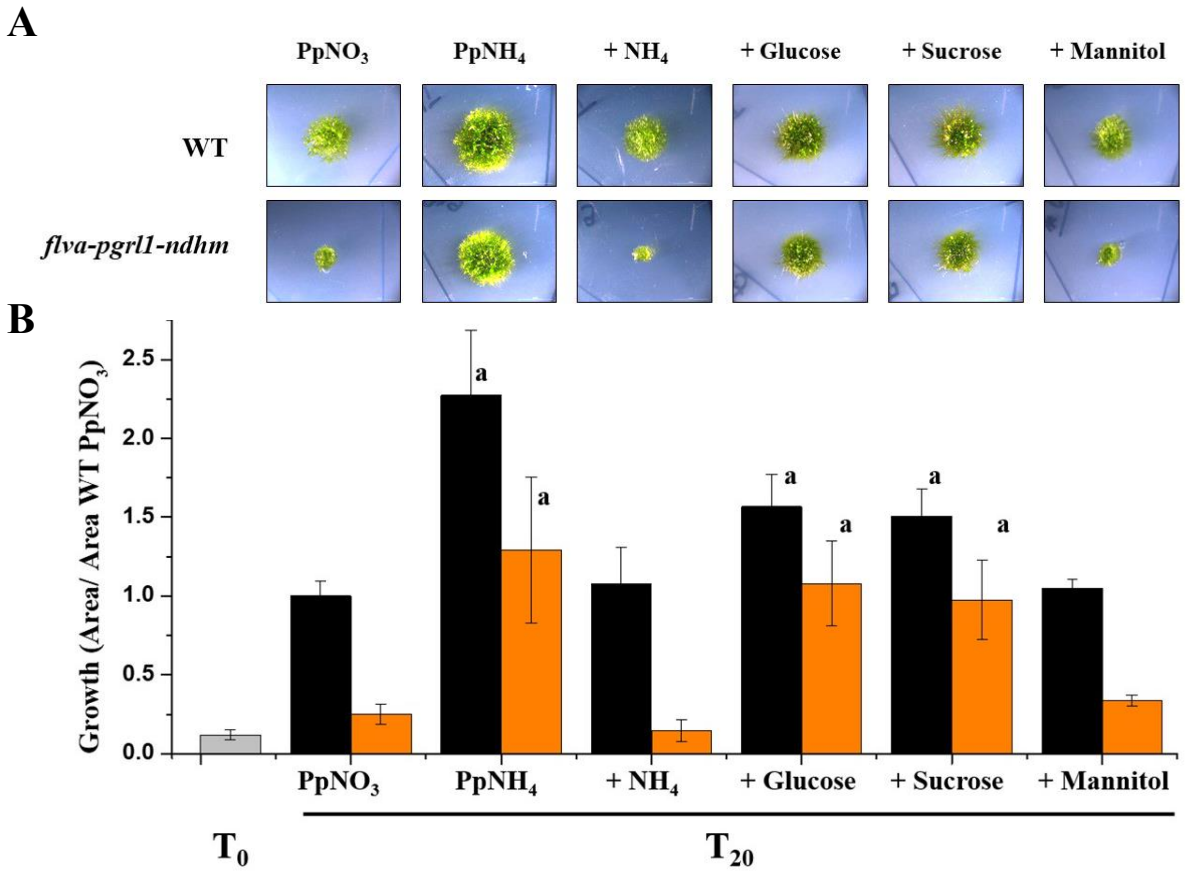

Figure 9 *P. patens* growth in different solid media. **A)** exemplificative colonies of WT and *flva-pgrl1-ndhm* grown in $PpNO_3$, $PpNH_4$ and $PpNO_3$ supplemented with NH4, glucose, sucrose or mannitol. **B)** Estimation of colony sizes (normalized to WT $PpNO_3$) of plants grown for 20 days in the same condition of panel A. WT is represented in black, flva-pgrl1-ndhm KO in orange, while T_0 in grey is the mean value of a representative set of colonies in the day of the inoculum. Letter a indicates significant increase in growth respect to photoautotrophic condition ($PpNO_3$) (Anova $p<0.001$, n=8-12)

It is interesting to observe that the presence of an organic carbon source not only supported the growth but also alleviated photosynthetic damage. *flva-pgrl1-ndhm* KO recovered Fv/Fm defect present in $PpNO_3$ respect to WT plants (Figure 10A). The content of PSI-LHCI significantly increased in *flva-pgrl1-ndhm* KO plants grown in the presence of glucose, while WT plants showed similar PSI-LHCI content in the two media (Figure 10B). Photosynthetic parameters analysis thus indicates that an external carbon source not only support growth by providing reducing power but also alleviates photodamage to PSI in *flva-pgrl1-ndhm* KO partially restoring PSI content and suggesting a functional interaction of respiration with photosynthetic electron transport (Larosa et al. 2017).

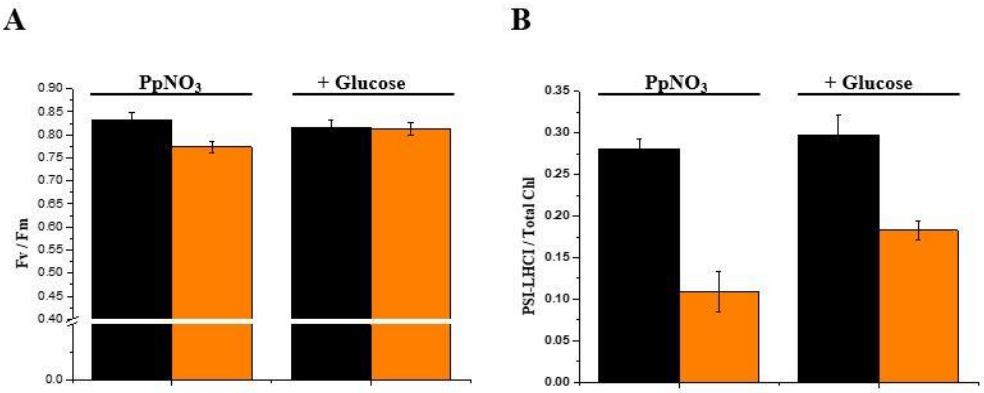

Figure 10 Comparison of photosynthetic parameters of plants grown in $PpNO_3$ or $PpNH_4$ (+ Glucose) medium. **A**) Fv/Fm (n=9-11 ± SD), **B**) PSI-LHCI of WT (Black) and *flva-pgrl1-ndhm* KO (orange) content in CN-PAGE (n=4 ± SD). PSI-LCHI content for $PpNO_3$ medium is the same shown in Figure 3 to allow a direct comparison with the values calculated for PSI-LHCI content for $PpNH_4$ medium.

DISCUSSION

In this work we generated two new *P. patens* photosynthetic mutants (Figure 1, Supplementary Figure 1), knocked out respectively for essential genes of CEF (*PGRL1*, *NDHM*) and for both CEF and PCEF (*FLVA*, *PGRL1*, *NDHM*). Previously isolated CEF single KO mutants, only marginally differs from WT plants in growth (Figure 2) and photosynthetic parameters (Figure 4, 7) even when cultured in stressing stressful light regimes (Figure 6). At the contrary plants depleted in multiple genes as *pgrl1-ndhm* and *flva-pgrl1-ndhm* KO showed severe alterations in growth and photosynthetic performances (Figure 2, 4, 7). These results highlight a strong synergy and high overlap between the functions of the three AEF pathways studied in this work. When only one mechanism is altered the others can

largely compensate but when multiple genes are affected there is a much stronger effect. Similar synergy was previously observed between the two CEF pathways in *Arabidopsis* (Munekage et al. 2004) and in *P. patens* depleted for FLV and PGRL1 activity (Chapter 3).

The phenotypes observed also clearly show the seminal role of AEF in photosynthesis. Both the double and triple KO mutants suffered extensive PSI photoinhibition even in optimal growth conditions (Figure 3). The reduced PSI amount together with the strong PSI acceptor side limitation observed (Figure 3, 4) can easily explain the increased saturation of PQ pool and the consequent reduced yield of PSII (Figure 7). In chapter 3, similar effect emerged when FLV and PGRL1 were depleted, but only in specific light conditions while here they were evident in all cases. Thus, AEF are seminal to protect PSI, revealing an intrinsic instability of the complex in absence of appropriate regulatory mechanisms. This has been largely underestimated in the literature since PSII is believed to be more unstable and sensitive to illumination (Sonoike 2011) and it can be actually true only because mechanisms for PSI photoprotection are highly effective.

Previous works demonstrated that FLV activity is transient and particularly relevant after dark to light transition, with their role fundamental to cope with fluctuating light (Gerotto et al. 2016; Jokel et al. 2018). Here we can compare *pgrl1-ndhm* and *flva-pgrl1-ndhm* KO which only differ for the presence of FLV. These showed significantly differential growth even in continuous light conditions (Figure 2) and lower level of active PSI when FLV were depleted (Figure 3). Moreover *flva-pgrl1-ndhm* KO electron transport rate was diminished compared to *pgrl1-ndhm* KO (Figure 8), explaining the decreased growth rate. At least in these plants, FLV are active even at steady state under constant illumination. Thus, FLV activation is not strictly dependent on dark to light transition but could occurs whenever stromal acceptor pool becomes saturated and it is not more able to accept electrons from LEF. These evidences could contribute to answer questions related FLV loss in angiosperms (Chapter 2). Indeed, if FLV are or at least can be active in all conditions, they can have a negative impact on photosynthetic efficiency, subtracting electrons for NADPH production.

Another interesting point is the phenotype observed when *flva-pgrl1-ndhm* KO were supplied with an organic carbon source (Figure 9). Growth recovery is attributable to respiratory metabolism which, in absence of efficient photosynthetic process, can sustain the energy demand of the cell. The mosses ability to use organic carbon source to support growth was already known (Thelander, Olsson, and Ronne 2005; Bricker et al. 2014) and is linked to the presence of sugars in the natural environment (Graham et al. 2010). Results presented however also showed that sugars alleviate photoinhibition of *flva-pgrl1-ndhm* KO (Figure 10), suggesting that mitochondrial metabolism can have a beneficial effect on photosynthesis. A tight relationship between mitochondrial and plastidial metabolism was

observed to be based on the exchange of ATP or NADPH equivalents between the two organelles (Bailleul et al. 2015; Larosa et al. 2017). In this case the influence of respiratory metabolism on photosynthesis still need to be elucidated, but several interaction between the two organelles are possible including the direct transfer of ATP, sugar catabolism intermediates or ascorbate (Nunes-Nesi, Araujo, and Fernie 2011). The two former will sustain the activity of Calvin Benson cycle promoting NADPH consumption and alleviating stroma overreduction, while ascorbate synthesized at the mitochondrial membrane can exert protective effects scavenging ROS and sustain PSI activity (Ivanov 2014).

MATERIAL AND METHODS

Plant material and growth

P. patens (Gransden) wild-type (WT) an KO lines were maintained in protonemal stage by vegetative propagation and grown in controlled conditions: 24°C, 16 h light/ 8 dark on photoperiod at 50 µmol photons $m^{-2}s^{-1}$ (Control light, CL) where not differently specified. Physiological and biochemical experiment were performed on 10 days old plants when grown in $PpNO_3$ medium or 7 days old plant when grown in $PpNH_4$ medium. Growth on different media and light conditions was evaluated on 2 mm diameters colonies of protonema, for 21 days and colonies size was measured as reported in chapter 3. Light condition used in this experiment were 10 (low light, LL) 50 (CL), 150 (medium light, ML), 500 (high light, HL) µmol photons $m^{-2}s^{-1}$ and fluctuating light (FL) of 9 min 25 µmol photons $m^{-2}s^{-1}$ and 3 min 525 µmol photons $m^{-2}s^{-1}$. Growth test with different nutrients were performed using $PpNH_4$ and $PpNO_3$ media or $PpNO_3$ supplemented with 0.5% Glucose, NH_4 0.05%, Sucrose 0.5% or Mannitol 0.5%.

Moss Transformation and mutant selection

PGRL1 KO (Kukuczka et al. 2014) and was used to remove the gene *PGRL1* from *ndhm* single KO genetic background, to obtain *pgrl1-ndhm* double KO mutants. After lines confirmation *PGRL1* KO construct was used to remove *PGRL1* from *flva-ndhm* background (Chapter 4), similarly *NDHM* KO construct (Chapter 4) was used to remove the gene from *flva-pgrl1* background (Chapter 3), obtaining

in both cases a triple KO mutant *flva-pgrl1-ndhm*. Transformation was performed by protoplast DNA uptake as described in (Alboresi et al. 2010). After two rounds of selection, *in vivo* chlorophyll fluorescence measure with Fluorcam 800 (photon system instrument) allowed to detect colonies with different fluorescence feature respect to background lines. These were homogenized using 3 mm zirconium glass beads (Sigma-Aldrich) and genomic DNA (gDNA) isolated with rapid extraction protocol (Edwards, Johnstone, and Thompson 1991) with minor modification. PCR reactions were performed with the primers described in Kukuczka et al. 2014; Gerotto et al. 2016 and chapter 4 on extracted gDNA. RT PCR was performed on cDNA (RevertAid Reverse Trancriptase, Thermo Scientific) synthesized after RNA extraction (Allen et al. 2006) to confirm *pgrl1-ndhm* and *flva-ndhm* lines.

Pulse amplitude modulation (PAM) in vivo analysis

In vivo chlorophyll fluorescence and $P700^+$ absorption were monitored simultaneously at room temperature with a Dual-PAM 100 (Walz) on protonemal tissues grown for 10 days in $PpNO_3$ or 7 days in $PpNH_4$. Before measurements, plants were dark-acclimated for 40 min, and Fv/Fm parameter calculated as (Fm-F0)/Fm. For induction curves, actinic red light was set at 50 or 540 µmol photons $m^{-2}s^{-1}$ and photosynthetic parameters recorded every 30 s. At each step photosynthetic parameters were calculated as following: Y(II) as (Fm'-Fo)/Fm', qL as (Fm'-F)/(Fm'-Fo') x Fo'/F and NPQ as (Fm-Fm')/Fm', Y(I) as 1-Y(ND)-Y(NA); Y(NA) as as (Pm-Pm')/Pm; Y(ND) as (1 - P700 red).
Fv/Fm parameter was evaluated on colonies during growth test experiment with a FluorCam FC 800 video-imaging apparatus (photosystem instrument).

$P700^+$ kinetics

Oxidation state of PSI was evaluated by $P700^+$ kinetics, measuring 705 nm absorption with a JTS-10 (Biologic). $P700^+$ was recorded for 15 s at different light intensity (45, 150, 320, 940, 2050 µmol photons $m^{-2}s^{-1}$) before actinic light switch off to reach the maximum $P700^+$. $P700^+$ levels were calculated by the differences of maximum $P700^+$ during light and minimum $P700^+$ and normalized to the same measurement perform in presence of 20 µM DCMU (3-(3,4-dichlorophenyl)-1,1-dimethylurea) and 150 µDBIMB to completely oxidize $P700^+$. Kinetic rates of P700 were estimated by reduction speed as $1/T_{1/2}$.

Electrochromic Shift (ECS) analysis

ECS spectra were recorded with JTS-10 (Biologic) on plants dark adapted and soaked with HEPES 20mM pH 7.5, KCl 10mM., 520 nm signal was subtracted by 546 nm background. Amount of functional photosystem was evaluated by single flash turnover using a xenon lamp, samples were infiltrated with 20 µM DCMU and 4 mM HA (hydroxylamine) to eliminate contribution of PSII and prevent PSI charge recombination. ETR was evaluated by DIRK (dark induced relaxation kinetic) analysis as in (Gerotto et al. 2016) and normalized to total amount of PS, after five minutes light was switch off for 20 s to follow relaxation kinetic and evaluate proton motive force generated during light treatment (Cruz et al. 2001).

Clear native (CN) gel and 2D electrophoresis

Gel were casted in 8x10 cm plates using buffer described by (Kügler et al. 1997), running gel was obtain by using an acrylamide gradient of 3.5-11%, and 3.5% acrylamide in the stacking. Thylakoids from dark adapted protonemal tissue were isolated as in (Gerotto et al. 2012) and resuspended in 25BTH20G buffer at 1 µg chl/ µl concentration. Thylakoids were solubilized as described in (Järvi et al. 2011), using 0.75 % DM (β-dodecylmaltoside) and adding deoxycholic acid (DOC 0.2%) to solubilized samples. Anode and cathode buffer were the same used by (Järvi et al. 2011) for CN gel, cathode buffer was addicted with 0.05% DOC and 0.02% DM. Gel were run for 4h with increasing voltage (75-200 V).

Pictures of the gel were analyzed with GelPro 31 software (Media Cybernetic Inc., Silver Spring, MD, USA) to calculate integrated density of the bands.

For 2D (two-dimensional) separation, lanes from CN were excised and proteins denatured by incubation in denaturation buffer (140mM Tris pH 6.8, 6M urea,20% glycerol, 4.3 % SDS and 5% β-mercaptoethanol) and then washed with the same buffer without β-mercaptoethanol. After solubilization the stripes were put on the top of SDS/PAGE gel (15% acrylamide, 6M urea) and sealed with the stacking gel (4% acrylamide). After running proteins were transferred on nitro-cellulose membrane for western blot detection using specific antibody for PsaD (Agrisera catalog number AS09 461) and homemade polyclonal CP47.

In vivo respiration and oxygen evolution

Protonemal tissue grown for 10 days at CL was put in a 2 ml closed chamber filled with water. O_2 consumed by respiration in the dark at 25°C was measured using a Clark-type O_2 electrode (Hansatech, King's Lynn, UK). Gross O_2 evolution was measured with the same setup during the exposure of protonemal tissue at 850 µmol photons $m^{-2}s^{-1}$ white light. O_2 consumption and evolution rates were normalized to the total chlorophyll content of each sample.

REFERENCES

Alboresi, Alessandro, Caterina Gerotto, Giorgio M Giacometti, Roberto Bassi, and Tomas Morosinotto. 2010. "Physcomitrella Patens Mutants Affected on Heat Dissipation Clarify the Evolution of Photoprotection Mechanisms upon Land Colonization." *Proceedings of the National Academy of Sciences of the United States of America* 107 (24): 11128–33. doi:10.1073/pnas.1002873107.

Allahverdiyeva, Y., H. Mustila, M. Ermakova, L. Bersanini, P. Richaud, G. Ajlani, N. Battchikova, L. Cournac, and E.-M. Aro. 2013. "Flavodiiron Proteins Flv1 and Flv3 Enable Cyanobacterial Growth and Photosynthesis under Fluctuating Light." *Proceedings of the National Academy of Sciences* 110 (10): 4111–16. doi:10.1073/pnas.1221194110.

Allahverdiyeva, Yagut, Janne Isojärvi, Pengpeng Zhang, and Eva-Mari Aro. 2015. "Cyanobacterial Oxygenic Photosynthesis Is Protected by Flavodiiron Proteins." *Life* 5 (1): 716–43. doi:10.3390/life5010716.

Allen, G C, M A Flores-Vergara, S Krasynanski, S Kumar, and W F Thompson. 2006. "A Modified Protocol for Rapid DNA Isolation from Plant Tissues Using Cetyltrimethylammonium Bromide." *Nature Protocols* 1 (5): 2320–25. doi:10.1038/nprot.2006.384.

Bailleul, Benjamin, Nicolas Berne, Omer Murik, Dimitris Petroutsos, Judit Prihoda, Atsuko Tanaka, Valeria Villanova, et al. 2015. "Energetic Coupling between Plastids and Mitochondria Drives CO 2 Assimilation in Diatoms." *Nature* 524 (7565): 366–69. doi:10.1038/nature14599.

Bricker, Terry M., Adam J. Bell, Lan Tran, Laurie K. Frankel, and Steven M. Theg. 2014. "Photoheterotrophic Growth of Physcomitrella Patens." *Planta* 239 (3): 605–13. doi:10.1007/s00425-013-2000-3.

Cove, David. 2005. “The Moss *Physcomitrella Patens*.” *Annual Review of Genetics* 39 (1): 339–58. doi:10.1146/annurev.genet.39.073003.110214.

Cruz, J. A., C. A. Sacksteder, A. Kanazawa, and D. M. Kramer. 2001. “Contribution of Electric Field (????) To Steady-State Transthylakoid Proton Motive Force (Pmf) in Vitro and in Vivo. Control of Pmf Parsing into ???? And ??PH by Ionic Strength.” *Biochemistry* 40 (5): 1226–37. doi:10.1021/bi0018741.

DalCorso, Giovanni, Paolo Pesaresi, Simona Masiero, Elena Aseeva, Danja Schünemann, Giovanni Finazzi, Pierre Joliot, Roberto Barbato, and Dario Leister. 2008. “A Complex Containing PGRL1 and PGR5 Is Involved in the Switch between Linear and Cyclic Electron Flow in Arabidopsis.” *Cell* 132 (2): 273–85. doi:10.1016/j.cell.2007.12.028.

Edwards, Keith, Christophe Johnstone, and C. Thompson. 1991. “A Simple and Rapid Method for the Preparation of Plant DNA for PCR Analysis.” *Nucleic Acids Research* 19: 1349–1349. doi:10.1073/pnas.0905845106.

Gerotto, C., A. Alboresi, A. Meneghesso, M. Jokel, M. Suorsa, E.-M. Aro, and T. Morosinotto. 2016. “Flavodiiron Proteins Act as Safety Valve for Electrons in Physcomitrella Patens.” *Proceedings of the National Academy of Sciences of the United States of America* 113 (43). doi:10.1073/pnas.1606685113.

Gerotto, Caterina, Alessandro Alboresi, Giorgio M. Giacometti, Roberto Bassi, and Tomas Morosinotto. 2012. “Coexistence of Plant and Algal Energy Dissipation Mechanisms in the Moss Physcomitrella Patens.” *New Phytologist* 196 (3): 763–73. doi:10.1111/j.1469-8137.2012.04345.x.

Gerotto, Caterina, Alessandro Alboresi, Andrea Meneghesso, Martina Jokel, Marjaana Suorsa, Eva-mari Aro, and Tomas Morosinotto. 2016. “Flavodiiron Proteins Act as Safety Valve for Electrons in Physcomitrella Patens.” *Proceedings of the National Academy of Sciences of the United States of America* 113 (43): 12322–27. doi:10.1073/pnas.1606685113.

Graham, Linda E., Eunsoo Kim, Patricia Arancibia-Avila, James M. Graham, and Lee W. Wilcox. 2010. “Evolutionary and Ecophysiological Significance of Sugar Utilization by the Peat Moss Sphagnum Compactum (Sphagnaceae) and the Common Charophycean Associates Cylindrocystis Brebissonii and Mougeotia Sp. (Zygnemataceae).” *American Journal of Botany* 97 (9): 1485–91. doi:10.3732/ajb.0900341.

Helman, Yael, Dan Tchernov, Leonora Reinhold, Mari Shibata, Teruo Ogawa, Rakefet Schwarz, Itzhak Ohad, and Aaron Kaplan. 2003. “Genes Encoding A-Type Flavoproteins Are Essential for Photoreduction of O2 in Cyanobacteria.” *Current Biology* 13 (3): 230–35. doi:10.1016/S0960-9822(03)00046-0.

Ivanov, B N. 2014. “Role of Ascorbic Acid in Photosynthesis.” *Biochemistry. Biokhimiĭa* 79 (3): 282–89. doi:10.1134/S0006297914030146.

Järvi, Sari, Marjaana Suorsa, Virpi Paakkarinen, and Eva-Mari Aro. 2011. “Optimized Native Gel Systems for Separation of Thylakoid Protein Complexes: Novel Super- and Mega-Complexes.” *Biochemical Journal* 439 (2): 207–14. doi:10.1042/BJ20102155.

Jokel, Martina, Xenie Johnson, Gilles Peltier, Eva Mari Aro, and Yagut Allahverdiyeva. 2018. “Hunting the Main Player Enabling Chlamydomonas Reinhardtii Growth under Fluctuating Light.” *Plant Journal* 94 (5): 822–35. doi:10.1111/tpj.13897.

Kügler, Marion, Lothar Jänsch, Volker Kruft, Udo K. Schmitz, and Hans Peter Braun. 1997. “Analysis of the Chloroplast Protein Complexes by Blue-Native Polyacrylamide Gel Electrophoresis (BN-PAGE).” *Photosynthesis Research* 53 (1): 35–44. doi:10.1023/A:1005882406718.

Kukuczka, B., L. Magneschi, D. Petroutsos, J. Steinbeck, T. Bald, M. Powikrowska, C. Fufezan, G. Finazzi, and M. Hippler. 2014. “Proton Gradient Regulation5-Like1-Mediated Cyclic Electron Flow Is Crucial for Acclimation to Anoxia and Complementary to Nonphotochemical Quenching in Stress Adaptation.” *Plant Physiology* 165 (4): 1604–17. doi:10.1104/pp.114.240648.

Larosa, Veronique, Andrea Meneghesso, Nicoletta La Rocca, Janina Steinbeck, Michael Hippler, Ildiko Szabo, and Tomas Morosinotto. 2017. “Mitochondria Affect Photosynthetic Electron Transport and Photo-Sensitivity in a Green Alga.” *Plant Physiology*, pp.01249.2017. doi:10.1104/pp.17.01249.

Mehler, Alan H. 1951. “Studies on Reactions of Illuminated Chloroplasts. II. Stimulation and Inhibition of the Reaction with Molecular Oxygen.” *Archives of Biochemistry and Biophysics* 34 (2): 339–51. doi:10.1016/0003-9861(51)90012-4.

Mehler, Alan H., and Allan H. Brown. 1952. “Studies on Reactions of Illuminated Chloroplasts. III. Simultaneous Photoproduction and Consumption of Oxygen Studied with Oxygen Isotopes.” *Archives of Biochemistry and Biophysics* 38 (1): 365–70. doi:10.1016/0003-9861(52)90042-8.

Munekage, Yuri, Mihoko Hashimoto, Chikahiro Miyake, Ken-ichi Tomizawa, Tsuyoshi Endo, Masao Tasaka, and Toshiharu Shikanai. 2004. “Cyclic Electron Flow around Photosystem I Is Essential for Photosynthesis.” *Nature* 429 (6991): 579–82. doi:10.1038/nature02598.

Munekage, Yuri, Masaya Hojo, Jörg Meurer, Tsuyoshi Endo, Masao Tasaka, and Toshiharu Shikanai. 2002. “PGR5 Is Involved in Cyclic Electron Flow around Photosystem I and Is Essential for Photoprotection in Arabidopsis.” *Cell* 110 (3): 361–71. doi:10.1016/S0092-8674(02)00867-X.

Nunes-Nesi, A., W. L. Araujo, and A. R. Fernie. 2011. “Targeting Mitochondrial Metabolism and

Machinery as a Means to Enhance Photosynthesis." *PLANT PHYSIOLOGY* 155 (1): 101–7. doi:10.1104/pp.110.163816.

Peltier, Gilles, Dimitri Tolleter, Emmanuelle Billon, and Laurent Cournac. 2010. "Auxiliary Electron Transport Pathways in Chloroplasts of Microalgae." *Photosynthesis Research* 106: 19–31. doi:10.1007/s11120-010-9575-3.

Rensing, Stefan A, Daniel Lang, Andreas D Zimmer, Astrid Terry, Asaf Salamov, Harris Shapiro, Tomoaki Nishiyama, et al. 2008. "The Physcomitrella Genome Reveals Evolutionary Insights into the Conquest of Land by Plants." *Science (New York, N.Y.)* 319 (5859): 64–69. doi:10.1126/science.1150646.

Rumberg, B, and U Smgel. 1968. "PH Changes in the Inner Phase of the Thylakoids during Photosynthesis" 622 (1963): 1968–70.

Shikanai, Toshiharu. 2015. "Chloroplast NDH: A Different Enzyme with a Structure Similar to That of Respiratory NADH Dehydrogenase." *Biochimica et Biophysica Acta - Bioenergetics*. Elsevier B.V. doi:10.1016/j.bbabio.2015.10.013.

Shikanai, Toshiharu, and Hiroshi Yamamoto. 2017. "Contribution of Cyclic and Pseudo-Cyclic Electron Transport to the Formation of Proton Motive Force in Chloroplasts." *Molecular Plant* 10 (1). Elsevier Ltd: 20–29. doi:10.1016/j.molp.2016.08.004.

Sonoike, Kintake. 2011. "Photoinhibition of Photosystem I Review 2011.Pdf." *Physiologia Plantarum* 142 (1): 56–64. doi:10.1111/j.1399-3054.2010.01437.x.

Suorsa, Marjaana, Michele Grieco, Markus Nurmi, Malgorzata Pietrzykowska, Marjaana Rantala, Virpi Paakkarinen, Mikko Tikkanen, Stefan Jansson, and Eva-mari Aro. 2012. "PROTON GRADIENT REGULATION5 Is Essential for Proper Acclimation of Arabidopsis Photosystem I to Naturally and Arti Fi Cially Fluctuating Light Conditions" 24 (July): 2934–48. doi:10.1105/tpc.112.097162.

Suorsa, Marjaana, Fabio Rossi, Luca Tadini, Mathias Labs, Monica Colombo, Peter Jahns, Martin M. Kater, et al. 2015. "PGR5-PGRL1-Dependent Cyclic Electron Transport Modulates Linear Electron Transport Rate in Arabidopsis Thaliana." *Molecular Plant*, no. February: 271–88. doi:10.1016/j.molp.2015.12.001.

Thelander, Mattias, Tina Olsson, and Hans Ronne. 2005. "Effect of the Energy Supply on Filamentous Growth and Development in Physcomitrella Patens." *Journal of Experimental Botany* 56 (412): 653–62. doi:10.1093/jxb/eri040.

Vries, Jan De, Amanda Stanton, John M Archibald, and Sven B Gould. 2016. "Streptophyte Terrestrialization in Light of Plastid Evolution." *Trends in Plant Science* xx. Elsevier Ltd: 1–10. doi:10.1016/j.tplants.2016.01.021.

Yamori, Wataru, and Toshiharu Shikanai. 2016. “Physiological Functions of Cyclic Electron Transport Around Photosystem I in Sustaining Photosynthesis and Plant Growth.” *Annual Review of Plant Biology* 67 (1): 81–106. doi:10.1146/annurev-arplant-043015-112002.

SUPPLEMENTARY MATERIAL

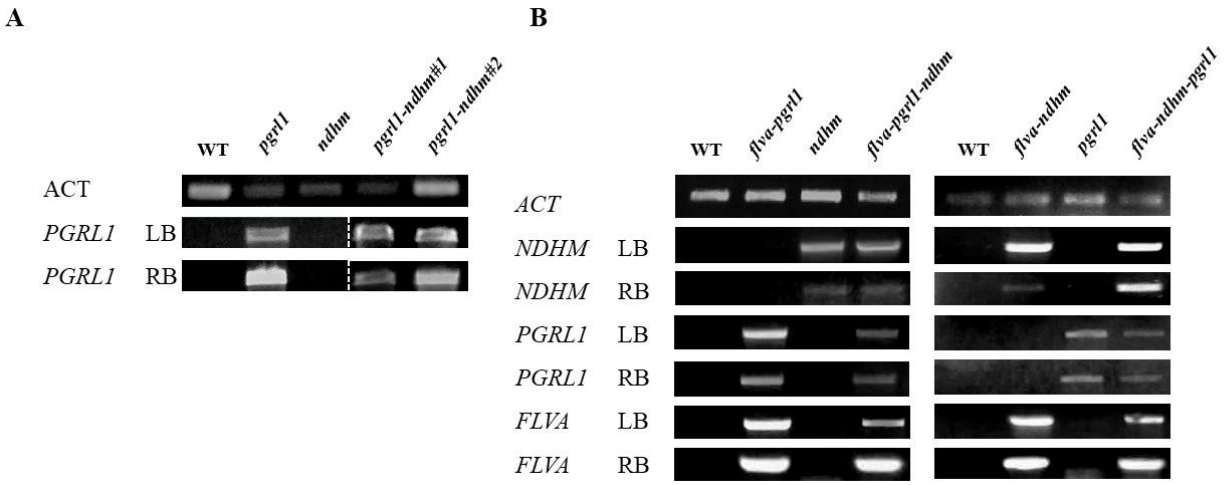

Supplementary 1 Isolation of KO lines: PCR on gDNA confirming insertion of resistance cassettes in targeted loci. Left border (LB) PCR with 5’-3’ primer of the insertion locus and 3’-5’ on resistance cassette. Right border (RB) 5’-3’ primer on resistance cassette and 3’-5’ primer on targeted locus. **A** characterization of two lines *pgrl1-ndhm* **B** characterization of triple mutants *flva-pgrl1-ndhm* and *flva-ndhm-pgrl1* and their respective background.

APPENDIX 1

Identification of *Physcomitrella patens* Ferredoxin-NADPH Reductase isoforms

CONTRIBUTIONS

In this Appendix Mattia Storti performed all the experiments and wrote most of the text. Most of experimental data presented were obtained during a visit in the laboratory of Dr Guy Hanke (Queen Mary University of London). Dr Guy Hanke and Laura Mosebach also contributed to experimental design and data analysis of results described in this chapter.

ABSTRACT

Photosynthetic linear electron flow sustains carbon fixation and all plant metabolism. Efficiency of this process is largely influenced by environmental condition which easily cause an imbalance between light dependent photosynthetic reactions and the rest of metabolism. These conditions can easily drive accumulation of reactive molecules and photodamage and photosynthetic organisms have therefore evolved different mechanisms to protect PSI and PSII, including alternative electron transfer pathways capable of dispersing electrons in excess from the PSI acceptors (Ferredoxin, NADPH). The final step of linear electron flow is mediated by the enzyme FNR which transfer electrons from reduced Ferredoxin to $NADP^+$. The efficiency and regulation of this last reaction clearly can have a major influence on the overall processes, making regulation of FNR in response to light intensities and redox state of photosynthetic apparatus potentially highly strategic. In this chapter we identified FNR isoenzymes in *Physcomitrella patens* and assessed their localization at tissue and subcellular level.

INTRODUCTION

As discussed in detail in previous chapters, alternative electron flow (AEF) pathways play a pivotal role in the regulation of photosynthesis. They are particularly important in protecting photosystem I (PSI) by dissipating excess reducing power to avoid its over-reduction and consequent damage. As shown in chapters 3 and 5, mutants impaired in these pathways suffer a decrease in photosynthetic performance and growth, especially when subjected to dynamic light regimes. This phenotype can largely be explained by a limitation in electron acceptors downstream of PSI, causing accumulation of reducing power with consequent oxidative damage. NADPH is synthesized through Ferredoxin-NADPH reductase (FNR) which transfers electrons from reduced Ferredoxin (Fd) to $NADP^+$. FNR activity thus has a major influence on the rate of Fd re-oxidation, and thus could have a major influence on PSI activity redox state by affecting the kinetics of regenerating its primary electron acceptor, oxidized Fd.

FNR is a flavin adenine dinucleotide (FAD)-containing enzyme of about 35 kDa. In higher plants two FNR types have be distinguished: (*i*) a Leaf-type FNR (LFNR) mediating the last step of photosynthetic electron transport, by transfering two electrons from Fd_{red} to a $NADP^+$ molecule (Batie

and Kamin 1984). (*ii*) a Root-type FNR (RFNR) which exploits Root-type Fd_{ox} allowing the transfer of an electron from NADPH to Fd (Hanke et al. 2004; Onda et al. 2000). RFNR allows production of reduced Fd in non-photosynthetic tissues for biosynthetic pathways requiring reducing power, such as NiR (Nitrite Reductase) and GOGAT (glutamine-oxoglutarate aminotransferase) involved in nitrogen uptake (Hachiya et al. 2016).

FNR are soluble proteins with no transmembrane helices, but in vascular plants they can associate to the thylakoid membrane thanks to the interaction with Tic62 (Balsera et al. 2007) or Trol (Jurić et al. 2009) mediated by FNR N-terminal domain (Twachtmann et al. 2012). Additionally, FNR was shown to interact with NDH-1 complex (Guedeney et al. 1996), PSI (Andersen, Scheller, and Møller 1992), Cyt b_6f (Clark et al. 1984) in higher plants and a PSI-Cyt b_6f super-complex including also FNR was detected in *C. reinhardtii* (Iwai et al. 2010). This evidence highlights a dynamic distribution of FNR on the membrane and it was hypothesized that different FNR localization could influence the fate of the electrons transported by Fd (Goss and Hanke 2014). It is in fact possible that a membrane bounded FNR could transfer more efficiently electrons to Cyt b_6f and plastoquinone pool while a soluble form would be more active with $NADP^+$. Joliot and Johnson (Joliot and Johnson 2011) suggested that FNR can work in a "CEF configuration" binding to Cyt b_6f, and transferring electrons to this complex rather than to $NADP^+$ and they consistently detected a decrease in CEF activity in FNR depleted plants (Joliot and Johnson 2011). It was also shown that FNR recruitment to PSI in *C. reinhardtii* is affected by the absence of PGR5 or PGRL1 (Mosebach et al. 2017). An opposite correlation between CEF and FNR activities was however also observed in (Talts et al. 2007), in particular after dark adaptation when FNR is inactive and CEF is instead more active. Available evidences thus point to the possibility that modulation of FNR localization and activity can play a significant influence on the fate of electrons downstream PSI, affecting cyclic, pseudo-cyclic and linear electron flow (CEF, PCEF and LEF), even if the mechanisms regulating this process are still unknown. In this context it should be considered that electrons in reduced Fd and NADPH not only supply CEF or carbon fixation but can be used by many other metabolic pathways and, as example Fd acts as electron donor for chlorophyll synthesis, nitrogen and sulphate metabolism.

FNR protein sequences, activity and membrane association has never been investigated in *P. patens* nor in other non-vascular plants to assess if its activity was altered during land colonization. Considering that plants and green algae show significant differences it is thus interesting to assess how this enzyme is regulated in this organism and its possible role in regulation of photosynthetic activity, also in connection with the mutants with altered photosynthetic electron transport described here. Here we identified 3 FNR isoforms in *P. patens* and we studied FNR distribution in the whole

plant and in chloroplast of WT and plants depleted for different AEF pathways with the aim to understand the correlation between FNR activity and the consequent flow of electrons in the different AEF pathways.

RESULTS

Identification of FNRs in *P. patens* genome

We first searched for FNR isoforms in *P. patens* latest genome available (V3.1, phytozome.jgi.doe.gov) using *A. thaliana* leaf type FNR (LFNR1, sp|Q9FKW6|) as query, identifying three potentially homologous sequences (Pp3c9_25700V3.1, Pp3c9_25950V3.1, Pp3c19_9770V3.1). Translated *P. patens* sequences were cross-checked against reference refseq_protein database using blastp (blast.ncbi.nlm.nih.gov) and first 50 results for each sequence aligned with FNR sequences of other species, supporting their identification as homologues. Two of the sequences identified in *P. patens* encode for an identical protein (Pp3c9_25700V3.1, Pp3c9_25950V3.1, these were named PpFNR1) and, since the coding *loci* are very closely located in the same chromosome, they probably derived from a recent duplication event, as observed in other cases in *P. patens* (Rensing et al. 2008). The other sequence was instead named PpFNR2. In vascular plants FNR binding to the membrane is mediated by Tic62 or Trol (Balsera et al. 2007; Jurić et al. 2009). *In silico* analysis did not allow identifying any Tic62 homologous in *P. patens* genome, while a protein similar to Trol is present. However the latter carries a conserved rhodanase-like domain but it lacks the C-terminal domain (Supplementary information) fundamental for recruitment of FNR, raising doubts on the conservation of its function in *P. patens*.

P. patens FNR protein sequences were aligned with sequences from non-vascular embryophytes, unicellular algae and vascular plant FNRs, including both LFNRs and RFNRs. In the corresponding phylogenetic tree algal FNRs all clustered in a single branch highlighting the presence of a specific algae type FNR (cluster 3, Fig 1A). As previously observed by (Goss and Hanke 2014) they are closer to plants Root-type FNRs than leaf isoforms. A single exception is the microalgal Tp FNR3, which clusters with LFNR sequences together with two cyanobacterial FNR proteins (A FNR, S FNR).

Most of non-vascular plant FNRs also clustered together and, as algal isoforms, their sequences are more similar to vascular plant RFNRs (cluster 4, Fig 1A). Two exceptions are the sequences of *M. polymorpha* and *S. mollendorffi* FNRs that instead cluster together with LFNRs (cluster 2, Fig 1A). In the case of *P. patens* both protein isoforms appear to be more similar to RFNRs (Fig 1A). In vascular plants the separation between RFNR and LFNR reflects also the different function of the enzyme but this is generally valid. In *P. patens* even if no Leaf-type FNR was identified an enzyme supporting photosynthetic NADPH production must be present.

FNR expression levels were investigated using "The Bio-Analytic Resource for Plant Biology" (bar.utoronto.ca) tool collecting available data on gene expression, revealing that PpFNR2 (Pp3c19_9770V3.1) is preponderantly expressed in non-photosynthetic tissues such as rhizoids and spores but also in caulonemata. Pp3c9_25700V3.1 encoding for PpFNR1 is almost equally expressed in rhizoids and phyllids but is more expressed in chloronemata, thus the tissues with high photosynthetic activity (Fig 1B). These expression data thus suggest that despite their sequence similarity FNR1 is more active in photosynthetic electron transport while FNR2 in heterotrophic activity.

The distribution of FNR proteins in *P. patens* was assessed on extracts obtained from protonema, phyllids, rhizoids and entire gametophores. Protonema and phyllids are photosynthetic tissues while rhizoids have limited photosynthetic activity, if any (as confirmed also by the absence of Rubisco, Fig 1B), they are mainly involved in anchoring to the soil and probably nutrient uptake (Cove 2005). The two former tissues should thus contain mainly photosynthetic FNR while rhizoids should contain heterotrophic FNR. Western Blotting revealed that, while in photosynthetic tissues (phyllids and protonema) PpFNR1 is more abundant, in rhizoids PpFNR2 (distinguishable from its higher molecular weight) and PpFNR1 amounts detected are similar (Fig1 C). In gametophores PpFNR2 is undetectable indicating that PpFNR1 is the main FNR enzyme in mature *P. patens* plants. Western blotting showed that in photosynthetic tissues PpFNR1 is the most abundant FNR enzyme, supporting the hypothesis of its involvement in photosynthesis, while PpFNR2 was consistently detected only in rhizoids thus probably works in heterotrophic direction.

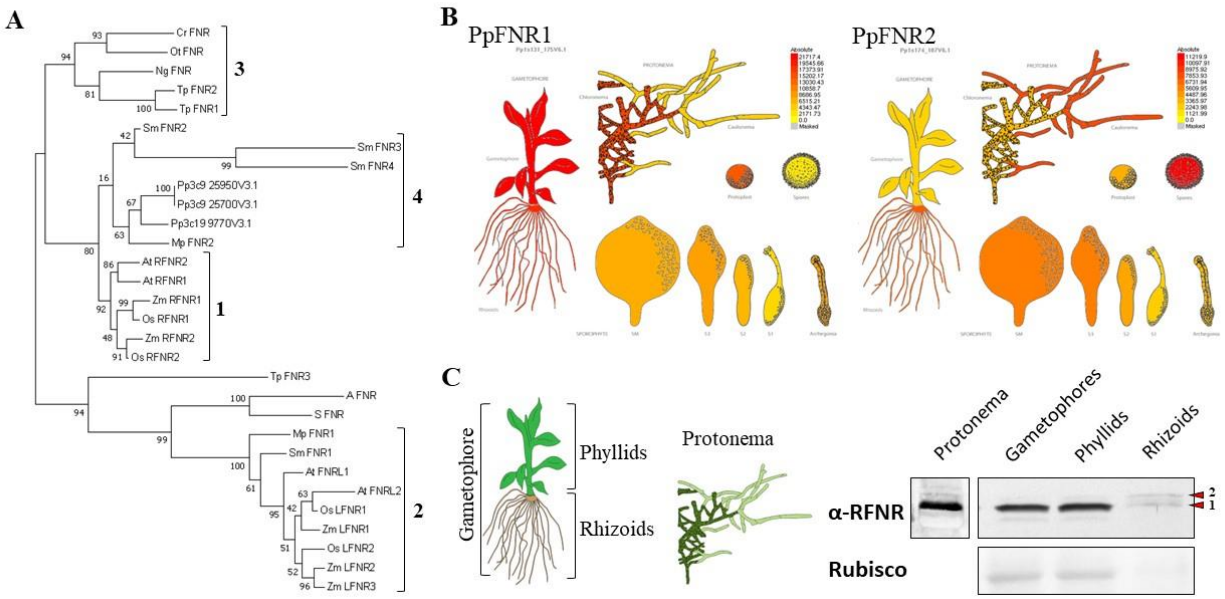

Figure 1: *P. patens* FNR enzymes. A) *FNRs phylogenetic tree:* ***1*** *RFNR,* ***2*** *LFNR (vascular plants: Arabidopsis thaliana, Zea mays, Oryza sativa),* ***3*** *algae specific (Chlamydomonas reinhardtii, Nannochloropsis gaditana, Thalassiosira pseudonana) FNR,* ***4*** *non-vascular plant FNR (Selaginella mollendorffii, Physcomitrella patens, Marcanthia polymorpha), other (Nostoc, Synechocystis).* **B)** Blot on *P. patens* extracts (α-Maize RFNR), Ponceau staining of Rubisco and representation of utilized tissues. **C)** FNR1 FNR2 genes expression levels, Lower: FNR3 expression levels. Red color is attributed to higher expression in of the gene while yellow colored tissues have relatively lower expression. According to PhytoMine data (phytozome.jgi.doe.gov) the two genes coding PpFNR1 are coexpressed (correlation index=0.991) and represented by the same panel.

P. patens FNR is found largely in the soluble form.

FNR distribution at sub-chloroplast level is expected to affect its activity. To assess FNR localization thylakoid membranes were separated from soluble stromal fraction and tested using both western blotting and activity assays. Thylakoid membranes were isolated from protonemal cells and washed twice with low salinity buffer to prevent protein dissociation from the membranes while completely removing soluble proteins (Figure 2A). Western blot analysis revealed that most of the FNR enzyme is found as soluble (S) while a smaller but significant fraction is also found in the membrane thylakoids (M). This fraction of FNR appears however to be stably bounded to the membrane since it is maintained during several washes (Figure 2 B).

We evaluated if the association of FNR to the membrane can influence its enzymatic activity exploiting an assay that quantifies its heterotrophic activity. This is based on the addition of external NADPH that is used by FNR to reduce an external electron acceptor, in this case DCPIP (Dichlorophenolindophenol). DCPIP turns from blue to colourless when it is reduced and following 600 nm absorbance during time it is thus possible to determine the kinetic rate of the enzyme (Figure

2B). Enzymatic kinetics was evaluated in the first 30 seconds after DCPIP addition, in soluble phase (S), thylakoid membranes (M) and the first wash step (W1) which still contain soluble FNR. The activity in the wash (W1) fractions was negligible, while higher NADPH oxidation rates were observed in fractions containing soluble enzymes (S) and on resuspended membranes (M, Figure 2B). The NADPH oxidation rate observed in the soluble phase was much larger than the one measured in thylakoids samples. In particular FNR in soluble fraction has 5.8 ±1.6 higher activity compared to the membrane, a value that is very consistent with the western blotting analysis that suggest a 4.7 ± 1.1 higher protein content (Figure 2C). Both experiments thus consistently showed that most FNR is found as soluble in *P. patens* even if a significant fraction is also detected associated to the thylakoid membranes. Independently from the localization enzymatic activity is similar.

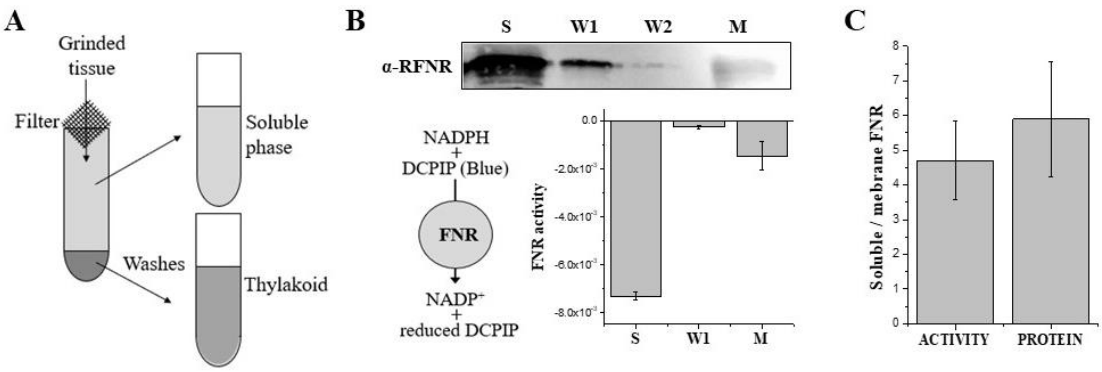

Figure 2: Soluble and membrane bounded FNR. A) Schematic representation of soluble and thylakoid membrane bounded proteins preparation, the same volume of buffer was used for grinding, washes and thylakoid resuspension to compare the protein amount in the different phases. **B)** Sub-cellular localization of PpFNR enzymes in WT plants. Upper: Immunodetection of FNR in soluble phase (S), first wash (W1), second wash (W2) and purified thylakoids (M). Button: Scheme of heterotopic assays reaction with DCPIP and FNR activity estimates from DCPIP absorption (600 nm) during the first 30s after DCPIP addition. Black bar: membrane extracts, grey bar: soluble extracts. **C)** Sub-cellular localization of PpFNR abundance and activity, derived from data in B. Ratio of soluble to membrane associated FNR activity, and of soluble to membrane associated FNR protein content detected by Western blot after integrated density quantification of the bands. n=5 ± SD.

Light dependent $NADP^+$ reduction mediated by membrane associated FNR was also assessed using a Dual PAM 100 supplied with DUAL-DNADPH detector (Walz, Germany). Purified thylakoids were added with external $NADP^+$ and Fd, that were lost during purification (Figure 3). As expected photosynthesis was almost inactive in isolated thylakoids and no NADPH formation was observed (Figure 3). To restore photosynthetic electron flux from PSI to $NADP^+$ we added ascorbate that serves as electron donor for PSI via plastocyanin (Trubitsin et al. 2014)(Figure 3). When ascorbate was added, a light dependent NADPH synthesis was detected by the increase of 465 nm fluorescence

signal. NADPH increase showed 3 different phases upon light switch on: an initial lag phase, a second linear phase and finally a decrease in activity due to NADPH accumulation which inhibits FNR photosynthetic activity (Figure 3, (Schreiber and Klughammer 2009)). Maximum rate of NADPH formation in the linear phase is known to be dependent on FNR activity and thus the signal kinetic was thus quantified (Figure 3).

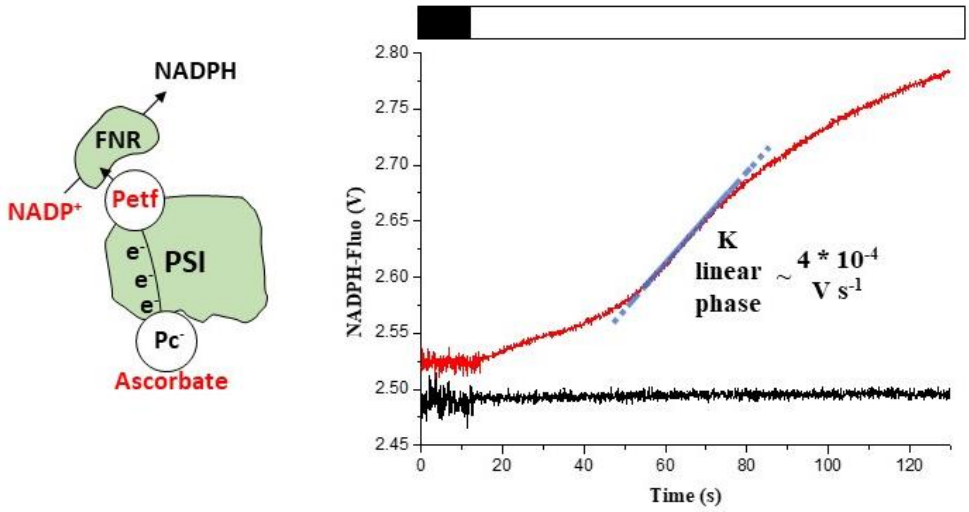

Figure 3: FNR activity in photosynthetic direction. Representative trace of light induced NADPH production. On the right traces of NADPH fluorescence upon light switch on (timing indicated by the upper bar) with (red) or without (black) ascorbate. On the left experimental scheme: soluble stromal components are lost during thylakoids isolation thus added (in red) to allow FNR to work in the photosynthetic direction.

FNR sub-chloroplast localization in Alternative Electron Flow mutants

We assessed FNR activity in mutants affected in CEF and PCEF (chapter 3,4) to see if altered redox balance in the chloroplast influences FNR activity and/or localization. In this case both localization and heterotrophic enzymatic activity results were very similar to what observed for WT plants. Soluble FNR in all cases is more abundant than the fraction associated to the membrane fractions (4 to 6-fold higher upon quantification, Figure 4A) and a higher FNR activity was consistently detected in the soluble phase rather than in the membrane (Figure 4B). Both Western blot and heterotrophic FNR assay did not evidence any significant difference in the localization of FNR enzymes at sub-cellular level in CEF and PCEF KO mutants respect to WT plants, showing that alteration of the

electron transport activities does not have major effects on FNR distribution and activity. We also compared the activity of membrane associated FNR of WT and mutants of CEF and PCEF following light dependent $NADP^+$ reduction (Figure 4C). Even in this case we still did not detect any significant differences between WT and CEF and PCEF KO mutants analysed.

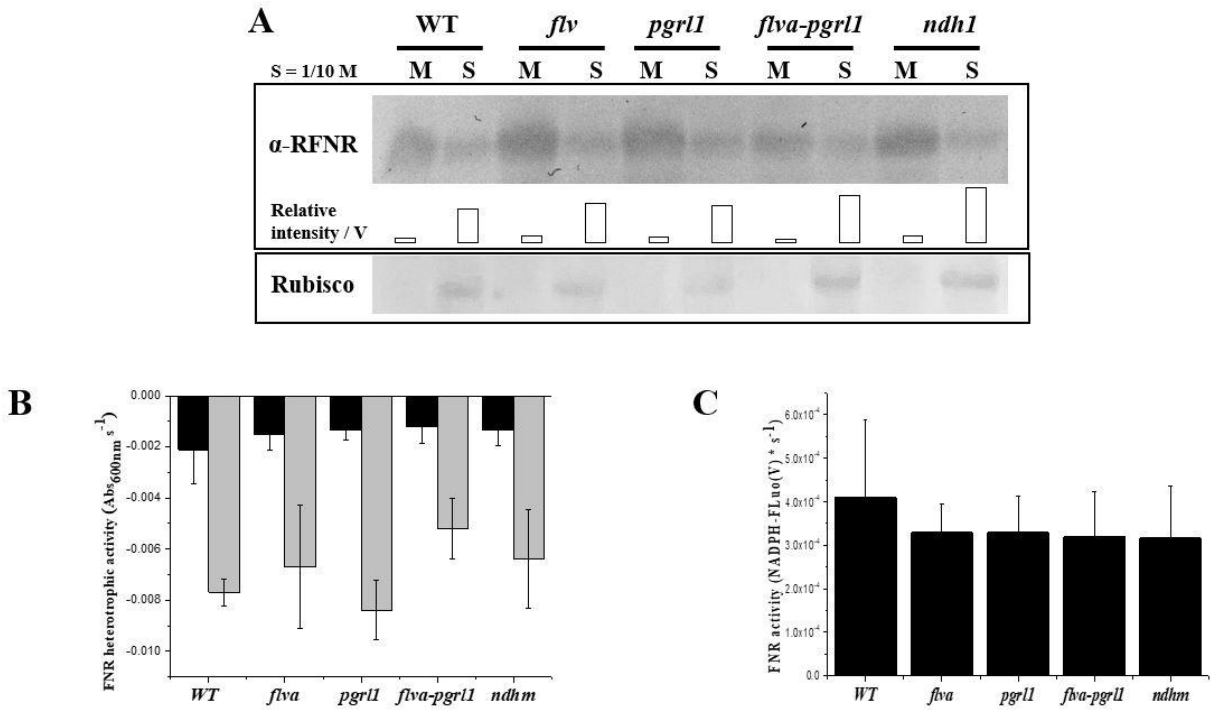

Figure 4: FNR activity and localization in CEF and PCEF KO mutants. A) FNR detected by Western blot on soluble (S) and membrane (M) extracts. S are 1/10 volume compared to M samples. Quantification of FNR in different soluble and membrane fractions normalized to the volume of each fraction. Soluble enzyme Rubisco was used as loading control. **B)** FNR heterotrophic assay on soluble (gray bar) and thylakoid membranes (black bar). n=3 ± SD. **C)** Kinetic rates of NADPH synthesis calculated by maximum slope (K) of NADPH fluorescence tracks. Data shown are the average value of 2 biological replicates (3 technical replicates ± SD).

DISCUSSION

Here we analysed FNR enzymes of *P. patens* and identified 3 different genes with differential expression profiles in photosynthetic and non-photosynthetic tissues. PpFNRs do not show a clear differentiation between leaf type and root type FNR at sequence level as for vascular plants and all PpFNR show more similarity to root type FNR. Clearly one of the two isoforms must be working in light dependent NADPH photosynthesis and gene expression and western blotting analyses suggests that PpFRN1 is likely more involved that the other isoform. This thus suggests that separation between root and leaf type FNR in plants is not necessarily correlated with their functional

specialization but that still it is advantageous to have isoforms specialized in autotrophic or heterotrophic metabolism. Since, as also shown here, FNR appears to be active in both directions and the reaction likely depends on the redox conditions they are in and the availability of substrates, it is not clear what advantage having distinct FNR isoforms brings to the plant. One possibility is that having multiple genes allows an independent regulation of FNR isoforms accumulation. In fact considering that FNR catalyses both activities it is likely important to regulate FNR activities differently in photosynthetic and heterotrophic tissues.

PpFNR enzymes are found mostly soluble enzymes and only approx. 15% are associated to the thylakoid membrane (Figure 2), at difference from what observed for angiosperms in which membrane bounded FNRs can be predominant (Hanke et al. 2005). This can be a consequence of the absence of proteins know to favour a stable association of FNR to the membrane in *P. patens* (e.g. Trol and Tic62).

It is interesting to observe that this difference in FNR localization with angiosperms is correlated with another difference identified in this work, the presence of FLV proteins (Chapter 2). In the dark chloroplasts are still active metabolically using starch reserves as energy source. Since FNR can be active heterotrophically, in the dark they can use available reducing power to reduce the Fd pool. As soon as the light is switched on, however, if Fd is reduced it can cause PSI acceptor side limitation and consequently damage, as discussed extensively in chapters 2,3 and 5. FLV proteins in *Physcomitrella patens* are fundamental to dissipate these extra electrons on the PSI acceptor side upon dark to light transitions. As discussed extensively in other chapters, Angiosperms lost FLV during evolution and it is possible that they can prevent some PSI acceptor side limitation by sequestering FNR in the dark thanks to Trol/Tic62 association. This hypothesis is consistent with the finding that FNR-Trol/Tic62 association is favoured in acidic/neutral pH conditions in the stroma that are found when chloroplast is in the dark (Alte et al. 2010). If this true, Trol/Tic62 can avoid accumulation of extra electron in PSI, keeping acceptors more oxidised and readier to accept electrons as soon as the light is switched on.

METHODS

Total proteins extraction from P. patens tissues

Frozen gametophores, rhizoids e phyllids were ruptured with plastic pestles. Homogenized material was resuspended in phosphate buffer (20 mM phosphate buffer pH 7, 0.1 v/v β-mercaptoethanol, 0.05 W/v triton X-100). Proteins amount in solubilized samples was quantified by Bradford assay (Sigma Aldrich). 20 µg of proteins were used for Western blot detection after resuspension in SB buffer (10% glycerol, 45 mM TRIS (pH 6.8), 0.03 M dithiothreitol and 3% SDS). In the case of protonema, tissue was grinded in SB buffer and 4 µg of chl were loaded in SDS page for Western blot detection. For Western blot antisera against maize RFNR was used, the latter allowed better detection of PpFNR compared to other antisera available during preliminary test.

Total membrane purification

Membrane were purified from 10 days protonema tissue grown at 50 µmol photons m^{-2} s^{-1} in long photoperiod 16/8 hours at 24 ± 2 °C. Frozen sample were grinding using a glass potter and resuspended in B1 buffer (400 mM Sorbitol, 5 mM $MgCl_2$, HEPES (NAOH) pH 7, supplemented with protease inhibitor) in the case of photoreduction assay or in Assay Buffer (100 mM NaCl, 50 mM Tris pH 7.5) for heterotrophic assay. Ungrounded material was filtered through a 20 µm nylon cloth and membrane were pelleted at 8000xG for 5 min. Membranes were than washed twice using the same buffer used for the extraction and finally resuspended in the desired volume buffer (for heterotrophic assay and Western blotting the resuspension volume is the same used for grinding to directly compare the amount/ activity of the proteins in the two samples).

$NADP^+$ photoreduction assay

$NADP^+$ photoreduction was measured using a DUAL PAM 100 (Walz) equipped with a NADPH/9-AA module. Membranes (10 µg/chl) were resuspended in 2 ml measure buffer (400 mM Sorbitol, 10 mM NaCl, 5 mM $MgCl_2$, 100 mM KH_2PO_4 pH 7.5). The reaction was supplemented with 200 µM

$NADP^+$ as FNR electron acceptor and 50 mM Ascorbate to sustain PSI activity and 0.1 % Triton X-100 to allows its permeabilization in the membranes. Moreover, 10 µM CrPetf (Mosebach et al. 2017) was added was used as electron donor for PpFNR. CrPetf was chosen because highly similar to main Fd isoform in *P. patens* (Pp3c4_8330V3.1). NADPH accumulation was measured 3 minutes in the dark to assure reaction stability e specificity, after that actinic light (578 µM photons s^{-1} m^{-2}) was switch on to initialize $NADP^+$ photoreduction. Reaction was carried on without mechanical mixing to allow membrane settle and remove signal noise.

Heterotrophic NADPH oxidation assay

Membrane extracts containing 5 µg of chlorophyll (or the corresponding volume of soluble extract) were resuspended in assay buffer (100 mM NaCl, 50 mM Tris pH 7.5) together with 500 µM NADPH in a total volume of 100 µl. The same volume of 100 µM DCPIP was injected during the measurement to achieve a final concentration of 50 µM. DCPIP absorbance at 600 nm was evaluated for 30 s after its injection in a multi-well plate using a FLUOstat OMEGA (BMG LABTECH) plate reader. Enzymatic kinetic was evaluated by MARS Data Analysis Software (BMG LABTECH).

REFERENCES

Alte, Ferdinand et al. 2010. "Ferredoxin:NADPH Oxidoreductase Is Recruited to Thylakoids by Binding to a Polyproline Type II Helix in a PH-Dependent Manner." *Proceedings of the National Academy of Sciences of the United States of America* 107(45):19260–65. Retrieved (http://www.pubmedcentral.nih.gov/articlerender.fcgi?artid=2984204&tool=pmcentrez&rendertype=abstract).

Andersen, Birgitte, Henrik Vibe Scheller, and Birger Lindberg Møller. 1992. "The PSI-E Subunit of Photosystem I Binds Ferredoxin:NADP+oxidoreductase." *FEBS Letters* 311(2):169–73.

Balsera, Mónica, Anna Stengel, Jürgen Soll, and Bettina Bölter. 2007. "Tic62: A Protein Family from Metabolism to Protein Translocation." *BMC Evolutionary Biology* 7.

Batie, Christopher J. and Henry Kamin. 1984. "Electron Transfer by Ferredoxin:NADP+ Reductase."

The Journal of Biological Chemistry 259(19):11976–85.

Clark, R. D., M. J. Hawkesford, S. J. Coughlan, J. Bennett, and G. Hind. 1984. "Association of Ferredoxin-NADP+oxidoreductase with the Chloroplast Cytochrome b-f Complex." *FEBS Letters* 174(1):137–42.

Cove, David. 2005. "The Moss *Physcomitrella Patens*." *Annual Review of Genetics* 39(1):339–58. Retrieved (http://www.annualreviews.org/doi/abs/10.1146/annurev.genet.39.073003.110214).

Goss, Tatjana and Guy Hanke. 2014. "The End of the Line: Can Ferredoxin and Ferredoxin NADP(H) Oxidoreductase Determine the Fate of Photosynthetic Electrons?" *Current Protein & Peptide Science* 15(4):385–93. Retrieved (http://www.eurekaselect.com/openurl/content.php?genre=article&issn=1389-2037&volume=15&issue=4&spage=385).

Guedeney, Geneviève, Sylvie Corneille, Stéphan Cuiné, and Gilles Peltier. 1996. "Evidence for an Association of Ndh B, Ndh J Gene Products and Ferredoxin-NADP-Reductase as Components of a Chloroplastic NAD(P)H Dehydrogenase Complex." *FEBS Letters* 378(3):277–80.

Hachiya, Takushi et al. 2016. "Arabidopsis Root-Type Ferredoxin: NADP(H) Oxidoreductase 2 Is Involved in Detoxification of Nitrite in Roots." *Plant and Cell Physiology* 57(11):2440–50.

Hanke, Guy T., Genji Kurisu, Masami Kusunoki, and Toshiharu Hase. 2004. "Fd: FNR Electron Transfer Complexes: Evolutionary Refinement of Structural Interactions." *Photosynthesis Research* 81(3):317–27.

Hanke, Guy Thomas et al. 2005. "Multiple Iso-Proteins of FNR in Arabidopsis: Evidence for Different Contributions to Chloroplast Function and Nitrogen Assimilation." *Plant, Cell and Environment* 28(9):1146–57.

Iwai, Masakazu et al. 2010. "Isolation of the Elusive Supercomplex That Drives Cyclic Electron Flow in Photosynthesis." *Nature* 464(7292):1210–13.

Joliot, P. and G. N. Johnson. 2011. "Regulation of Cyclic and Linear Electron Flow in Higher Plants." *Proceedings of the National Academy of Sciences* 108(32):13317–22. Retrieved (http://www.pnas.org/cgi/doi/10.1073/pnas.1110189108).

Jurić, Snježana et al. 2009. "Tethering of Ferredoxin:NADP+ Oxidoreductase to Thylakoid Membranes Is Mediated by Novel Chloroplast Protein TROL." *Plant Journal* 60(5):783–94.

Mosebach, Laura et al. 2017. "Association of Ferredoxin : NADP + Oxidoreductase with the

Photosynthetic Apparatus Modulates Electron Transfer in Chlamydomonas Reinhardtii." *Photosynthesis Research* 0(0):0.

Onda, Y. et al. 2000. "Differential Interaction of Maize Root Ferredoxin:NADP(+) Oxidoreductase with Photosynthetic and Non-Photosynthetic Ferredoxin Isoproteins." *Plant physiology* 123(3):1037–45. Retrieved (http://www.pubmedcentral.nih.gov/articlerender.fcgi?artid=59067&tool=pmcentrez&rendertype=abstract).

Rensing, Stefan A. et al. 2008. "The Physcomitrella Genome Reveals Evolutionary Insights into the Conquest of Land by Plants." *Science (New York, N.Y.)* 319(5859):64–69. Retrieved (http://www.sciencemag.org/content/319/5859/64).

Schreiber, Ulrich and Christof Klughammer. 2009. "New NADPH / 9-AA Module for the DUAL-PAM-100 : Description , Operation and Examples of Application ." 1–13.

Talts, Eero et al. 2007. "Dark Inactivation of Ferredoxin-NADP Reductase and Cyclic Electron Flow under Far-Red Light in Sunflower Leaves." *Photosynthesis Research* 94(1):109–20.

Trubitsin, Boris V., Mahir D. Mamedov, Alexey Yu Semenov, and Alexander N. Tikhonov. 2014. "Interaction of Ascorbate with Photosystem I." *Photosynthesis Research* 122(2):215–31.

Twachtmann, M. et al. 2012. "N-Terminal Structure of Maize Ferredoxin:NADP+ Reductase Determines Recruitment into Different Thylakoid Membrane Complexes." *The Plant Cell* 24(7):2979–91. Retrieved (http://www.plantcell.org/cgi/doi/10.1105/tpc.111.094532).

Supplementary Information

TROL sequence alignment: *P. patens* TROL (PpTROL) aligned with *A. thaliana* (AtTROL) isoform using CLUSTALW. Asterixis indicate identity, colons indicate residues similarity, periods indicate weak similarity. Highlighted on the AtTROL sequence are: the putative mature protein start (pink); the 2 transmembrane domains (yellow); the rhodanase domain (blue), with the specific aspartic acid residue proposed to eliminate TROL rhodanase activity (black); and the FNR binding domain (green).

```
PpTROL      MEVLSRVKFAAPTCSISEGSSSPTHAQVGQSSSSLFVAVSRRPH-------AFVGSLLAS
AtTROL      MEALKTATFS-PMSVLSEKRSEPRK---PFSLPNLFPPKSQRPISQESFLKRFNGGLALL
            **.*. ..*: * . :**  *.* :     *  .**   *:**         * *.*

PpTROL      TVSVIASVPAGLALNYDEFVKGGSNAAASATSAADSFSFDVPDIIDFDAATDFMSSNPVA
AtTROL      TSVLSSATAPAKSLTYEEALQQS---------MTTSSSFDSDGL--IEGISNFVTDNPLV
            *  : ::.  . :*.*:* :: .          : * ***  .:  ::. ::*::.**:.

PpTROL      ALAGLAAVAVPLIAFR-ASAAPQNFGSVSALEAFTKLSDPEQNAQLLDIRAPEDIKSEGT
AtTROL      IAGGVAALAVPFVLSQVLNKKPKSWGVESAKNAYTKLG-TDDNAQLLDIRATADFRQVGS
              .*:**:***::  :  .  *:.:*  ** :*:***.  ::*********  *::. *:

PpTROL      PNLKSLRKKAVQVPYTAAD-DSFLDKVFAKYRDAENTTVYILDQLDGNSLAVAKILANNG
AtTROL      PNIKGLGKKAVSTVYNGEDKPGFLKKLSLKFKDPENTTLYILDKFDGNSELVAELVALNG
            **:*.* ****.. *.. *  .**.*:  *::* ****:****::****  **:::* **

PpTROL      FEKAYSIKGGVEGPKGWLSSELPWQLPRKGFSLDLSGLKDLLSGNADPS--LVPTTLGAA
AtTROL      FKSAYAIKDGAEGPRGWLNSSLPWIEPKKTLSLDLSSLTDSISGVFGESSDGVSVALGVA
            *:.**:**.*.***:***.*.***  *:* :*****.*.* :**  . *   * .:**.*

PpTROL      AAAGIGVAVFTEAETVLQLLGSAAFVQIFFKKFMFAEDREKTVKEIQTFLDTKIAPKEFV
AtTROL      AAAGLSVFAFTEIETILQLLGSAALVQLAGKKLLFAEDRKQTLKQVDEFLNTKVAPKELV
            ****:.* .*** **:********:**:  **::*****::*:*::: **:**:****:*

PpTROL      DEIKEVGRVLLPKDGESSSAVTKGD------GASVNSSKVDSVAVE-----AAGEKVKAA
AtTROL      DELKEIGKALLPQSTSNKALPAPATVTAEAESATATTTTVDKPVPEPETVAATTTTVDKP
            **:**:*:.***:. ...:  : .       .*:..::.**. . *     *:  .*.

PpTROL      ------------------------------------------------------------
AtTROL      VPEPEPVPEPVPVPAIEAAVAAQVITEPTETEAKPKPHSRPLSPYASYPDLKPPSSPMPS

PpTROL      --
AtTROL      QP
```

APPENDIX 2

Systemic Calcium Wave Propagation in *Physcomitrella patens*

Authors name and affiliation

Mattia Storti[1], Alex Costa[2], Serena Golin[1], Michela Zottini[1], Tomas Morosinotto[1], Alessandro Alboresi[1]

1. Department of Biology, University of Padova, Via Ugo Bassi 58B, 35121 Padua, Italy

2. Department of Bioscience, University of Milano, Via Giovanni Celoria 26, 20133 Milan, Italy

THIS APPENDIX WAS PUBLISHED IN PLANT AND "*CELL PHYSIOLOGY*" (2018)

CONTRIBUTION

In this work MS performed most of the experiments on *P. patens*, including isolation of mutant lines, imaging experiments on protonema and gametophores of mutants line and analyzed the data.

ABSTRACT

The adaptation to dehydration and rehydration cycles represents a key step in the evolution of photosynthetic organisms and requires the development of mechanisms by which to sense external stimuli and translate them into signaling components. In this study, we used genetically encoded fluorescent sensors to detect specific transient increases in the Ca^{2+} concentration in the moss *Physcomitrella patens* upon dehydration and rehydration treatment. Observation of the entire plant in a single time-series acquisition revealed that various cell types exhibited different sensitivities to osmotic stress and that Ca^{2+} waves originated from the basal part of the gametophore and were directionally propagated towards the top of the plant. Under similar conditions, the vascular plant *Arabidopsis thaliana* exhibited Ca^{2+} waves that propagated at a higher speed than those of *P. patens*. Our results suggest that systemic Ca^{2+} propagation occurs in plants even in the absence of vascular tissue, even though the rates can be different.

INTRODUCTION

Land plants form a monophyletic clade that evolved from freshwater charophyte macroalgae approximately 450 million years ago (Bowman 2013, de Vries et al. 2016). Land colonization by plants represents one of the most significant evolutionary events in the history of life on planet Earth and had a major impact on the Earth's biosphere. During adaptation to their new environment, plants acquired the ability to survive cycles of dehydration and rehydration (Oliver et al. 2005), as well as exposure to stronger mechanical forces and more oxidative conditions (i.e. high light intensities, light enriched in UV wavelengths and high oxygen availability) (Kenrick and Crane 1997, Dahl et al. 2010). Because they diverged from their angiosperm ancestors soon after land colonization, bryophytes are a useful model system for the identification of early plant adaptations to the terrestrial environment. In particular, the moss *Physcomitrella patens* is used as a model plant for the study of evolution and development due to its evolutionary position and the availability of several molecular tools (Cove 2005, Rensing et al. 2008).

The perception of external stimuli is pivotal for plant fitness, and these pathways probably involve calcium (Ca^{2+}), a common second messenger that triggers cell responses in prokaryotes and eukaryotes during development, stress and long-distance signal transduction. Different external

stimuli cause Ca^{2+} transient increases, waves and oscillations that are interpreted by cells as signals themselves (Whalley and Knight 2013, Choi et al. 2017).

Ca^{2+} measurement in *P. patens* plants has been successfully performed using ratiometric dyes (Tucker et al. 2005, Qudeimat et al. 2008), the Ca^{2+}-sensitive genetically encoded sensor aequorin from *Aequorea victoria* (Haley et al. 1995, Russell et al. 1996, Saidi et al. 2009) and GCaMP3 (Kleist et al. 2017). This allowed the assessment of the role of Ca^{2+} in the regulation of physiological and developmental processes at the level of protonemata cells in *P. patens*, including the UV-A response (Tucker et al. 2005) and thermal sensing mediated by cyclic nucleotide-gated calcium channels (CNGCs) (Finka et al. 2012). Moreover, two glutamate receptor-like ion channels (GLRs) were shown to be involved in the regulation of the cytoplasmic Ca^{2+} concentration in *P. patens* sperm cells. Changes in intracellular Ca^{2+} levels modulate sperm orientation towards the archegonium, thereby affecting the overall fertility of the plant (Ortiz-Ramírez et al. 2017).

In this work, Cameleon YC3.60 (Nagai et al. 2004), a Förster resonance energy transfer (FRET)-based genetically encoded fluorescent sensor, was exploited to monitor the Ca^{2+} concentration *in vivo* with high spatiotemporal resolution inside different cell types and compartments of *P. patens* plants during osmotic stress.

RESULTS AND DISCUSSION

The Cameleon YC3.60 sensor was targeted to the nucleoplasm, mitochondria and cytoplasm using specific N-terminal transit peptides or proteins previously utilized in *Arabidopsis thaliana* (Krebs et al. 2012, Loro et al. 2012, Costa et al. 2017). The presence of a clear homogeneous fluorescence signal in the expected compartment was verified by confocal laser scanning microscopy (Fig. 1a; Supplementary Fig. S1). The stability of fluorescent protein expression and the absence of major interference with cell physiology were verified by assessing plant growth, development and photosynthetic efficiency. Transgenic lines affected by the expression of the sensor were not used in further analyses (refer to Supplementary Fig. S1).

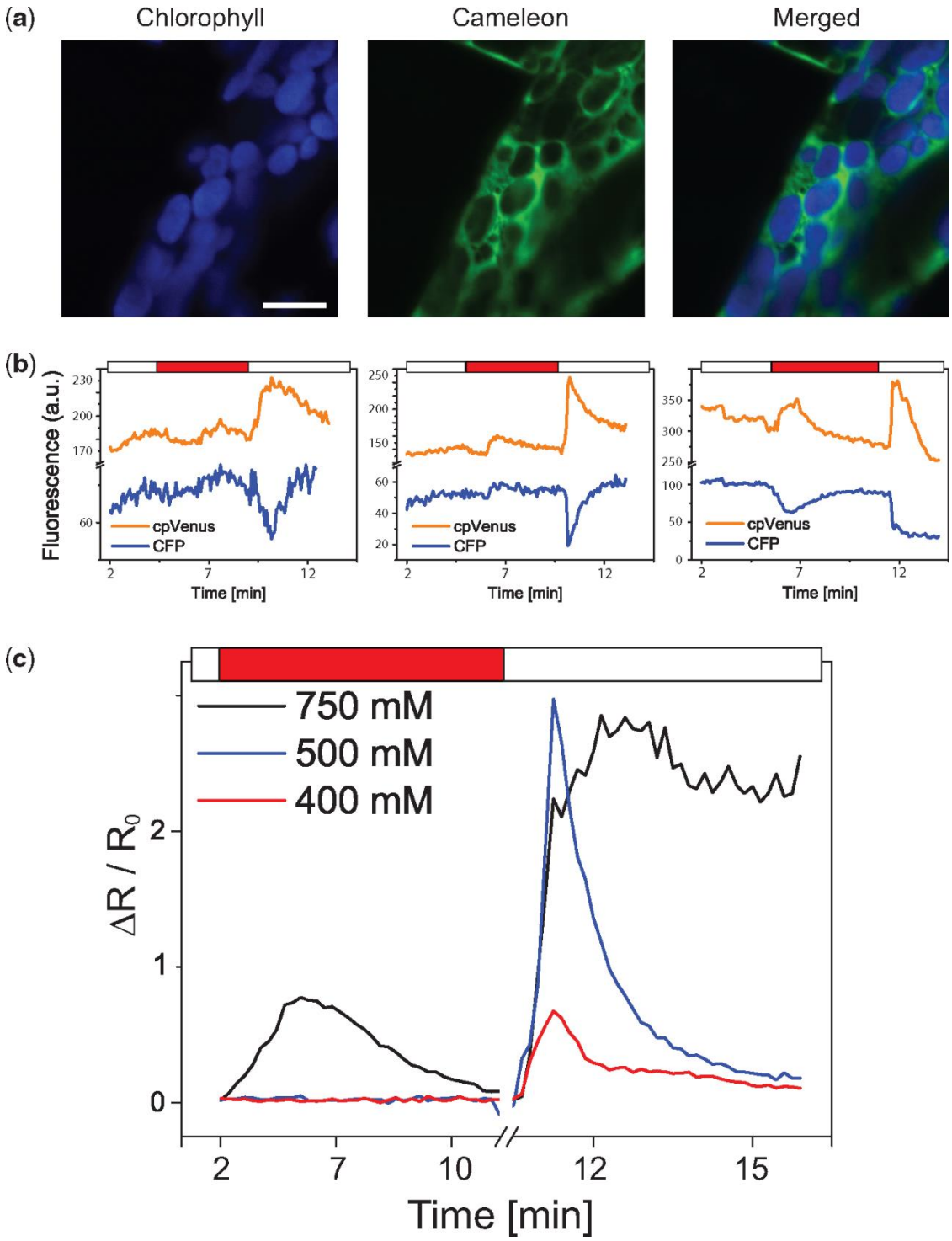

Figure 1: Expression of Yellow Cameleon 3.60 (YC3.60) and analysis of Ca^{2+} dynamics in *Physcomitrella patens* protonema cells. (a) The YC3.60 sensor was expressed under control of the constitutive *7113*promoter and was targeted to the cytoplasm. Chl and YC3.60 signals were independently acquired by confocal laser scanning microscopy and were then merged. Scale bar = 10 µm. (b, c) Changes in Ca^{2+}concentration in protonema cells in response to osmotic stress. CFP and cpVenus emissions were detected simultaneously after CFP excitation, and the cpVenus/CFP fluorescent ratio over that time is expressed as $\Delta R/R_0$. Osmotic stress was applied by continuous perfusion with solutions containing 400, 500 or 750 mM mannitol, which are represented by red, blue and black lines, respectively. The white and red bars on top of the panel indicate the absence and the presence, respectively, of mannitol in the perfusion solution. Data are shown as the mean of at least four independent plants.

Drought and salt stresses are major abiotic constraints affecting plant growth and productivity. The acquisition of tolerance to dynamic water availability is considered a keystone in land colonization (Rensing et al. 2008). Ca^{2+} concentration in response to salt and osmotic stress was assessed *in vivo* by imaging analyses of YC3.60 transgenic lines. Protonema cells were treated with various concentrations of NaCl, sorbitol and mannitol, and then the osmotic stress was released. Cyan fluorescent protein (CFP) and circularly permutated Venus (cpVenus) fluorescence signals were simultaneously acquired for the duration of the treatment to detect Ca^{2+}-induced FRET transient efficiency change (Fig. 1b; Supplementary Fig. S2). Both the addition (hyperosmotic treatment) and removal of the osmoticum (hypo-osmotic treatment; mannitol was used) caused a detectable increase in Ca^{2+} concentration in various cell compartments, as shown by the clear change in $\Delta R/R_0$ (Fig. 1c; Supplementary Fig. S1). For all compartments, the transient increase in Ca^{2+} was more intense during the hypo-osmotic response than during the hyperosmotic response (Fig. 1c; Supplementary Fig. S1; Supplementary Table S1). *Vicia faba* and *A. thaliana* guard cells, as well as *A. thaliana* leaves and roots, exhibited similar trends (Hayashi et al. 2006, Zhang et al. 2007, Loro et al. 2012), suggesting that the strong hypo-osmotic response is highly conserved. The detected Ca^{2+} transients exhibited different intensities and kinetics depending on the mannitol concentration used (400, 500 or 750 mM) and on the cellular compartments examined, revealing that Ca^{2+} dynamics are differentiated within the cell and also transduce information regarding stress severity (Fig. 1c; Supplementary Figs. S1, S3; Supplementary Table S1). Control experiments run in the absence of mannitol showed that the perfusion solution itself had no effect on Ca^{2+} dynamics (Supplementary Fig. S4).

In vivo imaging analyses were implemented using lower magnification to observe more extended portions of the sample and different cell types simultaneously. It was possible to observe entire young *P. patens* gametophores, a significant advantage over *A. thaliana*, *Oryza sativa* and other plants of greater size in which the Cameleon sensor has already been expressed. Lines expressing YC3.60 in the cytoplasm were used preferentially because they showed more homogeneous and stable expression of the sensor in different cell types, especially old gametophores (Supplementary Fig. S5).

Similar to previous observations in protonema, the exposure of entire young gametophores to 500 mM mannitol generated a concomitant increase in cpVenus fluorescence emission and a decrease in CFP fluorescence emission (Fig. 2b; Supplementary Videos S2, S3). The most intense Ca^{2+} transient was recorded again after the relief of the osmotic stress (Fig. 2b). The Ca^{2+} response, however, was not homogeneous throughout the plant but was more intense in the basal part of the gametophore than

in the phyllids, demonstrating that different cell types have different sensitivities to the same stimulus (Fig. 2c, d; Supplementary Video S1). An independent quantitative analysis of the gametophore base and phyllids confirmed that Ca^{2+} responses are more intense in the former but are present in the latter, exhibiting a delay of approximately 1 min before reaching maximal signal intensity (Fig. 2d). Of note, our calibration of Ca^{2+} estimates that the maximum concentration of cytosolic Ca^{2+} at the base of the gametophore (634 ± 28 nM) was almost four times higher than in phyllids (152 ± 32) nM. Also in the case of gametophores, control experiments run in the absence of mannitol showed that the perfusion solution itself had no effect on Ca^{2+} response (Supplementary Fig. S6).

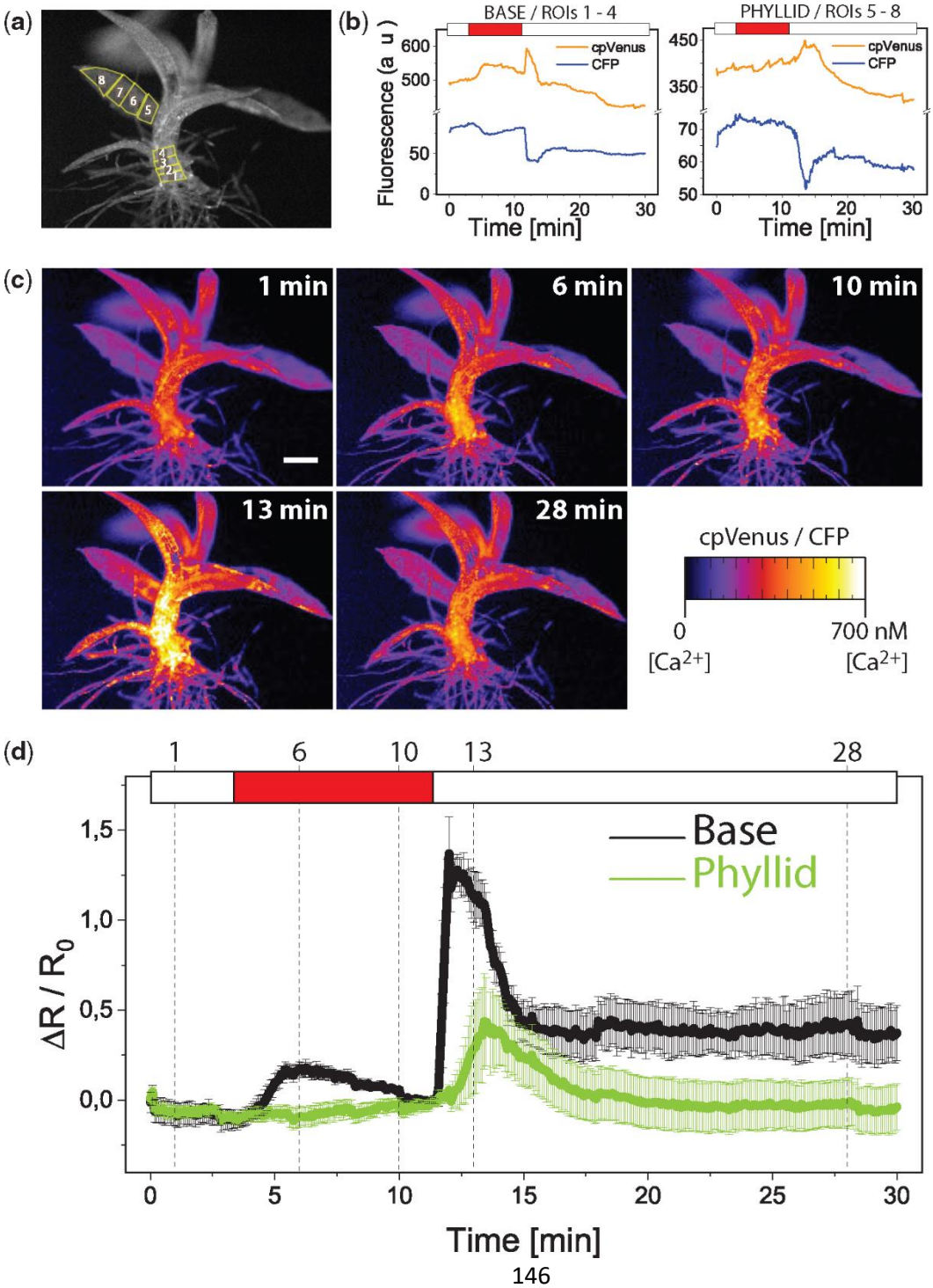

Figure 2: *In vivo* analysis of Ca^{2+} dynamics in response to osmotic stress throughout *P. patens* gametophores expressing CYT–YC3.60. (a) Representative snapshot of one gametophore; yellow boxes correspond to the regions of interests (ROIs 1–8) outlined to follow CFP and cpVenus fluorescence emission with time. (b) The signal is the result of the average signal emitted in ROIs 1–4 (left graph, base) and ROIs 5–8 (right graph, phyllid). (c) Snapshots of fluorescence ratio imaging acquisition during continuous perfusion with hyperosmotic (6 and 10 min) and hypo-osmotic (1, 13 and 28 min) solutions. False colors reflect the ratio of the cpVenus fluorescence emission to the CFP fluorescence emission at the specified time point. Scale bar = 500 μm. (d) Quantitative analysis of cpVenus/CFP fluorescent ratio measurements calculated as $\Delta R/R_0$ for the gametophore base and phyllids shown in (a–c). White and red bars on top of each graph indicate the presence and the absence of mannitol, respectively. The full acquisition cpVenus, CFP and cpVenus/CFP can be visualized as supplementary material(Supplementary Videos S1–S3).

The delay measured in phyllids was due to the directional propagation of Ca^{2+}transients from the base towards the tip of the plant (Fig. 3a–e, Supplementary Videos S4, S5). The directionality of propagation did not depend on the orientation of the plant with respect to the point of stress application. In Supplementary Video S4, the lower portion of the gametophore is closer to the entry point of the buffer (Fig. 3a), while in Supplementary Video S5 the orientation is reversed (Fig. 3b). In both cases, however, Ca^{2+} waves emanated from the lower part of the gametophore and propagated towards the phyllid. The dynamics of the osmo-induced Ca^{2+}increase were also analyzed independently at the base of the gametophore (Supplementary Fig. S7) and in phyllids (Fig. 3c–e). We also examined the same Ca^{2+}waves at the highest magnification available and found that only a few cells were in focus, thus precluding an analysis of long-distance transmission (Supplementary Fig. S8). In order to understand if a local mannitol stimulus could elicit Ca^{2+}propagation throughout gametophores, a local stress system was set up, in which gametophores were covered by a block of agarized perfusion solution and then subjected to the perfusion experiment (Supplementary Fig. S9). Even if the upper part of the plant was in less direct contact with mannitol solution, we still observed a retarded increase in cytoplasmic Ca^{2+} concentration in phyllids as compared with the base of the gametophore, suggesting the existence of a proper long-distance Ca^{2+}wave propagation in *P. patens*.

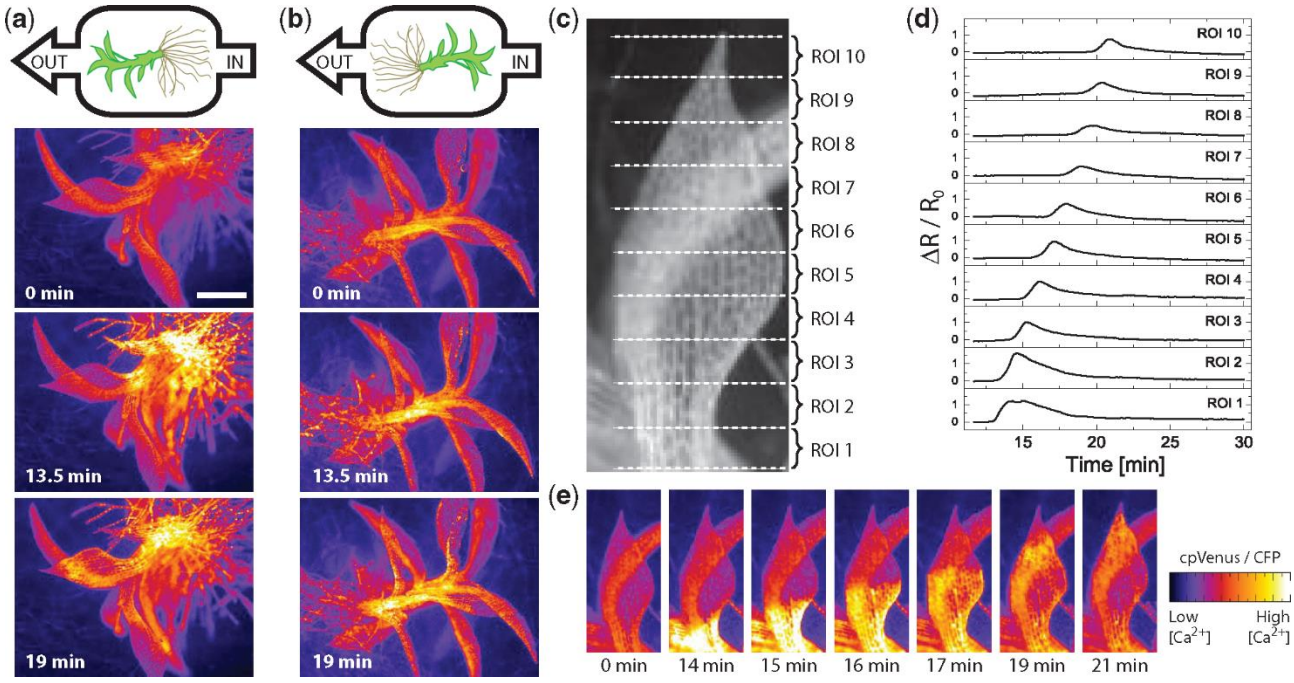

Figure 3: *In vivo* analysis of Ca^{2+} dynamics in response to osmotic stress in young *Physcomitrella patens* plantlets. (a, b) The response of two representative gametophores was in the same direction as or the direction opposing osmotic flow. From top to bottom, a sketch representing the direction of flow in the plant, and three snapshots of fluorescence ratio imaging acquisition corresponding to 0, 13.5 and 19 min. (c) Detail of one phyllid shown in (a). White dashed lines correspond to the regions of interest (ROIs 1–10) designated to follow CFP and cpVenus fluorescence emission during the indicated time. (d) Ca^{2+} concentration variation ($\Delta R/R_0$) during the hypo-osmotic phase. ROIs from 1 to 10 correspond to those drawn in (c). (e) Ratiometric false-color images from representative time series of a basal portion of a *P. patens* gametophore. The false colors represent the intensity of the cpVenus/CFP fluorescent ratio. The time (min) below each snapshot corresponds to the signal reported in (d). The full acquisitions are included as supplementary material (Supplementary Videos S4, S5). Scale bar = 250 µm. Ratio images are representative of $n \geq 3$.

Ca^{2+} waves are known to be involved in systemic acquired acclimation response to abiotic stress in *A. thaliana* (Choi et al. 2014, Choi et al. 2017). Four-day-old *A. thaliana* plantlets expressing CYT–YC3.60 (Loro et al. 2012) (Supplementary Fig. S10; Supplementary Video S7) were treated with the same protocol used for *P. patens* for a direct comparison of their local and systemic Ca^{2+} responses. In this case, a Ca^{2+} wave was recorded and could be observed following the time needed to reach $\Delta R_{max}/R_0$ in four independent regions of interest (ROIs) from the root tip to the shoot (Supplementary Fig. S10).

To better compare the Ca^{2+} propagation rates of the model plants *A. thaliana* and *P. patens*, ROIs of 400 µm were drawn and kymographs of the corresponding FRET signals were extrapolated (Fig. 4). In *A. thaliana*, Ca^{2+} waves moved at approximately 58.5 ± 18.9 µm s^{-1}. In *P. patens*, both at the base of the gametophore and in phyllids, the speed of propagation was instead 4.5 ± 3.8 µm s^{-1}, a value compatible with what has been measured using Fura-2-dextran ratio images in protonema apical cells in response to UV-A light (3.4–8.4 µm s^{-1}) (Tucker et al. 2005). It is interesting to note that with our

set-up, we managed to measure cell–cell communication in entire gametophores rather than simply the communication between two adjacent cells. The fast propagation measured in *A. thaliana* (Fig. 4; Supplementary Fig. S10) is in agreement with what has been reported previously for different tissues and stressors. Ca^{2+} waves traveled at 60–290 μm s^{-1} along the leaf veins of *A. thaliana*after exposure of the roots of plants expressing a bioluminescence resonance energy transfer (BRET)-based green fluorescent protein (GFP)–aequorin reporter to salt stress (Xiong et al. 2014). The response was fastest (400 μm s^{-1}) when measured through root tissues at lower salt concentrations (Choi et al. 2014). Thus, the main component of Ca^{2+} wave propagation in *P. patens* is slower than that measured in *A. thaliana* roots and leaves. In order to understand whether extracellular Ca^{2+} was involved in Ca^{2+} wave propagation, we performed experiments by perfusing plants with a low Ca^{2+} concentration and lanthanum (III) chloride, a blocker of non-selective cation channels and stretch-activated Ca^{2+}-permeable channels (Supplementary Fig. S11). The application of lanthanum has effectively reduced the amplitude of the Ca^{2+} increase in response to osmotic stress relaxation. On the other hand, we could still detect the propagation of a long-distance Ca^{2+} wave (Supplementary Fig. S11), suggesting that intracellular Ca^{2+} storage is involved in this process or that there are Ca^{2+} channels/transporters at the level of the plasma membrane that are insensitive to lanthanum. Moreover the rate of propagation is similar to calcium-induced calcium release measured in single cells (Jaffe 2010). Further work may elucidate whether Ca^{2+} waves serve a signaling function in the moss system and to uncover the molecular system responsible for the propagation of Ca^{2+} waves. Different models have been proposed for the interaction of propagating Ca^{2+} signals with electric signals and reactive oxygen species (ROS) waves through symplastic or apoplastic pathways (Choi et al. 2014, Choi et al. 2017). Vasculature seems to be fundamental for the propagation of Ca^{2+} waves when the signal is triggered by wounding or herbivore attack (Mousavi et al. 2013, Kiep et al. 2015). Interestingly, the aphid *Myzus persicae* elicits elevated cytosolic Ca^{2+} concentrations around piercing sites in the epidermal and mesophyll cells of *A. thaliana* (Vincent et al. 2017). This phloem-independent radial propagation proceeds at a speed of approximately 6 μm s^{-1} over an area of approximately 110 μm^2 (Vincent et al. 2017). In the case of roots, transmission is likely to be supported by the activity of Ca^{2+} pumps and channels and their regulators within cortical and endodermal cells (Choi et al. 2016). Differences in the speed of Ca^{2+} propagation could be due to the obvious lack in *P. patens* of a proper vascular tissue. However, it is possible that different systems control Ca^{2+} homeostasis in the two model species. This second hypothesis is supported by genomic surveys highlighting the existence of transport systems differing in composition and complexity compared with other members of the Viridiplantae lineage (Edel and Kudla 2015). For example, GLRs have been identified as potential mediators of systemic electric signals in *A. thaliana* (Mousavi

et al. 2013, Salvador-Recatalà 2016). *P. patens* encodes a small family of GLRs consisting of only two members (Edel and Kudla 2015, De Bortoli et al. 2016) that are thought to be involved in plant reproduction rather than gametophytic cell–cell signal transduction (Ortiz-Ramírez et al. 2017).

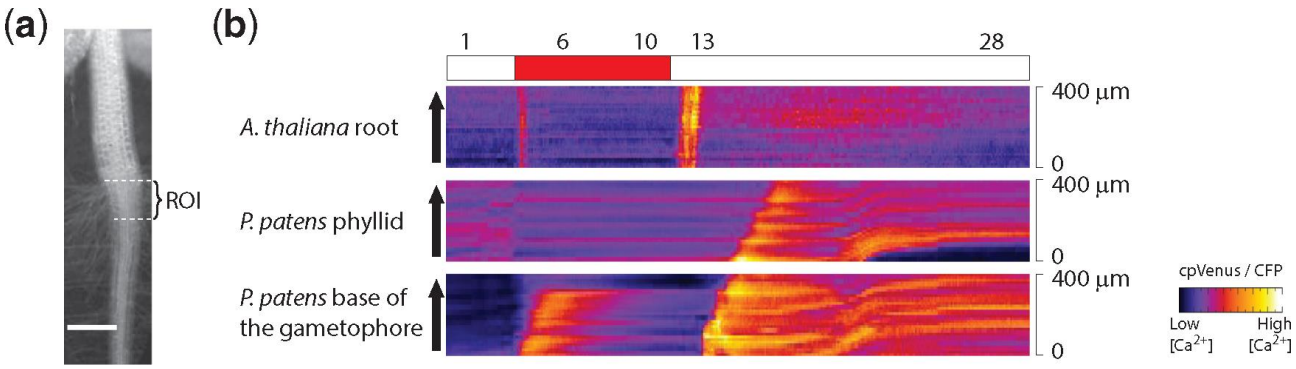

Figure 4: Kymographs illustrating Ca^{2+} wave dynamics in *Arabidopsis thaliana* and *Physcomitrella patens* lines expressing the cytoplasmic sensor (CYT–YC3.60). Ratiometric data (cpVenus/CFP fluorescent ratio) were extracted from a region of interest (ROI) of 400 µm parallel to the plant axis. For *A. thaliana*, the last segment of root before the hypocotyl was considered (Supplementary Fig. S10), while for *P. patens*, gametophores and phyllids were analyzed independently. The arrows indicate the tipward direction followed to draw the ROIs. The white and red bars represent the absence and the presence, respectively, of mannitol in the perfusion solution.

The present work reveals the existence of long-distance transmission of Ca^{2+} waves in response to an osmoticum in the body of *P. patens*. The ability to propagate systemic Ca^{2+} waves, an important component for osmotic stress perception and osmotolerance in general, was present during land colonization.

MATERIALS AND METHODS

Plant material and growth conditions

Protonemal tissue of *P. patens* (the Gransden wild-type strain and YC3.60-expressing lines) were grown on minimum $PpNO_3$ medium under controlled conditions: 24°C, a 16 h light/8 h dark photoperiod and a light intensity of 50 µmol photons m^{-2} s^{-1}. Ten-day-old plants were used for protonemal tissue imaging, and gametophores were observed between 1 and 2 months of growth. *Arabidopsis thaliana* plants expressing cytoplasmic Cameleon (CYT–YC3.60) were used in this

study (Krebs et al. 2012). Seeds were surface-sterilized and sown on half-strength Murashige and Skoog medium (MS including vitamins; Duchefa) supplemented with 0.1% (w/v) sucrose and 0.05% (w/v) MES, adjusted to pH 5.8 with KOH, and solidified with 0.8% (w/v) plant agar (Duchefa). After stratification at 4°C in the dark for 2–3 d, the seeds were transferred to a growth chamber with a 16/8 h light cycle (70 µmol photons m^{-2} s^{-1}) at 24°C.

Constructs

Standard plasmid construction methods were used to obtain pMAK1-7113::YC3.60 plasmids. All PCRs were carried out using high-fidelity KAPA HiFi PCR Kits (Kapa Biosystems), according to the manufacturer's instructions. PCR products were cloned into a pJET1.2/blunt vector (Thermo Fisher Scientific) and were sequenced after transfer to the expression vector pMAK1 (http://www.nibb.ac.jp/evodevo/PHYSCOmanual/17Overdriveplasmid/pMAK1.htm) under control of the constitutive promoter 7113 (Mitsuhara et al. 1996, Gerotto et al. 2012). The primers used to amplify the sequences and add signal sequences for mitochondrial or nucleoplasmic subcellular localization are as follows: MIT/NUC-for (5'-CTCGAGAGAGGACAGCCCAAGCTTATG-3') and MIT/NUC-rev (5'-GGGCCCTTTCAGCGTACCGAATTCTTA-3'). The PCR product was cloned with *Xho*I and *Apa*I. The primers used to amplify the sequences with cytoplasmic subcellular localization were: CYT-for (5'-GGGCCCATGCTGCAGAACGAGCTTGCTCTT-3') and CYT-rev (5'-GAATTCGTGCCAAGCTTCGATTGATG-3'). The PCR product was cloned with *Apa*I and *Eco*RI. Plant expression vectors were used as templates to perform the PCRs (Krebs et al. 2012, Loro et al. 2012, Costa et al. 2017). The Tnos terminator sequence in the pMAK1 plasmid was used to control the expression of the mitochondrion- and nucleoplasm-localized versions of YC3.60. The cytoplasm-localized version of YC3.60 was amplified together with the rbcs terminator, which was substituted for the Tnos terminator sequence in the pMAK1 plasmid.

YC3.60 is targeted to the nucleoplasm by its fusion with the nuclear-localized *Xenopus laevis*nucleophosmin, to the mitochondrial matrix by four repeats of the mitochondrial targeting sequence from subunit VIII of human Cyt *c* oxidase (MIT) and to the cytoplasm by a nuclear export signal (CYT) of rabbit heat-stable protein kinase inhibitor α.

Chl fluorescence measurements and growth tests

To test plant performance, 10-day-old plants grown on PpNO3 were transferred to new plates as multiple independent spots of 2 mm diameter. In vivo Chl fluorescence was measured using Fluorcam 800MF (Photon Sytems Instruments) to evaluate the F_v/F_m parameter as $(F_m - F_0)/F_m$. Pictures of the same plates were taken regularly, and plant growth was evaluated by measuring the size of different plant spots using ImageJ software (http://rsb.info.nih.gov/ij/) after background exclusion was performed with the 'TRESHOLD COLOUR' PLUGIN (http://www.mecourse.com/landinig/software/software.html).

Confocal microscopy

Laser scanning confocal microscopy analyses were performed using a Leica SP5 imaging system (Leica Microsytems). Images were acquired using a ×40 objective (HCX PL APO CS 40/1.25–0.75 oil) with different degrees of digital zoom. cpVenus was excited by the 514 nm line of the argon laser and the emission was collected between 525 and 540 nm. Chl fluorescence emission was collected simultaneously between 660 and 750 nm. Images were merged using ImageJ software (http://rsb.info.nih.gov/ij/).

FRET-based calcium imaging

For FRET measurements, plant material was removed from the plate and placed in an open-top chamber overlaid by cotton soaked in imaging solution (5 mM KCl, 10 mM MES and 10 mM $CaCl_2$; adjusted to pH 5.8 with Trizma® base). Osmotic stress was achieved by adding imaging solutions containing different concentrations of mannitol or NaCl, using a continuous perfusion system. After 8 min, the hyperosmotic solution was replaced by the initial imaging solution to restore the baseline condition. We ensured that the increase in Ca^{2+} concentration was the result of osmotic stress and not mechanical stimulation by performing experiments with and without osmoticum (Supplementary Figs. S4, S6). Images were collected every 5 s using an inverted fluorescence microscope (Nikon Ti-E or Leica DMI6000) as described by Loro et al. (2012, 2016). Excitation was provided using a fluorescent lamp equipped with a 436/20 nm filter, and emission signals were filtered at 483/32 nm for CFP and at 542/27 nm for cpVenus with a dichroic mirror (510 nm). Experiments examining

Ca^{2+} propagation throughout entire plants were carried out with a Nikon Ti-E microscope using a ×4 CFI 4 0.13 NA (numerical aperture), whereas for protonema cells, a ×20 CFI Plan APO VC, 0.75 NA dry objective was used (Loro et al. 2012, Loro et al. 2016).

False-color images were obtained using the ImageJ 'RATIO PLUS PLUGIN' (Palmer and Tsien 2006). Fluorescence intensity was determined over ROIs corresponding to a single cell or organelle (in the case of nuclei) or to different plant tissues. The mean cpVenus and CFP signals of each ROI were used for ratio (R) calculation. Background subtraction was performed independently for both channels before calculating the ratio. To calculate the $\Delta R/R_0$, we used the following formula $(R - R_0)/R_0)$. The $\Delta R/R_0$ was plotted vs. time.

In situ calibration was performed by raising Ca^{2+} to saturating levels for YC3.60. This was attempted by permeabilizing plants for 5 min with 200 µM digitonin dissolved in a solution that we called Intracellular Like Medium (ILM: 100 mM K-gluconate, 1 mM $MgCl_2$, 10 mM HEPES, pH 7.5 adjusted with Trizma®) in the presence of 5 mM EGTA to chelate Ca^{2+}. Plants were then transferred to the imaging chamber where they were continuously perfused with ILM solution supplemented with 5 mM EGTA and imaged (acquiring CFP and cpVenus wavelengths) every 5 s for 6 min to measure the R_{min}. To measure the R_{max}, the plants were then perfused for 5 min with a modified ILM solution in which 5 mM EGTA was replaced with 10 mM $CaCl_2$ and imaged. Plants were then perfused again with the ILM supplemented with 5 mM EGTA and imaged for 6–7 min. To make the R_{min} and R_{max} calculations, we averaged the traces of four independent experiments performed with two independent transgenic lines used herein. R_{max} was 15.93 ± 0.09, R_{min} was 5.11 ± 0.02 and the corresponding dynamic range was 3 and 11. In order to calculate the Ca^{2+} concentration, we considered the in vitro K_d and the Hill coefficient (n) of the YC3.60 reported in Nagai et al. 2004 corresponding to 250 nM and 1.7, respectively. We then used the equation previously published for the calculation of Ca^{2+} concentration in Palmer and Tsien (2006): $[Ca^{2+}] = \{K_d\text{^}n\times[(R - R_{min})/(R_{max} - R)]\}\text{^}1/n$.

ACKNOWLEDGMENTS

This study was supported by the European Research Council [ERC starting grant BIOLEAP no. 309485 to T.M. and A.A.]; the Università degli Studi di Milano [PIANO DI SVILUPPO DI ATENEO 2016 to A.C.]; the Università degli Studi di Padova, Dipartimento di Biologia [BIRD173749/17 to A.A.].

AUTHOR CONTRIBUTIONS

T.M., A.A. and A.C. planned and designed the research. A.A., A.C. and M.S. performed most of the experiments and analyzed the data. M.S., S.G. and M.Z. performed imaging analyses of protonemata cells. T.M. and A.A wrote the manuscript, which all authors revised and approved.

REFERENCES

Bowman J.L. (2013) Walkabout on the long branches of plant evolution. *Curr. Opin. Plant Biol.* 16: 70–77.

Choi W.-G., Hilleary R., Swanson S.J., Kim S.-H., Gilroy S. (2016) Rapid, long-distance electrical and calcium signaling in plants. *Annu. Rev. Plant Biol.* 67: 287–307.

Choi W.-G., Miller G., Wallace I., Harper J., Mittler R., Gilroy S. (2017) Orchestrating rapid long-distance signaling in plants with Ca^{2+}, ROS and electrical signals. *Plant J.* 90: 698–707.

Choi W.-G., Toyota M., Kim S.-H., Hilleary R., Gilroy S. (2014) Salt stress-induced Ca^{2+} waves are associated with rapid, long-distance root-to-shoot signaling in plants. *Proc. Natl. Acad. Sci. USA* 111: 6497–6502.

Costa A., Luoni L., Marrano C.A., Hashimoto K., Köster P., Giacometti S., et al. (2017) Ca^{2+}-dependent phosphoregulation of the plasma membrane Ca^{2+}-ATPase ACA8 modulates stimulus-induced calcium signatures. *J. Exp. Bot* . 29: 1007–1018.

Cove D. (2005) The moss *Physcomitrella patens*. *Annu. Rev. Genet.* 39: 339–358.

Dahl T.W., Hammarlund E.U., Anbar A.D., Bond D.P.G., Gill B.C., Gordon G.W., et al. (2010) Devonian rise in atmospheric oxygen correlated to the radiations of terrestrial plants and large predatory fish. *Proc. Natl. Acad. Sci. USA* 107: 17911–17915.

De Bortoli S., Teardo E., Szabò I., Morosinotto T., Alboresi A. (2016) Evolutionary insight into the ionotropic glutamate receptor superfamily of photosynthetic organisms. *Biophys. Chem*. 218: 14–26.

de Vries J., Stanton A., Archibald J.M., Gould S.B. (2016) Streptophyte terrestrialization in light of plastid evolution. *Trends Plant Sci* . 21: 467–476.

Edel K.H., Kudla J. (2015) Increasing complexity and versatility: how the calcium signaling toolkit was shaped during plant land colonization. *Cell Calcium* 57: 231–246.

Finka A., Cuendet A.F.H., Maathuis F.J.M., Saidi Y., Goloubinoff P. (2012) Plasma membrane cyclic nucleotide gated calcium channels control land plant thermal sensing and acquired thermotolerance. *Plant Cell* 24: 3333–3348.

Gerotto C., Alboresi A., Giacometti G.M., Bassi R., Morosinotto T. (2012) Coexistence of plant and algal energy dissipation mechanisms in the moss *Physcomitrella patens*. *New Phytol.* 196: 763–773.

Haley A., Russell A.J., Wood N., Allan A.C., Knight M., Campbell A.K., et al. (1995) Effects of mechanical signaling on plant cell cytosolic calcium. *Proc. Natl. Acad. Sci. USA* 92: 4124–4128.

Hayashi T., Harada A., Sakai T., Takagi S. (2006) Ca^{2+} transient induced by extracellular changes in osmotic pressure in Arabidopsis leaves: differential involvement of cell wall–plasma membrane adhesion. *Plant Cell Environ.* 29: 661–672.

Jaffe L. (2010) Fast calcium waves. *Cell Calcium* 48: 102–113.

Kenrick P., Crane P.R. (1997) The origin and early evolution of plants on land. *Nature* 389: 33–39.

Kiep V., Vadassery J., Lattke J., Maaß J.-P., Boland W., Peiter E., et al. (2015) Systemic cytosolic Ca^{2+} elevation is activated upon wounding and herbivory in Arabidopsis. *New Phytol.* 207: 996–1004.

Kleist T.J., Cartwright H.N., Perera A.M., Christianson M.L., Lemaux P.G., Luan S. (2017) Genetic ally encoded calcium indicators for fluorescence imaging in the moss *Physcomitrella*: GCaMP3 provides a bright new look. *Plant Biotechnol. J.* 15: 1235–1237.

Krebs M., Held K., Binder A., Hashimoto K., Den Herder G., Parniske M., et al. (2012) FRET-based genetically encoded sensors allow high-resolution live cell imaging of Ca^{2+} dynamics. *Plant J.* 69: 181–192.

Loro G., Drago I., Pozzan T., Schiavo F.L., Zottini M., Costa A. (2012) Targeting of Cameleons to various subcellular compartments reveals a strict cytoplasmic/mitochondrial Ca^{2+} handling relationship in plant cells. *Plant J* . 71: 1–13.

Loro G., Wagner S., Doccula F.G., Behera S., Weinl S., Kudla J., et al. (2016) Chloroplast-specific in vivo Ca^{2+} imaging using Yellow Cameleon fluorescent protein sensors reveals organelle-autonomous Ca^{2+} signatures in the stroma. *Plant Physiol*. 171: 2317–2330.

Mitsuhara I., Ugaki M., Hirochika H., Ohshima M., Murakami T., Gotoh Y., et al. (1996) Efficient promoter cassettes for enhanced expression of foreign genes in dicotyledonous and monocotyledonous plants. *Plant Cell Physiol*. 37: 49–59.

Mousavi S.A.R., Chauvin A., Pascaud F., Kellenberger S., Farmer E.E. (2013) GLUTAMATE RECEPTOR-LIKE genes mediate leaf-to-leaf wound signalling. *Nature* 500: 422–426.

Nagai T., Yamada S., Tominaga T., Ichikawa M., Miyawaki A. (2004) Expanded dynamic range of fluorescent indicators for $Ca^{2+}$by circularly permuted yellow fluorescent proteins. *Proc. Natl. Acad. Sci. USA* 101: 10554–10559.

Oliver M.J., Velten J., Mishler B.D. (2005) Desiccation tolerance in bryophytes: a reflection of the primitive strategy for plant survival in dehydrating habitats? *Integr. Comp. Biol* . 45: 788–799.

Ortiz-Ramírez C., Michard E., Simon A.A., Damineli D.S.C., Hernández-Coronado M., Becker J.D., et al. (2017) GLUTAMATE RECEPTOR-LIKE channels are essential for chemotaxis and reproduction in mosses. *Nature* 549: 91–95.

Palmer A.E., Tsien R.Y. (2006) Measuring calcium signaling using genetically targetable fluorescent indicators. *Nat. Protoc.* 1: 1057–1065.

Qudeimat E., Faltusz A.M.C., Wheeler G., Lang D., Holtorf H., Brownlee C., et al. (2008) A PIIB-type Ca^{2+}-ATPase is essential for stress adaptation in *Physcomitrella patens*. *Proc. Natl. Acad. Sci. USA* 105: 19555–19560.

Rensing S.A., Lang D., Zimmer A.D., Terry A., Salamov A., Shapiro H., et al. (2008) The Physcomitrella genome reveals evolutionary insights into the conquest of land by plants. *Science* 319: 64–69.

Russell A.J., Knight M.R., Cove D.J., Knight C.D., Trewavas A.J., Wang T.L. (1996) The moss, *Physcomitrella patens*, transformed with apoaequorin cDNA responds to cold shock, mechanical perturbation and pH with transient increases in cytoplasmic calcium. *Transgenic Res* . 5: 167–170.

Saidi Y., Finka A., Muriset M., Bromberg Z., Weiss Y.G., Maathuis F.J.M., et al. (2009) The heat shock response in moss plants is regulated by specific calcium-permeable channels in the plasma membrane. *Plant Cell* 21: 2829–2843.

Salvador-Recatalà V. (2016) New roles for the *GLUTAMATE RECEPTOR-LIKE 3.3*, *3.5*, and *3.6* genes as on/off switches of wound-induced systemic electrical signals. *Plant Signal Behav*. 11: e1161879.

Tucker E.B., Lee M., Alli S., Sookhdeo V., Wada M., Imaizumi T., et al. (2005) UV-A induces two calcium waves in *Physcomitrella patens*. *Plant Cell Physiol.* 46: 1226–1236.

Vincent T.R., Avramova M., Canham J., Higgins P., Bilkey N., Mugford S.T., et al. (2017) Interplay of plasma membrane and vacuolar ion channels, together with BAK1, elicits rapid cytosolic calcium elevations in Arabidopsis during aphid feeding. *Plant Cell* 29: 1460–1479.

Whalley H.J., Knight M.R. (2013) Calcium signatures are decoded by plants to give specific gene responses. *New Phytol.* 197: 690–693.

Xiong T.C., Ronzier E., Sanchez F., Corratgé-Faillie C., Mazars C., Thibaud J.B. (2014) Imaging long distance propagating calcium signals in intact plant leaves with the BRET-based GFP–aequorin reporter. *Front. Plant Sci.* 5: 43.

Zhang W., Fan L.-M., Wu W.-H. (2007) Osmo-sensitive and stretch-activated calcium-permeable channels in Vicia faba guard cells are regulated by actin dynamics. *Plant Physiol*. 143: 1140–1151.

ABBREVIATION

- **CFP** cyan fluorescent protein
- **cpVenus** circularly permutated Venus
- **FRET** Förster resonance energy transfer
- **GFP** green fluorescent protein
- **GLR** glutamate receptor-like ion channel
- **NA** numerical aperture
- **ROI** region of interest

SUPPLEMENTARY DATA

Supplementary videos 1-7 are available at PCP online

Supplementary Video 1. In vivo analysis of Ca2+ dynamics in the *Physcomitrella patens* plant reported in Fig. 2.

Supplementary Video 2. Dynamics of cpVenus fluorescence emitted by the *Physcomitrella patens* plant reported in Fig. 2.

Supplementary Video 3. Dynamics of CFP fluorescence emitted by the *Physcomitrella patens* plant reported in Fig. 2.

Supplementary Video 4. In vivo analysis of Ca2+ dynamics in the *Physcomitrella patens* plant reported in Fig. 3 and having the base of the gametophore towards the entry point of the osmoticon.

Supplementary Video 5. In vivo analysis of Ca2+ dynamics in the *Physcomitrella patens* plant reported in Fig. 3 and having the tip of phyllids towards the entry point of the osmoticon.

Supplementary Video 6. In vivo analysis of Ca2+ dynamics in the *Physcomitrella patens* plant reported in Supplementary Fig. 6.

Supplementary Video 7. In vivo analysis of Ca2+ dynamics in the *Arabidopsis thaliana* plant reported in Fig. 4.

		$\Delta R_{max}/R_0$		t/2 [s]	
	Mannitol	Hyper-osmotic	Hypo-osmotic	Hyper-osmotic	Hypo-osmotic
Nucleoplasm	400 mM	0.036 ± 0.031	1.339 ± 0.750	n.d.	7.93 ± 0.33
	500 mM	0.593 ± 0.465	5.909 ± 1.786	5.60 ± 0.91	15.51 ± 0.66
	750 mM	0.813 ± 0.258	6.598 ± 3.936	21.97 ± 1.82	12.93 ± 1.37
Mitochondria	400 mM	0.132 ± 0.038	0.717 ± 0.110	7.08 ± 1.22	13.68 ± 1.14
	500 mM	0.497 ± 0.229	1.085 ± 0.308	45.71 ± 5.07	n.d.
	750 mM	1.240 ± 0.388	2.142 ± 1.126	23.87 ± 2.07	8.11 ± 2.93
Cytoplasm	400 mM	0.048 ± 0.016	0.674 ± 0.340	n.d.	17.44 ± 1.82
	500 mM	0.051 ± 0.024	2.972 ± 0.442	n.d.	20.05 ± 0.34
	750 mM	0.775 ± 0.132	2.853 ± 0.335	142.89 ± 56.92	n.d.

Supplementary table 1. Maximum Ca^{2+} peak values (ΔRmax/R0) reached in the nucleoplasm, mitochondria and cytoplasm during the hyperosmotic and hyposmotic treatment with various doses of mannitol. The recovery time of resting calcium concentration here expressed as t/2 was calculated after a fitting analysis reported in supplementary Fig. 3. n.d. = not determined, indicate samples for which there was no change in ΔRmax/R0 or that did not recover during the experiment.

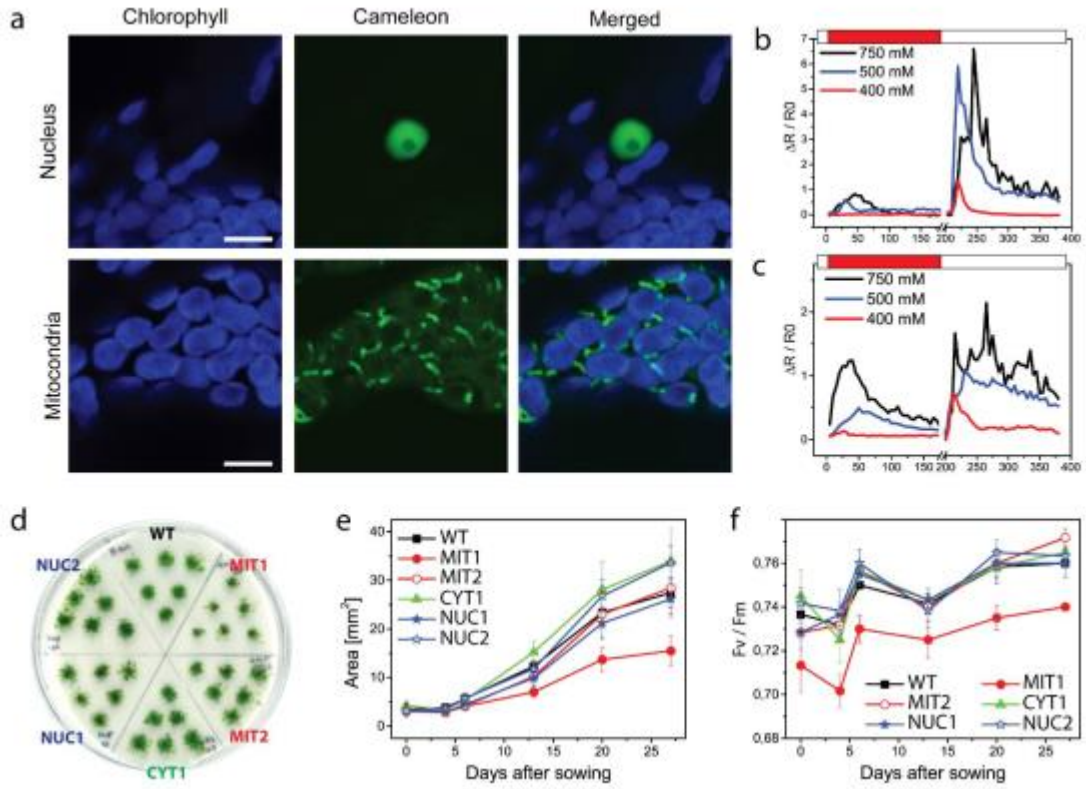

Supplementary Fig. 1. Expression of Yellow Cameleon 3.60 (YC3.60), plant growth and photosystem II maximum efficiency. a, The YC3.60 sensor was expressed under control of constitutive 7113 promoter and targeted to the nucleoplasm and nucleoplasm. Chlorophyll and YC3.60 signals were independently acquired by confocal laser scanning microscopy and then merged. Scale bar corresponds to 10 µm. **b-c**, Changes in Ca^{2+} concentration in protonema cells in response to osmotic stress in nucleoplasm (b) and mitochondria (c). CFP and cpVenus emissions were detected simultaneously after CFP excitation and cpVenus/CFP fluorescent ratio over the time is expressed as ΔR/R0. Osmotic stress was applied by continuous perfusion with a solution containing 400, 500 and 750 mM mannitol, respectively represented by red, blue and black lines. White and red bars on top of the panel indicate respectively the absence and the presence of mannitol in the perfusion solution. Data are shown as the mean of at least 4 independent plants. **d-f**, example of *P. patens* growth test on minimum medium. Plate diameter is 9 cm and contain 4-week-old plants. **e**, Growth curve and **f**, maximum efficiency of photosystem II measured by chlorophyll fluorescence video imaging of the plants shown in panel **d**. WT, wild type; MIT, CYT and NUC are lines expressing YC3.60 respectively in mitochondria, cytoplasm and nucleoplasm. MIT1 is a representative line not considered for further experiments because of its growth defects if compared to the wild-type.

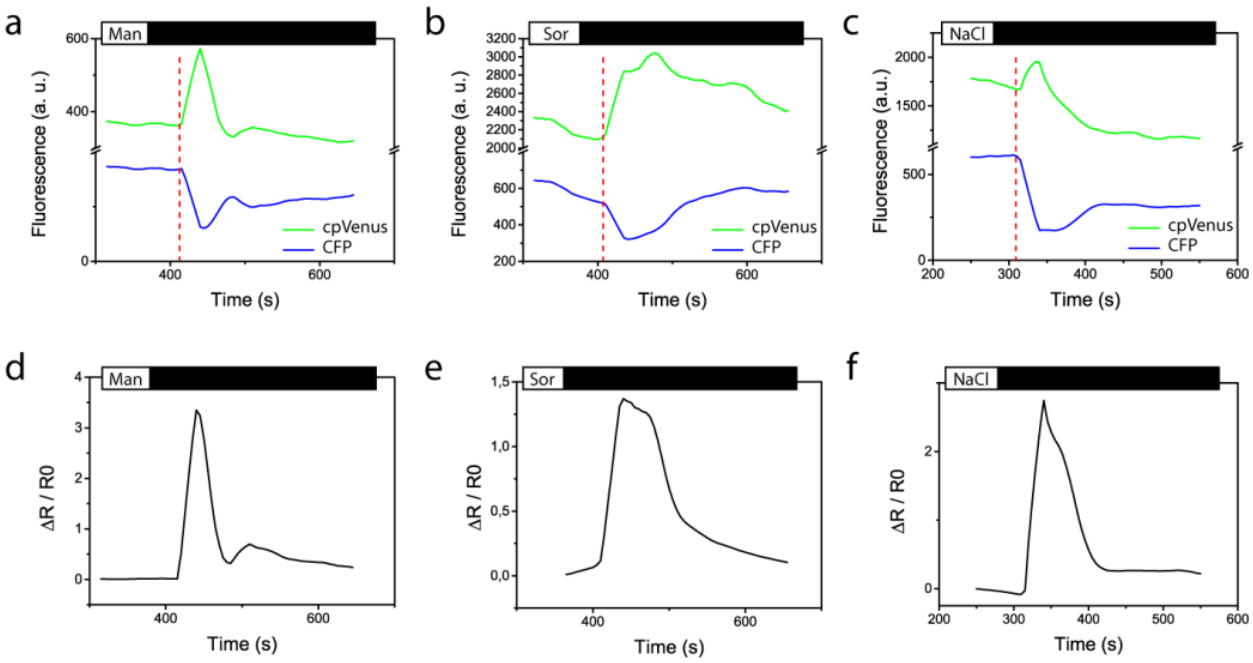

Supplementary Fig. 2. Representative examples of the analysis of Ca^{2+} dynamics in protonema cells of *P. patens* in response to osmotic stress. The anti-parallel behaviors of cpVenus and CFP is symptomatic of a true sensor conformational change and variation of the FRET efficiency hence faithfully reporting a change in Ca^{2+} concentration. Of note, the ratiometric calculation allows the abolition of artifacts that are generated by the movement of the sample, its shrinking or out-of-focus effects 20,41 possibly occurring during treatment. **a - c**) CFP and cpVenus emissions were detected simultaneously after CFP excitation in plants expressing YC3.60 in the nucleus. **d - f**) The ratio between cpVenus and CFP emission was subtracted of the initial cpVenus/CFP ratio and normalized to it (ΔR/R0). Osmotic stress was applied by continuous perfusion with a solution either containing 400 mM mannitol (a and d), 400 mM sorbitol (b and e) or 250 mM NaCl (c and f). Red dashed lines indicate the points in which cpVenus fluorescence signal started to increase while CFP signal started to decrease, generating an increase in ΔR/R0. White and black bars on top of each panel indicate respectively the presence and the absence of mannitol, sorbitol and NaCl in the perfusion solution.

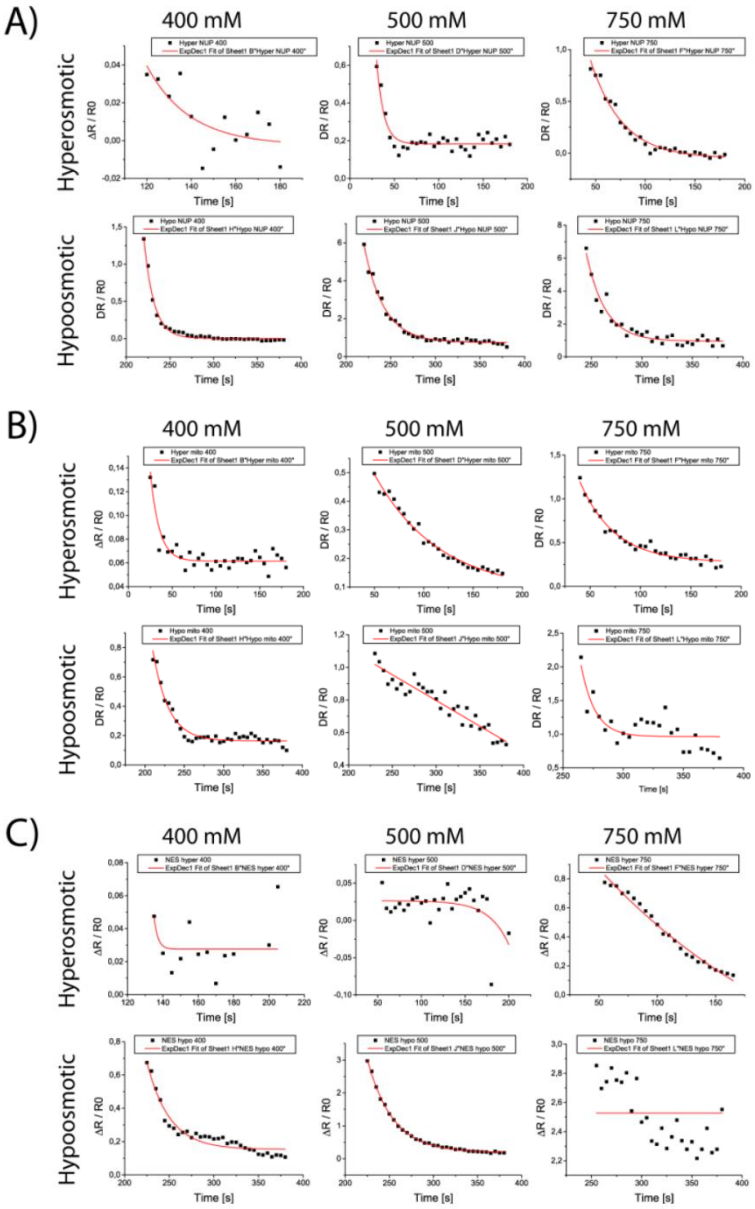

Supplementary Fig. 3. Fitting analysis of Ca^{2+} decrease. Both hyper- and hypo-osmotic kinetics were studied for transgenic lines expressing Cameleon YC3.60 sensor in the nucleoplasm (**a**), mitochondria (**b**) and cytoplasm (**c**). Three doses of mannitol were considered and reported on the top of each panel (400, 500 and 750mM). ΔR/R0 values are represented by black dots while the fitting line is represented in red. The analysis was used to calculate t/2 reported in Supplementary table 1.

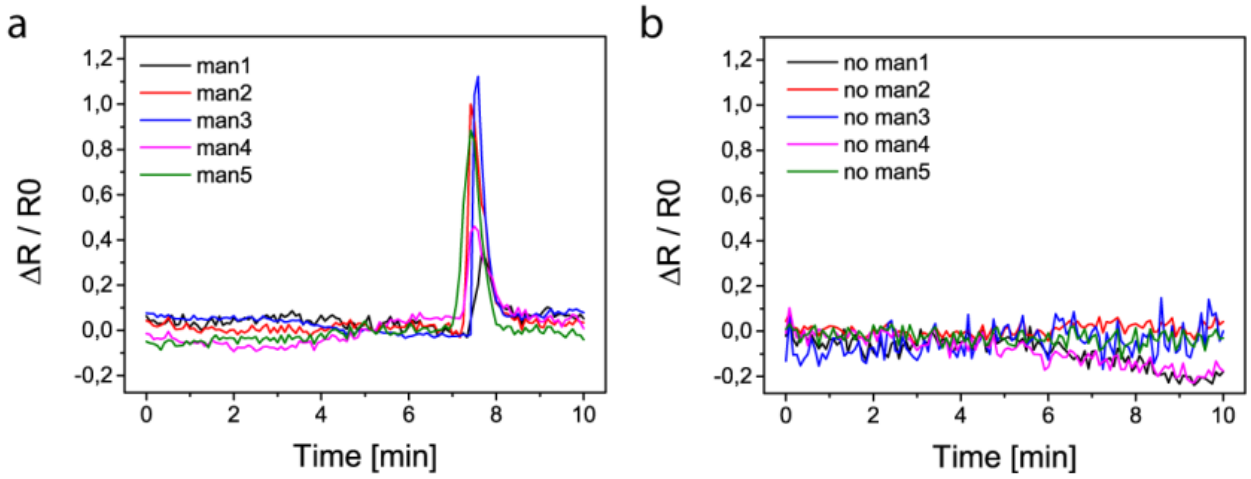

Supplementary Fig. 4. In vivo analysis of Ca^{2+} dynamics in response to osmotic stress in protonema cells of *Physcomitrella patens*. Variations in Ca^{2+} concentration (ΔR/R0) during the hypo-osmotic phase (**a**) or in the continuous perfusion in the absence of mannitol (**b**) was measured in 5 independent protonema samples.

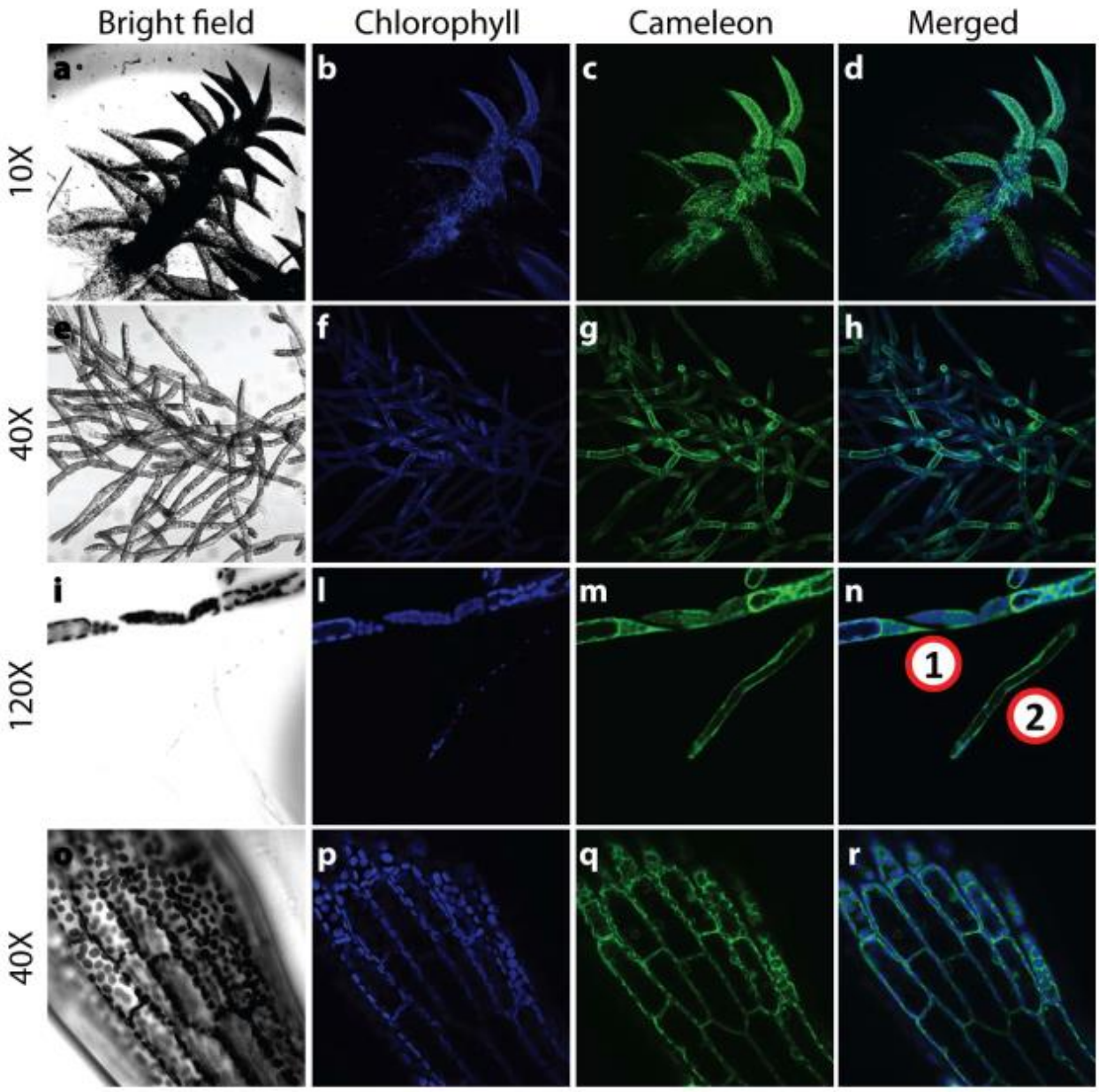

Supplementary Fig. 5. Expression of cytoplasm localized Yellow Cameleon 3.60 (CYT-YC3.60) in different cell types of *Physcomitrella patens*. Bright field (**a**, **e**, **i**, **o**) and the signal of chlorophylls (**b**, **f**, **l**, **p**) and YC3.60 (**c**, **g**, **m**, **q**) was acquired by confocal laser scanning microscopy independently and the two images were then merged together (**d**, **h**, **n**, **r**). Panels a – d show entire gametophores; e -h show protonema; i – n show chloronema (1) and caulonema (2); o - r show a phyllid.

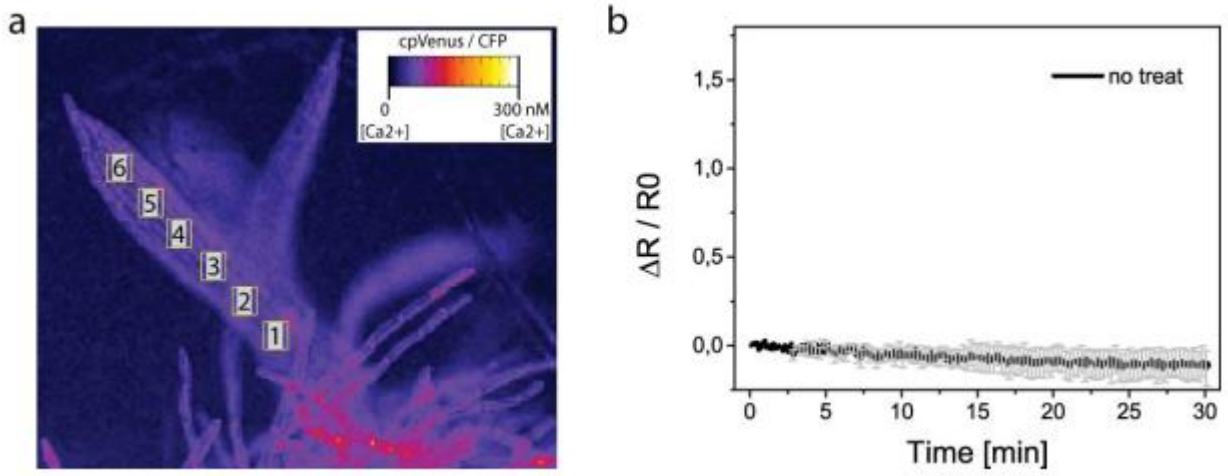

Supplementary Fig. 6. In vivo analysis of Ca2+ dynamics in the absence of osmotic stress in gametophores of *Physcomitrella patens*. (**a**) Representative snapshot of a control experiment run in the absence of mannitol during perfusion solution. Numbers from 1 to 6 identify the ROIs that were chosen to calculate changes of cpVenus/CFP. (**b**) Variations of Ca^{2+} concentration (ΔR/R0) were measured in 6 independent ROIs.

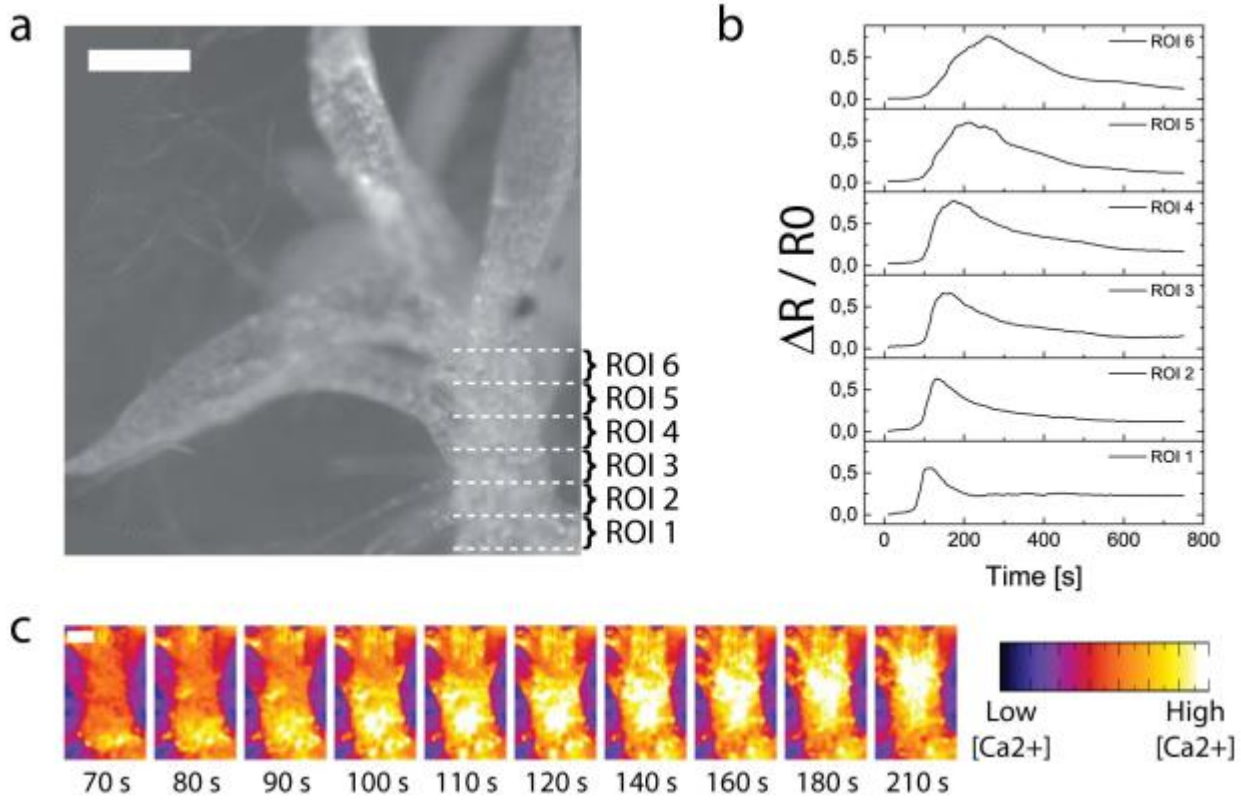

Supplementary Fig. 7. *In vivo* analysis of Ca^{2+} dynamics in response to osmotic stress in entire gametophores of *P. patens* expressing CYT-YC3.60. Plants were treated with hyper-osmotic solution (500 mM mannitol) and then returned to a non-mannitol added solution (hypo-osmotic solution). **a**, Representative snapshot of a gametophore. White dashed lines correspond to the Regions Of Interests (ROIs form 1 to 6) outlined to follow CFP and cpVenus fluorescence emission during the time. Scale bar is 500 µm. **b**, Variations of Ca^{2+} concentration (ΔR/R0) during the hypo-osmotic phase. ROIs from 1 to 6 correspond to those drawn in panel a. **c**, ratiometric false-color images from representative time series of a basal portion of the gametophore of *P. patens*. the false color represents the intensity of cpVenus/CFP ratio. Time (s) below each snapshot corresponds to the signal reported in panel b. The full acquisition can be visualized as supplementary material (Supplementary video 6). Scale bar is 2 50 µm.

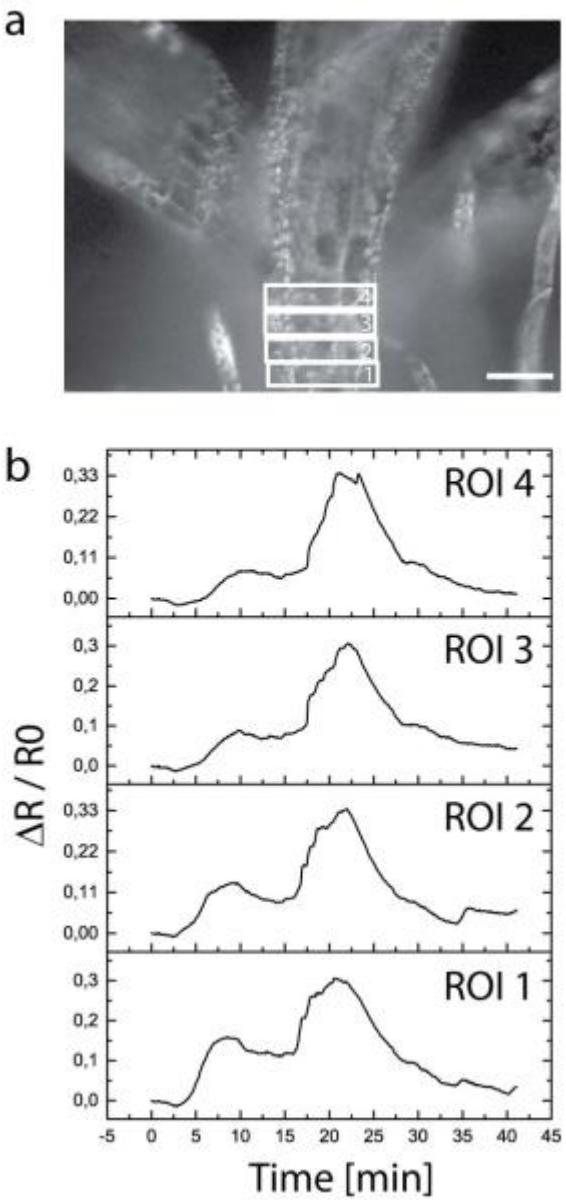

Supplementary Fig. 8. *In vivo* analysis of Ca^{2+} dynamics in response to osmotic stress in gametophores of *P. patens* observed at high magnification. Plants were treated with hyper-osmotic solution (500 mM mannitol) and then returned to a non-mannitol added solution (hypo-osmotic solution). **a**, Representative snapshot of a phyllid, white boxes correspond to the Regions Of Interests (ROI form 1 to 4) outlined to follow CFP and cpVenus fluorescence emission during the time. Scale bar = 50 µm. **b**, Variations in Ca^{2+} concentration (ΔR/R0) during the hypo-osmotic phase. ROIs from 1 to 4 correspond to those drawn in panel a.

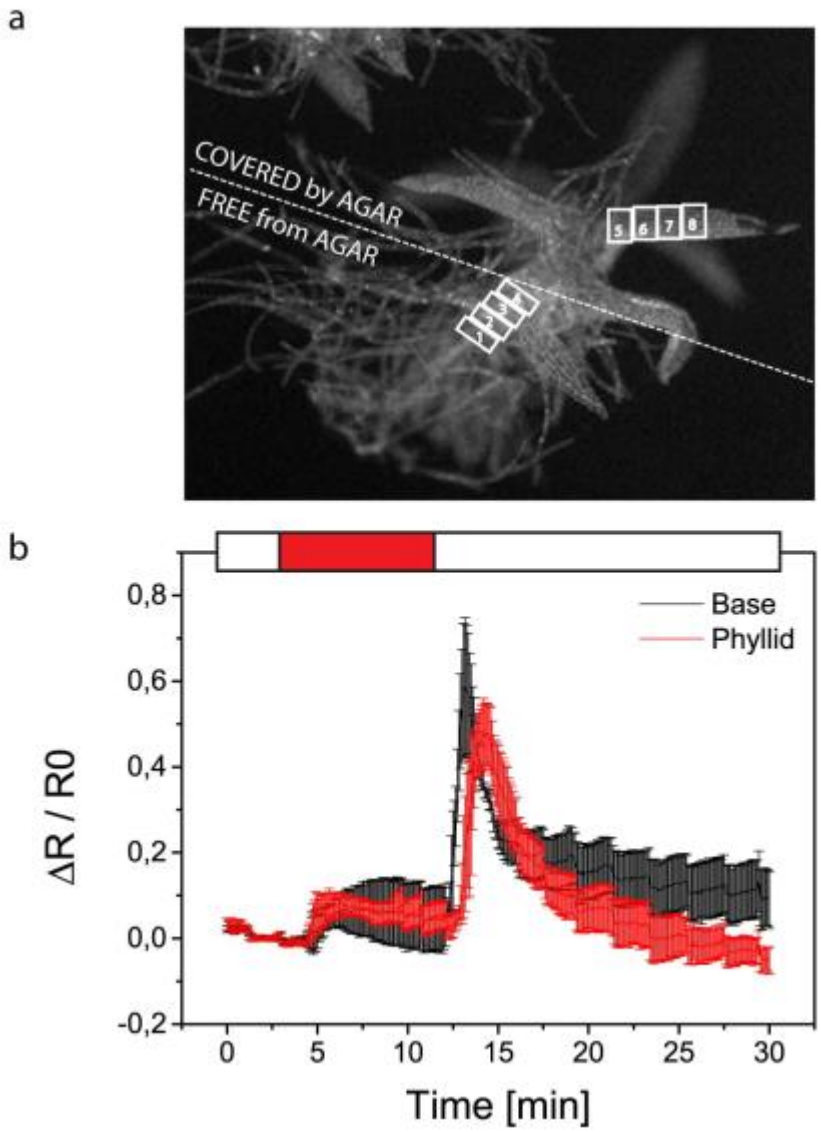

Supplementary Fig. 9. *In vivo* analysis of long-distance Ca^{2+} dynamics in response to osmotic stress in gametophores of *P. patens*. Plants were covered by a block of agarized (1% w/v) imaging solution and then treated with hyper-osmotic solution (500 mM mannitol) and returned to a non-mannitol added solution (hypo-osmotic solution). **a**, Representative snapshot of a gametophore, white boxes correspond to the Regions Of Interests (ROI) outlined to follow CFP and cpVenus fluorescence emission during the time (form 1 to 4, base of the gametophore; form 5 to 8 phyllid). **b**, changes in Ca^{2+} concentration (ΔR/R0) at the base of the gametophore (black line) and in phyllids (red line).

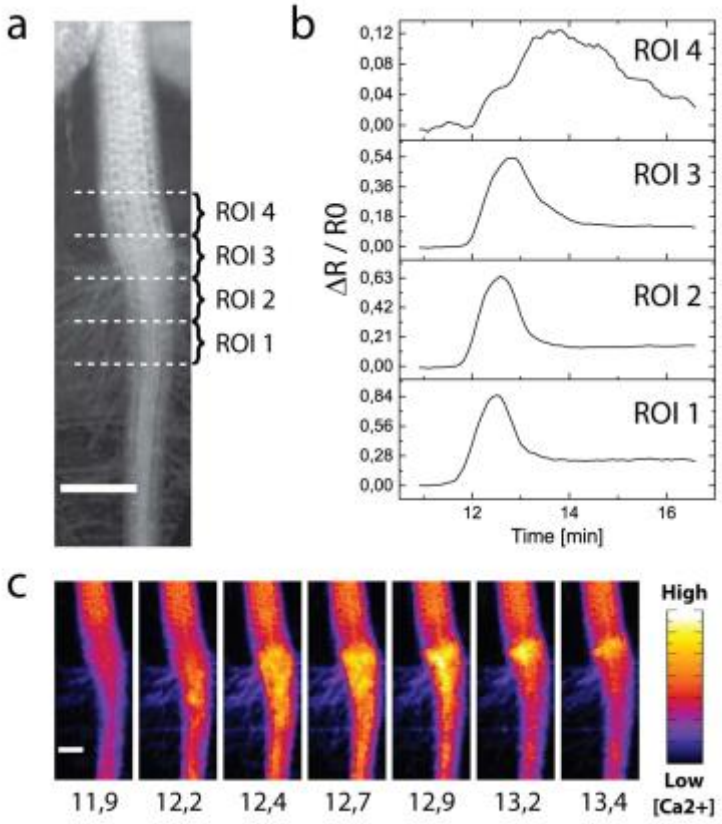

Supplementary Fig. 10. *In vivo* analysis of Ca^{2+} dynamics in response to osmotic stress in young plantlets of *Arabidopsis thaliana* expressing the cytoplasm localized probe (CYT-YC3.60). a, representative snapshot of a 4-day-old plantlet of *A. thaliana* as reported in Fig. 4a. Cotyledons are visible in the upper part of the panel. White dashed lines delimit the Regions Of Interests (ROIs form 1 to 4) outlined in the region between the hypocotyl and the radicle to follow CFP and cpVenus fluorescence emissions during the time. Scale bar, 500 µm. **b**, Variation of Ca^{2+} concentration (ΔR/R0) during the hypo-osmotic phase. ROIs from 1 to 4 correspond to those drawn in panel a. **c**, ratiometric false-color images from representative time series of a basal portion of the gametophore of *P. patens*. Time (min) below each snapshot corresponds to the signal reported in panel b. The false colors represent the intensity of cpVenus/CFP ratio. The full acquisition can be visualized as supplementary material (Supplementary video 7). Scale bar, 250 µm. Ratio images are representative of n = 4.

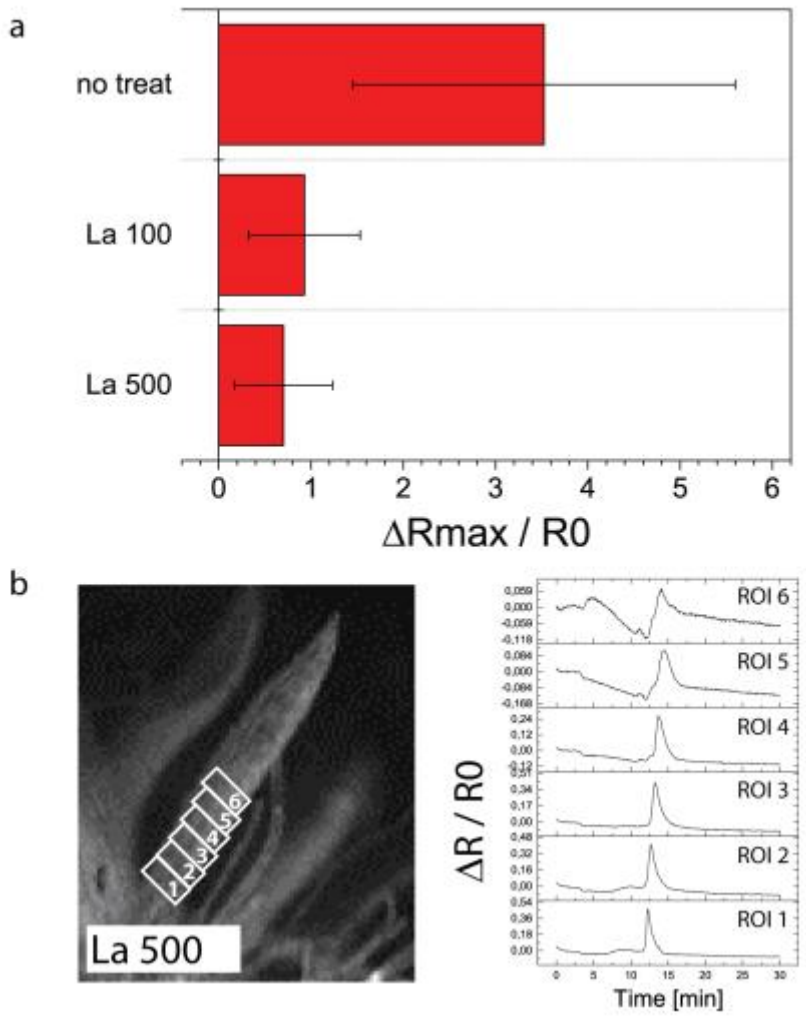

Supplementary Fig. 11. Effect of Lanthanum (III) chloride on osmotically-induced Ca^{2+} transients. a, Effect of Lanthanum (III) Chloride on the maximum increase of cytoplasmic Ca^{2+} concentration at the base of *P. patens* gametophores. **b**, Representative phyllid used to measure ΔR/R0 and therefore Ca2+ wave propagation in the presence of 500 µM Lanthanum (III) Chloride. Ca^{2+} waves are still propagated even in the presence of Lanthanum (no treat, La 100 and La 500 stands respectively for perfusion Lanthanum (III) Chloride 0, 100 and 500 µM). In the experiments with Lanthanum (III) Chloride we used a modified imaging solution with 50 µM instead of 10mM $CaCl_2$.

ABBREVIATION LIST

AEF: Alternative Electron Flow

AL: Actinic Light

Car: Carotenoids

CEF: Cyclic Electron Flow

Chl: Chlorophyll

Cyt: Cytochrome

EDB: Electron Binding Domain

Fd: Ferredoxin

FLV: Flavodiiron protein

FMN: Flavin MonoNucleotide

FNR: Ferredoxin-$NADP^+$ reductase

FQR: Ferredoxin Plastoquinone Reductase

LEF: Linear Electron Flow

NDH-1 / NDH: NADH DeHydrogenase like-1

NPQ: Non-Photochemical Quenching

OEC: Oxygen Evolving Complex

Pc: Plastocyanin

PCEF: Pseudo-Cyclic Electron Flow

PGRL1: PGR5-like 1

PGR5: Proton Gradient Regulator 5

pmf: Proton Motive Force

PQ: Plastoquinone

PQH_2: Pastoquinol

PS: Photosystem

RC: Reaction center

ROS: Reactive Oxygen Species

WT: Wild Type